The early stages of biofilm formation by *Staphylococcus epidermidis* studied by XPS and AFM

Thesis submitted in accordance with requirements of the University of Chester for the degree of Doctor in Philosophy by Radhika Bava

September 2019

Declaration

The material being presented for examination is my own work and has not been submitted for an award of this or another HEI except in minor particulars which are explicitly noted in the body of the thesis. Where research pertaining to the thesis was undertaken collaboratively, the nature and extent of my individual contribution has been made explicit.

Acknowledgements

I would firstly like to thank the University of Chester for providing me with the opportunity and funding to complete this PhD. I would also like to thank my supervisor Professor Graham Smith at the University of Chester. The door to Professor Smith's office was always open, and it is not often that one finds an advisor and colleague that always finds the time for listening to the little problems and roadblocks that unavoidably crop up in the course of performing research. His technical and editorial advice was essential to the completion of this thesis and has taught me innumerable lessons and steered me in the right the direction whenever he thought I needed it.

Thank you to the University of Chester Biology department for gifting me the bacteria *S. epidermidis ATCC35984.* Without this gift the thesis would have not been completed, and I will always be grateful to the department. Thank you to Alice Gillet for the preparation of the bacterial lawn samples for XPS analysis, it provided an additional depth to my analysis, confirming what was happening at the surface of the bacteria. Thank you to all my colleagues and friends at the University of Chester, completing this work would have been all the more difficult were it not for their support, friendship and passionate participation. They aided with keeping my morale and I will always be indebted to them all.

I must express my very profound gratitude to the ultimate role models, my parents, my elder brother Jay and my sister in law Darshna. They have assisted with keeping my focus have provided me with unfailing support and continuous encouragement throughout my years of study and through the process of researching and writing this thesis. I would also like to thank my amazing nieces Arianna and Sienna, who have provided me with great happiness and have definitely assisted with maintaining my morale. This accomplishment would not have been possible without them.

I would also like to thank the rest of my family and in particular my uncle Bipin and auntie Tilly. Without them I would not only have been introduced to Professor Smith, but they also took me under their wings and provided me with love and accommodation, allowing me easier access to the university. My family have always believed in me and always wanted the best for me.

Finally, I would like to thank God, who without, I would have not got through any of the stages that have been set out to me, not only during this PhD, but in life as well.

Contents

Abstract

Staphylococcus epidermidis is an opportunistic bacteria which forms pathogenic biofilms in medical implant environment. Biofilm formation is a complex multistage process within which the initial stages of adhesion are deemed the most critical target for preventing biofilms.

This research involves the characterisation of *S. epidermidis (ATCC35984 and NCTC13360)* by using X-ray photoelectron spectroscopy (XPS) and atomic force microscopy (AFM) on model substrates including glass, muscovite mica, silicon (111) wafer, sputter-coated titanium and sputter-coated silver, focusing on the effect of chemical properties of the material on adhesion by using surfaces with minimal roughness.

AFM was used to image the surface, from which bacterial coverage can be estimated. AFM was also used to probe adhesion forces and local mechanical properties of all samples through the use of force-distance curves. AFM images were also used to estimate the bacterial coverage. XPS was used to investigate the surface chemistry from the layer thicknesses, the percentage coverage and potential composition of the overlayer. The combination of these techniques allow the relationships between the surface chemistry of the substrate and the bacteria to be correlated with changes in coverage and properties of bacterial films.

Data on incubated bacterial samples were compared with those from the reference substrates, both before and after autoclaving, and from samples prepared using protein rich growth medium (tryptic soy broth) in the absence of bacteria as well as a pure bacterial pellet in an assumed non-biofilm forming state.

The research indicates the potential differences between biofilm and non-biofilm former strains, with both strains being covered by an organic layer with little influence of the growth media used to incubate the bacteria. This research also shows how XPS and AFM data can be combined and applied to bacterial adhesion.

Chapter 1 Introduction

Biofilms are microbes that are connected through an extracellular matrix that can attach to a surface. This can lead to a range of problems in various situations. In medical devices, biofilm formation can give rise to infections (Chen, Yu, & Sun, 2013) and within the body are known to be the cause of various health problems such as cystic fibrosis lung infections and meningitis (Bjarnsholt, 2013). In processing systems, biofilms formed can detach in lumps, causing contamination in processing plants or can give rise to fouling layers, reducing performance of heat exchangers. In pipelines, they are a source of corrosion and failure and therefore cost to industry (Tan, Chew, Tan, Givskov, & Yang, 2014).

Formation of bacterial biofilms is a defence mechanism for the microbes, in that they behave differently from planktonic bacteria, especially in terms of antimicrobial resistance and the ability to survive in nutrient deprived environments. Chemical signalling between the bacteria, known as quorum sensing, plays a pivotal role in biofilm formation by stimulating the bacteria to multiply and form colonies, as well as a means of communication within a biofilm allowing multi-strain biofilms to survive at different metabolic rates. There is consequently a significant amount of research into the structure of biofilms research and methods to prevent their formation (Wright et al., 2013).

The growth of biofilm communities is quite well understood, the first stages of adherence is not. The exact mechanism of attachment is generally not known, but involves complex intracellular pathways, such as quorum sensing whereby cells can communicate with each other. Overall, the trigger point for biofilm formation is likely to have some generic factors (e.g. cell density) and some species/substrate-dependent factors (Campoccia, Montanaro, & Arciola, 2013).

With the recent rise in antibiotic resistance, the understanding of biofilms becomes even more important. It should be noted that biofilms are not just a problem, they can also be used constructively within industry. They can provide an excellent way of harnessing microbes for industrial transformations. The most widespread use of biofilms is in wastewater treatment ‘trickle bed’ processes in which a community of bacteria growth on pebbles and degrade contaminating species to produce less harmful effluent. There are also other exciting potential applications(Al-Mailem, Kansour, & Radwan, 2014). A recently discovered class of hydrocarbonoclastic (hydrocarbon degrading) bacteria have been used in oil elimination from polluted water(Naz, Saroj, Mumtaz, Ali, & Ahmed, 2015).

This project addresses this critical first stage of adhesion of the microbe to the surface, before the development of any extra-cellular material or any signalling between co-located bacteria. The objective is to use the classical analytical techniques of surface science and apply them to this difficult biological problem. The precise elemental composition, chemistry and layer structure of the substrate/biofilm interface will be addressed using X-ray photoelectron spectroscopy (XPS), and high resolution images of the bacterial films will be generated by atomic force microscopy (AFM). AFM will be used to probe the surface mechanical properties of individual bacteria cells, including the adhesion force, and the possibility of imaging and mechanical property measurement in-situ while the film is under the liquid will be investigated.

S. epidermidis was chosen as the model bacterium for this work as it is an opportunistic bacteria which is a part of the human flora (Otto, 2009) and frequently forms problematic antimicrobial resistant biofilms in medical implant environments (Campoccia et al., 2013).

Chapter 2 Literature Review

Bacterial biofilms cause a multiple problem across a range of situations, including with medical devices and the effectiveness of equipment in processing plants. Formation of a biofilm is a defence mechanism, especially in terms of antimicrobial resistance and the ability to survive in nutrient deprived environments. Although the pathway of biofilm growth is understood, the mechanism of the first stage of adhesion is still being researched.

2.1 Biofilm growth mechanism

The essential steps in biofilm formation are summarised schematically in Figure 2.1. Initially, a clean surface is present in a microbe-containing environment. Because of media flow and microbe movement, individual microbes arrive at the surface. Initially they are free to move, and the attachment is reversible. At some point, triggered by population density or other chemical or physical phenomena, the attachment becomes irreversible and a biofilm begins to develop in the form of microcolonies. The attached bacteria start to produce extracellular polymer substances (EPS), which allows the attachment of secondary colonisers and the adaption of the bacteria in the biofilm to different metabolic states. The microbes continue to multiply until the full biofilm is reached, where dynamic growth and dispersal occurs, allowing dispersed bacteria to form new colonies (Myszka & Czaczyk, 2011).

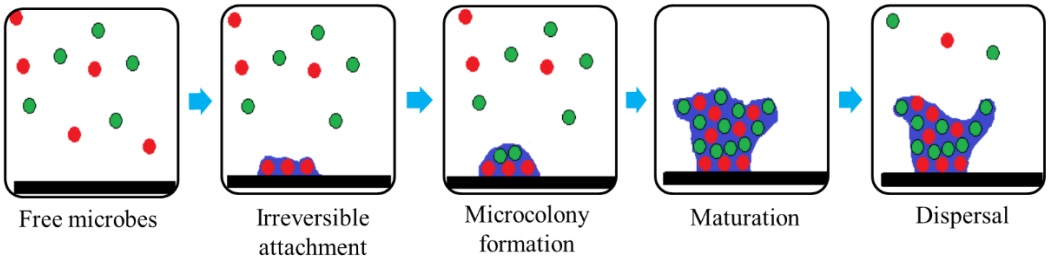

Figure 2.1 Diagram depicting the growth of biofilms where green and red represent different bacteria.

There are multiple theories discussing the factors that included in the initial attachment of microbes, including the role of extracellular polymeric matrix (EPS) (Arciola, Campoccia, Speziale, Montanaro, & Costerton, 2012; Flemming & Wingender, 2010), quorum sensing (QS)(Kalia, 2013), adhesins and environment (Campoccia et al., 2013).

Extracellular polymeric substance (EPS), is the substance produced by the microbes which helps to form a matrix for the microbes to survive in. EPS is made up of a number of things including DNA, polysaccharides and proteins (Arciola et al., 2012). EPS acts a barrier around the bacteria and fungi, protecting it from external influences (Flemming & Wingender, 2010).

This makes finding agents to remove biofilms harder as they must penetrate the EPS, which contributes to the resistant nature of biofilms.

EPS also contributes to the structure of the biofilm, allowing the transfer of nutrients through channels to various layers as well as communication by quorum sensing systems. It is thought that the EPS is important in the binding of bacteria to a surface and the subsequent formation of a biofilm (Tan et al., 2014).

There are theories into the fact only a few species can make the initial attachment to a surface and subsequently other species that bind at a later time, to make a multispecies biofilm (Supernak & Świeczko-Żurek, 2010).

Quorum sensing helps facilitate the formation of a biofilm as a method of communication between bacteria of different species. The number of bacteria corresponds to the amount of quorum sensing compound and as a result correlates to if a biofilm is formed through facilitating colony formation.

Within biofilms quorum sensing (QS) agents can change the biological environment to allow multiple strains of microbes to survive in the same environment in different metabolic states (Supernak & Świeczko-Żurek, 2010). The amount of QS molecules can determine the formation of a biofilm, if the critical amount is reached (Kalia, 2013). The amount of QS compound can be related to the amount of a certain species of bacteria. QS can also allow bacteria to communicate with each other in either cooperative or competitive manner.

There are various types of QS sensing systems in bacterial biofilms including oligopeptides (Kalia, 2013) and N-acyl hormoserine lactones(Dickschat, 2010).

One of the main reason's biofilms are formed is to survive the change in environmental conditions. Biofilms can consist of multiple species of microbes which survive in a nutrient deprived state, relying on other microbes to cooperate and metabolise compounds needed for survival which the microbe may not be able to use in its planktonic form. Another advantage of microbial cooperation is antibiotic resistance. There are several theories on why biofilms are antibiotic resistant. These include the role of EPS, nutrient deprived state of bacteria and the potential to share antimicrobial resistant genes within the biofilm community (Bjarnsholt, 2013).It is important to note not all microbes will form biofilms, or cooperate with all species of microbe present. In these cases, a biofilm can release anti-biofilm compounds, to prevent other biofilms from forming, reducing the competition for space and nutrients. The attachment of a microbe to the surface irreversibly is the start of

the growth of a biofilm. This can be affected by a range of qualities including pathogen, environment and surface properties (Campoccia et al., 2013).

The size and shape of the bacteria affect adhesion, in terms of the area of contact the pathogen has on a surface and if there are gaps on the surface it can get caught in. The strain of bacteria also plays a role in adhesion, as this can affect the adhesins the bacteria expresses.

Another factor is the environment the bacteria is in; the temperature and nutrients available can easily affect the bacteria's survival, as well as how the bacteria acts. These properties can differ in vivo, however from an in vitro perspective, temperature and pH are controllable.

As an extension of the environment, the location of adhesion to the surface can affect the formation of a biofilm. This can be split into the morphology, looking at the roughness and porosity of the material, in relation to the size of the bacteria, and the physiochemical properties of the material itself, including functional groups available and hydrophobicity. This is a diverse section which will be discussed in more detail in a later section, discussing mechanisms used currently in biofilm prevention. The physiochemical properties offer a wide range of possibilities to explore, looking at hydrophobicity, charge and functional group effects. There are a range of ways to modify the properties of the surface, which will not be discussed here.

2.2 Biofilm prevention methods

Although biofilms are complex and varying in structure and composition, there has been research into the environment and surface qualities that contribute to the likelihood of bacterial attachment, and therefore the formation of biofilms.

There are numerous ways the formation of biofilms can be prevented, each with their own set of advantages and disadvantages. These include, but not limited to, phage therapy (Campoccia et al., 2013), quorum sensing inhibitors (Kalia, 2013) and enzyme treatments (Gomes, Teixeira, & Oliveira, 2014).

While there is a wide range of treatments involved in preventing biofilms, the focus in this research is the material contribution to biofilm formation.

The inclusion of anti-infective treatments within the material is the most direct route and include a range of chemicals (Campoccia et al., 2013). These treatments usually end in microbe death. One of the main problems with this is the resistance build-up from the microbe, which is enhanced by the formation of a biofilm, through the key changes in

qualities of microbes from free to biofilm. This has led to a wider range of biofilm prevention methods. Not all anti-microbial treatments are ineffective, there are some in development which can be used on biofilms (Campoccia et al., 2013). However, an issue with microbe death compounds being imbedded into a surface, is the build-up of dead organisms on the surface. The dead microbes cover the surface, reducing the contact with live organisms, and hence the antimicrobial activity, leading to ineffective biofilm prevention method (Campoccia et al., 2013). Alternatively these compounds can be introduced through the use of nanoparticles (Sharma et al., 2014) or metal organic frameworks (Sancet et al., 2013), however the advantages of these methods will not be discussed here.

The texturing of a surface can be altered to change the attachment of a microbe to the surface. General theory suggests that the smoother the surface, the less biofilm attaches to it (Campoccia et al., 2013).

However, the limitation of this is the space between the texturing. If the gaps are sufficiently large enough the microbes may be able to orientate themselves to fit into these gaps and therefore form a biofilm across the surface (Halder et al., 2013). This becomes more complex to design a surface for a range of microbes, as they vary in size and shape.

Roughness has also been used to mimic the structure of hydrophobic parts of plants, leading to the reduction in adhesion by limiting the contactable surface points (Chung & Toh, 2014).

Leading on from changing the roughness of a material to prevent adhesion, there are a range of nanofeatures that can affect the adhesion of microbes to a surface, including nanotubes and pillars.

By altering the arrangement of nanofeatures, adhesion can be reduced, and by forming larger patterns with the layout of nanostructures can change the microbial adhesion to a surface (Desrousseaux, Sautou, Descamps, & Traore, 2013). There have been conflicting results with the change of patterns, however this could possibly be due to the change in surface chemistry affecting the groups. From this it may be interesting to look at the why the surface chemistry alters in such a way that adhesion is prevented

Through use of nanotubes on a surface, we can use patterning to deliver drug compounds, in this case antimicrobials, to the site of action (Ercan, Taylor, Alpaslan, & Webster, 2011).

The hydrophobicity of the material can affect the microbial adhesion. This is due to the external features of the microbe involved in microbial adhesion. The level of hydrophobicity

required depends on the strain of microbe, however as a rule more hydrophobic surfaces have a higher rate of adhesion. However, the interaction between a surface and bacteria is more complex, and therefore relies on other factors such as surface tension of the media (Desrousseaux et al., 2013). The hydrophobicity is proportional to the roughness of the sample, so both must be taken into account in determining bacterial adhesion (Ivanova et al., 2011).

Salinization of a surface leads to a positively charged, highly adhesive antimicrobial surface which depends on the terminal group of the polymer. If a saline coat is applied through using an atmospheric plasma jet, the coating becomes superhydrophobic, making it an effective antimicrobial, reducing protein absorption. Combining a saline coating with nitric oxide reduces the microbial adhesion to a surface. Using a trimethylsaline coating, *S. epidermidis* biofilms are reduced, through the lack of EPS binding, therefore making it more susceptible to antibiotic treatment (Ma et al., 2012). Saline coats can also be functionalised using salioxides to covalently attach biomolecules, which can prevent nonspecific attachments (Rodriguez-Cano et al., 2013).

2.3 Material choices

To analyse bacterial growth several materials were chosen to analyse effect of initial adhesion.

Glass was chosen due to its frequency in surface studies of biofilm growth, and the material was selected for this work to enable comparison with previous results where applicable. Some key references include (Bernstein et al., 2014; Mitik-Dineva et al., 2009; Preedy, Perni, Nipic, Bohinc, & Prokopovich, 2014),

Silicon was chosen as an idealised substrate with high purity, low surface contamination levels and low surface roughness. Silicon has been analysed for adhesion of *S. aureus* (Müller, Ruhl, Hiller, Schmalz, & Schweikl, 2007).

Muscovite mica is well known as near-atomically smooth substrate often used for AFM studies of biological structures (Kan, Tan, Wu, Si, & Chen, 2015).

Titanium was chosen for the frequency of titanium alloys in medical implant devices (Antoci et al., 2008; Braem et al., 2014; Truong et al., 2009) and therefore studies on this material would provide insight into biofilm growth on a medically-relevant substrate. Nanoparticles of coated titanium dioxide have been used in antifouling coatings (Khalil et al., 2014).

Silver was chosen as a well-known anti-microbial material (Chen et al., 2013) and was used (i) to provide a contrast to the titanium substrates and (ii) to provide an opportunity to study the mechanism of its anti-microbial action. Silver nanoparticles have been used to treat biofilms (Jena, Mohanty, Mallick, Jacob, & Sonawane, 2012; Taraszkiewicz, Fila, Grinholc, & Nakonieczna, 2013).

The choice to sputtercoat was to ensure the substrate was a smooth layer, which is unaffected by the use of polishing. The use of sputtercoated titanium based materials has been previously used in bacterial adhesion research (C. Oliveira et al., 2011). Silver-titanium based films have also been analysed for its interaction with *S. epidermidis* (Carvalho et al., 2013).

2.4 *S. epidermidis*

S. epidermidis is a coagulase-negative gram positive bacteria which normally colonizes the skin and mucus of the human body as part of the human flora (Hu, Ulstrup, Zhang, Molin, & Dupres, 2011). The outer structure of a gram positive bacteria consists of a thick peptidoglycan layer with teichoic acids bound to the cell wall passing through the peptidoglycan layer (Figure 2.2 (van der Mei, de Vries, & Busscher, 2000)). While the outer structure of the bacteria may vary between strains the core structure remains similar (Figure 2.3 (Sadovskaya, Vinogradov, Li, & Jabbouri, 2004)and 2.4 (Fournier & Philpott, 2005)).

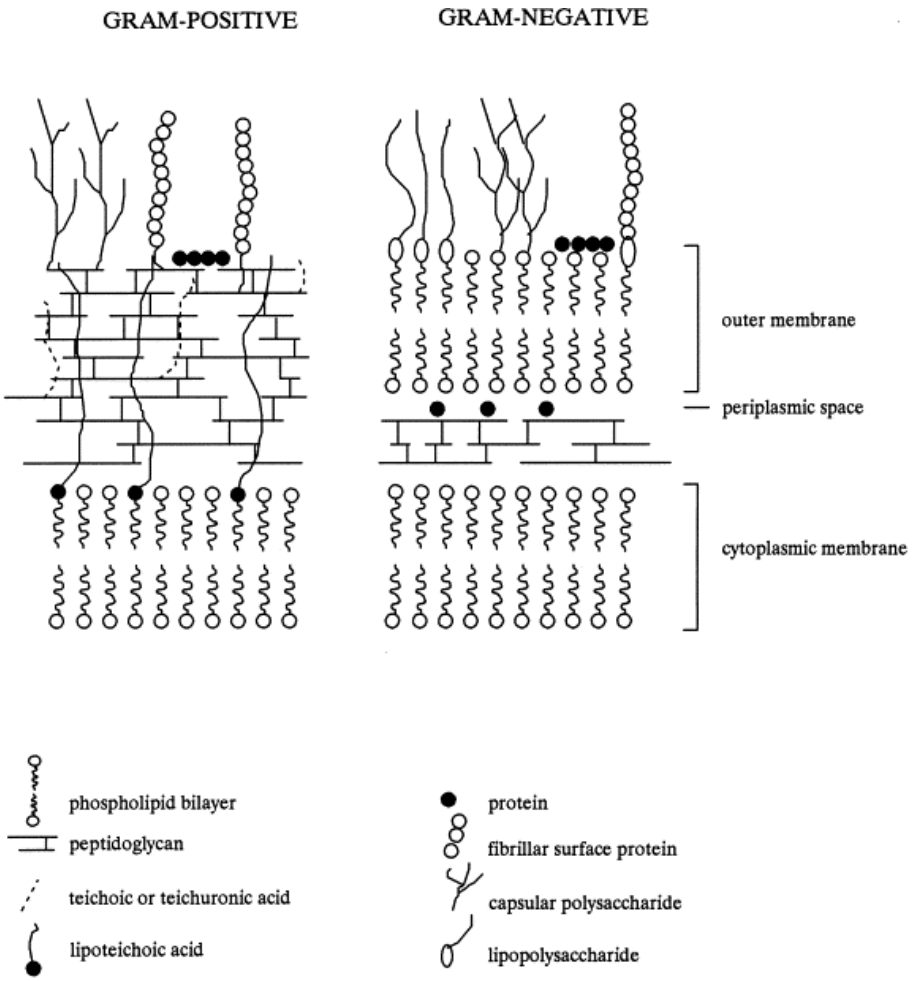

Figure 2.2 Schematic structure of the outer structure of gram-positive and gram-negative bacteria taken from van der Mei (2000)

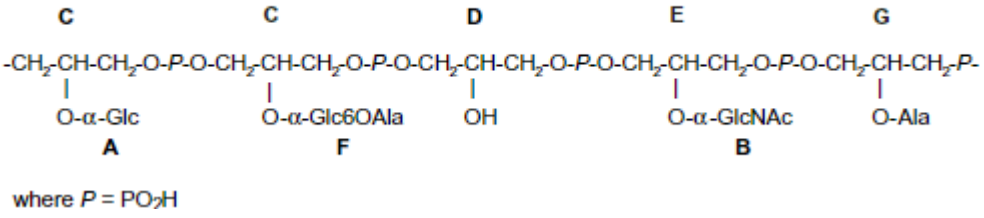

Figure 2.3 Chemical structure of teichoic acids in *S. epidermidis* taken from Sadovskaya, (2004)(Sadovskaya et al., 2004).

Certain strains have the ability to form biofilms such as *ATCC35984* (Ista et al., 2009; Méndez-Vilas et al., 2004) while others do not (*NCTC13360*). Both strains chosen are used frequently in research as model bacteria (Hu et al., 2011).

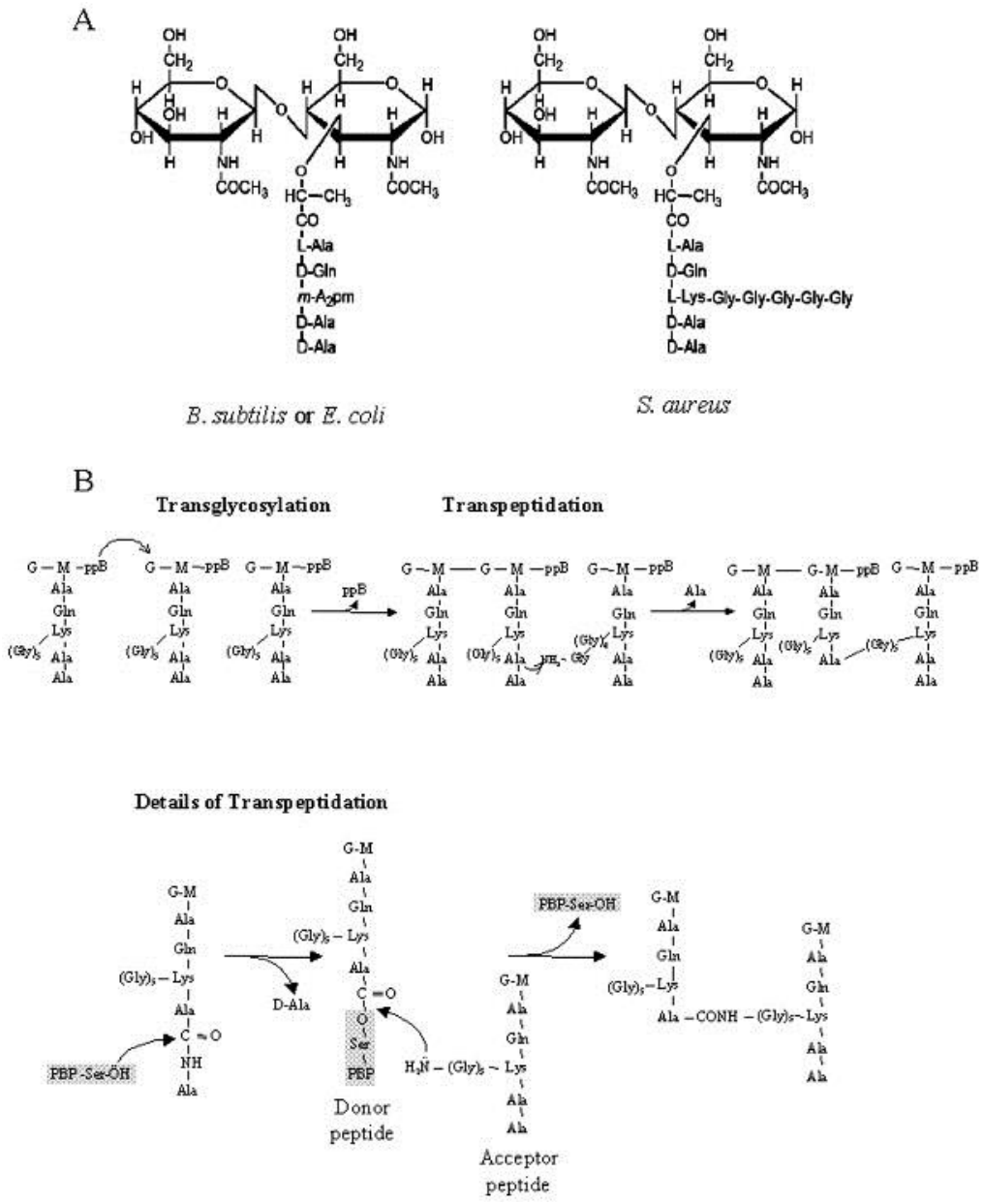

Figure 2.4 Chemical structure of peptidoglycan of *S. aureus, E.coli and B. subtillus* taken from Fournier (2005)(Fournier & Philpott, 2005).

2.5 Use of Surface Techniques in Biofilms and Biological investigations

2.5.1 X-ray Photoelectron Spectroscopy

Techniques used to analyse biological systems give insight into the specific biological processes. To analyse the chemical specific information, surface analysis techniques are applied to biological interactions (McArthur, Mishra, & Easton, 2014). X-ray photoelectron spectroscopy can be used to determine the elemental composition of the samples, and can be used to characterise specific functional groups related to the element(McArthur et al., 2014).

A range of XPS studies have looked at the outer structure of the bacterial cell (Cerca, Pier, Vilanova, Oliveira, & Azeredo, 2005; Ploszaj-Pyrek, Talik, & Piotrowska-Seget, 2014; van der Mei, van de Belt-Gritter, Reid, Bialkowska-Hobrzanska, & Busscher, 1997).

Research into the use of XPS for bacterial samples focuses on the variation of the outer structure of bacterial pellets. XPS data can be used to determine the biological compounds on the surface (McArthur et al., 2014), which can be applied to the structure of bacteria (Cerca et al., 2005; Ploszaj-Pyrek et al., 2014; Rouxhet & Genet, 2011; van der Mei et al., 2000). From the spectra, the percentage composition of each element can be calculated, and the bond type determined. By comparing this to expected outcomes and previous models, it is possible to calculate the compounds present within the sample. For example, by looking at the structure of a phospholipid, the ratio of phosphate to positively charged nitrogen, there is a 1:1 ratio. However, there is a limit to how XPS can be used to identify the compounds, and the effects of depth and complexity of the mixtures within the sample need to be considered. There are models that use this data to calculate the composition, however, these prove to be difficult to use between different species of bacteria. Two key models within this are proposed by Rouxhet (Equations 5-7,(Rouxhet & Genet, 2011)) and van der Mei (Equations 1-4 (van der Mei et al., 2000)).

$$\frac{N}{C} = 0.270\,\mathrm{Pr} + 0.200\,Pg$$

$$\frac{O}{C} = 0.320\,\mathrm{Pr} + 0.500\,Pg + 1.2Ta$$

$$\frac{P}{C} = 0.170Ta$$

$$\frac{C}{C} = 1 = \mathrm{Pr} + \mathrm{Pg} + \mathrm{Ta} + \mathrm{Ps} + \mathrm{Hc}$$

Equations 1-4: Model of bacterial outer cell wall as determined by XPS using the model proposed by van der Mei(van der Mei et al., 2000) where Pr is protein, Pg is peptidoglycan, Ta is teichoic acids, Ps are polysaccharides and Hc are hydrocarbons.

The van der Mei model uses ideal structures of the components of the bacterial cell wall. Analysis of the van der Mei Model takes into account the teichoic acids and peptidoglycan layer of the bacterial cell. However, for the equations to be solvable, the model has to assume the glycoprotein layer is zero, which leads to overestimates the protein content of the material, leading to an underestimate of sugars at the surface. The alternate way proposed is to use the decomposition data, but this was shown to be less reliable.

$$\frac{N}{C} = 0.279\left(\frac{Pr}{C}\right)$$

$$\frac{(O-4P)}{C} = 0.325\left(\frac{Pr}{C}\right) + 0.833\left(\frac{Ps}{C}\right)$$

$$\frac{C}{C} = \left(\frac{Pr}{\mathrm{C}}\right) + \left(\frac{Ps}{C}\right) + \left(\frac{Hc}{\mathrm{C}}\right) = 1$$

Equations 5-7: Model of bacterial outer cell wall as determined by XPS adapted from Rouxhet (Rouxhet & Genet, 2011) where Pr is protein, Ps are polysaccharides and Hc are hydrocarbons.

The model from Rouxhet also uses ideal compounds to model biological systems. The model considers the presence of peptidoglycan through its subunits of protein and polysaccharides. The paper discusses that the original equation would not work for noticeable phosphate oxygen bonding, as seen with *S. epidermidis* and includes the modification of (O-4P) to account for phosphate oxygens in the sample. Beyond this, the model does not consider the structure of the teichoic acids. While these equations are likely to work for some bacteria, the use of idealised compounds may not be as relevant as more complex systems which contain different types of binding between biological compounds calculated leads to errors in calculations.

The neglect of teichoic acids for gram positive bacteria would also lead to miscalculations as the outer layers of gram positive bacteria have a high amount of teichoic acids. The van der Mei model includes the calculations for some of these complex structures, however it neglects the peptidoglycan layer which is also a key part of the bacterial structure.

The limitations of both models are observed through samples that have a higher phosphate content. As phosphates have a high oxygen content, when factored in it is found that these models could potentially predict an oxygen content that is negative, causing the models to fail.

Errors also arise in the van der Mei model from estimates of phosphates not bound to other compounds, i.e. DNA binding. This extends to other compounds e.g. glycoproteins and teichoic acids. This can cause errors in oxygen calculations by overestimating the oxygen.

The use of idealised compounds may be useful for simple structures, however for more complex systems, flaws in the calculations become evident. Additionally, it is important to note, both biological composition models are not based on incubated samples on a range of substrates, but on pelleted bacteria. It may be possible to define the interaction between media and pellet with these models, but they lack the ability to consider the possibility of

substrate-media binding and substrate-bacteria binding, such that X-O-C (where X is the surface) is a possibility. While it is reasonable to assume these are independent, these interactions are also possible, and in the cases where it is, it is inevitable the organic oxygen will be miscalculated.

Due to the limitations of these equations they were not used for bacteria incubated samples. Rather the ratios involved in the models were used to qualitatively address the composition of the sample, as quantitative determination was not possible.

One of the limits of the material chosen for this research is the inclusion of oxygen within most materials. To overcome this, the XPS analysis of the sample must be used to determine the organic oxygen content of the material.

One of the methods proposed is the use of the C 1s peak fit to determine the organic oxygen content (Rouxhet & Genet, 2011).

$$\frac{O_{org}}{C} = \frac{(C_{286.3} + C_{288} + C_{289} - N)}{C}$$

Equation 8 Organic oxygen estimated by Rouxhet (Rouxhet & Genet, 2011).

While this equation works for simple compounds, they are likely to fail in more complex systems by neglecting the effect of multiple heteroatom bonds to the same carbon, as seen in carboxylic acid groups.

Rather, knowledge of the substrate was used to determine the oxygen contribution to signal. An example of this is the use of the silicon 2p peak where the peak can be separated into element and oxide components, which can then be used to estimate the oxygen composition of the substrate (Van der Marel et al., 2004).

2.5.2 Atomic Force Microscopy

Scanning tunnelling microscopy (STM) was developed to measure ultra-small forces on particles as small as atoms into atomic force microscopy (AFM). AFM measures the motion of a cantilever beam with an ultra-small mass to image the surface. The spring of the AFM tip is soft enough to measure the maximum deflection of a force, and stiff enough to minimise sensitivity to vibrational noise(Binnig, Quate, & Gerber, 1986).

AFM has become of more interest to bacterial systems (Robichon, Girard, Cenatiempo, & Cavellier, 1999) to image the effects of biological compounds (Rouxhet & Genet, 2011))and of microbes (Y. F. Dufrene, 2014).

Unlike other analytical techniques, AFM has the advantage that the surface does not have to be under vacuum. This makes it a more desirable analytical method for biological systems. AFM can be used to detect samples in liquid (Moreno-Herrero, Colchero, Gomez-Herrero, & Baro, 2004), making it desirable method to measure a biofilm *in situ*. However, the main difficulty is the mobility of the bacteria (Robichon et al., 1999).

Typically, AFM has been used in a way such that the tip is in contact with the surface, however in some cases, such as biofilms, this can cause problems. For biofilms contact can disrupt the surface, potentially changing the structure and can also end up with bacteria on the tip, which changes the force measurements (Moreno-Herrero, Colchero, Gómez-Herrero, & Baró, 2004). To overcome this a non-contact mode can be used to prevent the tip contacting the biofilm, or alternatively a tapping mode (semi-contact mode) can be used to ensure the contact with the sample is minimal and minimises the damage. Semi-contact mode is better than non-contact mode as it is easier to determine the presence of bacteria and any change in topography.

AFM can also be used in the observation of various properties of biofilms. Qin (Qin et al., 2009) shows how biofilm formation starts with a single bacterium that forms its own colony, then associates it with other colonies, as well as identifying their compounds work against *S. epidermidis* initial attachment rather than established films. Missirlis (Missirlis & Katsikogianni, 2007) discusses the use of AFM for measuring interaction forces at microbial surfaces.

AFM can also be used to determine bacteria morphology and can obtain detailed information on bacterial features such as vesicle size. As a result it is possible to be able to identify the bacteria type, which is an advantage in deciding treatment of infections. (Germano, Bramanti, Arcuri, Cecchetti, & Cicciu, 2013). As an extension from this, it is also possible to detect live processes within the cell (Wright, Shah, Powell, & Armstrong, 2010).

AFM can be used in more technical ways by altering the probe using different features of the material. An example of this is to change the chemical properties of the tip and observe the change in force with materials (Dufrene, 2015). Alternatively, biologically active compounds can be used to coat the tip, from which the force between substrate and receptor can be measured (Dufrêne, 2015).

Moving on from chemical modifications, another development with altered AFM tips is to attach single microorganisms, including bacteria, leading to single cell force microscopy

(SCFM). There are a number of ways the tip can be functionalised to immobilise the microorganism onto the tip (Wright et al., 2010). The immobilisation method of bacteria needs to be done in such a way to ensure cell viability (Wright et al., 2010), which will be discussed later on. After each experiment, the tip needs to be examined to ensure the bacteria is still present, and not been damaged in previous experiments.

The advantage of using single cell force microscopy is to analyse directly the effects of attachment of a microbe to a surface or biofilm (Harimawan, Zhong, Lim, & Ting, 2013). This is done by bringing the functionalised tip into contact with the surface, and by analysing the force-distance curves the adhesive forces can be measured. From this it is possible to identify the adhesive (Ivanov et al., 2012) or anti adhesive properties (Friedrichs, Zieris, Prokoph, & Werner, 2012) of a surface or treatment. However, there are limitations through the effects of immobilisation and contact time between the modified probe and surface.

As mentioned previously, AFM has the capability to analyse live cells. One of the main issues with live cell AFM analysis is the potential deformation or delocalization of bacterial cells (Muller & Ziegler, 2013) as well as the mobility and turgid shape of the sample (Wright et al., 2010). To overcome this there are a range of immobilisation methods available, including chemical fixation, surface functionalization and porous membranes. However, one of the problems with immobilising is the change in properties of the sample (Muller & Ziegler, 2013) which influences the measured interaction force (Vadillo-Rodriguez et al., 2004). One of the main issues with fixing bacteria is the potential effect on cell viability (Wright et al., 2010).

One of the main methods used is to dry the sample on the surface to be analysed. This leads to the question of change in properties on drying. It has been found that if the samples are grown in humid air, then dried, there is little change compared to those dried form a liquid media (Auerbach, Sorensen, H.G., & Holden, 2000).

Not all methods affect cell viability, as there are cases of a few methods that have been used to immobilise cells on AFM tips (Vadillo-Rodriguez et al., 2004).

Force-distance curve measurements can be carried out on bacteria, to determine the forces between the bacteria and the tip. From this it is possible to determine the adhesive nature of the top layer of a bacteria. Another use of force distance curves on bacteria is to determine the spring constant of the bacteria under certain conditions, which is relevant for the SCFM experiments and modelling the forces of bacteria on a range of surfaces. It is important to

note these methods are not independent of each other, but rather complement each other, so when possible should be done under similar conditions.

Chapter 3 Experimental Methods

This chapter describes the source and preparation of the substrates and bacterial strains, the incubation and growth of the bacterial films, and the application of the analysis methods of Atomic Force Microscopy (AFM) and X-ray Photoelectron Spectroscopy (XPS).

3.1 Substrate materials

Silicon (111) wafers were sourced from Agar Scientific Ltd (catalogue number G3336-3) and were used as-received with no further preparation. Glass microscope slides and cover slips were sourced from VWR Ltd. Freshly cleaved ruby muscovite mica sheets were sourced form Agar Scientific Ltd (catalogue number G250-3) and used as-received with no further preparation.

Titanium coatings of approximately 15 nm thickness were sputter-coated onto Si (111) substrates using an automated sputter coat unit with quartz crystal microbalance film thickness monitor (Agar Scientific Ltd B7341 with B7348 thickness monitor). Films were sputter-coated onto silicon (111) to provide titanium substrates of a well-characterised, smooth and flat form.

Silver coatings of 50 nm thickness were made on Si (111) substrates pre-coated with approximately 15 nm of titanium. The pre-coating was found necessary to ensure good adhesion of the silver layer.

In all the film growth experiments described here, all substrates were autoclaved at 121°C for 15 minutes before incubating any bacterial films, and subsequently handled in a sterile manner according to standard microbiological protocols.

3.2 Bacteria strains

Two strains of *S. epidermidis* was used in this work. *ATCC35984*, a biofilm former strain, was obtained from stock from the University of Chester Department of Biological Sciences. A second strain *NCTC13360* (also known as *ATCC12228* (Hu et al., 2011)) and was sourced from Public Health England(England, 2016) .

In both cases give maximum cell densities of 0.9 for *NCTC13360* ($3x10^6$) Colony Forming Units (CFU) and 1.2 for the *ATCC35984* (1.2x107 CFU).

3.3 Incubated samples

Overnight cultures of the bacterial strains in tryptic soy broth (TSB, Sigma- Aldrich) were diluted to an initial optical density at 600nm (OD600) of 0.01. The optical density was chosen based on literature. 4 mL of the inoculated media was added to polystyrene petri dishes (Falcon, 35 mm x 10 mm) containing the silicon, mica, glass, silver-coated silicon or titanium-coated silicon substrate samples (separate petri dishes for each sample) and incubated at 37°C as required for the experiment concerned. Control samples with no *S. epidermidis* were similarly treated. The composition of the TSB growth medium is shown in Table 3.1.

Component	Concentration (g/L)
Casein peptone (pancreatic)	17
Dipotassium hydrogen phosphate	2.5
Glucose	2.5
Sodium Chloride	5
Soya Peptone (papain digest.)	3

Table 3.1 Composition of tryptic soy broth TSB.

Samples for analysis by Atomic Force Microscopy (AFM) were rinsed and kept in ¼ strength Ringer's solution before analysis. Samples were kept in buffer for a minimal amount of time before analysis.

Samples for analysis by X-ray Photoelectron Spectroscopy (XPS) were rinsed in flowing distilled water to remove non-adherent bacteria, air-dried vertically for 2 minutes and immediately inserted into the ultra-high vacuum air lock of the XPS instrument.

3.4 Bacterial pellet and lawn

To produce the bacterial pellets, 1 mL of an overnight culture in tryptic soy broth (TSB, Sigma-Aldrich) was centrifuged for 10 minutes at 9630 *g*. The resulting pellet was rinsed twice with sterile distilled water and centrifuged again. It was then resuspended in sterile water (2 µl) and dried onto a silicon wafer to produce a uniform surface representative of the bacteria in its original i.e. non-biofilm state suitable for analysis.

Lawn samples were prepared by Alice Gillet using the following method: -

S. epidermidis (*ATCC35984* and *NCTC13360*) were grown in tryptic soya broth overnight at 37^{o}C. Cells were harvested by centrifugation, washed twice and suspended in NaCl saline (0.85% w/v). The bacterial substrata for XPS analysis were prepared by collecting bacterial cells on a cellulose triacetate filter (pore diameter 0.45 µm; Sartorius) to a density of

approximately 108 cells per mm^2. Bacterial lawns were left to air dry for 30 minutes, until a plateau lawn was achieved.

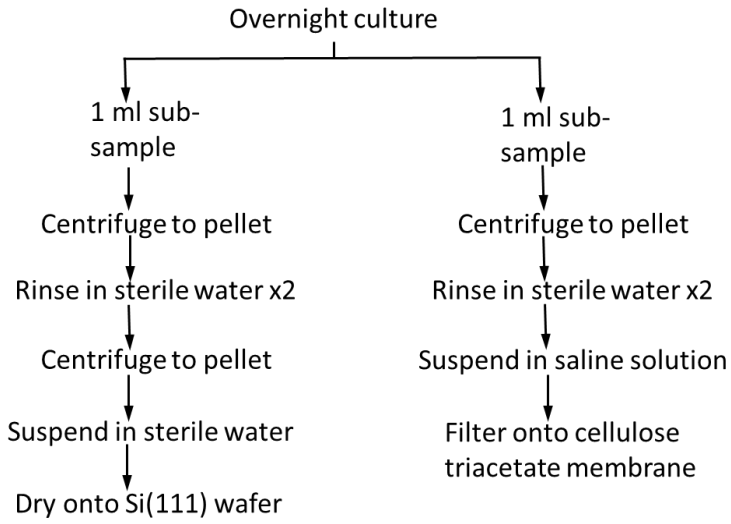

Figure 3.1 Schematic flow diagram showing the processes used in the preparation of bacterial pellet and lawn samples.

3.5 Atomic Force Microscopy

Atomic force microscopy (AFM) has become established as a well-known method for producing very high-resolution images of surface structures and topography (Dufrene, 2001).

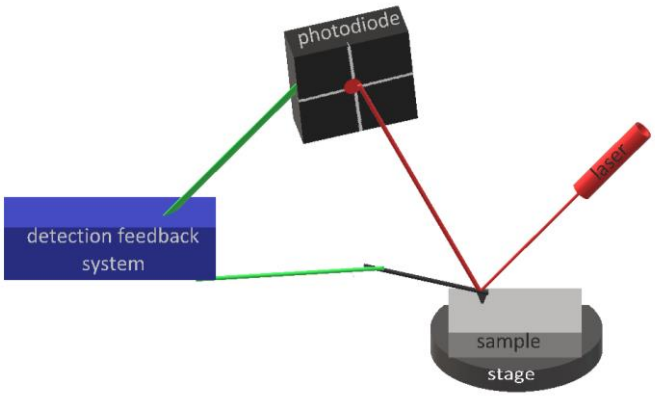

Figure 3.2 Schematic of AFM detection method.

In summary, the technique relies of scanning a very fine tip across the specimen surface while monitoring the vertical displacement of the tip through a laser reflection and photodiode system. Practical realisations involve a feedback system to maintain sample tip distance or some other characteristic of the tip/sample interaction. This is shown schematically in Figure 3.2, with an SEM image of the AFM tip shown in Figure 3.3.

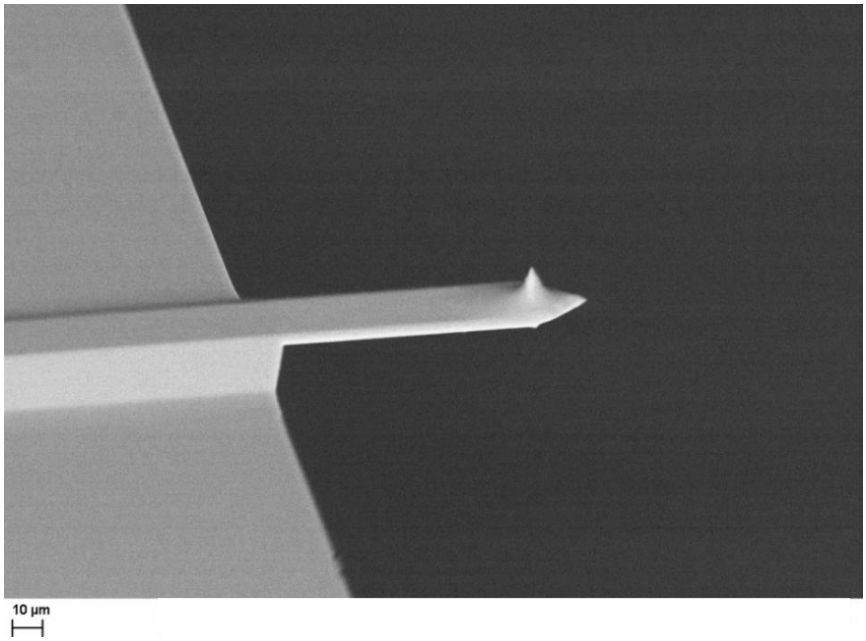

Figure 3.3 SEM image of AFM cantilever NT-MDT NSG10.

In the work described here, a NT-MDT Solver Next Atomic Force Microscope (AFM) with NT-MDT NSG10 silicon nitride tips in Semi-contact mode and NT-MDT Nova PX software was used to generate AFM images and force-distance curves. The semi-contact mode was chosen over contact mode as the oscillating tip used in this mode is less likely to cause damage to the soft materials examined in this study.

Attempts were made to investigate the use of liquid-mode AFM to image the early stages of bacterial adhesion and biofilm growth on the substrates used. However, the movement of the cantilever was found to disrupt and damaged the bacteria, which were not in any way fixed to the substrates. Liquid mode was not pursued further.

Force distance curves were measured between -100 – 500 nm gand were analysed through the Nova Px image analysis software. Spring constants for the cantilevers used were individually calculated through the software corrections. Note that the software does not directly measure the force in nN but rather the change in photodiode current, which is related to the degree of bending of the cantilever with tip - sample distance.

Determination of the spring constant of the cantilever in the Nova Px software is calculated by the Sader method (equation 1,(Gibson, Smith, & Roberts, 2005)) and confirmed by thermal noise calibration(Butt & Jaschke, 1995). This calibration was needed to give a true measure of force applied by the cantilever to the sample.

$$k_n = 0.1906 L\omega^2 \rho_i Q_f \Gamma_i (2\pi v)^2 \quad (1)$$

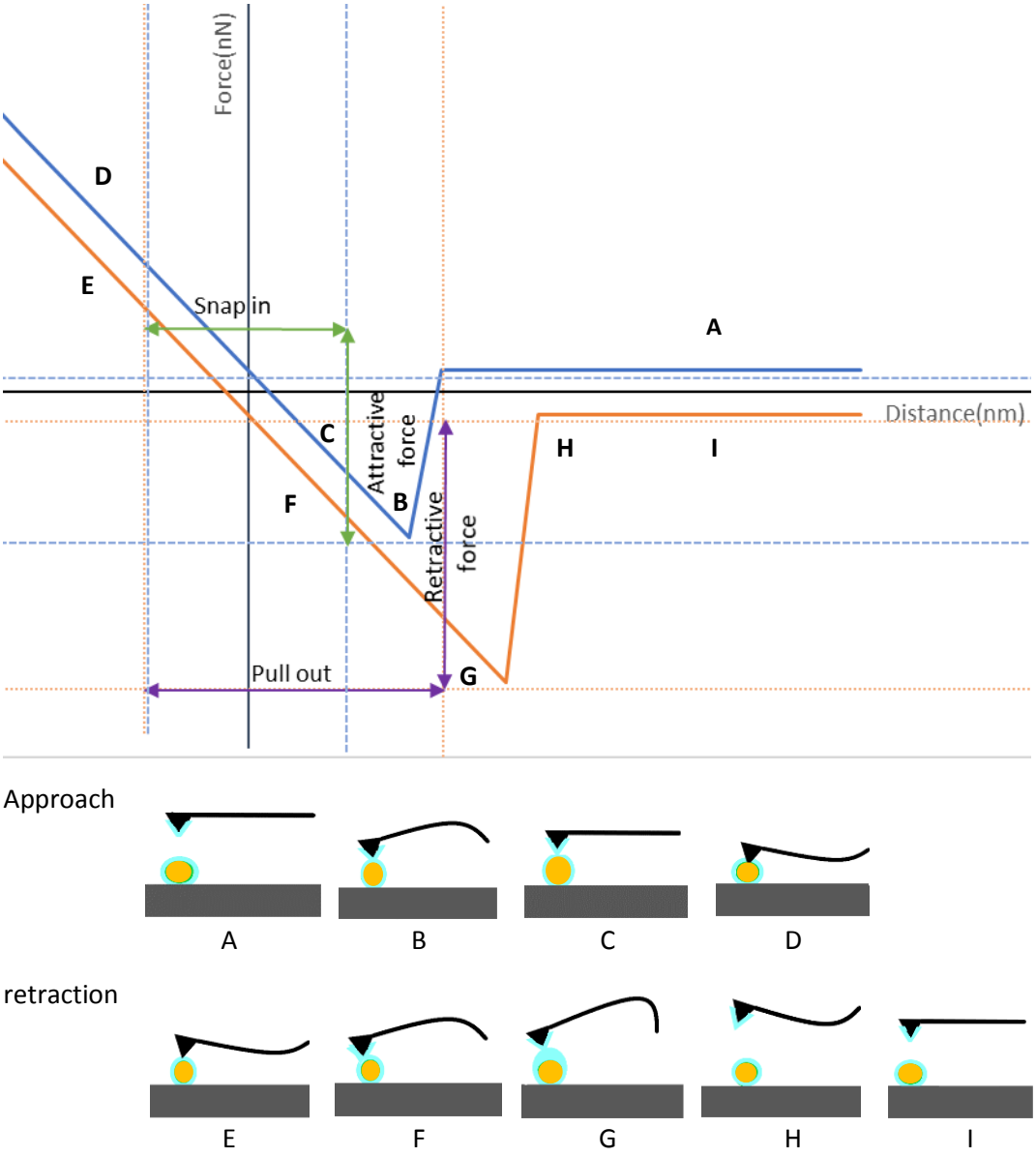

Figure 3.4 Cantilever deflection in response to changes in force distance curve where blue is the cantilever on approach, and orange is the cantilever on retraction. Letters on the curve refer to specific interactions in images below. Blue refers to force interactions and are not part of the substrate, tip or bacteria.

The change in the cantilever deflection as a measure of force applied at a single point on the specimen was used to produce force-distance (F-D) curves. The expected variation of force with distance for an idealised surface is shown in Figure 3.4. In this scheme, the tip is slowly moved closer to the surface (A) until there is sufficient attractive force between the surface and tip for there to be contact (B). The tip then continues to be moved towards the surface (C) and experiences a repulsive force (D). The tip is then retracted from the surface (E). After passing the point of initial contact (F), the tip is then affected by attraction to the surface (G) until the tip overcomes the adhesive force (H) and leaves the specimen surface to follow the line of zero force (I).

Analysis of force distance curves gives insight *to* various physical properties of the surface. Attractive forces are measured on approach (B) as contact between the tip and sample is made, as well as on retraction (G-H) as the bond between the tip and sample is broken. Retractive forces are higher than approach forces due to the difference in energy of bond formation compared to bond breaking. Indications of the types of adhesive bonding of the surface can be determined from the distance the tip travels on retraction between no net forces to maximum adhesion known as pull out distance. Snap in distance is a measure of resistive properties of the material and defined as the distance the tip travels from maximum adhesion to the point where resistive and attractive forces are equal. Pull out distance is a measure of adhesive properties of the material and is defined as the distance the tip travels on retraction between the point where attractive and repulsive forces are equal to the point of maximum attractive force.

3.6 X-ray Photoelectron Spectroscopy

3.6.1 Experimental

X-ray photoelectron spectroscopy (XPS) uses a focused x-ray source directed at the sample. This excites the electrons in the sample to a higher energy state, to the extent an electron is released through the photoelectric effect. This photoelectron emission can be detected and used to plot a spectrum based on the energy of photoelectrons released. XPS has become the standard technique of quantitative and chemically-specific surface analysis (Briggs & Grant, 2003).

X-ray photoelectron spectroscopy (XPS) analyses were performed using a bespoke ultra-high vacuum chamber fitted with Specs GmbH Phoibos 150 analyser, Focus 500 monochromator and F20 charge neutralizing gun. Base pressure of the UHV chamber was $< 3 \times 10^{-10}$ Torr. Where possible, spectra were acquired using the Al monochromatic source at 1486.6 eV. X-ray energy with an analysis area approximately 2mm diameter using the Specs GmbH FG20 low energy electron flood gun for charge neutralisation. In a minority of cases it was not possible to obtain satisfactory charge neutralisation with the monochromator source and therefore the Al twin anode source was used. The flood of low energy secondary electrons from the thin Al window over the end of the twin-anode source gives better charge neutralisation, higher intensity peaks than with the monochromator source, but broader lines photoelectron lines. Survey scans were measured from 1100 – 0 eV binding energy with a pass energy of 50 eV, and individual line scans were measured at 20 eV pass energy. The

angle between the X-ray beam and the analyser axis is 55o and therefore the angle of incidence (θ) is also 55° when the sample is horizontal, and emission is normal to the surface.

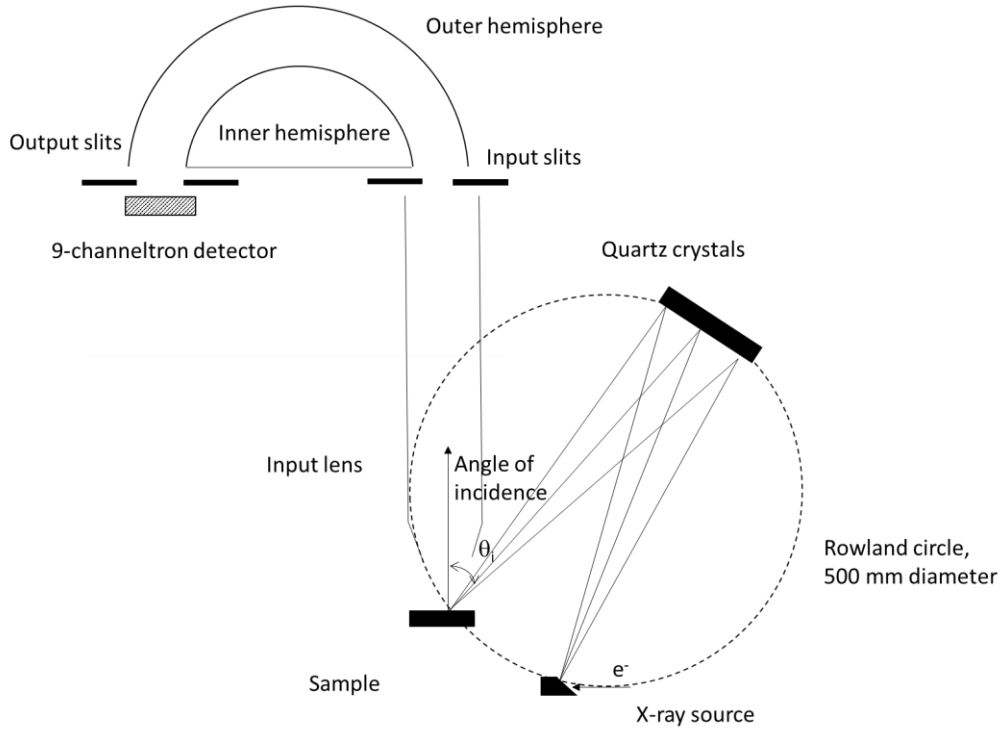

Figure 3.5 Schematic diagram of Thornton XPS instrument.

3.6.2 Data interpretation

All data was initially analysed through Casa XPS ("Casa XPS v2.3.17," 2015) for identification of photoelectron lines and quantitative analysis. All scans were charge corrected to the hydrocarbon component of the C 1s peak, which was set at 285.0 eV in accordance with standard practice for organic materials (Beamson & Briggs, 1992). Spectra were quantified after subtraction of Shirley backgrounds (Shirley, 1972) using relative sensitivity factors based on Scofield cross-sections (Scofield, 1976)corrected for the energy dependence of the effective electron attenuation length and of the analyser sensitivity. In this method, the relative sensitivity factor is normalised to carbon 1s = 1, and is given by:

$$RSF(element, line) = \frac{cross\ section\ (element,line)}{cross\ section\ (C\ 1s)}\left(\frac{kinetic\ energy\ (element,line)}{kinetic\ energy(C\ 1s)}\right)^{m+n} \quad (2)$$

Where *m* is the exponent in the energy dependence of the analyser sensitivity and *n* is the exponent in the energy dependence of the effective electron attenuation length. This approach gives good accuracy over a wide range of compounds of known composition and can be improved further by the use of an overlayer correction (Smith, 2005).In the work described here, the intensity exponent factor in CasaXPS was calibrated for individual instrument conditions using the F 1s: C 1s ratio for fresh, pure PTFE. A value of -0.52 was

found for aluminium monochromator spectra using the 7 mm diameter entrance slit, open exit slits, 50 eV pass energy, medium area lens mode and with the lens iris set to 30 mm diameter. In a small number of cases where a smaller analysis area was required, values were recalibrated accordingly.

Chemical state information was determined by curve-fitting high resolution photoelectron data to known reference standards using the facility available in CasaXPS(Fairley, 2016) and Oliveria et al.(C. Oliveira et al., 2011).

For organic materials, reference data for the C 1s and O 1s peaks were taken from Beamson and Briggs (1992 (Beamson & Briggs, 1992)).

Element	Signal	Example	Approximate electron energy (eV)
Carbon	C 1s	1 C-C	285.0
		2 C-O-C	286.5
		3 O-C=O	288
Nitrogen	N 1s	1 C-NH_2	400
		2 NO_3	402
Oxygen	O 1s	1 O-R	532.7 – 533.2
		2 O=R	531.7 – 532.3
Silicon	Si 2p	1 pure silicon	99.4
		2 silicon oxide	103.5
Titanium	Ti 2p	1 pure titanium	454.1
		2 TiO_2	458.5
Phosphorus	P 2p	1 phosphide	128.5
		2 phosphate	133
Silver	Ag 3d	1 pure silver	368.2
Sodium	Na 1s	NaCl	1071.1
Potassium	K 2s	KCl	292.9
Aluminium	Al 2p	Al metal	72.6
		Al-O	74.6
Sulphur	S 2p	Thiol R-SH	164
		Metal sulphate	169
Calcium	Ca 2p		347.3
Magnesium	Mg 2p		52

Table 3.2 XPS approximate binding energies values.

Separation of substrate and overlayer oxygen contributions to spectra

Oxygen was present in the bulk of the glass and mica substrates and as a thin layer in the surface oxide of the silicon substrates. Oxygen was also found associated with the silver and the titanium substrates. Oxygen was also expected to be present in the organic layers resulting from the surface treatments and bacterial growth on these substrates. It was therefore necessary to develop procedures to allow the percentage oxygen that relates to the substrate and that which relates to the organic overlayer on the surface to be determined.

To overcome the difficulties in determining the percentage oxygen, several approaches were used.

Estimations of organic oxygen content from C 1s peak fit was used to determine the organic oxygen for materials before autoclaving only, as the compounds on the surface are assumed to be simple, mostly hydrocarbon state.

$$O_{org(inital)} = O_{total-}\left(\frac{C_{286}}{C} + \frac{C_{288}}{C}\right) \quad (3)$$

For unknown organic layers, the organic layer may be more complex, therefore using the carbon peak fit data has the potential to miscalculate the organic oxygen content. Instead, knowledge of the surface composition was used to determine the oxygen content of the substrate alone, from which the remaining oxygen must relate to the organic overlayer.

$$O_{organic} = O_{total} - O_{substrate} \quad (4)$$

In the following equations, D is defined as defining peak and refers to a high percentage element that is independent of any subsequent overlayers. Samples referred to with the subscript initial relate to measurements done on samples before autoclaving, whereas those with the subscript substrate relate to after treatment or incubation samples discussed in later chapters.

For substrates with no oxide layer, such as glass, the ratio of oxygen and defining peak (D), in this case silicon, is constant, therefore the formula below was used. To determine the organic oxygen in the substrates initial state the organic oxygen content was determined from the carbon 1s peak, as the compounds on the surface are assumed to be simple, mostly hydrocarbon is state.

$$\frac{D_{initial}}{O_{initial}} = \frac{D_{substrate}}{O_{substrate}} \quad (5)$$

Where initial values refer to the sample before autoclaving and substrate refers to the sample being analysed.

In the case of silicon, 3 layers are involved namely the pure silicon, silicon oxide and organic layer. To determine the organic oxygen on silicon, the Si 2p peak was used to calculate the percentage of silicon oxide to pure silicon, from which the oxygen relating to the oxide layer can be determined. The oxide layer was estimated to be SiO_2.

$$Si\ 2p_{total} = Si_{oxide} + Si_{pure} \quad (6)$$

$$2Si_{oxide} = O_{substrate} \quad (7)$$

For samples which consist of multiple oxygen contributing layers, such as titanium coated silicon, the calculations are more complex. Knowledge of both layers are required to calculate oxygen contributions from the substrate, so that a similar calculation to a single oxygen contributing substrate layer can be used).

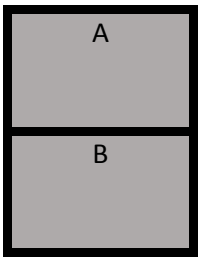

Figure 3.6 Multi-layered system for XPS layer calculations.

$$O_{substrate} = O_A + O_B \quad (8)$$

$$O_A = O_{total} - (\ O_B + (C_{286} + C_{288})_{inital\ A}) \quad (9)$$

Where A and B relate to the substrate layer as seen in diagram below, and where initial values refer to the sample before autoclaving and substrate refers to the sample being analysed. In the case of sputtercoated titanium, A is titanium layer and B is silicon.

$$\frac{D_{inital\ B}}{(O_{inital\ B} - O_{org\ inital\ B})} = \frac{D_{substrate\ B}}{O_{substrate\ B}} \quad (10)$$

$$\frac{D_{initial\ A}}{(O_{initial\ A} - O_{Org\ inital\ A} - O_{substrate\ B})} = \frac{D_{substrate\ A}}{O_{substrate\ A}} \quad (11)$$

Effect of attenuation

All samples, including as received samples, are assumed to consist of multiple layers. For example, a simple model consists of an inorganic and an organic overlayer. Differentiating between the two in this sample is relatively simple, with the exception of oxygen. To analyse multilayer samples, the effect of signal attenuation must be taken into account.

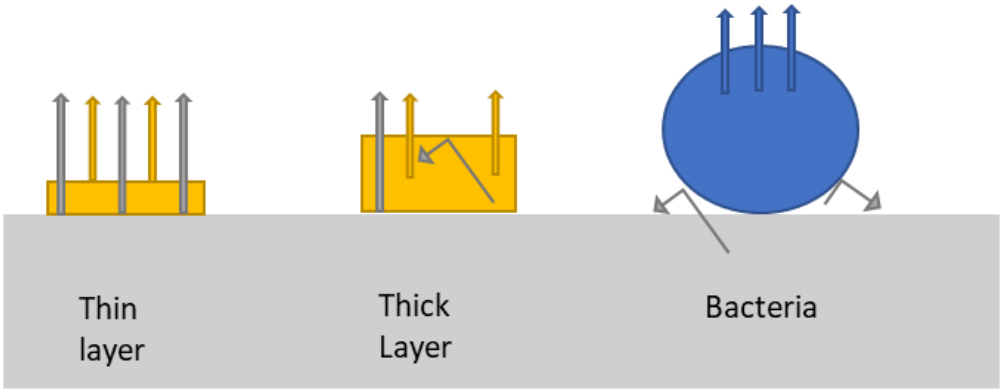

Figure 3.7 Effects of attenuation on signal on different layer systems.

Signal attenuation occurs when the overlayer prevents the photoelectrons from the lower layer passing through and being detected. Figure 3.7 shows how different layers affect the signal detection. For a thin layer, the signal from the lower layer can pass through and be detected. As the layer becomes thicker, the photoelectrons from the lower layer become harder to detect, until only the overlayer is detected, which is about 10nm thick overlayer.

Signal attenuation considerations also apply to bacterial systems. The bacteria used in this study was about 500nm, considerably thicker than that being detected by XPS. If the surface is fully bacterial, the signal from the substrate will not be detected. This is the basis of the calculation of coverage in bacterial coverage, where the change in substrate defining peak (Si 2p, Ti 2p or Ag 3d) is an estimation of bacterial coverage.

$$\frac{Si\ 2p_{incubated}}{Si\ 2p_{initial}} = Bacterial\ coverage$$

Once bacterial coverage can be determined, the composition of the organic layer in terms of bacteria and other organic compounds can be determined and calculations as to if the layer covers the bacteria or uncovered substrate can be estimated.

Layer Thickness calculations

Using information known about the sample, for example, the elemental composition of a layer, the thicknesses of overlayers can be calculated by considering the attenuation of the photoelectron signals due to electron transport (Tanuma, 2003). To a good approximation, signals are exponentially attenuated by a thin overlayer according to

$$\frac{I}{I^o} = \left[1 - \exp\left(\frac{-d}{L\,cos\theta}\right)\right] \quad (12)$$

Where:

I is the signal measured from the overlayer

I_o is the signal that would be expected to be measured from a 100% pure sample of the overlayer material

d is the thickness of the overlayer

L is the effective electron attenuation length of the photoelectrons from the overlayer element in the overlayer

Θ is the angle of photoelectron emission relative to the surface normal

For the signal of C 1s passing through a hydrocarbon layer where θ =0 the equation can be written as

$$\frac{I_c}{I_c^o} = [1 - \exp\left(\frac{-d_2}{L_{C\,1S}^{HC}}\right)] \quad (13)$$

The depth of each layer can be determined by the effective attenuation length and the ratio of the signal intensity between that measured and pure compound being equivalent to the % atomic concentration, as calculated through the XPS analysis through Casa XPS.

The effective attenuation length is the path electrons takes once it has been excited, and can be calculated if the density of the sample and concentration of each element in a given layer, using NIST standard reference database 82 (Powell & Jablonski, 2011). XPS data can be used not only to determine the elemental composition of the surface but also the thickness of the organic layer deposited on the surface from atmospheric contamination.

With more layers the calculation becomes more complex as the effect of each layer on the observed signal must be considered. The example below shows the calculation used for silicon, which includes the calculation of the thickness of silicon oxide layer also. Within the NIST SRD82 software, the Gries method was used (Gries, 1996),as this avoids arbitrary assumptions of band-gap parameters and gives a consistent approach to the complex nature of the organic layer.

Within these calculations the organic layer was determined by XPS survey spectrum with the oxygen being calculated as described above. The hydrogen content was estimated to be on average 1.5 times that of carbon content.

$$\frac{I_c}{I_c^o} = \left[1 - \exp\left(\frac{-d_1}{L_{O\ 1S}^{SiO2}}\right)\right] \tag{14}$$

$$\frac{I_o}{I_o^o} = Xox\left[1 - \exp\left(\frac{-d_1}{L_{O\ 1S}^{SiO2}}\right)\right]\left[\exp\left(\frac{-d_2}{L_{O\ 1S}^{HC}}\right)\right] \tag{15}$$

Where

	effective attenuation length of
$L_{O\ 1S}^{SiO2}$	O 1s signal passing through the silicon oxide layer
$L_{O\ 1S}^{HC}$	O 1s signal passing through the hydrocarbon layer
$L_{C\ 1S}^{HC}$	C 1s signal passing through hydrocarbon layer

Where $L_{C\ 1S}^{HC}$ corresponds to the effective attenuation length of the sample corresponding to the layer it is passing through (HC, hydrocarbon) and the signal attenuated (C 1s peak). $\frac{I_o}{I_o^o}$ refers to the overall signal measured from the data for the relevant element. Depths calculated in this case are d_1 is the depth of the oxide layer and d_2 is the thickness of the hydrocarbon layer. From knowledge of the effective attenuation length and the NIST standard reference database 82, the thickness of the relevant layer can be calculated. These values were calculated for each relevant layer to be used to calculate the depth of each layer, which can be seen in Table 3.3.

Element signal	Electron energy (eV)	Kinetic energy (eV)	Symmetry
C 1s	284.4	1202	2
O 1s	533.4	953.4	2
Ti 2p	454.2	1032.9	1.41

Table 3.3 Values inserted into the NIST 82 database for signal.

Sample	Layer calculated	Effective EAL
Silicon as received	$L_{C\ 1S}^{HC}$	5.086
	$L_{O\ 1S}^{SiO2}$	2.338
	$L_{O\ 1S}^{HC}$	4.211
Glass as received	$L_{C\ 1S}^{HC}$	4.713
Mica as received	$L_{C\ 1S}^{HC}$	4.520
Titanium as produced	$L_{C\ 1S}^{HC}$	5.408
	$L_{Ti\ 2p}^{Ti02}$	1.831
	$L_{Ti\ 2p}^{HC}$	4.768
Silver as produced	$L_{C\ 1S}^{HC}$	4.708

Table 3.4 effective attenuation length of as acquired samples.

Sample	Layer calculated	effective EAL
Silicon autoclaved	$L_{C\ 1S}^{HC}$	4.577
	$L_{O\ 1S}^{SiO2}$	2.338
	$L_{O\ 1S}^{HC}$	3.786
Glass autoclaved	$L_{C\ 1S}^{HC}$	4.522
Mica autoclaved	$L_{C\ 1S}^{HC}$	4.520
Titanium autoclaved	$L_{C\ 1S}^{HC}$	4.994
	$L_{Ti\ 2p}^{Ti02}$	1.831
	$L_{Ti\ 2p}^{HC}$	4.402
Silver autoclaved	$L_{C\ 1S}^{HC}$	4.519

Table 3.5 effective attenuation length of autoclaved materials.

Sample	Layer calculated	effective EAL
TSB incubated silicon 24h	$L_{C\ 1S}^{HC}$	2.439
	$L_{O\ 1S}^{SiO2}$	2.338
	$L_{O\ 1S}^{HC}$	2.016
TSB incubated glass 24h	$L_{C\ 1S}^{HC}$	2.354
TSB incubated mica 24h	$L_{C\ 1S}^{HC}$	2.47
TSB incubated titanium 24h	$L_{C\ 1S}^{HC}$	2.603
	$L_{Ti\ 2p}^{Ti02}$	1.831
	$L_{Ti\ 2p}^{HC}$	2.290
TSB incubated silver24h	$L_{C\ 1S}^{HC}$	2.423
TSB incubated silicon 1h	$L_{C\ 1S}^{HC}$	2.482
	$L_{O\ 1S}^{SiO2}$	2.338
	$L_{O\ 1S}^{HC}$	2.051
TSB incubated silicon 2h	$L_{C\ 1S}^{HC}$	2.608
	$L_{O\ 1S}^{SiO2}$	2.338
	$L_{O\ 1S}^{HC}$	2.153
TSB incubated silicon 3h	$L_{C\ 1S}^{HC}$	2.697
	$L_{O\ 1S}^{SiO2}$	2.338
	$L_{O\ 1S}^{HC}$	2.226
TSB incubated silicon 5h	$L_{C\ 1S}^{HC}$	2.631
	$L_{O\ 1S}^{SiO2}$	2.338
	$L_{O\ 1S}^{HC}$	2.172
TSB incubated silicon 6h	$L_{C\ 1S}^{HC}$	2.595
	$L_{O\ 1S}^{SiO2}$	2.338
	$L_{O\ 1S}^{HC}$	2.141
TSB incubated silicon 8h	$L_{C\ 1S}^{HC}$	2.762
	$L_{O\ 1S}^{SiO2}$	2.338
	$L_{O\ 1S}^{HC}$	2.264
TSB incubated silicon 9h	$L_{C\ 1S}^{HC}$	2.551
	$L_{O\ 1S}^{SiO2}$	2.338
	$L_{O\ 1S}^{HC}$	2.107

Table 3.6 effective attenuation lengths of TSB incubated samples.

Separate samples were used for AFM and for XPS analysis. In one case, the effect of the XPS system vacuum and X-ray exposure was investigated by analysing the sample by AFM before and after the XPS analysis.

3.6.3 Biological models

Within the literature there are a few models used to determine the ratio of biological compounds on the surface from XPS data, discussed further in Chapter 2. The application of the model proposed by Rouxhet is used to estimate the protein and sugar composition on

the surface (equation 1-3) using the measured XPS data of incubated samples and organic oxygen calculations discussed above. The formula was modified to include the effect of phosphorus on oxygen content, as well as estimating the biological composition as a percentage of the entire overlayer.

$$\frac{N}{C} = 0.279\left(\frac{Pr}{100}\right) \tag{16}$$

$$\frac{(O-4P)}{C} = 0.325\left(\frac{Pr}{100}\right) + 0.833\left(\frac{Ps}{100}\right) \tag{17}$$

$$\frac{C}{C} = \left(\frac{Pr}{100}\right) + \left(\frac{Ps}{100}\right) + \left(\frac{Hc}{100}\right) = 1 \tag{18}$$

Where

Pr	Proteins
Ps	Polysaccharide
Hc	Hydrocarbon

These calculations offer only an estimate and the limitations of any biological compound model is discussed in Chapter 2.

3.7 Scanning Force Microscopy

Scanning force microscopy (SEM) images were produced using a Zeiss 1455VP SEM operating at 20 kV with beam currents typically 10 – 30 pA in secondary or backscattered electron detection modes. Images of bacterial samples were acquired using uncoated samples, with backscattered electron detection.

3.8 Surface energy

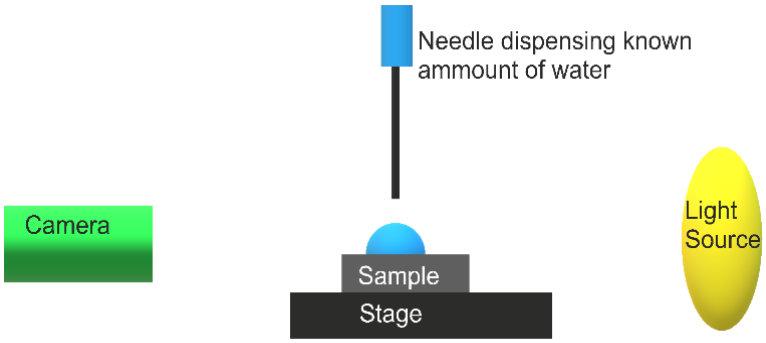

Figure 3.8 Measurement of contact angles (left) and contact angle measurement (right).

Surface energy was measured using Dataphysics OCA Contact Angle System with Dataphysics XYZ SCA 202 v4.5.11 software. A 0.01ml drop of water was dropped on the substrate and the captured on camera. From this the angle formed between the liquid-surface interface and air-liquid interface (contact angle) can be measured and applied to contact angle

models(Zenkiewicz, 2007). The angle formed between the surface and liquid can also indicate the hydrophobic nature of a material.

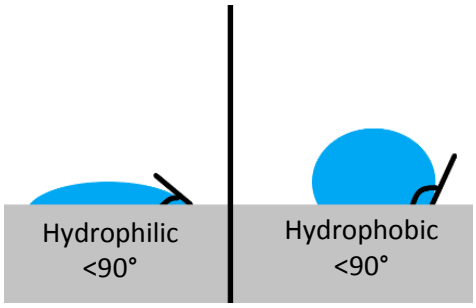

Figure 3.9 Contact angle measurement and using contact angle to determine hydrophobicit

Knowledge of the surface energy of a known liquid and the contact angle it forms on a solid surface can be used to model the surface energy of the surface. Several models for calculating the surface energy exists, however for this work the Neumann's equation of state was chosen(Neumann, Good, Hope, & Sejpal, 1974).

$$Cos\theta = 2\sqrt{\frac{\sigma^s}{\sigma^l}}e^{-B(\sigma_l-\sigma_s)^2} - 1 \qquad (19)$$

Where B=0.0001247

σ^s is the surface free energy of the solid

σ_l is the surface free energy of the liquid

The Neumann equation of state calculates the surface energy using only one liquid, and for the interest of this work, only water was used to determine the surface energy of the material as an identification of hydrophobicity of the material.

Chapter 4 Characterisation of Substrate Materials

Substrate materials were characterised for surface composition by XPS, surface topography by AFM and surface energy using the sessile drop technique as described in Chapter 3. This set of data give reference values to be used in the interpretation of subsequent experiments on adsorption of the TSB growth medium and on biofilm formation.

The biofilm growth experiments were carried out on autoclaved substrates to ensure sterility and minimise the potential for contamination. Therefore, the substrates were characterised as-received and after autoclaving at 121^{o}C for 15 minutes. Autoclaving was chosen instead of other sterilisation techniques to prevent chemical contamination to the samples.

4.1 Chemical characterisation

XPS data was used to characterise the surface composition and chemical state of the substrates. The methods described in Chapter 3, were used to determine the layer thicknesses of the hydrocarbon, silicon dioxide and titanium dioxide as appropriate. In the following sections, the results of XPS analysis of the substrate samples are presented as-received and after autoclaving, separated by sample material.

4.1.1 Silicon

The silicon (111) wafer sample was analysed as-received and after autoclaving. The as-received survey scan and C 1s spectra are shown in Figure 4.1, and the results of quantification of the data are shown in Table 4.1.

	As acquired	Autoclaved
C 1s	9.9	21.1
O 1s	23.2	22.6
O_{org}	5.6	3.0
Si 2p	66.9	56.3
C285	68.7	87.9
C286.5	29.0	8.8
C288	2.3	3.3
Thickness hydrocarbon	0.54nm	1.08nm
Thickness SiO_2	1.41nm	1.41nm

Table 4.1 Surface composition of silicon (111) before and after autoclaving.

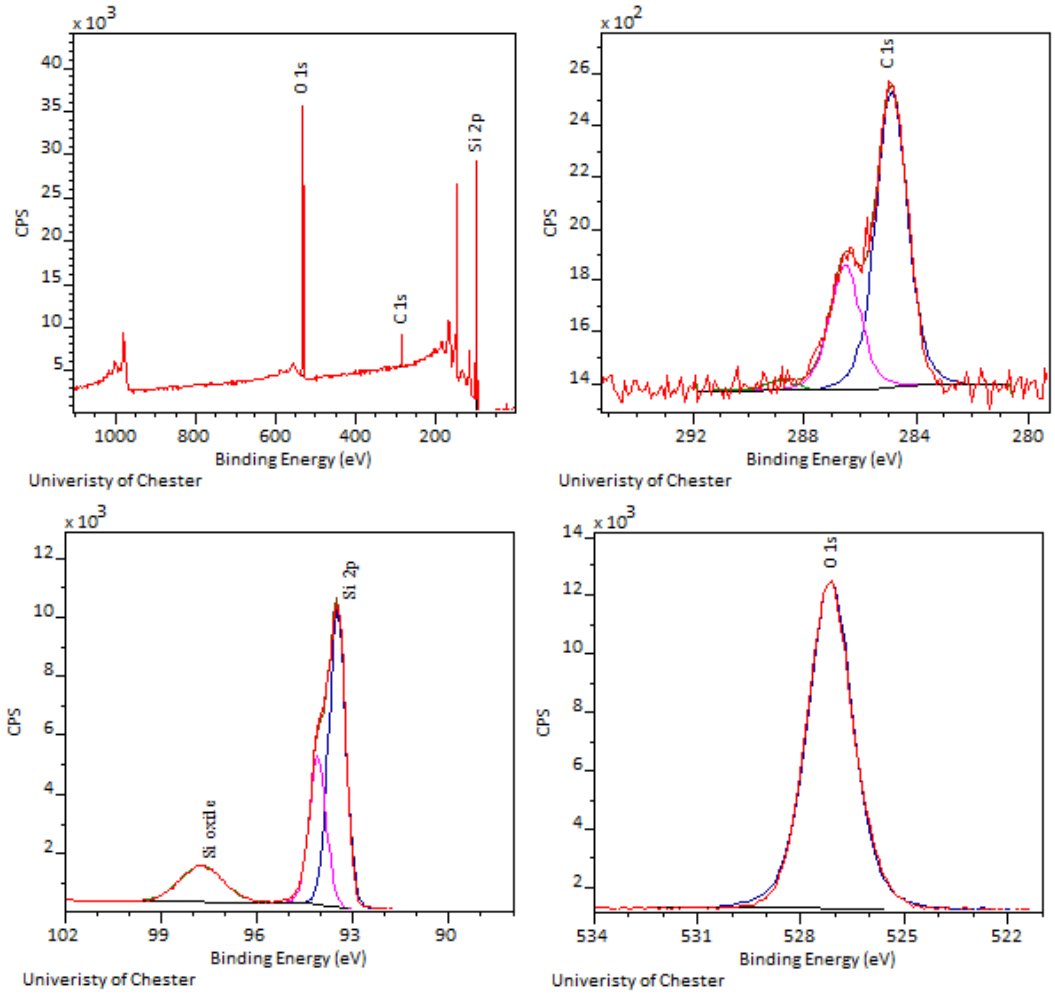

Figure 4.1 XPS survey spectrum, C 1s peak fit, Si 2p and O 1s of silicon as received.

The percentage oxide layer of silicon sample is calculated from the Si2p peak fit. Along with the estimation of the oxide composition the inorganic oxygen for all silicon samples are determined, therefore the organic oxygen is known. This is summarised by equations 4, 6 and 7 in Chapter 3.

The sample showed strong Si 2p and 2s peaks, as expected, with strong plasmon loss structures on their higher binding energy sides. The strong O 1s peak was attributed to the presence of a thin surface layer of SiO_2, as expected from the chemically-shifted oxide components visible in the Si 2p and Si 2s peaks. The relatively low carbon intensity was attributed to the presence of adventitious hydrocarbon contamination on the surface as a result of exposure to the laboratory environment. Autoclaving resulted in an increase in the carbon intensity and corresponding reductions in the O 1s and Si 2p signals, due the build-up of further surface hydrocarbon during autoclaving. The carbon 1s peak fit showed an increase in the component at 285eV, relating to the increase of hydrocarbons at the surface, with a decrease in peaks at 286.5eV and 288eV.

From layer the thickness calculations, the organic layer thickness almost doubles in thickness, as the silicon oxide layer remains almost constant. As there is a thicker layer of atmospheric contamination at the surface, it is assumed the layer of silicon oxide decreases, however the similarities in values suggest the layer of silicon dioxide increases, probably as a result of thermal oxidation of the silicon wafer.

4.1.2 Glass

At the start of this work, glass microscope slide coverslips were considered for use as substrates. However, as-received coverslips showed the presence of small particles in AFM and SEM images. XPS data showed the surfaces to be typical overall of borosilicate glass, suggesting that the particles are fragments of glass. It was considered likely that attempts to remove these particles by physical or chemical cleaning procedures would result in the presence of potential contaminants which may affect the results of subsequent adsorption and growth experiments. Therefore, glass microscope slide coverslips were not considered further as suitable substrates for these experiments.

Glass microscope slides were investigated as alternatives to the coverslips. These did not show the surface particle contamination visible on the coverslips and were used as model glass substrates for the remainder of this work.

The data were quantified as described in Chapter 3 section 3.6 to give the surface composition shown in Table 4.2. The table also shows the composition as measured after autoclaving.

XPS spectra for the as received glass microscope slide are shown in Figure 4.2. The survey spectrum is shown in the left panel, and a higher resolution scan over the C 1s / K 2p / Mg KLL region is shown in the right hand panel.

The organic oxygen content was calculated for as received glass microscope slide surface from the carbon 1s peak using the method described in Chapter 3 in equations 3 to 5. The ratio of inorganic oxygen to silicon was then determined for the as-received sample. This was assumed to be representative of the glass, and then used to determine the proportion of organic oxygen on the autoclaved surface.

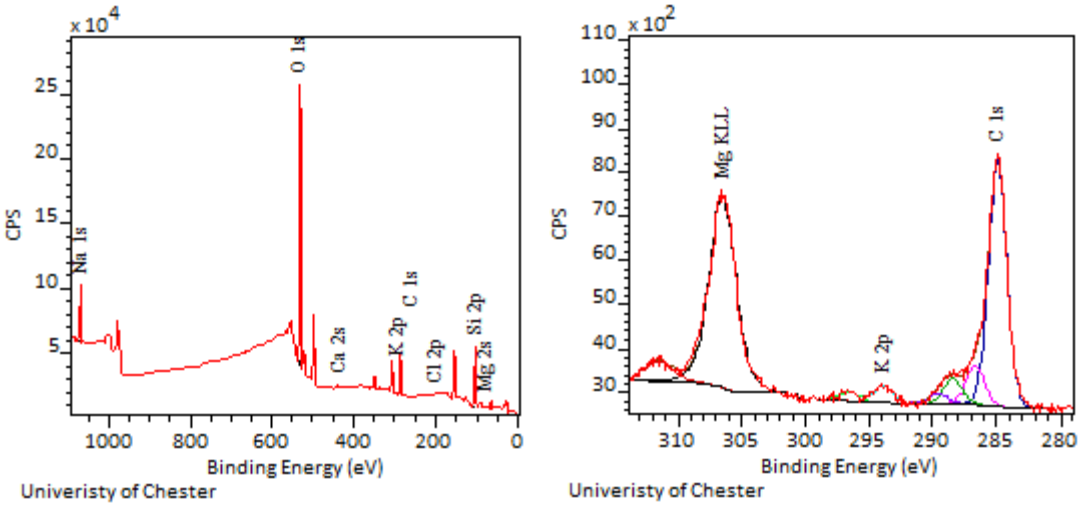

Figure 4.2 XPS spectra and C 1s peak fit from the representative glass microscope slide.

	As acquired	Autoclaved
C 1s	17.2	42.3
O 1s	48.1	32.9
O_{org}	4.0	4.1
N 1s	0.0	0.6
Si 2p	26.6	17.3
Na 1s	4.2	3.1
Ca 2s	0.6	0.8
Mg 2p	3.0	3.0
C285	76.9	76.2
C286.5	12.1	4.9
C288	8.0	5.5
C289	3.0	1.9
C283	0.0	11.5
Thickness hydrocarbon	0.88nm	2.49nm

Table 4.2 Surface composition of the representative glass microscope slide as-received and after autoclaving.

Overall, the XPS data indicated the microscope slide surface to be composed of a sodium/magnesium silicate glass with a small amount of potassium and calcium. The calcium content was determined from the Ca 2s peak rather than the strong Ca 2p peak as the 2p peak shows an overlap with a minor X-ray excited Mg KLL Auger peak. Similarly, the potassium content was estimated from the K 2s peak rather than the more intense K 2p doublet as the 2p peaks are close to the C 1s peak and intensities may be affected by the rising background of inelastically scattered electrons behind the carbon peak. Autoclaving the sample resulted in an increase in the surface carbon level and the appearance of a small

amount of nitrogen. This was accompanied by a reduction in the relative intensities of the other elements, to below the detection limit in the case of K, Ca and Mg.

4.1.3 Mica

The XPS survey spectrum and C1 s / K 2p spectral region as-received are shown in Figure 4.3. Both the C 1s and the K 2p peak show slight asymmetry in the form of broadening on the low binding energy side. Although this can be fitted using an additional low-intensity component as shown in Figure 4.3 for the C 1s peak, this is an artefact due to imperfect charge neutralisation on this highly non-conducting sample and should be ignored. In this case, the C 1s peak is essentially symmetric, after accounting for the charging effect, and is indicative of carbon in hydrocarbon bonds. The results of quantification of the XPS data acquired before and after autoclaving are shown in Table 4.3. The table also shows the data from Liu at al. (1998) (Liu & Brown, 1998) and the expected bulk composition calculated from its elemental composition.

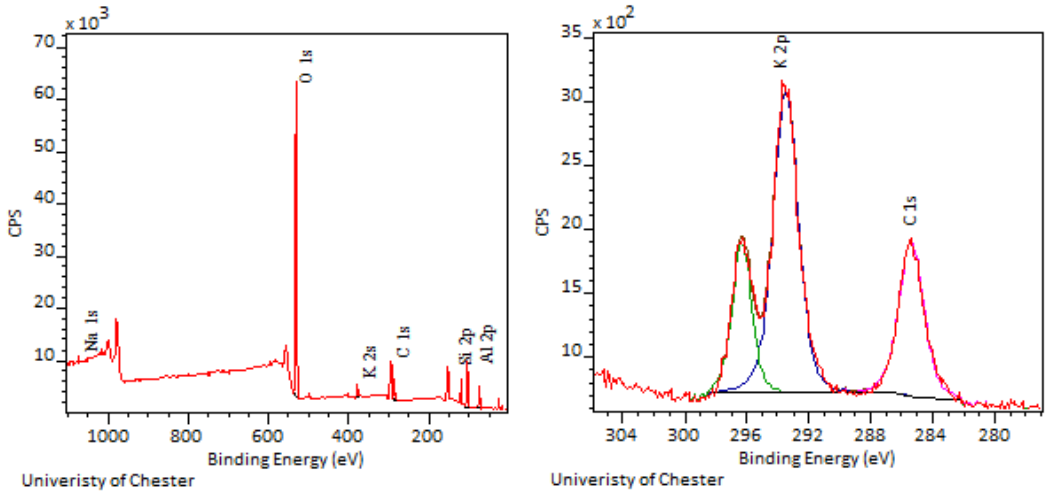

Figure 4.3: XPS survey spectrum and C1 s / K 2p spectral region from the as-received muscovite mica surface.

The as-received XPS spectrum showed relatively strong peaks due to oxygen, silicon and aluminium, in addition to weak peaks from sodium and potassium. Carbon was also detected and attributed to adventitious contamination from the laboratory environment.

Element	XPS data, as-received	Paper (Liu & Brown, 1998, 4h)	XPS data, autoclaved	Expected bulk composition (atom %, excluding H)
Potassium	4.0	2.3	3.7	5.3
Aluminium	17.0	20.9	13.3	15.8
Silicon	23.1	24.6	19.5	15.8
Fluorine	0		0.3	
Oxygen	47.6	44.1	44.3	63.2
O_{org}	0		0.7	
Carbon	7.9	8.1	18.5	
Hydrogen	N/A	N/A	N/A	
Sodium	0.3	-	0.4	
C285	100	-	89.1	
C286.5	0	-	7.4	
C288	0	-	3.7	
Thickness hydrocarbon	0.36nm	-	0.95nm	

Table 4.2 Surface composition of Muscovite mica before and after autoclaving and compared to results and expected bulk composition taken from (Liu & Brown, 1998).

In Table 4.2, the bulk composition is that for ruby muscovite mica which has the general formula $KAl_2Si_3O_{10}Al(OH)_2$ (Liu & Brown, 1998). The expected bulk composition shown in the Table 4.2 was obtained from this composition with the atom % values normalised to 100 % excluding hydrogen which is not detected by XPS. Compared to the ideal composition, the measured data showed a relatively lower level of K and relatively higher levels of Si and Al than expected. In addition, the proportion of aluminium to silicon was lower than the 1:1 ratio expected for the ideal material. These differences can be attributed to the relative depth of the various structural layers in the mica, and to the presence of the surface atmospheric hydrocarbon contamination. In the schematic structure of muscovite mica shown in Figure 4.4 (De Poel, Pintea, Drnec, Carla, & Felicic, 2014), it is clear that attenuation of the K signal by the Si/Al-containing sheets during photoemission could occur and result in a reduced relative K signal intensity as observed experimentally.

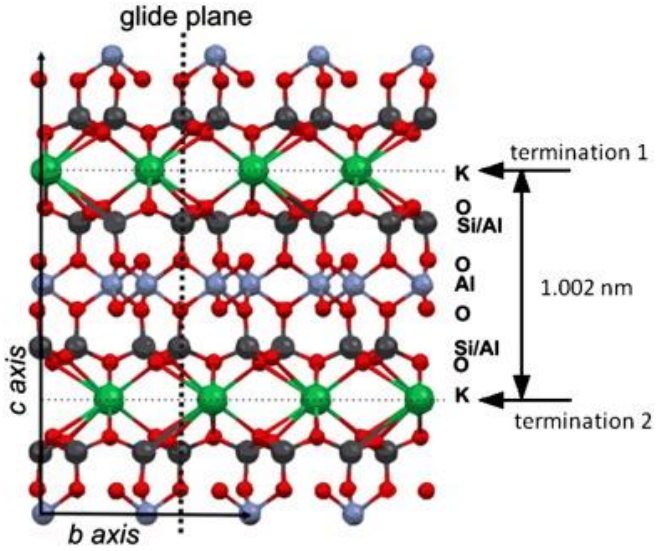

Figure 4.4 Structure of muscovite mica taken from (De Poel et al., 2014).

As mica has a well-defined oxygen to silicon ratio the measured oxygen content can be used in subsequent calculations of the organic oxygen content of any new overlayer using the method described in equations 3 to 5 in Chapter 3.

On autoclaving, the mica surface showed an increase in carbon, and lower levels of surface aluminium and silicon, with little effect on the concentration of potassium.

4.1.4 Titanium

XPS survey spectra and C 1s spectra of sputter-coated titanium on silicon wafer are shown in Figure 4.4 and quantification of data before and after autoclaving are shown in the Table 4.4. Sputtercoating of samples was carried out in batches to ensure even coverage, and analysis of two batches are shown in Table 4.4.

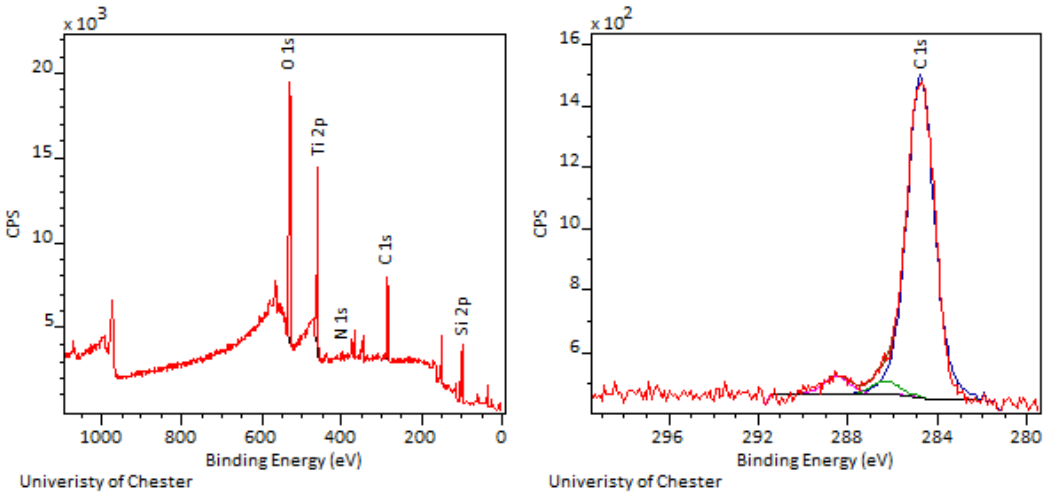

Figure 4.5 Survey spectrum and C 1s peak fitting for sputter-coated titanium.

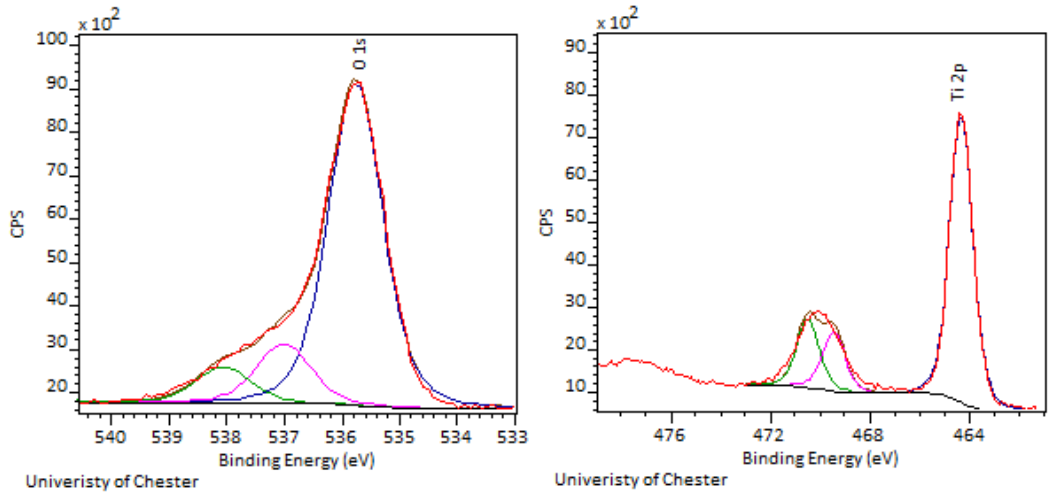

Figure 4.6 XPS O 1s and Ti 2p for autoclaved sputtercoated titanium.

The sputter coated titanium layers on Si (111) were found to have two layers of oxide, namely the TiO_2 layer and the SiO_2 layer on the underlying Si (111) wafer. Therefore, a combination technique was used to determine the organic oxygen content, as described in Chapter 3 equations 4 and equations 8-11.

	As Acquired	Autoclaved	As acquired 2
C 1s	26.3	46.7	42.9
O 1s	40.1	35.7	39.6
O org	1.2	21.2	
N 1s	0.8	1.6	1.0
Si 2p	23.2	3.5	2.4
Na 1s	1.3	0.0	0.0
Ti 2p	9.7	12.5	14.2
Ag 3d	0.7	0.0	0.0
Ca 2s	1.4	0.0	0.0
C285	90.4	89.4	-
C286.5	4.4	7.1	-
C288	5.2	3.6	-
Thickness Hydrocarbon	1.41nm	3.13nm	-
Thickness TiO_2	0.84nm	1.51nm	-

Table 4.3 Surface composition of sputtercoated titanium before and after autoclaving where XPS analysis of 2 different as prepared batches are compared.

The titanium surface was found to be in form of titanium dioxide, as determined by the observed shifted position of the Ti 2p peak from 454eV for pure titanium to 458eV for titanium dioxide. This is likely to have been due to air exposure after sputter coating or the

effect of unavoidable residual oxygen in the atmosphere of the sputter-coater unit. The presence of the Si 2p peak indicated that either the sputter coated titanium layer was not sufficiently thick to suppress the silicon signal, or that the titanium layer was patchy, and areas of the underlying silicon substrate were exposed. If the first case, then the titanium layer thick could be calculated as 0.37 nm using the methods of Chapter 3. Nitrogen was also found on the surface, suggesting some contamination on the surface, possibly from nitrogen incorporation from the residual vacuum of the sputter coater. Traces of silver found on the sample were attributed to contamination from sputter coating, however this was not seen in samples after autoclaving and is therefore unlikely to affect the final result.

On autoclaving the C 1s peak increased sufficiently to supress the silicon signal. Initially the carbon was found to be in a more hydrocarbon state, with low level signal at C286.5 and C288. On autoclaving, the carbon was still strongest at C285, but with increased amounts of carbon at C286.5 and C 288.

4.1.5 Silver

The XPS survey spectrum and the curve-fitted C 1s spectrum from the sputter-coated silver substrate is shown in Figure 4.7. The results of quantification of the data from the as-received (as-prepared) and the autoclaved surfaces are shown in Table 4.5.

The organic oxygen of the silver sample once prepared, is estimated from the C 1s peak fit data. From the inorganic oxygen content to silver ratio, and the oxygen content of the autoclaved sample, the organic oxygen content can be determined as explained in equations 3 to 5 in Chapter 3.

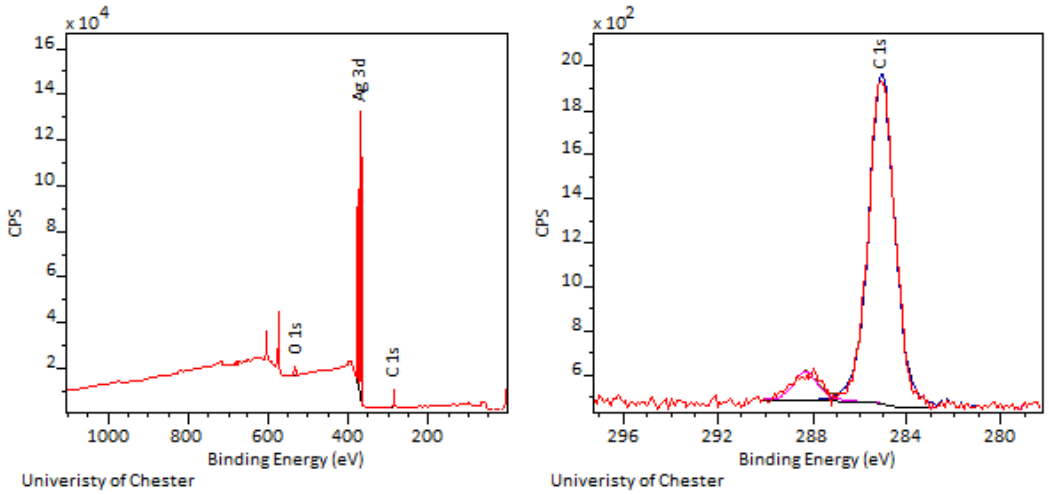

Figure 4.7 XPS survey and C 1s peak fit of sputtercoated silver.

	As Acquired	Autoclaved
C 1s	40.5	48.9
O 1s	7.5	8.6
O_{org}	3.2	8.3
Ag 3d	52.1	42.5
C285	92.0	93.7
C286.5	8.0	6.3
Thickness Hydrocarbon	2.44nm	3.03nm

Table 4.5 Surface composition of sputtercoated silver before and after autoclaving.

On observation the silver signal, at 367eV, was found to be strong enough to supress the signal of the lower titanium and silicon layers, suggesting the layer of silver to be thicker than 50 nm, in agreement with values measured by the quartz crystal balance of the sputter-coater during preparation. Carbon and low levels of oxygen show the contamination layer was mostly hydrocarbon in state. This was confirmed by the carbon peak fitting, with some carboxyl carbon at C 288 accounting for the O 1s peak detected. This also confirms the silver layer is pure silver.

Autoclaving the silver sample increased the C 1s peak intensity, mostly in the form of hydrocarbons as shown by the increase at C285.

4.2 Physical characterisation

The substrates were imaged using the NT-MDT AFM in Semi-contact mode and roughness values were determined from the AFM images using the NT-MDT Nova-Px software. Surface energy values were obtained using the Dataphysics OCA Contact Angle System with Dataphysics XYZ SCA 202 v4.5.11 software, as described in Chapter 3. Representative AFM images from the mica and the silver-coated surfaces are shown in Figure 4.8. Roughness and surface energy values from all substrates used are summarised in Table 4.6.

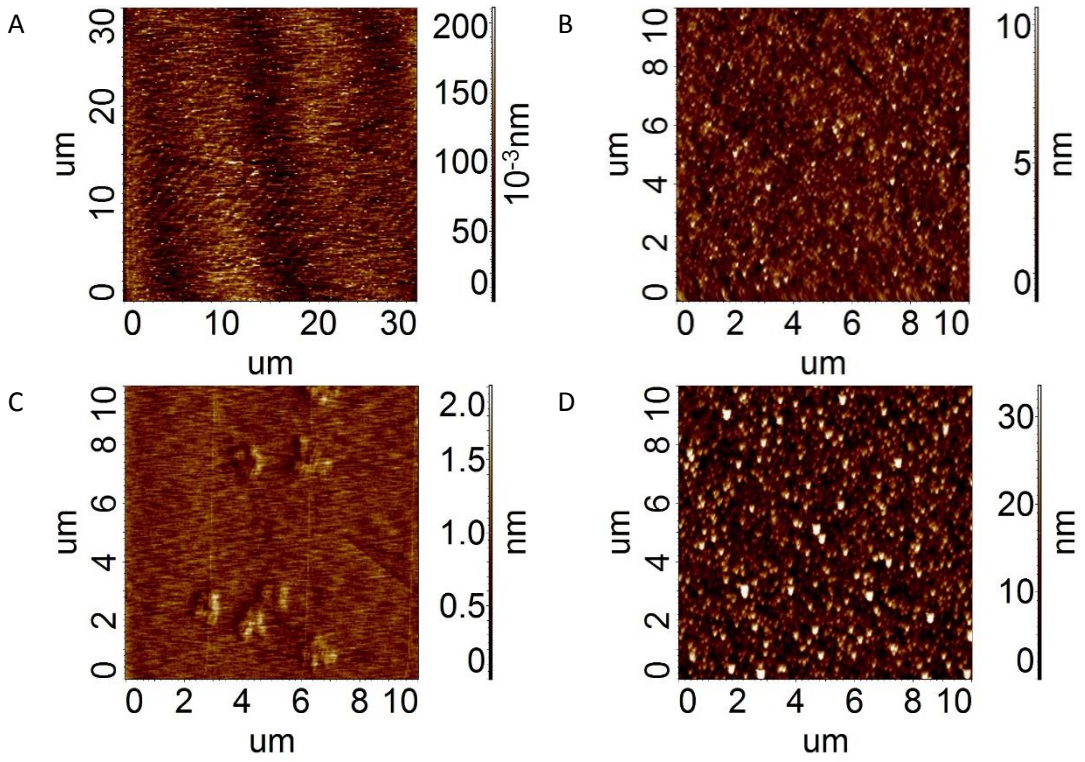

Figure 4.8: Representative AFM images from the mica (A and C) and silver (B and D) surfaces to illustrate the scale of observed roughness. As received are on top (A and B) with autoclaved images are listed below (C and D).

	As-received			Autoclaved		
Substrate	AFM Roughness		Surface energy	AFM Roughness		Surface energy
	RMS (nm)	Ra (nm)	(mJ m^{-2})	RMS (nm)	Ra (nm)	(mJ m^{-2})
Silicon	2.9	1.3	40.2	1.6	0.83	72.8
Glass	24.4	12.6	69.6	23.3	11.71	60.6
Mica	0.2	0.1	40.2	4.3	2.64	N/A (69.4)
Titanium	2.4	1.0	36.2	2.1	1.58	29.5
Silver	1.7	1.3	24.0	7.0	5.33	26.6

Table 4.6 Summary of AFM roughness measurements and surface energy values on as-received and autoclaved substrates.

Surface energy measurements on silicon and mica, and to some extent on silver showed an increase on autoclaving the surfaces whereas the glass and titanium surfaces showed a small decrease. It was noted that the surface energy measurements on autoclaved mica initially showed full wetting and therefore was only measured after allowing the mica to air dry for 15 minutes, which was not the case for any other analysis of mica. Therefore, the surface energy of freshly autoclaved mica is assumed to be significantly higher than the value recorded here.

All the materials were relatively smooth, with majority having a roughness root mean squared of less than 3 nm. The exception to this is that of glass, where a value of 24 nm was found. This was believed to be due to the occasional occurrence of larger particles on the surface. For both sputter-coated samples roughness was sufficiently low to support the assumption that the sputter-coated layers were continuous.

The AFM data showed that the roughness of the surfaces altered with autoclaving. Roughness values decreased on autoclaving glass, silicon and titanium. This is thought to be related to the increase of organic layer on the surface as seen in the XPS data (see above). This organic layer was assumed to be softer than the underlying substrate, and therefore tending to fill in any troughs or pits on the surface and so contributing to a reduction in roughness. Roughness values increased on autoclaving mica and silver.

The increase in roughness values on autoclaving the mica could be due to two possibilities. Firstly, mica consists of thin sheets, which are easily cleavable to relative smooth surfaces, and therefore some analyses may have taken place at positions where surface steps were present. Alternatively, the surface of mica has a high affinity to water and the surface layers have retained some trapped water on cooling after autoclaving, and this trapped water has resulted in distortion of the surface layers. The presence of small particles on the surface was noted. These may be potentially due to damage to the surface on autoclaving

The roughness values of silver were found to increase on autoclaving. The silver substrates were constructed using an intermediate layer of titanium to bind to the underlying silicon. The roughness increase may have been related to exposure to water vapour during autoclaving and the subsequent damage and partial disintegration of the silver layer. This reflects the observation of silver delamination from the underlying Si (111) substrate when sputter-coated directly to silicon without the intermediate titanium layer. AFM images of the autoclaved surface showed the presence of larger particles on this surface, supporting this

hypothesis. From XPS data, the lack of Ti 2p peak shows there is a significant amount of silver on the surface required for this experiment.

AFM force-distance curves were acquired on all five substrates before and after autoclaving. Typically, 3 scans with 9 representative points were recorded for force distance curves. Results are summarised in Table 4.7. In the table, for each substrate the upper row shows the mean recorded value and the lower row the population standard deviation of the results recorded.

Material	As received				Autoclaved			
	Snap in (nm)	Adhesive force (nN)	Pull out distance (nm)	Retractive force (nN)	Snap in (nm)	Adhesive force (nN)	Pull out distance (nm)	Retractive force (nN)
Silicon	3.3	8.7	3.9	32	5.0	25.7	21.3	144
	1.5	5.4	0.6	3	2.5	22.1	10.0	66
Glass	6.7	43.7	10.9	90	8.1	45.2	14.0	106
	1.3	11.3	1.9	26	2.8	27.5	2.8	25
Mica	1.2	5.0	2.5	16	6.6	52.4	29.2	256
	0.3	1.7	0.4	5	0.7	3.5	2.4	22
Titanium	3.3	21.3	6.7	54	2.0	6.5	2.4	13
	0.8	7.8	2.3	19	0.8	3.8	0.8	4
Silver	1.7	6.8	4.4	30	2.4	8.5	3.3	22
	0.7	5.3	1.7	14	0.6	4.2	1.5	10

Table 4.7 Snap in distance (nm) attractive force (nN), pull out distance (nm) and adhesion force (pull-off force, nN) for the as-received and the autoclaved surfaces. The top number is the average value and the bottom is the standard deviation of the data

The data in Table 4.7 are presented graphically in Figures 4.9 and 4.11 to 4.12. The error bars at the tops of the columns are the population standard deviations taken from Table 4.2. The force curve data were found to vary between each substrate material, reflecting differences in the materials and in any absorbed overlayers as a result of autoclaving. In the histograms in sections 4.2.1 – 4.2.4 below the height of the bar represents the mean value of the property indicated and the error bars on top of the bar represent the population standard deviations. In some cases, with apparently large error bars, the frequency distributions of the measurements were plotted to help determine whether the large range was due to genuine statistical variations or to, for example, bi-model or other non-Gaussian distributions. The results presented in the sections below form a base-line for interpretation of data on the growth of media and bacterial layers on these substrates discussed in later chapters.

4.2.1 Snap in distance

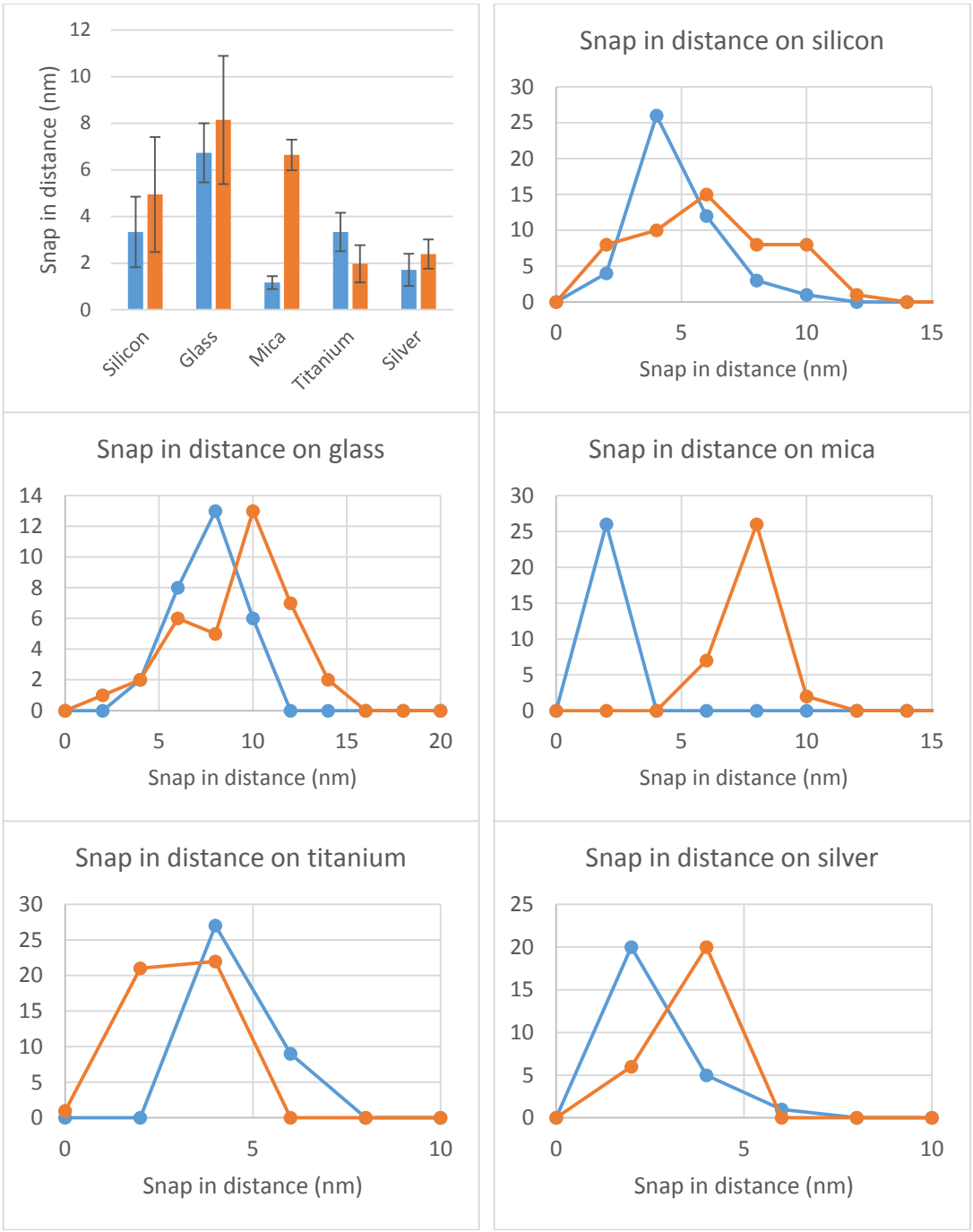

Figure 4.9 AFM snap in distances for the as-received and the autoclaved substrates (top left) and the frequency distribution of snap in distances as received and autoclaved materials. Blue refers to the as received material and orange relates to the autoclaved material.

Snap in distance is a measure of the resistive properties of the material in relation to the tip. Autoclaving materials, in most cases, increased the snap in distance by variable amounts, with an increase in standard deviation. On plotting frequency distributions, a wider distribution is measured, which in some cases is extended on both sides of the average, indicating the organic layer not only added to but redistributed unevenly.

The glass and silver substrates showed a slight increase in AFM snap in distance with autoclaving, but the effect was small and within the statistical uncertainty of the measurement.

Silicon shows a larger increase than that of glass, relating to a more elastic material on the surface and possibly consistent with the presence of an increased hydrocarbon-like overlayer.

The results on mica suggested the material was most likely to have formed a thicker layer of absorbed water on the surface, resulting in higher snap in values as a result of capillary forces.

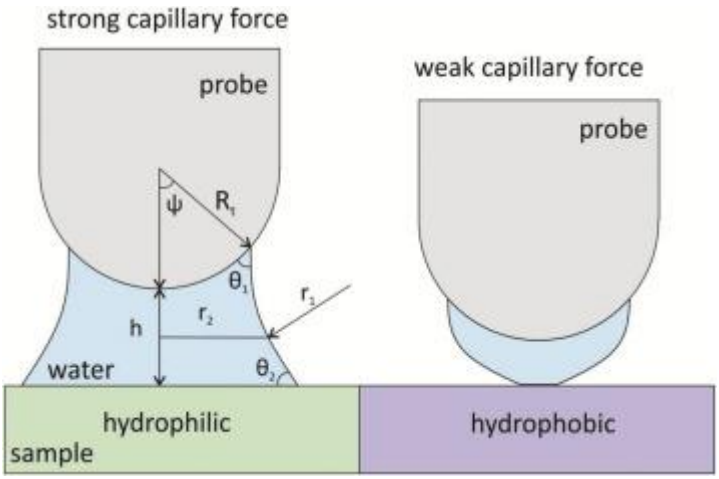

Figure 4.10 Capillary force effects in AFM taken from Trotsenko 2016(Trotsenko, Koestner, Roiter, Tokarev, & Minko, 2016)

Titanium is an exception, where a decrease in the snap in distance was seen on the autoclaved substrate compared to the initially prepared material.

4.2.2 Attractive force

Attractive force values show the maximum attractive forces of the substrate. The trends across adhesion values follow that of snap in distances, implying these results are complimentary to each other, and that attractive force values therefore reflect similar characteristics between the material resistivity and attractive forces, most likely from the substrate material.

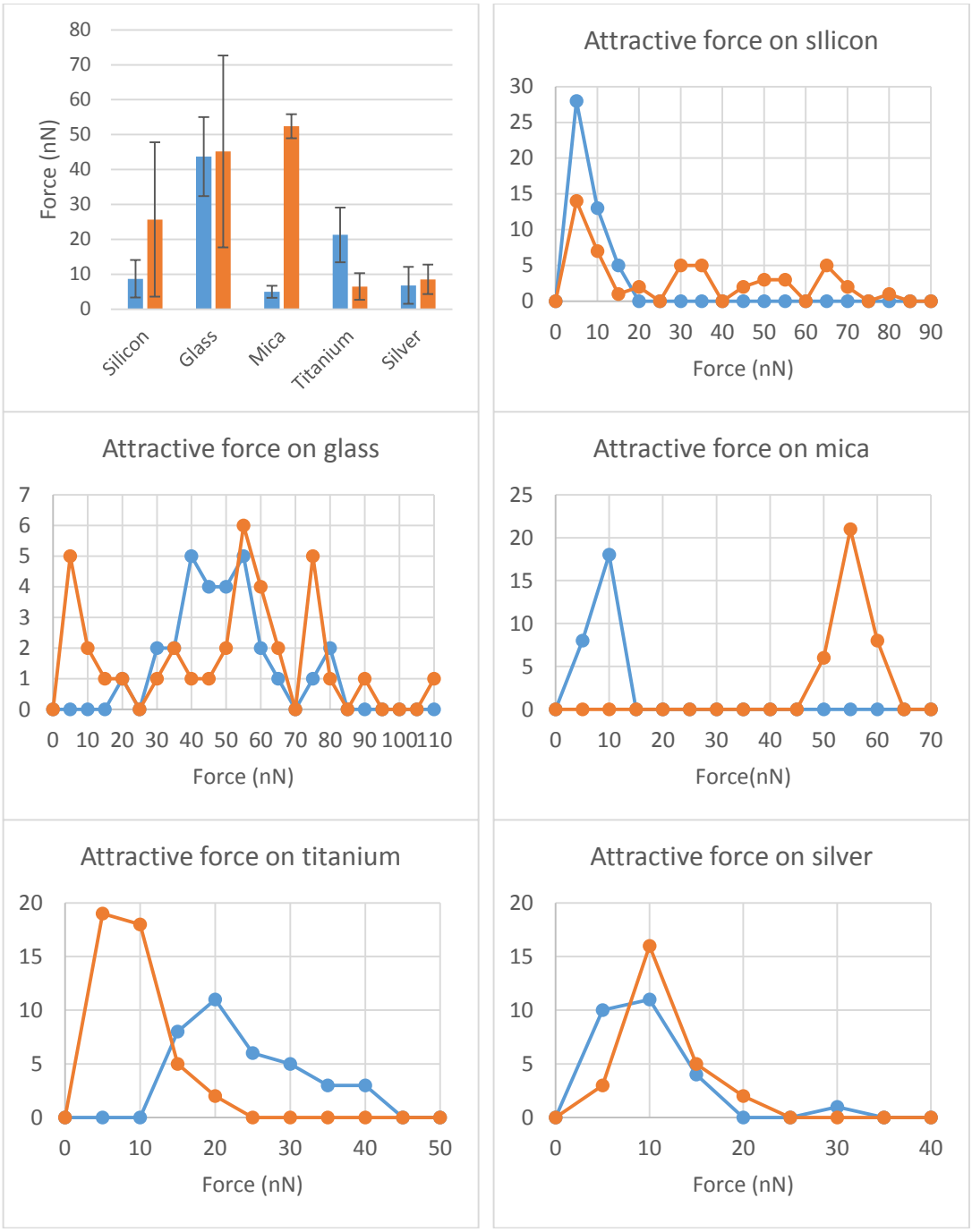

Figure 4.11 AFM attractive forces for the as-received and the autoclaved substrates (left) and the frequency distribution of attractive forces on glass as received and autoclaved glass (right). Blue refers to the as received material and orange relates to the autoclaved material.

4.2.3 Pull out distance

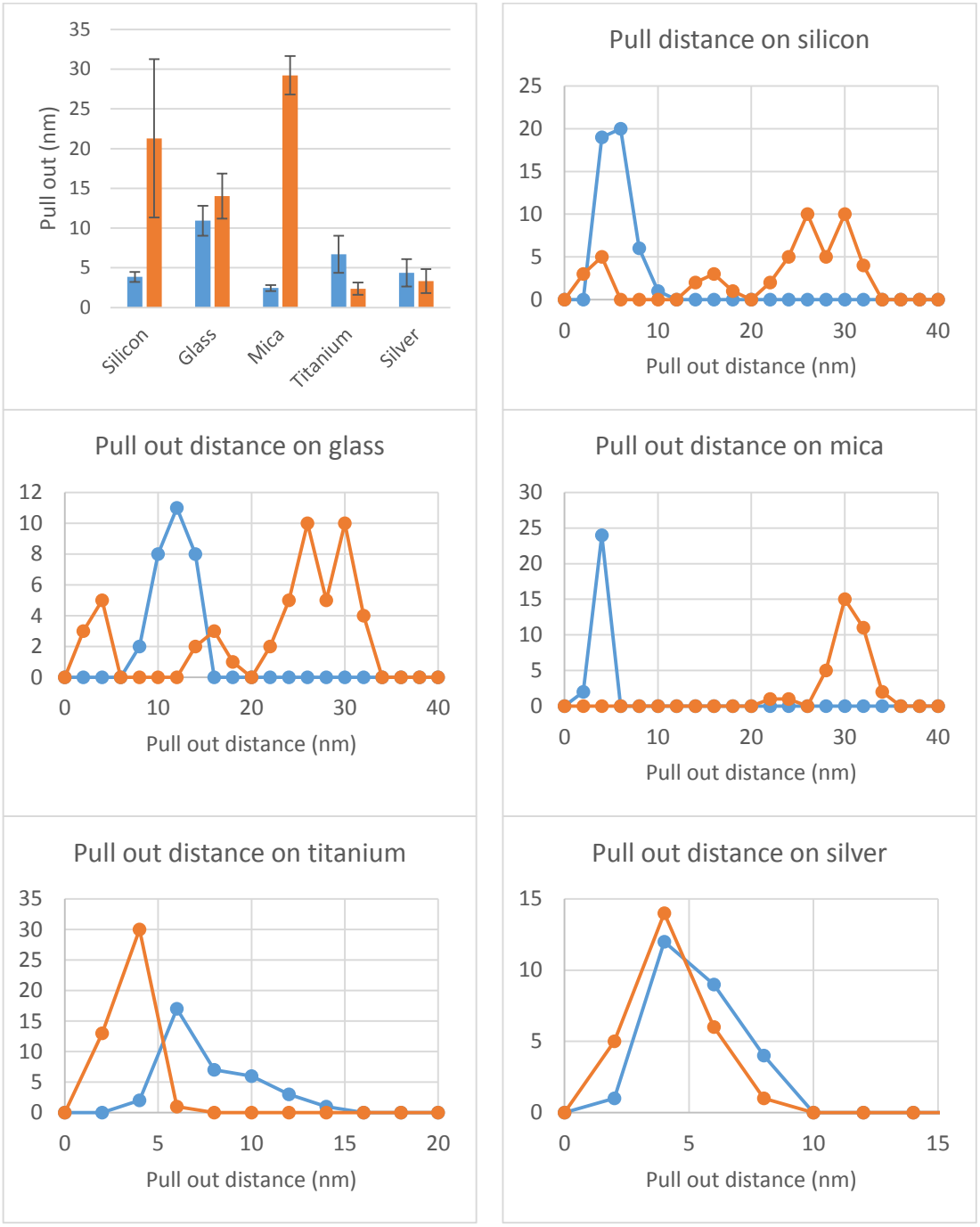

Figure 4.12 AFM pull out distances for the as-received and the autoclaved substrates (left) and frequency distribution of pull out distances of as received and autoclaved glass samples. Blue refers to the as received material and orange relates to the autoclaved material.

Pull out distance indicates the elasticity of the material and can also indicate the type of adhesive bonding present. Mica showed the largest increase in pull out distances on autoclaving followed by silicon. The larger pull out forces on silicon and mica indicate the greater distance travelled by the tip before removal from the surface overlayers on these materials. Of the chosen substrates, only glass showed a slight increase in pull out distance

on autoclaving, suggesting there was no significant change in the binding properties of the organic layer and substrate. As previously noted, titanium was an exception to the general trend of autoclaved samples, by showing a decreasing instead of increasing pull out distance. Silver, on retraction, also followed the same trend as titanium with a slight decrease. As noted above, the roughness of the silver increased on autoclaving possibly because of some damage to the silver layer. It is therefore possible that the AFM pull out distance was affected by an effect of the titanium substrate. However, the difference between the measurements before and after autoclaving are within the standard deviation, and this may indicate that the results were dependant on where the sample was probed.

4.2.4 Retractive force

Retractive forces followed the same trend as pull out values, showing the similarities in the types of forces and bonds being broken. The tip is therefore showing the bonds formed and broken are predominantly related to that of an organic layer.

Mica showed the greatest change in retractive forces on autoclaving. This may be due to the clay-like properties of the material, allowing it to absorb a higher level of water on the surface, resulting in higher capillary forces measured by AFM. In this case, capillary forces would add an additional bond type to break, thereby increasing the retractive force.

The increases in retractive force observed on the silicon substrate relate to the increase in the thickness of the silicon oxide layer because of autoclaving. As a more elastic material, as defined by Young's Modulus (kim, 1996) the tip can move further through the oxide layer, before feeling repulsion, some of which is from the pure silicon lager underneath.

The glass substrate showed very little increase in retractive force on autoclaving. Chemically, the material was not observed to change significantly on autoclaving. Any variations were therefore likely to be related to the increase in atmospheric contamination. Silver also showed little variations on autoclaving.

On autoclaving the titanium, significant decreases in retractive forces were observed, suggesting a less adhesive surface.

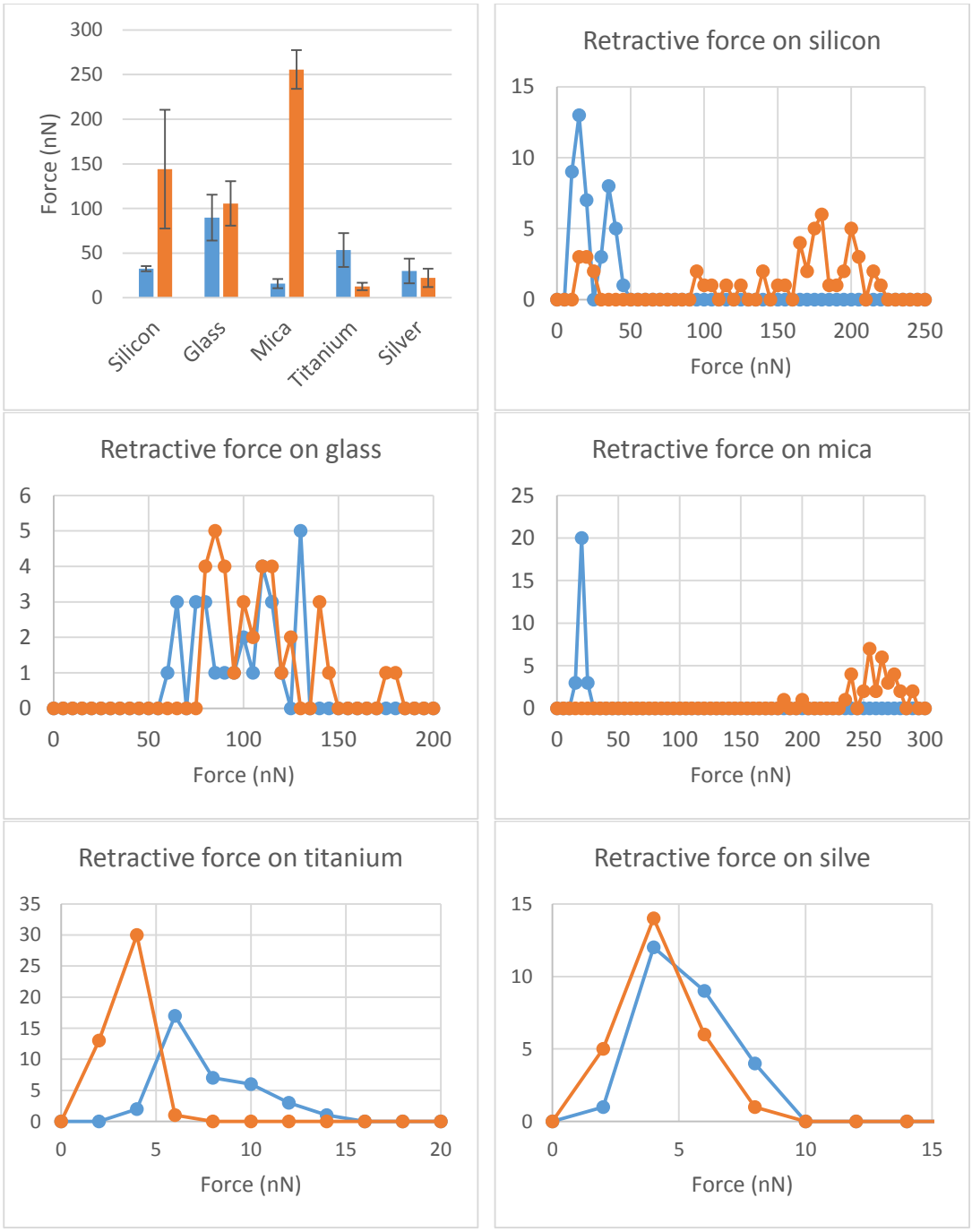

Figure 4.13 AFM retractive forces for the as-received and the autoclaved substrates (left) and the frequency distribution of retractive forces on as received and autoclaved glass (right). Blue refers to the as received material and orange relates to the autoclaved material.

4.2.5 Summary of XPS sample analysis

Overall, incubating substrates in tryptic soy broth after autoclaving showed there was binding of proteins and polysaccharides to the surface of the substrate. Figure 5.13 shows the calculated biological composition of the organic layer in each sample. The proportion of protein and polysaccharides on the surface varied depending on material, which may influence bacterial adhesion to the surface discussed in later chapters. While components of

media displaced some of the atmospheric hydrocarbon on the surface, XPS data indicated there was still some residual hydrocarbon on the surface. Comparing the defining element to the carbon content, focusing on the peak at 284eV before and after incubation, there was a correlation between the carbon content, relating to that of the atmospheric carbon bound to the surface. The presence of hydrocarbons was confirmed by the biological compound composition data.

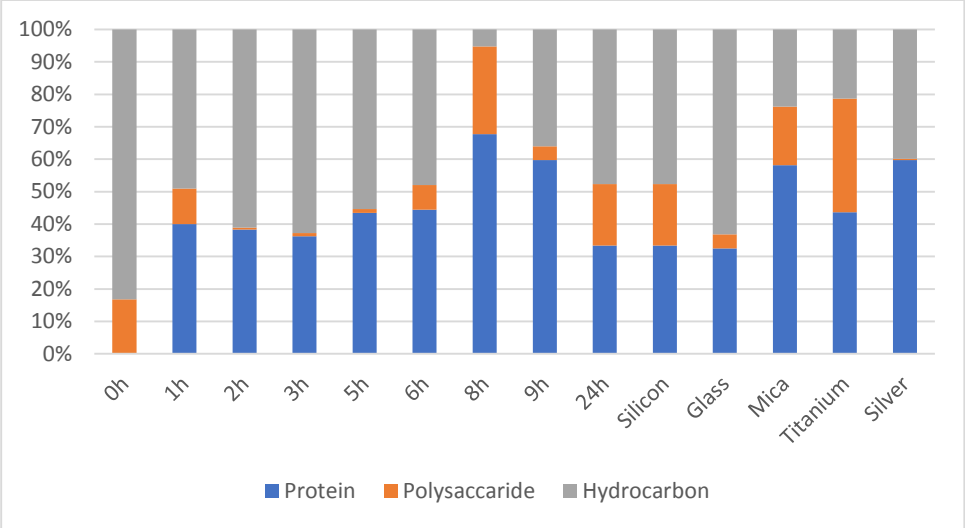

Figure 4.1 Biological composition calculation of the organic layer of TSB incubated samples where blue represents protein content, orange is polysaccharide content and grey represent hydrocarbon content.

4.3 Concluding remarks

Overall the chemical structure, as determined by XPS, was found to be approximately as expected for each of the substrate materials, with the addition of a thin layer of hydrocarbon-based material as a result of atmospheric contamination. The thickness of the atmospheric contamination layer varied across the substrate materials, however the layer was always less than 3nm. From analysis of the carbon peak, the majority of the carbon was found to be in hydrocarbon form. The layer thicknesses determined on the substrates before and after autoclaving as summarised in Table 4.8.

Layer	As received	Autoclaving
Silicon hydrocarbon	0.54nm	1.09nm
Silicon SiO_2	1.41nm	1.40nm
Glass hydrocarbon	0.89nm	2.49nm
Mica Hydrocarbon	0.36nm	0.95nm
Titanium hydrocarbon	1.41nm	3.13nm
Titanium TiO_2	0.37nm	0.88nm
Silver hydrocarbon	2.44nm	3.03nm

Table 4.8 Layer thickness as calculated using XPS data and attenuation lengths.

Sterilising substrates was necessary to prevent any contamination, giving the substrates equal conditions for later experiments. While other methods of sterilisation exist, autoclaving was chosen to prevent chemical alterations to the surface, which can influence sample roughness and organic layer binding. Consequently, the substrates' chemical and physical properties were characterised before and after autoclaving.

Chemically, autoclaving was found to increase the organic layer present on the surface, by an amount which varied between samples. This indicates substrate dependant binding of organic compounds to the surface, which may influence subsequent layer formation, the increase of carbon in the organic layer was found to be in the form of hydrocarbons and carbonyls, as seen in the C 1s peak fit data. These agree with the increase of oxygen and, in some cases, nitrogen signals on autoclaving. This indicates the organic layer at this stage was predominantly atmospheric carbon. The composition and thickness of this layer varied, indicating material effects which affected overlayer formation. Autoclaving silicon also increased the thickness of the silicon dioxide layer on the silicon wafer, but not changing the chemical properties of the substrate overall.

Image analysis of AFM data showed that the substrates were relatively smooth. Glass was the roughest material with 24 nm roughness, but all sample roughness values were noted to be much lower than the average dimensions of the bacteria to be used in this study. Autoclaving had some influence on surface roughness, and this varied between the substrate materials. The roughness was found to increase on autoclaving mica and silver but to decrease with the other substrates.

The shapes of the AFM force curves, and variations between them, indicated the nature of the material and the changes on autoclaving. Variations in force curve data were attributed to the differences between substrate materials. Differences on autoclaving were interpreted in terms of the effect of the organic layer and its interactions with the AFM tip.

From AFM force curve data, the variations in snap in and adhesive forces were related to changes in organic layer. Overall, the similarities before and after autoclaving showed the force curves were substrate dependant. The larger increases on mica was due to the effect of capillary forces, likely as a result of water retention between the layers of the clay-like mica structure. Titanium did not follow the trend of other substrate materials on autoclaving. This may be related to the layer thickness formed during sputter-coating. Layer thickness calculations were used to show the variations in thickness of titanium layer, between the

simple titanium layer substrate and the silver substrate with the titanium interlayer. As the lower titanium layer on the silver-coated substrate was observable by XPS then there is also a possibility this contributes to force curve data.

The material characterisation presented here forms a base for the interpretation of chemical and mechanical data as a consequence of layer growth and bacterial adhesion.

Chapter 5 Tryptic soy broth incubated samples

The *Staphylococcus epidermidis* bacteria used in this study were incubated in tryptic soy broth (TSB) as a growth medium. It was therefore likely that TSB components would be either incorporated in the biofilms produced when the bacteria were incubated in the presence of a substrate or would form a conditioning film on the substrate prior to biofilm growth. To provide a baseline for the analysis of the biofilms, and to aid understanding of film growth, substrates were incubated in the TSB growth medium in the absence of bacteria and characterised by XPS and AFM. Results from these techniques on the silicon (111), glass, mica, titanium and silver substrate surfaces are presented here.

5.1 XPS analysis of media incubated material

Samples were analysed by XPS for elemental composition, biological compound composition and layer thickness after incubation in TSB for periods up to 24 hours. Data were interpreted according to the methods described in Chapter 3. Where necessary, the amount of oxygen in the organic layer was estimated taking into account the substrate composition and the presence of any oxide layer, as discussed in Chapter 3. The ratios of O_{org}/C and N/C were used to estimate the presence of polysaccharides and proteins respectively using the biological model discussed in Chapter 3.

When estimating layer thicknesses using the methods described in Chapter 3, an organic layer density corresponding to that of TSB was used rather than an assumed value for the atmospheric contamination layer. The organic layer density was assumed to be 1.59 g/cm, calculated from ideal density of individual components. Evidence to justify replacement of the atmospheric organic hydrocarbon layer by a TSB-derived layer was obtained from the measured changes in chemical composition of the organic overlayer, corresponding to compositions consistent with that of components of the TSB formulation. The higher density of the TSB layer had the effect of decreasing the calculated layer thickness compared to those of the atmospheric contamination layer discussed in Chapter 4, for an equivalent overall atom % composition.

5.1.1 Silicon time-dependent study

Samples of TSB incubated on silicon were removed from the incubating liquid at hourly intervals and analysed during the first 9 hours and after 24 hours of incubation. The timescale was chosen to reflect the time period of the initial growth of the bacteria, with the 24 hour sample representing the stationary phase for several hours, where biofilm formation was more likely to occur, due to competition for nutrients. XPS surface composition data for these

samples are summarised in Table 5.1, where compositions are in atomic % and the percentage of carbon in the three chemical state binding energies indicated are also given. The time zero data is the autoclaved sample data from the equivalent table in Chapter 4. Figure 5.1 shows the XPS survey spectra, C1s peak fit and N1s peak fit after incubating silicon with TSB after 24 hours. XPS spectra for other timed samples can be found in the Appendix.

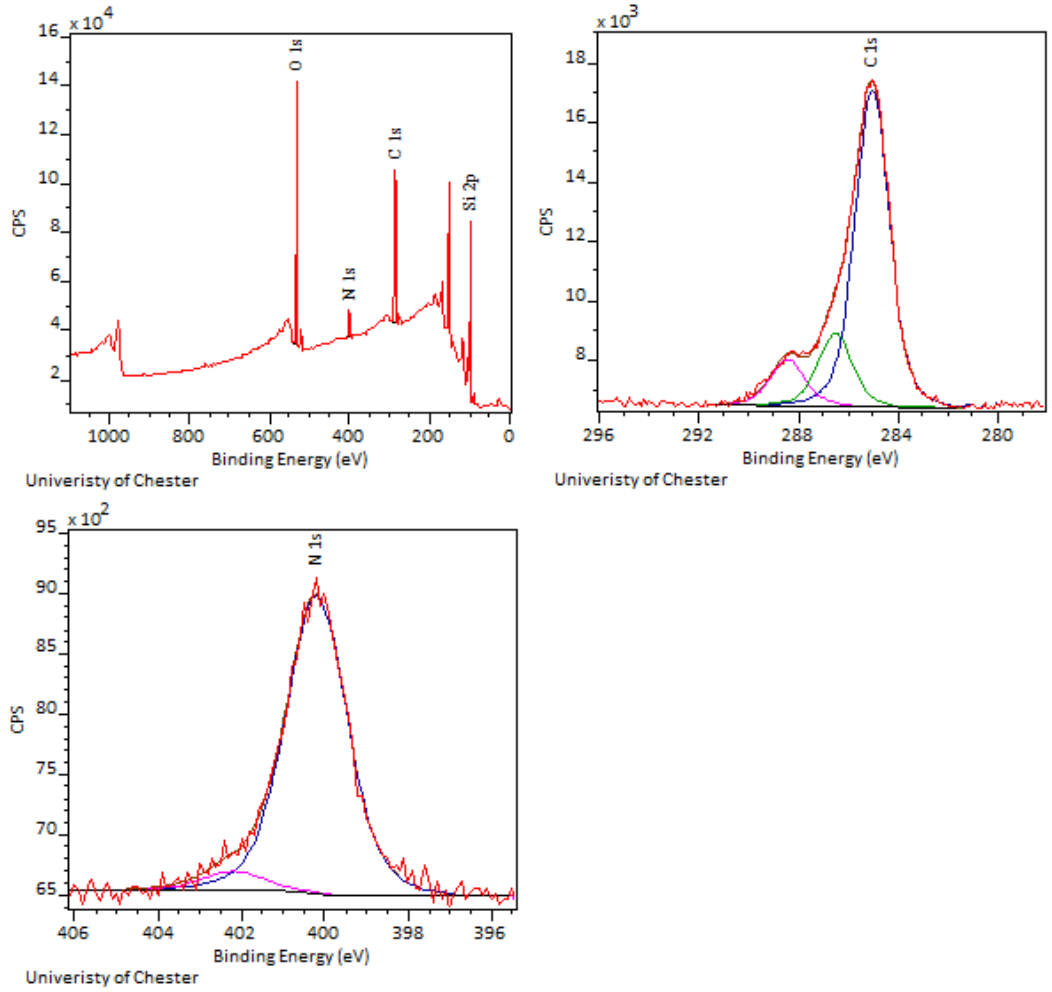

Figure 5.1 XPS survey spectra, C 1s peak fit, Si 2p peak fit and N 1s peak of silicon incubated in tryptic soy broth after 24 hours.

	Time taken from incubation (hours)								
	initial	1	2	3	5	6	8	9	24
C 1s	21.1	58.6	34.1	30.5	34.3	38.8	30.4	56.9	41.2
O 1s	22.6	19.3	22.3	21.1	24.7	22.1	22.3	20.6	23.5
O_{org}	3.0	13.0	4.4	3.8	5.2	8.1	7.6	16.2	11.0
N 1s	0.0	6.5	3.7	3.1	4.2	4.8	5.3	9.5	3.8
Si 2p	56.3	12.8	39.4	44.8	36.6	32.7	41.9	10.8	31.5
P 2s	0.0	0.0	0.0	0.0	0.0	0.0	0.0	0.3	0.0
Na 1s	0.0	0.9	0.1	0.0	0.2	0.7	0.1	0.9	0.0
Ca 2p	0.0	0.6	0.5	0.6	0.0	0.0	0.0	0.0	0.0
Cl 2p	0.0	1.4	0.0	0.0	0.0	0.9	0.0	1.1	0.0
C285	87.9	69.0	73.7	69.6	68.0	68.4	54.8	49.7	72.9
C286.5	8.8	17.9	13.6	19.4	19.8	18.5	27.5	30.7	16.6
C288	3.3	13.1	12.7	11.0	12.2	13.2	17.7	19.6	10.6
O_{org}/C	0.14	0.23	0.13	0.13	0.15	0.21	0.25	0.25	0.27
N/C	0.00	0.17	0.11	0.10	0.12	0.12	0.17	0.17	0.09
P/C	0.00	0.01	0.00	0.00	0.00	0.00	0.00	0.01	0.00
Proteins	0.0	40.0	38.3	36.3	43.5	44.4	62.0	59.7	33.3
Polysaccharides	16.8	11.0	0.6	0.9	1.1	7.6	5.9	8.5	19.0
Hydrocarbons	83.2	49.0	61.1	62.8	55.4	47.9	32.1	31.8	47.7
Organic layer thickness (nm)	1.08	2.07	1.04	0.93	1.05	1.23	0.96	2.04	1.29
Coverage (%)	84.2	19.1	58.9	67.0	54.8	48.9	55.2	16.2	47.1

Table 5.1 XPS survey spectrum and C 1s peak fit analysis of silicon incubated with tryptic soy broth as a function of time including layer thickness, coverage and analysis of XPS data in terms of biological composition described in Chapter 3. The initial sample is autoclaved silicon.

Variations between samples can be caused by a range of factors beyond changes to compounds binding to the surface. These include washing and sub sampling. Samples that have been removed from incubation for analysis could not be re-incubated, due to effects of analysis and potential for contamination. To overcome this, separate samples were removed from the growth medium for each measurement. However, this led to the possibility of variations in sample coverage, as well as external effects of chemical composition on the surface.

Additionally, there is also an issue with uneven coverage of the sample, which can also lead to variations in silicon signal. Although it was initially assumed the layer is smooth and even, it is more likely there were points on the sample the TSB layer is thicker than others. This results in different coverage of samples at different points, leading to variations in the XPS data. Figure 5.2 shows how the overlayer of the sample can affect the XPS data. On areas where the organic compounds only cover a small amount of the sample, the XPS data showed a stronger signal from the substrate than the organic layer, whereas in situations where high

coverage was observed the reverse is true. The same theory applies to different compounds adhered to the surface.

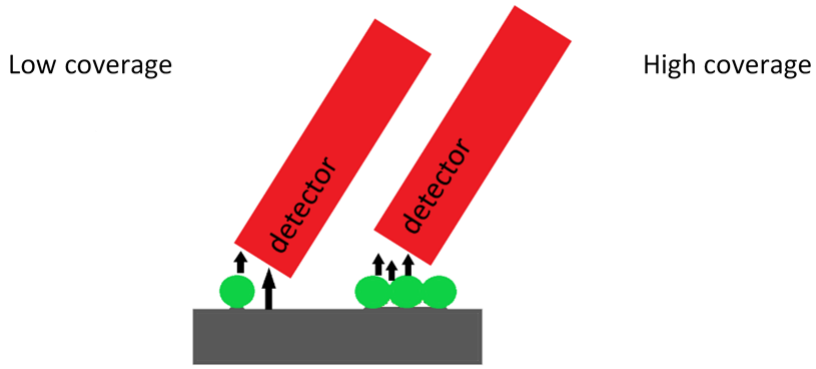

Figure 5.2 Diagrammatic representation of signal detection of high and low coverage.

The presence of variable coverage can be seen in the layer thickness calculations where the layer thickness varies from sample to sample with no clear pattern. The indication this was due to variable coverage can be seen in Figure 5.3 where apparent layer thickness and apparent coverage, both calculated from the reduction in intensity of the Si 2p peak, were shown plotted against each other. The figure shows a correlation between the calculated layer thickness and sample coverage, indicating that the estimated thickness of the organic overlayer is also an indication of sample coverage. The overlayer thickness calculation relates to coverage due to the neglect of atmospheric hydrocarbons within layer thickness calculations. A mixed layer of TSB and atmospheric hydrocarbon would have a lower density than TSB, and this may vary for each sample, depending on the amount of atmospheric carbon bound to the surface.

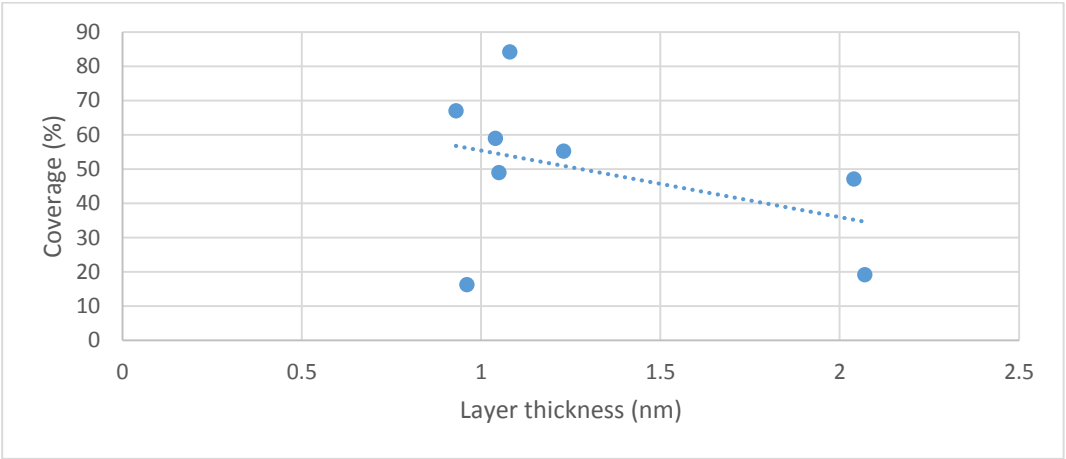

Figure 5.3 Graph of layer thickness vs. coverage calculated from change in Si 2p.

All samples showed the presence of silicon. Comparison of the spectra with the reference spectrum recorded for the autoclaved Si (111) wafer showed that the spectral backgrounds

on the high binding energy sides of the Si 2p peaks in this time-dependent series were raised to a similar degree to that seen for the reference spectrum. Therefore, the Si 2p signal originated from below a similar overlayer thickness to that on the reference sample (autoclaved but not incubated). This provides evidence that the Si 2p signals in the time-dependent series originated from silicon that was not covered in the TSB film. On this basis, it was possible to renormalize the data presented in the Table 5.1, taking into account the proportion of C 1s and O 1s associated with the exposed silicon (111) substrate, to give the approximate composition of the overlayer. Results are shown in the Table 5.2, and in Figure 5.4.

	0	1	2	3	5	6	8	9	24
C 1s	0.0	69.6	64.4	67.1	58.9	63.3	48.4	65.4	66.7
O 1s	0.0	18.3	21.6	15.1	28.6	21.4	34.1	20.1	24.7
N 1s	0.0	8.5	12.1	15.1	11.9	11.5	16.7	11.7	8.7
P 2s	0.0	0.0	0.0	0.0	0.0	0.0	0.0	0.4	0.0
Na 1s	0.0	1.2	0.5	0.0	0.6	1.6	0.8	1.1	0.0
Ca 2p	0.0	0.8	1.5	2.8	0.0	0.0	0.0	0.0	0.0
Cl 2p	0.0	1.8	0.0	0.0	0.0	2.2	0.0	1.4	0.0

Table 5.2 Approximate composition of the TSB layer, calculated assuming the layer was sufficiently thick to suppress all Si signals, and that the Si signals present in the spectra originated from exposed Si substrate.

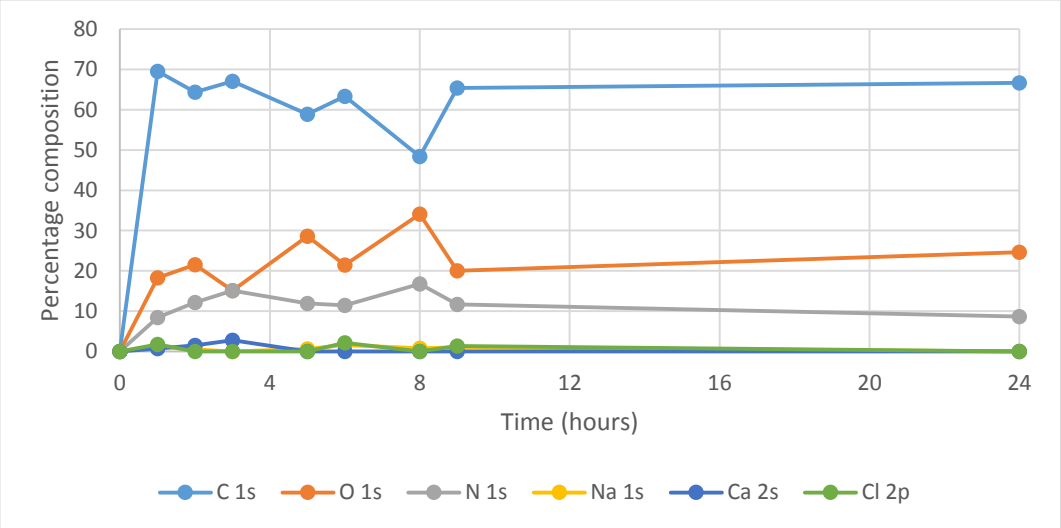

Figure 5.4 Approximate composition of the TSB layer, calculated assuming the layer was sufficiently thick to suppress all silicon signals, and that the Si signals present in the spectra originated from exposed Si substrate.

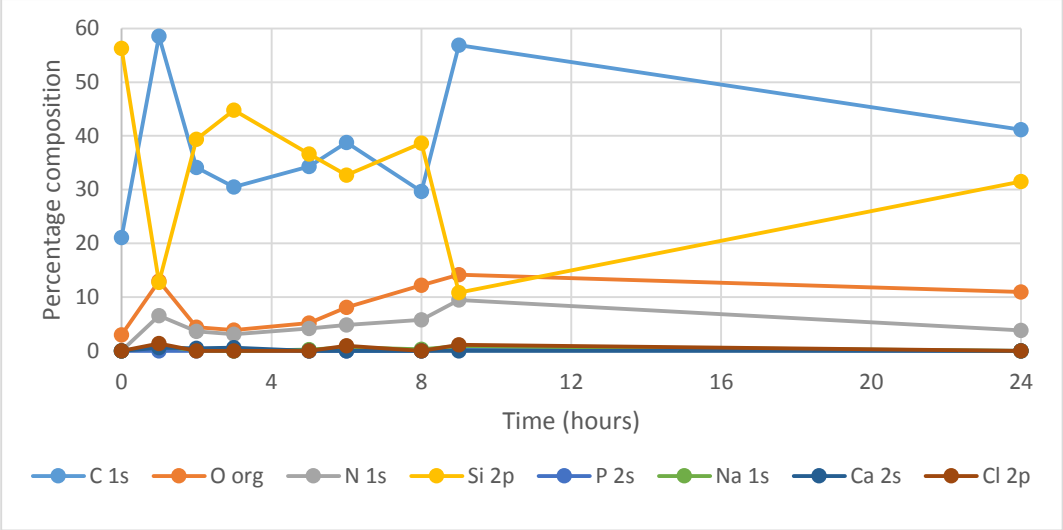

Figure 5.5 XPS survey analysis of silicon incubated in TSB over 24 hours included calculated organic oxygen from the Si 2p peak.

After the first hour of incubation, N 1s at 400 eV was seen in Figure 5.3. The binding energy was consistent with C-NH_2 (amine) bonding. Low levels of N 1s were also found at 402 eV in the spectrum recorded after 24 hours incubation and attributed to tertiary amines, consistent with the expected nitrogen bonding in protein. Na 1s and Cl 2p were detected in most samples and were assumed to be due to the presence of residual sodium chloride from the TSB incubation medium. Trace amounts of P 2s were detected on the 9 hour sample, likely due to phosphates in the media. The presence of Ca 2p in samples was observed for samples in the initial 1, 2 and 3 hours of incubation.

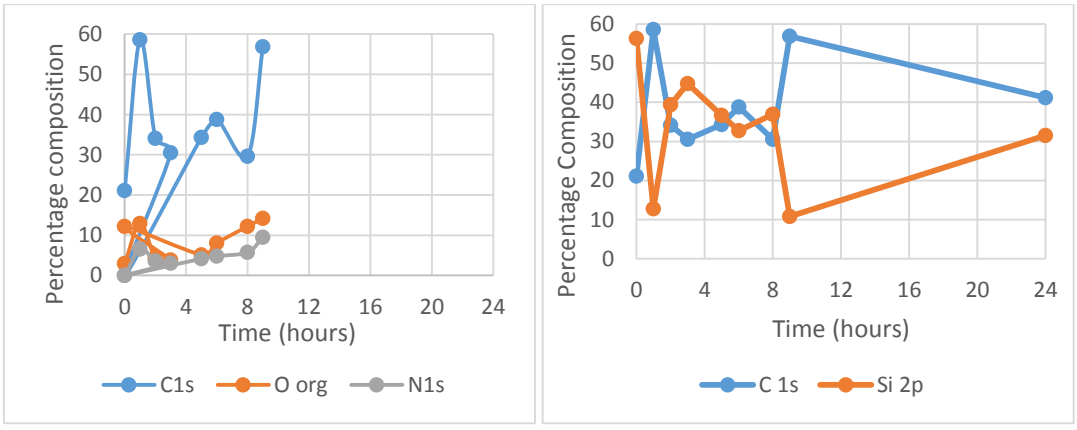

Figure 5.6 XPS survey spectrum analysis of elements against time for silicon incubated with tryptic soy broth (subset of data in Figure 5.5, replotted for clarity).

Analysis of survey spectra against time showed an inverse correlation between S 2p and C 1s compositions, confirming that increase in carbon relates to coverage of the silicon substrate. Correlations between carbon, nitrogen and organic oxygen indicate the change in biological compounds on the surface from atmospheric hydrocarbons to proteins and polysaccharides from the TSB, as discussed below.

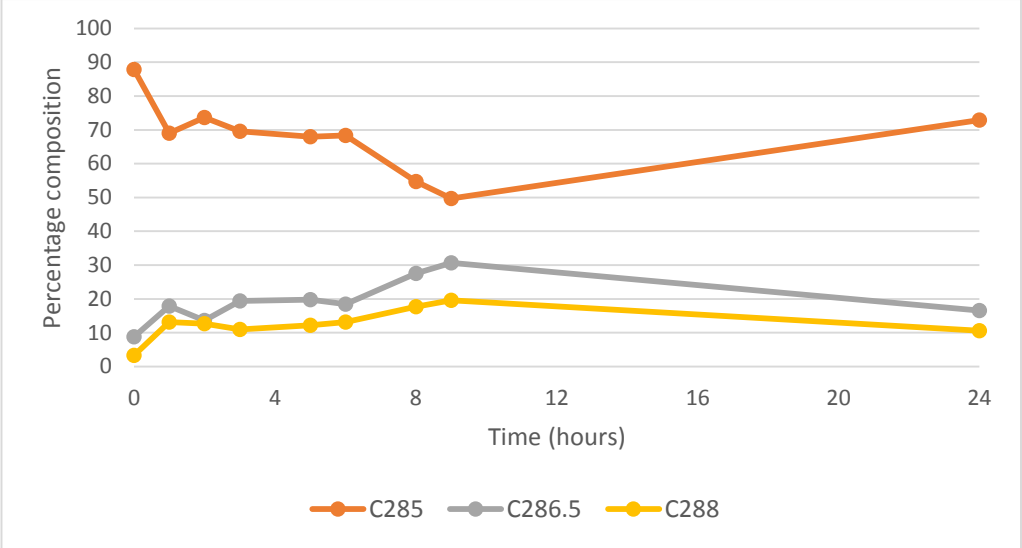

Figure 5.7 Carbon peak fit data from silicon wafer sample incubated with TSB over time.

The ratio of the components within the carbon peak fit varied during the timed experiment. The amount of C285 decreased as C286.5 and C288 increased for the first 9 hours of incubation, due to the increase in the quantity of media binding to the surface during this period. The reduction in C286.5 and C288 relative to C285 after 24 hours may be due to instability in the TSB film structure.

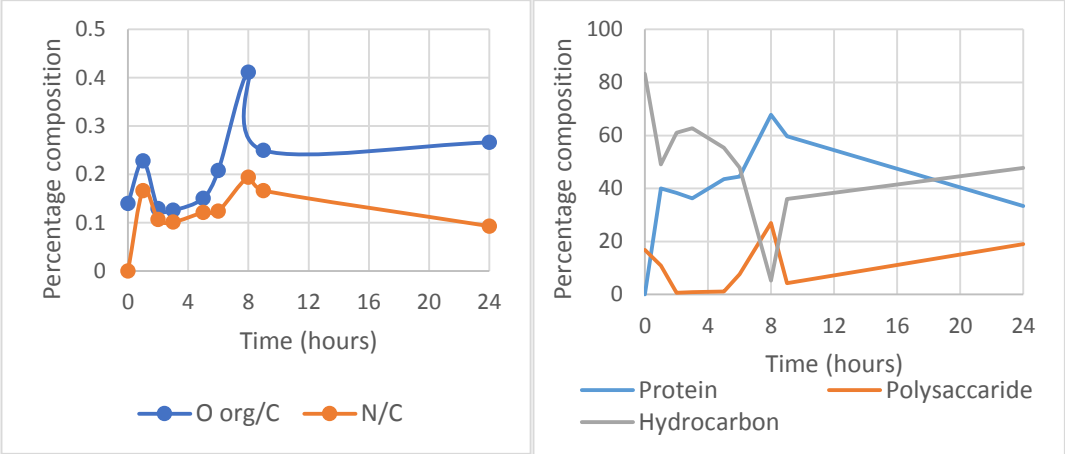

Figure 5.8: Elemental ratios (left panel) as a function of time and the calculated biological content (right panel) of the sample calculated using the elemental ratios and the model equations presented in Chapter 3.

Analysis of the N/C and O_{org}/C ratio was used to determine the protein and sugar content of the sample, from knowledge of model compounds as discussed in Chapter 3. For the first hour both the O_{org}/C and N/C increased, indicating an increase protein adhesion to the substrate. At 2 hours, there was a decrease in both O_{org}/C and N/C relating to a potential loss of organic compounds at the surface. The decrease in both O_{org}/C and N/C were at a similar rate, indicating the reduction was due to fewer proteins bound to the surface. After 2 hours, the O_{org}/C and N/C increase at a similar rate, indicating proteins binding to the surface. At 6

hours, the O_{org}/C rate increased at a quicker rate than N/C relating to both proteins and polysaccharides adhering to the surface. Analysis of the 24 hour sample compared to the 9 hour sample showed a decrease in N/C and a slight increase in O_{org}/C indicating polysaccharide adhesion was more dominant after the initial adhesion of proteins.

Analysis of the N/C and O_{org}/C ratio also correlate to the biological model modified from Rouxhet (2011). The additional points to observe were the polysaccharide content decreased for the first 2 hours and remains low until 6 hours, and the general decrease in hydrocarbon over time. The exceptions to the decrease in hydrocarbon over time was observed at 2 hours, where protein and sugar content decreases, and after 8 hours, where protein content decreases. Analysis of the calculated hydrocarbon contribution correlated to the Si 2p intensity, and by extension sample coverage, indicating a proportion of the hydrocarbon relates to exposed silicon. This was confirmed through the correlations between Si 2p and C285 observed in the carbon peak fit analysis.

5.1.2 Glass after 24 hours incubation with TSB

Glass was removed from incubation with TSB after 24 hours. The results of analysis of the incubated surface by XPS were compared to the reference autoclaved glass sample in Table 5.3. The XPS survey spectrum and carbon 1s spectrum are shown in Figure 5.9 and the results of the analysis are summarised in Table 5.3.

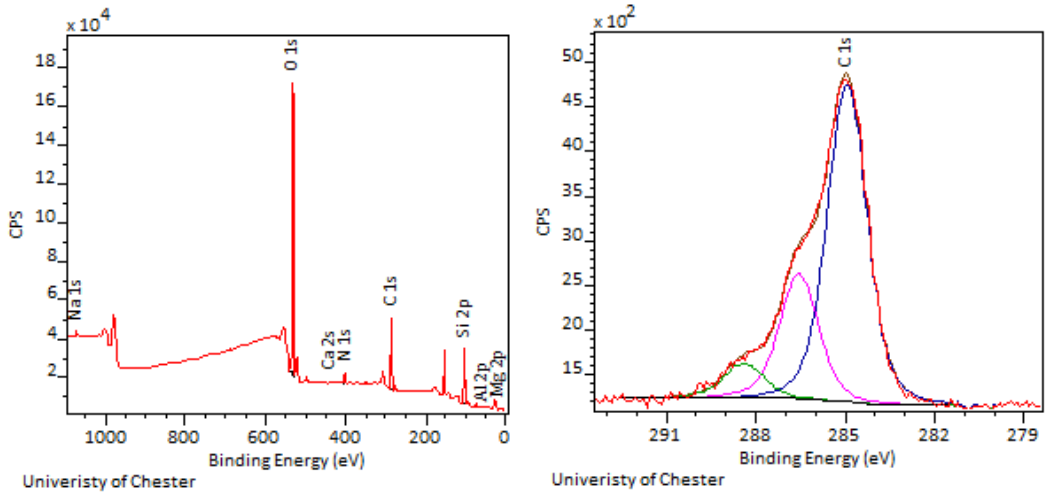

Figure 5.9 XPS survey and C 1s peak fit for 24 hour incubated glass in tryptic soy broth.

After incubation with media, C 1s peak decreased as Si 2p increased. This indicated the potential of replacing the atmospheric carbon layer to components of TSB, as seen in the decrease in coverage. The presence of TSB was assumed with an increase in N 1s and calculated O_{org} relating to proteins and polysaccharide content.

	Autoclaved glass	TSB incubated glass 24h
C 1s	42.3	30.6
O 1s	32.9	41.0
O_{org}	4.1	4.4
N 1s	0.6	2.8
Si 2p	17.3	22.1
Na 1s	3.1	0.3
Al 2p	0	1.6
Ca 2s	0.8	0.3
Mg 2p	3.0	1.3
C285	76.2	66.7
C286.5	4.9	26.1
C288	5.5	7.2
C289	1.9	0
C283	11.5	0
O_{org}/C	0.10	0.14
N/C	0.01	0.09
Protein	4.7%	32.5%
Polysaccharide	32.9%	4.4%
Hydrocarbon	62.4%	63.1%
Organic layer thickness	2.49 nm	0.86 nm
Coverage	74.1%	67.0%

Table 5.3 XPS analysis of glass incubated in tryptic soy broth after 24 hours

The XPS layer calculation showed the layer thickness decreases from 2.49 nm to 0.86 nm. This suggested that the some of the hydrocarbon layer formed on autoclaving was replaced on incubation with proteins and polysaccharides from TSB.

Analysis of C 1s peak fit indicated the presence of hydrocarbon as observed as a large peak at 285 eV on the surface, therefore the atmospheric layer could only be partially removed. The layer thickness decreasing to a value to similar to as received material confirms this and the presence of nitrogen and oxygen, with high density values showed the layer is a combination of atmospheric carbon and TSB components.

Using the O_{org}/C ratio and N/C ratio in biological compound models showed that the layer consisted of a high level of hydrocarbon (63.13%), potentially remaining from atmospheric hydrocarbons.

The biological model also showed low levels of proteins (32.45%) replacing some of the polysaccharides bound to the surface in the autoclaved sample.

5.1.3 Mica after 24 hours incubation with TSB

After 24 hours, mica was removed from incubation with TSB and analysed by XPS. Figure 5.10 shows the survey spectrum and C 1s peak fit, with Table 5.4 showing how the incubate sample compares to the autoclaved mica.

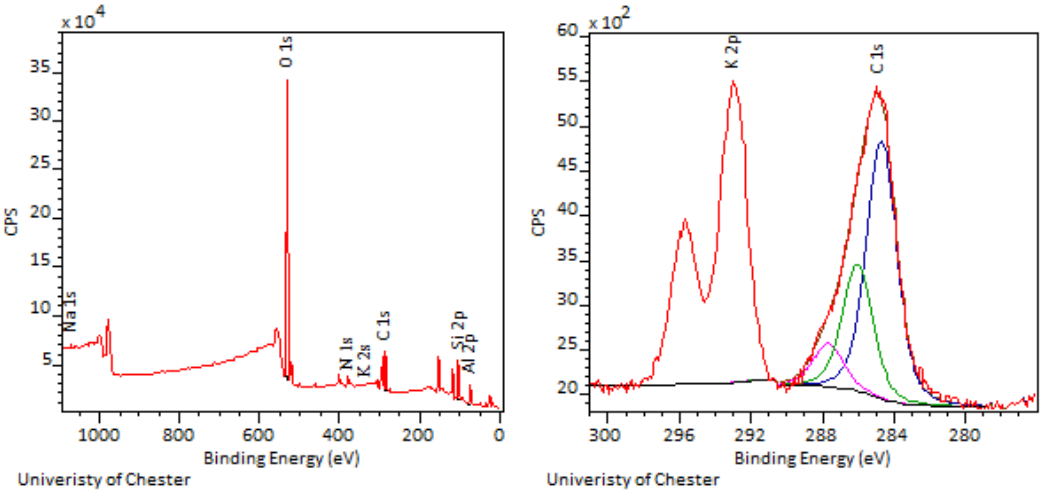

Figure 5.10 XPS survey spectrum and C 1s peak fit of TSB incubated muscovite mica after 24 hours.

	Autoclaved mica	TSB incubated mica 24 h
C 1s	18.9	17.6
O 1s	40.8	45.9
O_{org}	0.7	6.0
N 1s	0.0	2.9
Si 2p	21.4	18.8
Na 1s	0.4	0.2
K 2s	3.6	2.9
Al 2p	14.7	12.7
F 1s	0.2	0
C285	7.4	62.7
C286.5	89.0	27.9
C288	3.7	9.5
O_{org}/C	0.29	0.34
N/C	0	0.16
Proteins	0	58.1%
Polysaccharide	4.4%	18.1%
Hydrocarbon	95.6%	23.8%
Organic layer thickness	0.95 nm	0.48 nm
Coverage	7.5%	18.5%

Table 5.4 XPS analysis of mica incubated in tryptic soy broth after 24 hours compared to autoclaved mica.

The XPS spectra of mica incubated with TSB (Figure 8.10) shows the introduction of the N 1s peak as a representation of proteins on the surface. Apart from the introduction of nitrogen,

there are very little variations between before and after incubation. Analysis of the organic layer alone shows there was a slight increase in organic oxygen. The C 1s peak fit shows the decrease in hydrocarbons in the hydrocarbon layer as the layer is replaced with carbonyl and carboxyl groups as seen by the introduction of peaks at 286 eV and 288eV.

The O_{org}/C ratio was higher than that of N/C suggesting the layer formed was more protein like in nature**.** This was confirmed by modified biological models with some hydrocarbon (23.8%) and polysaccharides (18.05%) also present.

The layer thickness decreased, from 0.95 nm to 0.48 nm, which relates to the replacement of organic compounds at the surface, as the surface was predominantly proteins after incubation.

5.1.4 Titanium after 24 hours incubation with TSB`

Sputtercoated titanium was removed from incubation with TSB after 24 hours and analysed by XPS. Comparison of before and after incubating titanium in tryptic soy broth can be seen in Table 5.5. XPS peak analysis of the incubated sample can be seen in Figure 5.11. Two sets of coverage values were calculated, based on analysis of 2 batches of sputter-coated titanium in Chapter 4. One sample showed the atom percent of Ti 2p 9.68%, which was lower than subsequent samples, and the other showed an atom percent of Ti 2p 14.15%. The as received with a lower atom percent was used to calculate coverage 1, however as the atom percent is lower than that of the incubated sample, the calculated coverage is estimated to be negative.

The only additional peak observed was P 2s at 189eV which relate to low levels of phosphates from the media.

The increase in N 1s at 400eV peak and organic oxygen calculated in organic layer calculations showed there was an increase in both suggesting proteins and polysaccharides at the surface.

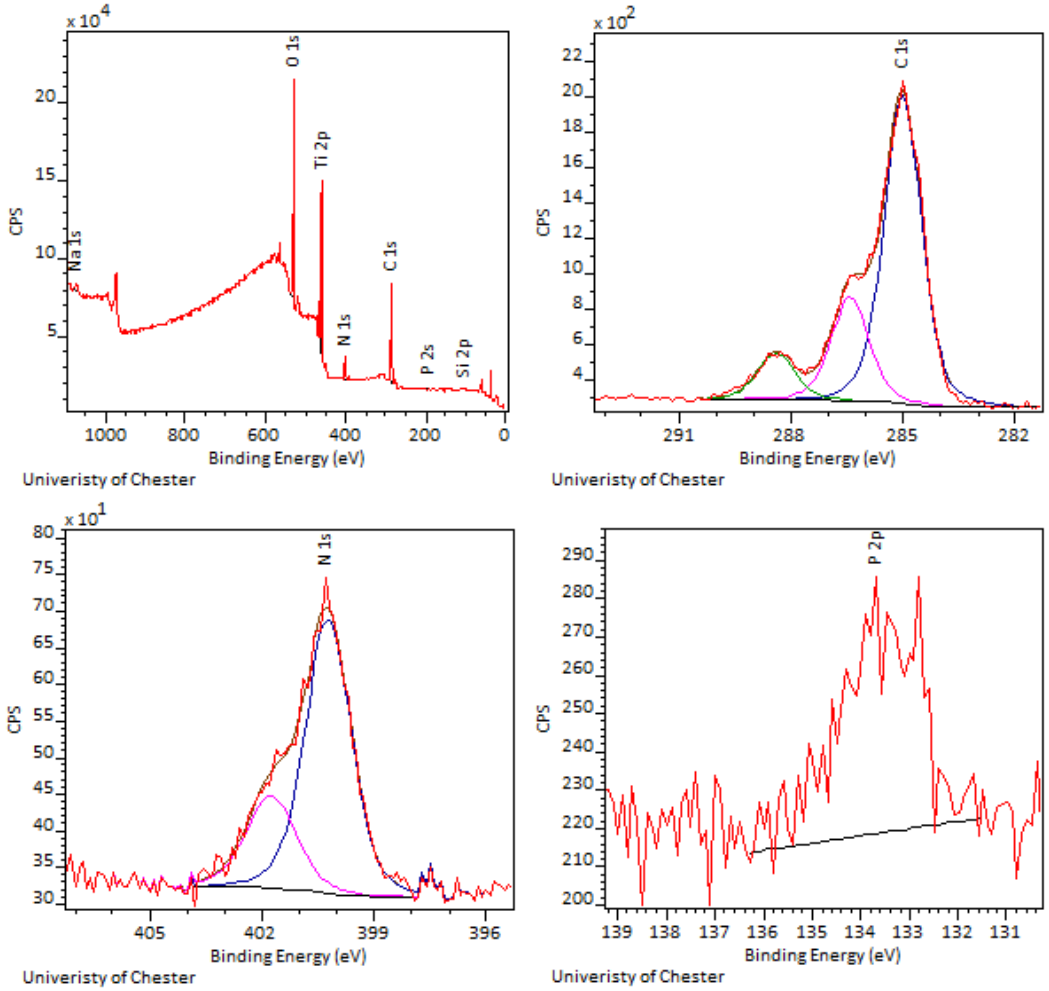

Figure 5.11 XPS survey spectrum (upper left), C 1s peak fit (upper right), N 1s (lower left) and P 2p (lower right) from the titanium sample after incubation in tryptic soy broth after 24 hours.

Decreases in the silicon and titanium signals showed that the substrate was covered by a material attenuating these signals, though did not correlate with an increase in the C 1s peak which was similar in value to autoclaved material.

This was also seen in the C 1s peak fitting, where the 284eV peak is reduced with stronger peaks at 286eV and 288eV, showing a replacement in hydrocarbon, to carbonyl and carboxyl groups, relating to proteins and polysaccharides. The increase in N/C ratio suggested there were more proteins at the surface. In comparison to the modified Rouxhet model, the surface had more proteins than polysaccharides on the surface, which was also reflected in the change in O_{org}/C.

Element	Autoclaved titanium	TSB incubated titanium 24h
C 1s	46.7	45.7
O 1s	35.7	36.0
O_{org}	18.4	22.2
N 1s	1.0	5.4
Si 2p	2.4	1.1
P 2p	0	0.6
Ti 2p	14.2	10.4
C285	89.4	67.3
C286.5	7.1	22.7
C288	3.6	10.0
O_{org}/C	0.39	0.49
N/C	0.04	0.12
Protein	12.5%	42.2%
Polysaccharide	42.4%	35.4%
Hydrocarbon	45.1%	22.4%
Organic layer thickness	3.13 nm	1.6 nm
Titanium dioxide layer thickness	1.51 nm	0.69 nm
Coverage 1	-29.1%	-7.0%
Coverage 2	11.7%	26.8%

Table 5.5 XPS analysis of sputter-coated titanium after 24 hour incubation in TSB compared to autoclaved titanium.

Changes in carbon bonding were observed as the Ti 2p and Si 2p intensities decreased. The decrease in layer thickness from 3.13 nm to 1.60 nm reflects a change in density of the material from atmospheric carbon to media constituents, with some effect of the hydrocarbon rinsed off the surface.

5.1.5 Silver after 24 hours incubation

Sputtercoated silver was removed from incubation with TSB after 24 hours and analysed by XPS. Table 5.6 shows the comparison between the samples before and after incubating with TSB. Figure 5.12 shows the XPS spectra and of the C 1s peak fit of the TSB incubated sample.

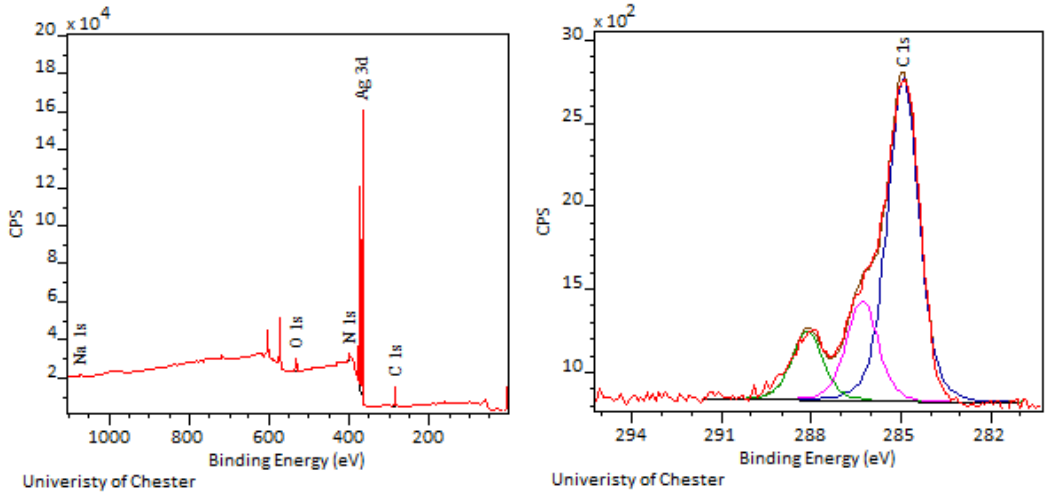

Figure 5.12 XPS survey spectrum and C 1s peak fit for silver incubated in TSB for 24 hours

Element	Autoclaved silver	TSB incubated silver 24h
C 1s	48.9	43.1
O 1s	8.6	11.8
O_{org}	8.3	8.4
N 1s	0	6.9
Na 1s	0	0.6
Ag 3d	42.5	37.5
C285	87.9	72.9
C286.5	8.8	16.6
C288	3.3	10.6
O_{org}/C	0.17	0.20
N/C	0	0.09
Protein	0	57.78%
Polysaccharide	20.5%	0.86%
Hydrocarbon	79.5%	41.35%
Layer	3.03 nm	1.4 nm
Coverage	18.3%	27.9%

Table 5.6 XPS analysis of autoclaved silver compared to silver incubated with TSB after 24 hours

The survey spectrum showed the presence of N 1s and Na 1s in addition to peaks expected from the autoclaved sample. The N 1s peak suggests the presence of protein whereas the Na 1s peak was most likely to be due to a residue from the NaCl in the media. The organic oxygen increased on TSB incubation. Together with the presence of N 1s this suggests the new layer consists of more polysaccharides and proteins.

The decrease in C 1s peak indicated the autoclaved layer was replaced by media constituents on incubation. This was further reflected in the change in layer thickness from 3.02 nm to 1.42 nm, which was a result of a denser layer formed of TSB components.

The decrease in Ag 3d signal supports the theory that layer formed was denser than that of the organic layer formed by autoclaving, therefore attenuating the silver signal to a greater degree.

Biological models based on O_{org}/C and N/C ratios showed there was a dominance of proteins (57.78%) on the surface with high levels of hydrocarbon (41.35%) also still observed, this was confirmed with the C 1s peak fit with a strong peak visible at 284eV and lower peaks at 286eV and 288eV.

5.2 AFM of media incubated materials

AFM data was analysed for coverage, roughness and force curve data. Force curve data is in Table 5.7 and graphed by measurement type in graphs in the relevant sections for further analysis. Frequency distributions were also used in the analysis of all measurements. Relevant examples are inserted in the sections below.

Coverage and roughness data were obtained through Nova PX software for each image and averaged over the number of images analysed. The depth chosen to calculate the coverage of the AFM images within the software were dependant on the size of features on each sample, larger than those of features on autoclaved samples.

Sample	Autoclaved substrate		TSB incubated substrate after 24 hours		
	Roughness AC RMS	Roughness AC RA	Roughness TSB RMS	Roughness TSB RA	Coverage TSB
Silicon	1.6	0.8	11.3	9.5	68.9%
Glass	23.3	11.7	14.1	10.4	87.0%
Mica	4.3	2.6	5.7	2.4	69.9%
Titanium	2.1	1.6	40.4	24.8	37.8%
Silver	7.0	5.3	19.9	12.8	57.9%

Table 5.7 AFM analysis of average roughness and root mean square roughness of the autoclaved and TSB incubated samples, as well as the TSB coverage of the sample estimated by AFM.

For most samples, roughness showed an increase after autoclaving, with the exception of mica and glass. As mica's roughness was similar to that of the autoclaved material, coverage calculations cannot be used, as it was assumed the coverage related to features on the sample. Glass showed a significant change in surface texture that coverage data was useable, with the decrease relating to washing of hydrocarbons on the surface, as defined by XPS data. Coverage data ranged from 37% to 87%. The image of glass incubated with TSB showed particles of a similar size to bacteria, however they were found to be thinner and of a slightly

different shape than bacteria used in this study. In this case is was assumed these particles were part of the glass residue and used in image analysis of coverage.

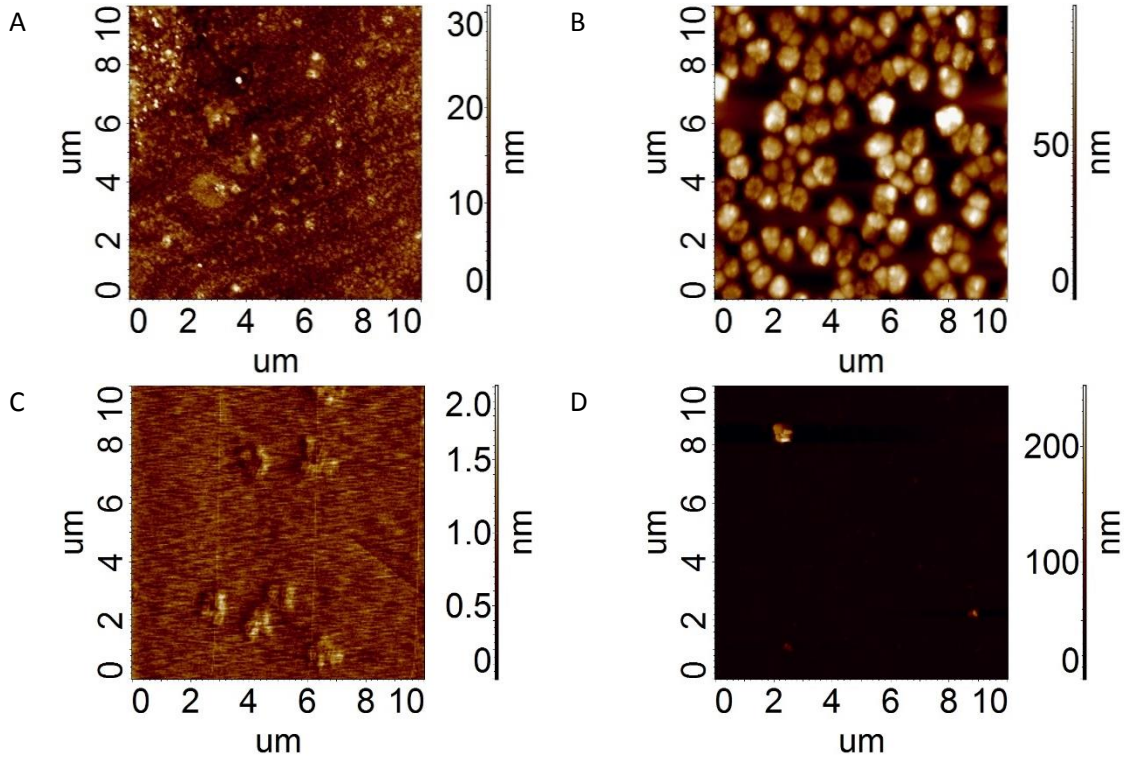

Figure 5.13 AFM images of glass and mica before and after incubation with TSB for 24 hours. A is autoclaved glass, B is glass incubated with TSB, C is autoclaved mica and D is mica incubated with TSB.

	Autoclaved				TSB			
Material	Snap in (nm)	Attractive force (nN)	Pull out distance (nm)	Retractive force (nN)	Snap in (nm)	Attractive force (nN)	Pull out distance (nm)	Retractive force (nN)
Silicon	5.0	25.7	21.3	144	6.1	49.1	8.8	77
	2.5	22.1	10.0	66	1.1	13.4	3.2	28
Glass	8.1	45.2	14.0	106	7.9	50.9	9.3	73
	2.8	27.5	2.8	25	3.0	25.4	4.9	40
Mica	6.6	52.4	29.2	256	1.2	11.3	3.0	47
	0.7	3.5	2.4	22	0.4	6.6	0.7	12
Titanium	2.0	6.5	2.4	13	3.3	23.7	9.1	76
	0.8	3.8	0.8	4	1.5	15.7	4.2	29
Silver	2.4	8.5	3.3	22	3.9	26.7	6.2	44
	0.6	4.2	1.5	10	1.2	13.2	1.6	13

Table 5.8 AFM force curve data and standard deviation for all substrates after 24 hour incubation compared to autoclaved force curve data. In all cases, the standard deviation is shown directly under the force curve data.

AFM force curves showed a range of variations across all materials. AFM data on media incubated samples were compared to that of the as acquired material and the autoclaved material. This was to define the effects of the over layer as a function of thickness, from autoclaved, and chemical structure, by as received data.

5.2.1 Snap in distance

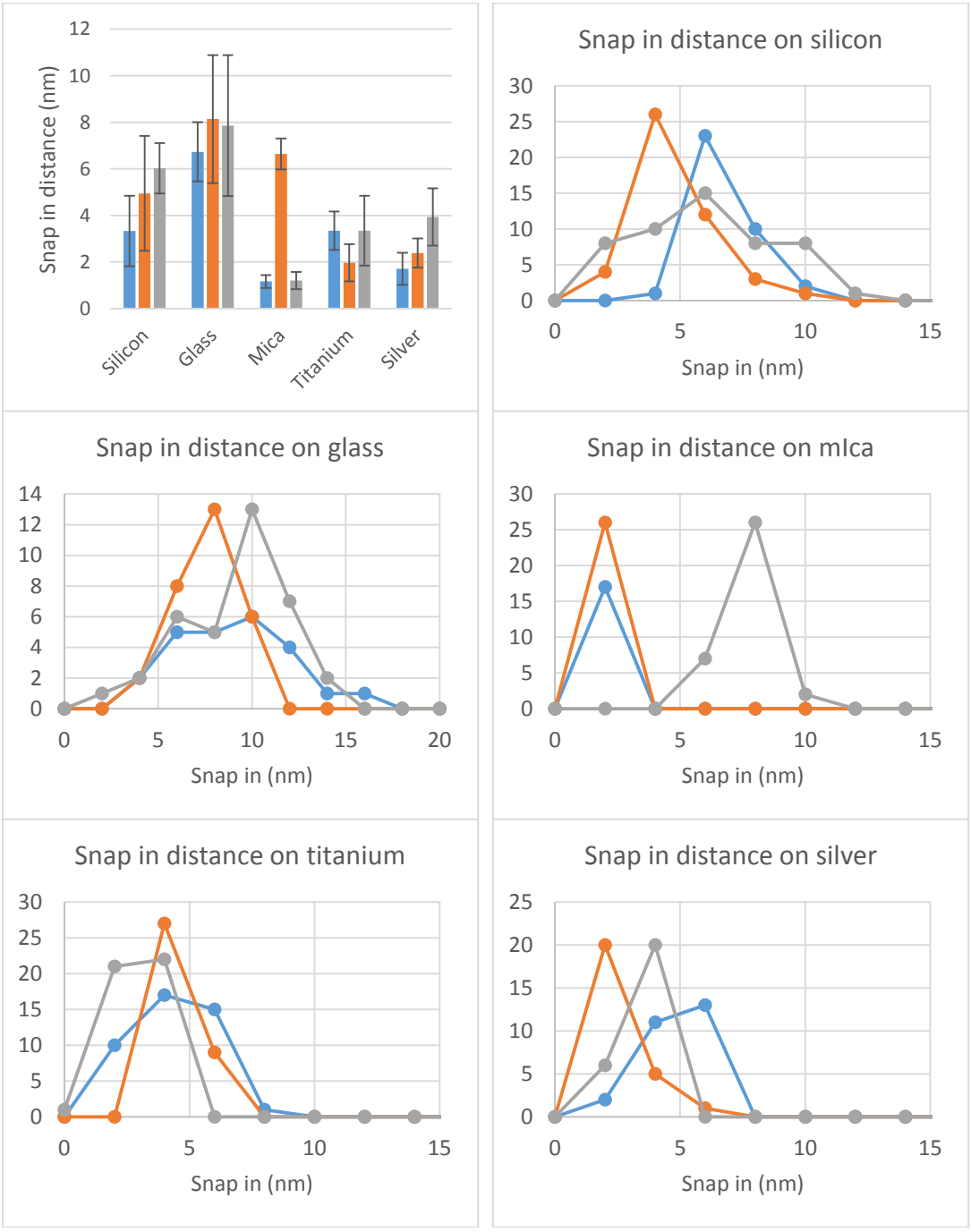

Figure 5.14 AFM snap in distances comparing the as-received, autoclaved and TSB incubated substrates (top left) with frequency distribution plots of the same data separated by material. Blue refers to the as received material, orange relate to the autoclaved material and grey relate to TSB incubated material.

On incubation, there was an increase in snap in distance on silicon, titanium and silver. There was a slight decrease on snap in distance on glass and a larger decrease in snap in distance on mica. On comparison to as received samples, titanium and mica media incubated samples were closest to as received samples. Silicon, glass and silver showed increases in snap in distance. This gives an indication to surface changes on incubation.

Standard deviations on silicon, titanium and glass incubated with TSB were large enough to overlap with that of the autoclaved sample, so frequency distribution plots were used to determine the extent of overlap. On incubation, frequency distributions on silicon showed smaller distributions on TSB incubated samples compared to autoclaved material. The reduction in distribution size relate to the decrease in variation in organic layer thickness.

Glass, silver and titanium showed a wider distribution, with the distribution of glass and titanium covering that of the as received and autoclaved, relating to the possibility of layer washing and layer replacement. Silver and silicon showed a shift to higher measured values, indicating the organic layer measured on autoclaving was covered.

Mica, as stated in Chapter 4, showed signs of capillary forces on autoclaving, which were lost on incubation with media. Snap in values for TSB incubated mica showed similarities to the as acquired substrate, showing the organic hydrocarbon layer was replaced on incubation, as snap in distance is a reflection of the layer thickness.

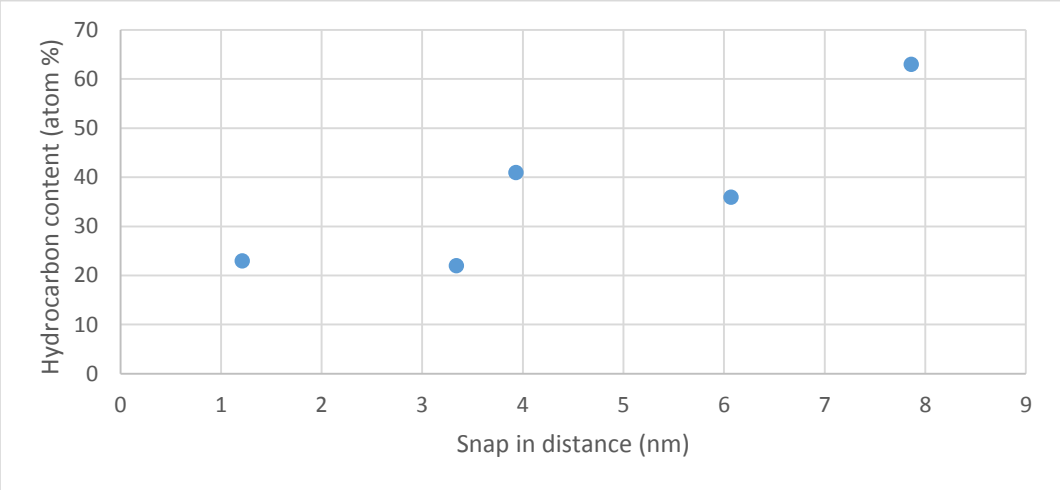

Figure 5.16 Scatterplot showing the correlation between snap in distance and hydrocarbon content.

Snap in distance variations relate to the resistive properties of the material and change of surface composition. Changes in snap in values relate to several factors, including surface composition and thickness of layers. The hydrocarbon content of the sample showed a direct correlation to snap in distances. As hydrocarbons are not as dense as proteins and sugars in

TSB, the AFM tip can pass easily through giving an indication of layer thickness. For proteins and sugars the tip finds more resistance on contact, giving lower snap in value. This indicates the snap in value was not a true representation of layer thickness, but an indication of surface composition with regards to media bound compounds.

5.2.2 Attractive force

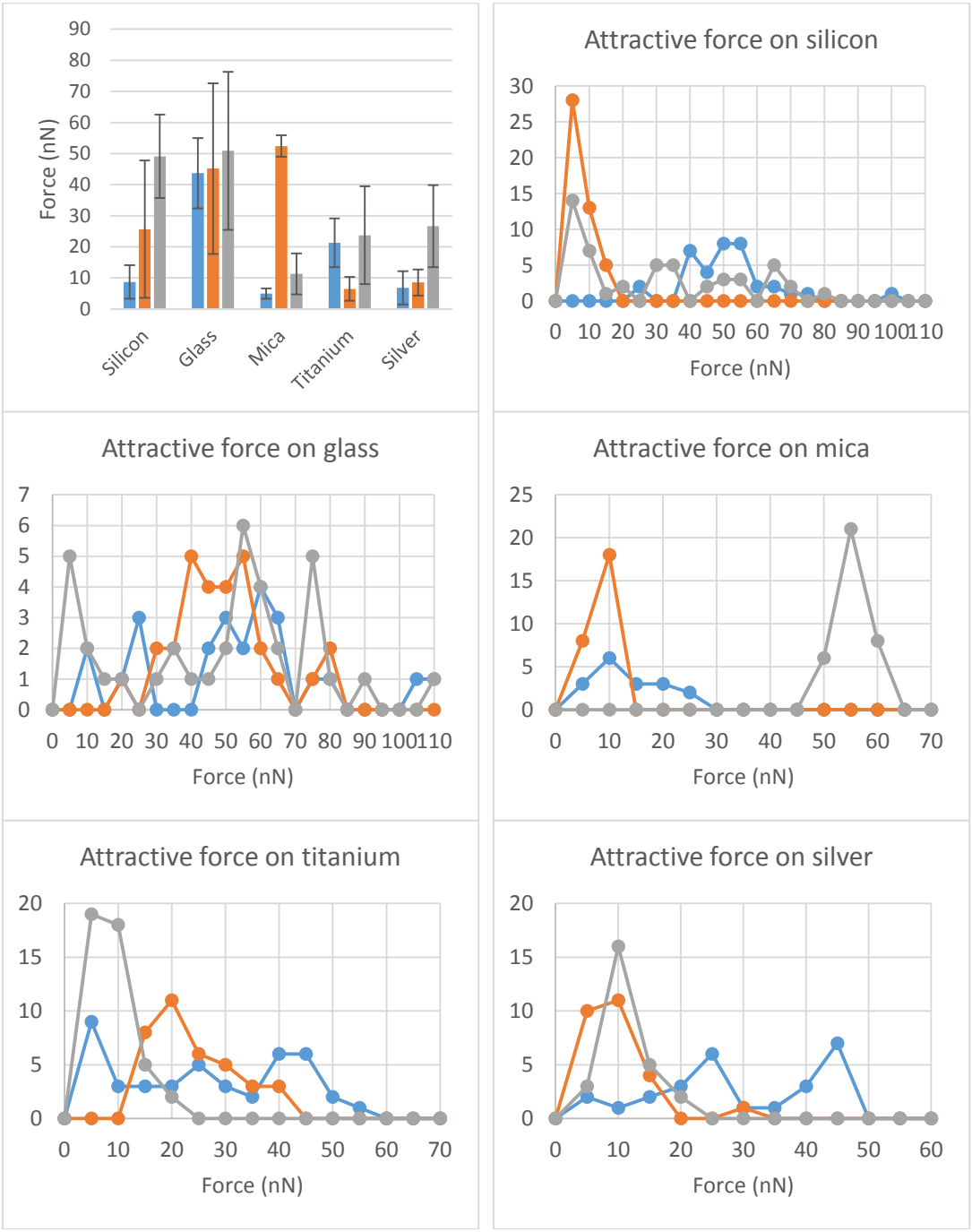

Figure 5.17 AFM attractive force comparing the as-received, autoclaved and TSB incubated substrates (top left) with frequency distribution plots of the same data separated by material. Blue refers to the as received material, orange relate to the autoclaved material and grey relate to TSB incubated material.

On incubation of autoclaved samples with media, most samples showed an increase in adhesive forces, relating to the property of the media. The exception to this was mica which showed a great decrease, which relate to loss of capillary forces. When comparing media incubated mica to as received mica, there was an increase in adhesive forces relating to a change in organic layer. On comparison to as received samples, all samples showed an increase in adhesion forces. Increases in attractive forces at the surface show the change in composition of the surface, to media components which were more adhesive than atmospheric hydrocarbons.

Frequency distribution plots for titanium and silver show a shift in attractive force for from autoclaved to TSB incubated samples, to higher values and wider range. Silicon and glass showed a smaller shift between autoclaved and TSB incubated sample.

5.2.3 Pull out distance

Comparing pull out distances of media incubated samples to autoclaved samples, there was a decrease observed on silicon, glass and mica. Titanium and silver increase in pull out distance. This is indicative of type of adhesive bonding. The increase showed there was a layer which is more adhesive than the original organic layer. The decrease in mica relates to capillary forces, whereas for glass and silicon, this decrease relates to the combination of hydrocarbons and polysaccharides at the surface being higher than the protein content, whereas the reverse was true for titanium and silver. The relevance of this refers to the internal bonding of these compounds, where proteins were long chains were known to show unfolding on retraction of the AFM tip, whereas polysaccharides do not show this feature and hydrocarbons were assumed to be too short to display this interaction. Frequency distributions showed overlap of autoclaved sample and TSB incubated sample, for silicon, glass, titanium and silver. Titanium showed 2 peaks, one of which overlaps with as acquired titanium, indicating the presence of patches of different types of organic compounds. Glass also showed multiple peaks that over the range of autoclaved and as received material, indicative of distinct regions of different organic material types. It was noted that the autoclaved glass substrate was the only sample to show a decrease in pull out distance on incubation in TSB.

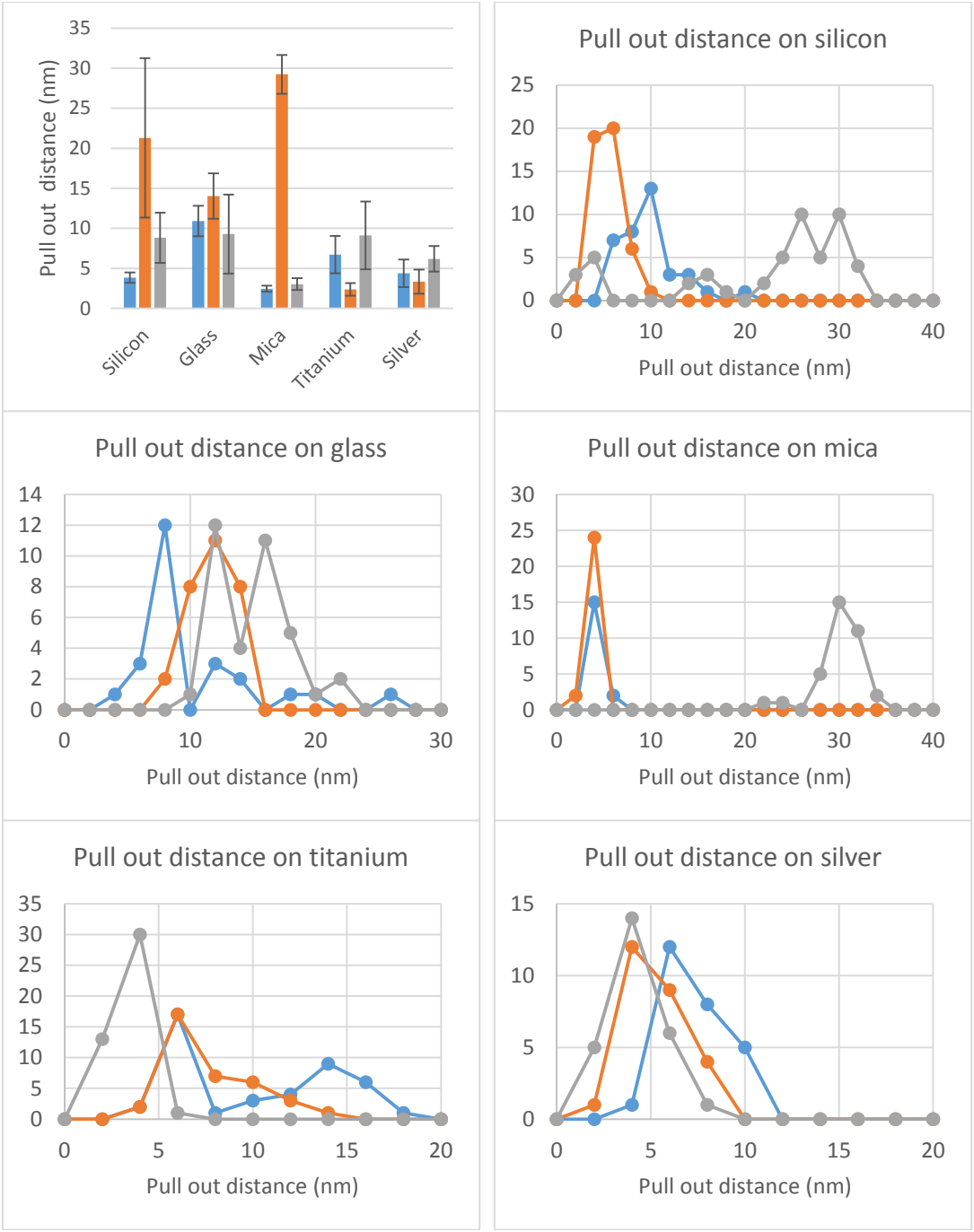

Figure 5.18 AFM pull out distance comparing the as-received, autoclaved and TSB incubated substrates (top left) with frequency distribution plots of the same data separated by material. Blue refers to the as received material, orange relate to the autoclaved material and grey relate to TSB incubated material.

5.2.4 Retractive force

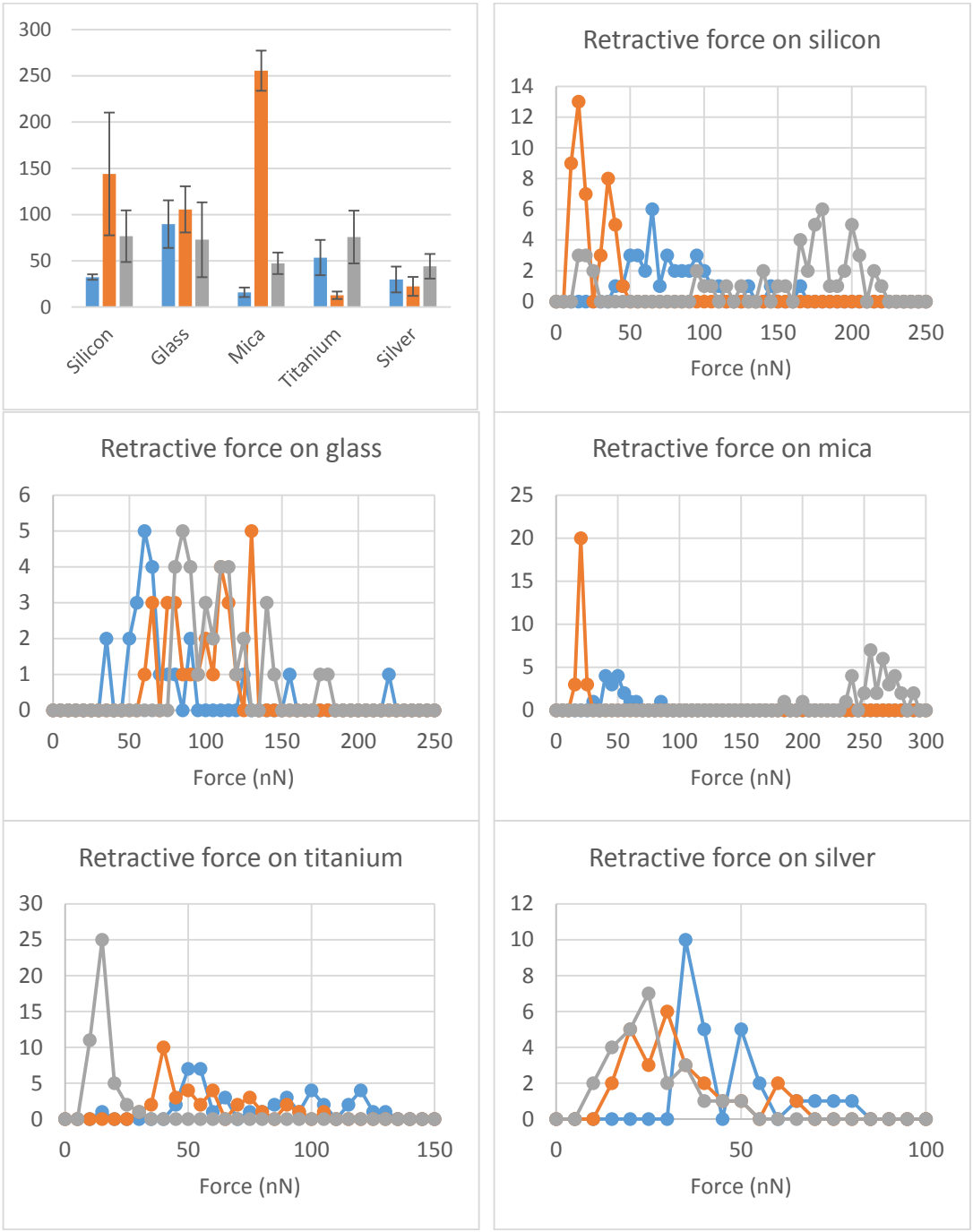

Figure 5.19 AFM retractive force comparing the as-received, autoclaved and TSB incubated substrates (top left) with frequency distribution plots of the same data separated by material. Blue refers to the as received material, orange relate to the autoclaved material and grey relate to TSB incubated material.

Retractive forces relate to the adhesive nature of the layer formed. On glass, silicon and mica, there was a decrease in adhesive force. Titanium and silver increase in retractive force. Apart from glass, all samples showed an increase in adhesion compared to as received materials. Glass showed a slight decrease, but within the standard deviation. Frequency distributions confirm this, and large ranges were seen on most sample, with silver and mica showing a

smaller range. Large ranges were indicative of patches of different organic compounds bound to the surface. Similarities between glass and silicon were observed, as well as similarities between mica and silver.

5.2.5 Summary of material analysis by AFM

Overall, AFM data showed some variations across materials which when combined with other information about the surface can be developed into a model of what is happening at the surface.

Mica showed the largest decrease across all measurements, showing capillary forces measured from autoclaving has been significantly reduced. Instead comparing to the as received sample, to ignore capillary action values were closer in value, the snap in and pull out values reflect the properties of the surface, with both samples having relatively thin organic layer, majority of attractive forces after initial content was related to the mica substrate. The adhesion value increase reflected the change in composition of the organic layer which was protein dominant.

Glass showed the least variation in AFM data, showing the material was the main contribution to force curve data. The small changes in values relate to the small amounts of protein on the surface. Overall, the organic layer on glass had not varied much on incubation with TSB, with higher levels of hydrocarbons remaining at the surface, indicating this was the predominant contributor to force curve data.

Silver showed an increase in all force curve data on incubation with TSB. As the surface was protein dominant, increases in adhesion was related to the change in surface composition. With the one highest amount of proteins on the surface, along with minimal polysaccharides, it was assumed that despite the overall layer thickness decreases, the overall probability of probing protein was higher and therefore reflected in the snap in and pull out distance. The increased sample roughness compared to other samples still play a role in adhesive properties, as titanium was more exposed in some areas, and may have some contribution to binding.

On incubation in TSB, the titanium surface showed an increase in the snap in, attractive force, pull out distance and retractive forces, measured by AFM. The media incubated titanium values were closer to that of the as received sample than to the autoclaved sample. This indicated the effect of autoclaving may have been temporary, with the film formed during autoclaving being displaced by TSB.

Silicon also had a higher protein to polysaccharide ratio, with higher levels of hydrocarbon. The increase in layer thickness showed the SiO_2 layer has a higher organic coverage. This was reflected in the snap in distance increase. The increase in attractive forces reflect the change in layer composition, and the decrease in retractive forces showed this change as a reduction in hydrocarbon bonding and increase in polysaccharide content. The pull out distances measured on polysaccharides were expected to be shorter than that of proteins due to the effect of protein unfolding. Retractive forces would also be lower. The resistive nature of the new layer was reflected in the decrease in pull out distance in comparison with the results from the autoclaved sample but increased in comparison to as received material. This showed the replacement of the autoclaved organic layer being with media, with some of the original hydrocarbon layer bound to the silicon was observed.

5.3 Conclusions

XPS data on all substrates showed an increase in organic oxygen and nitrogen. This suggests the incubation of TSB introduces the binding of proteins and polysaccharides to the surface, with some hydrocarbons still bound to the surface.

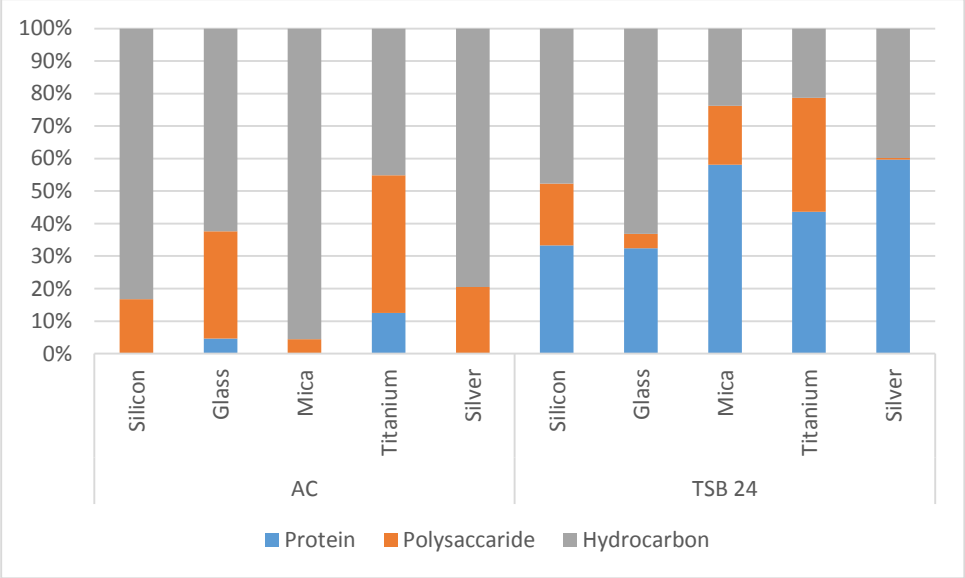

Figure 5.15 Diagrammatic representation of the change in biological composition after incubating with TSB for 24 hours. Note that the autoclaved samples does not have protein or polysaccharide on the surface, the apparent concentrations of these species are a result of applying the method of Rouxhet (2011) to the measured data.

Comparing the compounds on the surface of TSB incubated samples, there were variations between materials to the apparent ratio of proteins and polysaccharides bound to the surface, as determined through Rouxhet's modified model.

Comparing the C 1s peak fit and defining peak showed an anti-correlation between the two, and the possibility that atmospheric carbon still bound to the surface. This was confirmed with timed TSB incubated samples, with hydrocarbon coverage correlating to exposed silicon.

The presence of atmospheric carbon on the surface led to a miscalculation of layer thickness, however separating the layers based on XPS composition was also inaccurate due to the unknown nature and distribution of components on the surface, so the calculated layer thickness discussed is a good estimate. The composition of the layer is unknown, as detecting biological content from below the TSB layer is not possible.

A similar issue arose with timed samples, where if coverage was uneven, the XPS results varied between samples. Variation in coverage can arise from washing, but more likely occur from subsampling and uneven coverage. Subsampling was unavoidable due to issues with contamination and must be taken into account on analysis. By extension washing falls into the same issue as subsampling, as each sample was treated separately.

Sample	Autoclaved organic (nm)	TSB layer (nm)
Silicon	1.08	1.26
Glass	2.49	0.88
Mica	1.08	0.47
Titanium	2.87	1.54
Silver	3.02	1.42

Table 5.9 Layer thickness values before and after autoclaving.

Analysis of the coverage of the materials determined by XPS show a potential coverage of up to 80%. This poses a difficulty in measuring the bacterial coverage of the sample. High coverage data indicated either thick patches or mid-range thicknesses (3-5 nm) with the former being more plausible from AFM imaging and XPS variable coverage values. In either case, using the repression of silicon signal as an indication of further treatment, in particular bacterial adhesion, would result in overestimation of additional coverage giving inaccurate results.

The limitations of XPS has an effect on results analysed, but gives an overview of the surface composition, which can be used to model the components bound to the surface. This initial can be used to determine the approximate thickness and composition to determine its difference from bacterial excretions as well as the effect of biological compounds on the surface.

Analysis of formation of the growth medium incubated layer against time has shown that binding of proteins to the surface happens within the first hour, with further binding or replacement of proteins and polysaccharides occurred after about 5 hours. Analysis of how this relates to bacterial growth and adhesion is discussed in Chapter 7 and 8.

AFM force curves showed a range of variations across the different substrates. Attractive forces were typically higher across media incubated samples than on the autoclaved reference samples. Mica was the only sample not to show the same increase in attractive force when compared to autoclaved samples. This was believed to be due to the reduction in capillary forces measured on autoclaved mica samples.

Snap in distances measured overestimated the layer thickness when compared to XPS layer thickness calculations. However, analysis of biological composition indicated the higher the hydrocarbon content the higher the snap in value. Hydrocarbon content was assumed to be predominantly from exposed substrate, which was found to affect the accuracy of the layer thickness calculations. As previously noted, the exposed substrate influences the snap in value, indicating there was still some substrate material influence on overall snap in values for TSB incubated samples. Typically snap in distances were often overestimates of the layer thickness as there is a degree of attraction between sample and tip prior to the tip encountering the overlayer.

	Layer thickness calculated	Snap in average	Hydrocarbon (%)
Silicon	1.29	6.02	36.06
Glass	0.86	7.86	63.13
Mica	0.48	1.2	23.8
Titanium	1.60	3.34	22
Silver	1.40	3.93	41

Table 5.10 Layer thickness against snap in value and hydrocarbon content for samples incubated with TSB for 24 hours

Retractive forces showed a direct correlation with protein content, with higher adhesion values having a lower protein content. Similarly, pull out distance and protein content showed a similar trend. This showed that protein content can loosely be identified through retractive forces and pull out distances, as typically proteins are less adhesive than atmospheric carbon and polysaccharides and showed more resistance to the AFM tip.

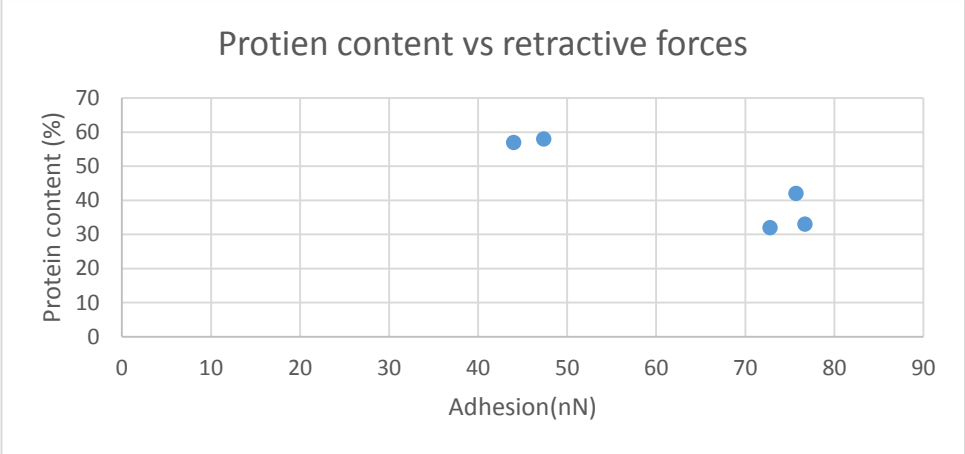

Figure 5.16 Correlation of protein content and retractive forces.

Overall, force curves showed correlations with the biological compound composition of the sample, predominantly proteins and hydrocarbons. The snap in distances appear to be related to the hydrocarbon content whereas protein content was more related to adhesion values (pull-off force). Differentiation between polysaccharides and hydrocarbons were difficult to distinguish by AFM alone but were clarified using XPS data.

Chapter 6 Analysis of Bacteria Surfaces in Native (non-Biofilm) State

As discussed in Chapter 3, *S. epidermidis* is a gram positive bacterium with the potential to form a biofilm and to adhere to surfaces. To provide reference data for the bacteria surfaces in their native state, i.e. prior to formation of a biofilm, analyses were carried out on bacteria prepared as (1) a re-dispersed pellet on either Si (111) wafer surfaces and (2) filtered as a lawn sample on a cellulose triacetate filter. Sample preparation was according to the method described in Chapter 3. Defining the chemical composition, elasticity and adhesive nature of the bacteria in this non-biofilm state contribute to understanding and modelling of the changes that occur on incubation to form biofilms.

The typical outer structure of gram positive bacteria in shown schematically in Figure 6.1 (Todar, 2008). The outer layer of the cell wall consists of several layers of peptidoglycan sheets with teichoic acid molecules passing vertically through them. This layer is based on a cytoplasmic membrane underlayer with phospholipids interspersed with protein molecules. The peptidoglycan sheets consist of alternating proteins and sugars linked together, with the base units being n-acetylglucosamine and n-acetylmuramic acid, as shown in Figure 6.2 (Romaniuk, 2015). In XPS, these would be expected to give approximate elemental compositions of C_7O_6N and C_9O_8N respectively. In both these structures the N 1s line would be expected at a binding energy corresponding to an amide-like (amino-) structure. The structure of the interpenetrating lipoteichoic acid is shown in Figure 6.2. With a repeat unit number of approximately 40, the structure shown would give an approximate expected XPS composition of $C_{35}O_{22}P_5N_5$. The cell wall thickness of gram positive bacteria is generally in the region of 15 – 80 nm (Todar, 2008), i.e. greater than the XPS information depth and therefore any phosphorous in the XPS spectra must have originated from the lipoteichoic acids. The nitrogen environment in the lipoteichoic acid is more amine-like compared to the amino environment of the peptidoglycan and therefore it should in principle be possible to distinguish between the two from the N 1s line binding energy.

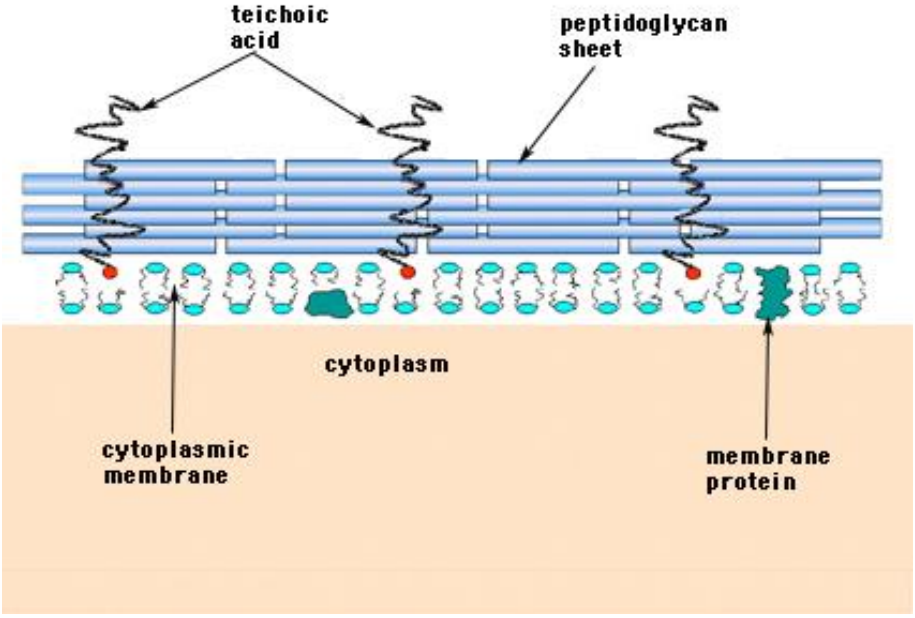

Figure 6.1 Structure of the outer structure of a gram positive bacterium. Todar, 2008).

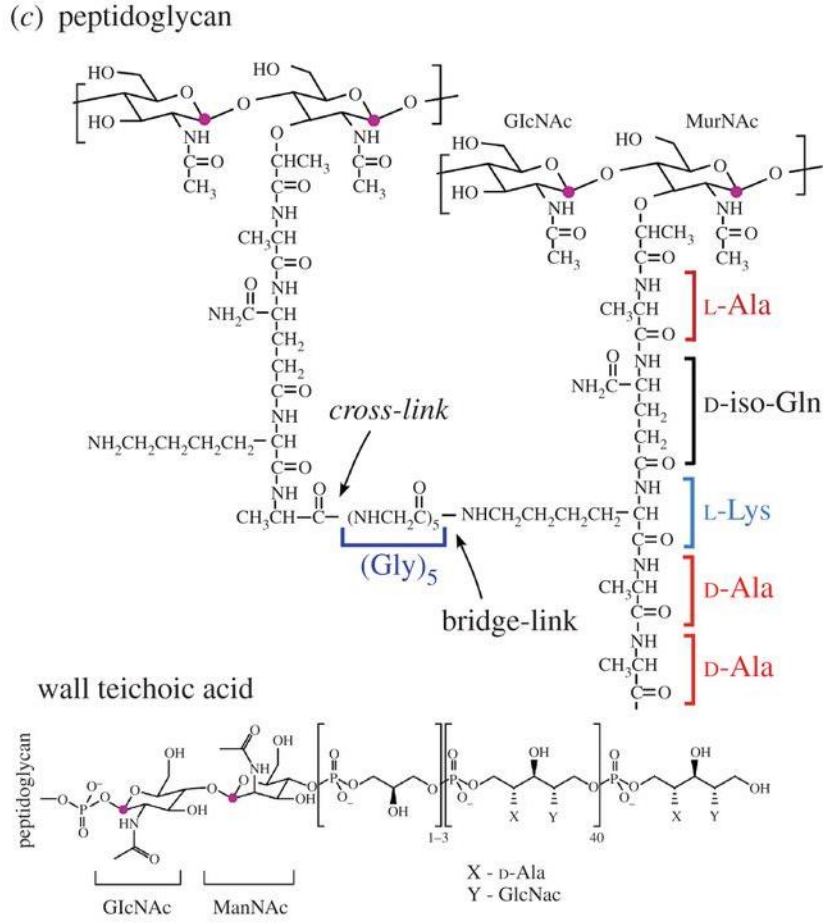

Figure 6.2 Schematic structure of peptidoglycan and teichoic acids of S. aureus taken from Romaniuk (2015)(Romaniuk & Cegelski, 2015), where GLcNAC is n-acetylglucosamine and MurNAC is n-acetylmuramic acid.

Knowledge of these can, in theory be applied to the biological model by Rouxhet (2011), described in Chapter 3, however the model is limited by the complexity of compounds at the surface of the bacteria. While Rouxhet et al. and van der Mei (1997) discuss methods to overcome this, both models are limited in the methods to calculate the biological structures on the surface. This was discussed further in Chapter 2. In this chapter, analyses of the bacterial structures were made using the O_{org}/C, N/C and P/C values.

6.1 XPS analysis

As described above, samples for XPS were prepared in 2 ways, either by redepositing a bacterial pellet on Si (111) using distilled water or by filtering the pellet material in saline onto a cellulose triacetate membrane. The absence of the TSB growth media in both cases should give data to which is purely bacterial. Both preparation methods have been reported in the literature (Cerca et al., 2005; van der Mei et al., 2000). Generally, the lawn preparation is preferred as the cells are kept closer to their physiological condition and the method is therefore less damaging.

	Pellet *NCTC13360*	Lawn *NCTC13360*	Pellet *ATCC35984*	Lawn *ATCC35984*	van der Mei, 1997 *ATCC35984*
C 1s	60.2	61.2	59.9	60.6	-
O 1s	25.1	25.9	25.7	23.4	-
O_{org}	23.9	25.9	25.1	23.4	-
N 1s	9.3	7.1	8.5	7.0	-
Si 2p	1.4	0	2.9	0	-
P 2s	3.7	3.5	2.5	1.9	-
Na 1s	0.1	1.1	0.4	2.1	-
Ca 2s	0.3	0	0	0	-
Cl 2p	0	1.3	0	5.0	-
285	48.9	49.6	38.3	39.1	-
286	35	40.6	44.4	44.9	-
288	16.2	9.8	17.4	16.0	-
O_{org} /C	0.40	0.42	0.42	0.39	0.552
N/C	0.16	0.12	0.14	0.12	0.147
P/C	0.06	0.06	0.04	0.03	0.048

Table 6.1 Results of XPS analysis of *ATCC35984* in pelleted and lawn form compared to literature data from van der Mei,1997(van der Mei et al., 1997).

XPS composition data for the lawn and redispersed pellet samples of the two bacterial strains are summarised in Table 6.1. The data of van der Mei et al (1997)(van der Mei et al., 1997) for one of the strains was also included. Survey spectra and scans over individual C 1s, O 1s, P 2p and N 1s spectra for the two samples are shown in Figure 6.3Figure 6.35.

The lawn sample was prepared to a density of approximately 10^8 cells per mm^2 as described in Chapter 3. Assuming a minimum cell size of approximately 0.5 µm in diameter and close-packing, this translates to a layer thickness of approximately 25 cells, or 12.5 µm. This is more than sufficiently thick to ensure that the XPS data reflect the composition of the bacteria alone, with no contribution from the underlying cellulose triacetate substrate.

S. epidermidis, *NCTC13360*, showed similarities between pelleted and lawn samples. The presence of teichoic acids was implied in the presence of P 2s peak, whereas potential proteins and polysaccharides were represented by oxygen and nitrogen peaks being detected. This was supported by the C 1s peak fit which showed the related higher carbon bonding of 286.5 eV and 288 eV, for carbonyl and carboxyl binding in the sample. The N 1s peak fit showed a dominant peak at 400ev indicative of amino groups. This was likely to be due to the external bacterial peptidoglycan layer.

The variation of O_{org}/C and N/C showed the presence of peptidoglycan, with low levels of P/C indicating the presence of teichoic acids. Variations between the pellet and lawn samples relate to the preparation method, with the pellet sample showing residual proteins on the surface or the lawn sample showing an additional source of carbon. The lower P/C ratio in the lawn sample indicate the additional carbon compound in the lawn sample was more likely, as the bacteria in this sample was assumed to be sufficiently thick to supress the signal from the underlying membrane.

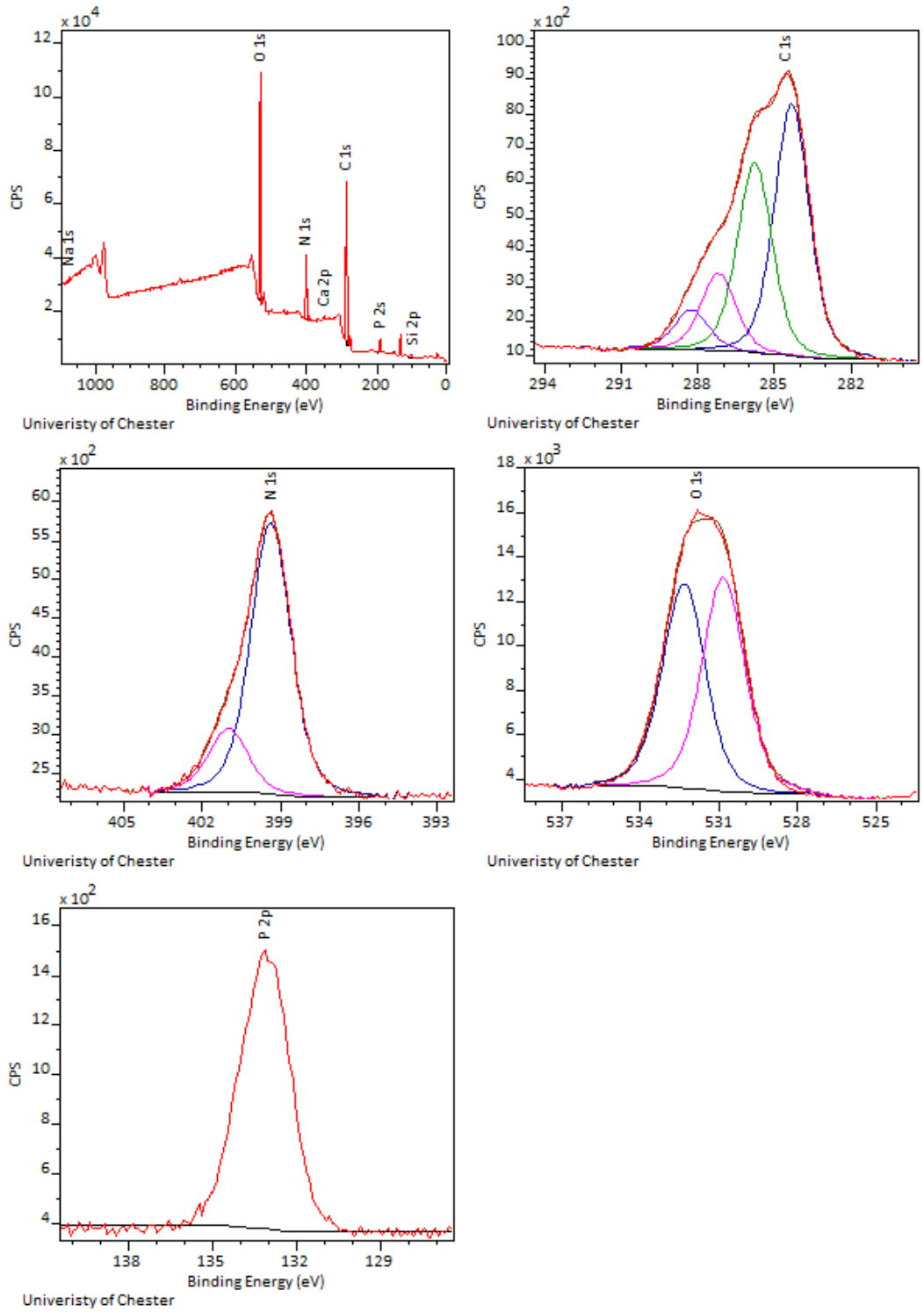

Figure 6.3 XPS survey, C 1s, N 1s, O 1s and P 2p peaks of *NCTC13360* pellet redispersed onto silicon.

For both pellet and lawn samples of *ATCC35984*, XPS data showed similarities in composition. The survey spectra showed high levels of C 1s, of which component peaks at 286.5 eV and 288 eV were considerably higher than was the case with silicon alone. The presence of N 1s and relatively high levels of oxygen suggest the presence of biologically relevant compounds.

The presence of the P 2p signal at 133 eV indicated the presence of teichoic acids, passing through the peptidoglycan layer.

The low value of P/C suggests the layer consisted of other compounds. Analysis of N/C and O_{org}/C suggests the presence of peptidoglycan, with the P/C ratio indicating the presence of teichoic acids. Variation in O_{org}/C, N/C and P/C was attributed to the presence of an additional carbon compound in the lawn sample, as all 3 values decrease. The O_{org}/C and P/C decrease in the lawn sample can be attributed to lower P 2s signal, assumed due to the phosphate component of peptidoglycan. This also decreased the O_{org}/C ratio significantly. Overall, this indicated the presence of less bacteria on the lawn sample or potentially the detection of an additional organic layer. The presence of an additional organic layer was more feasible as the lawn sample is assumed to be 100% bacterial.

S. epidermidis ATCC35984 was also compared to the results of van der Mei (1997), who prepared the samples by formation of a pellet as described in Chapter 3, followed by freeze drying and pressing into stainless steel cups. The analysis of *ATCC35984* as analysed by van der Mei discussed the cooperation of the O/C, N/C and P/C ratios of analysed bacteria, which is more reproducible. The data in the table are assumed to indicate the O/C as O_{org}/C, as the analysis of pellet samples as described by van der Mei (1997) does not discuss the detection of any non-bacterial signals.

In comparisons to van der Mei, values of N/C fall within a similar range to the pelleted sample, and higher than the lawn sample. The O_{org}/C ratio measured by van der Mei was higher than those measured through pellet and lawn samples, indicating the presence of an additional oxygen containing compound on the surface. This higher O_{org}/C ratio may be attributed to the higher amount of phosphate compounds on the surface as seen in the higher P/C ratio.

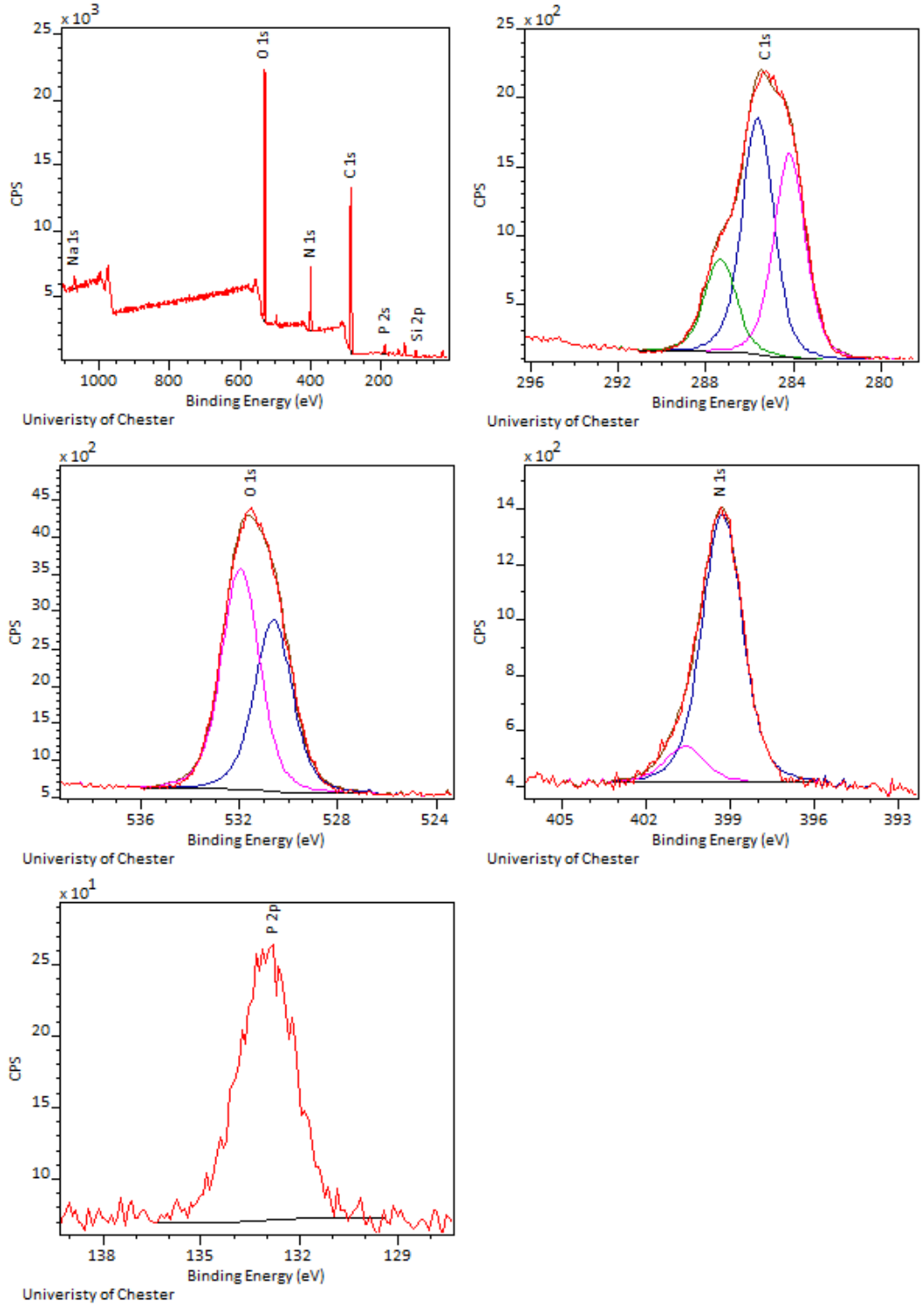

Figure 6.4 XPS survey spectra, C 1s, N 1s, O 1s and P 2p of *ATCC35984* pellet redispersed onto silicon along with N 1s peak fit and phosphorus peak.

Overall the composition of both bacteria showed similar compositions. A significant proportion of the composition was carbon based, with higher peaks at 286.5 eV and 288 eV which corresponds to the higher values of oxygen and nitrogen observed compared to autoclaved samples. The presence of phosphorus in both samples was to be expected, due of the presence of teichoic acids in the main bacterial structure, or DNA. The chemical

composition indicated the thick peptidoglycan layer, with teichoic acids passing through, as expected of the outer layer of a gram positive bacteria. An additional organic layer was detected in the lawn samples, confirmed by the reduction of P/C.

6.2 AFM analysis

Non incubated bacteria were analysed by AFM on pellet samples only. This was to allow characterisation of the bacteria without any external influence of the membrane on the force curve data. Additionally, as bacteria were deposited on silicon, it is easier to characterise substrate effects due to the tip consisting of silicon nitride, as well as the comparison between adhered bacteria to silicon in later chapters. Images of both strains of bacteria in Figure 6.5 indicated the presence of bacteria for XPS analysis as well as the similarities in structure of both bacteria.

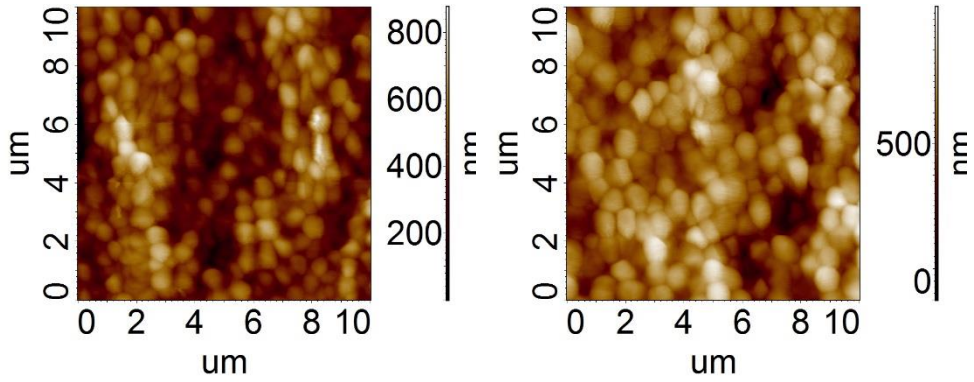

Figure 6.5 AFM images of *ATCC35984* (left) and *NCTC13360* (right) pellets deposited (redispersed) on silicon

The force curve data in Table 6.2 compare the results for *S. epidermidis* to previous silicon samples, to TSB incubated silicon after 24 hours and to autoclaved silicon on which the pellet was deposited. The data is also shown graphically as frequency distributions in Figures 6.6 and 6.7.

	Snap in (nm)	Attractive force (nN)	Pull out (nm)	Retractive forces (nN)
Autoclaved silicon	5.0	26.8	21.4	144
	2.7	23.3	9.7	64
TSB incubated silicon	6.0	49.1	8.8	77
	1.1	13.4	3.1	28
ATCC35984 pellet	3.1	2.8	6.8	11
	2.1	2.5	6.8	6
NCTC13360 pellet	2.5	3.4	7.8	14
	1.4	2.4	4.7	8

Table 6.2 AFM force curve data and standard deviations comparing bacterial pellets on silicon, 24 hour incubated silicon in media and autoclaved silicon. For each sample, the first row shows the average values and the row underneath shows the standard deviations.

Force curve data between each strain of bacteria were similar, relating to the similarities between the outer structures of the bacteria. Adhesion force differ from that of TSB incubated silicon, relating to adhesive properties of media discussed in Chapter 5. High standard deviation values on pelleted bacteria led to the use of frequency distribution plots instead of histograms to determine the nature of interactions.

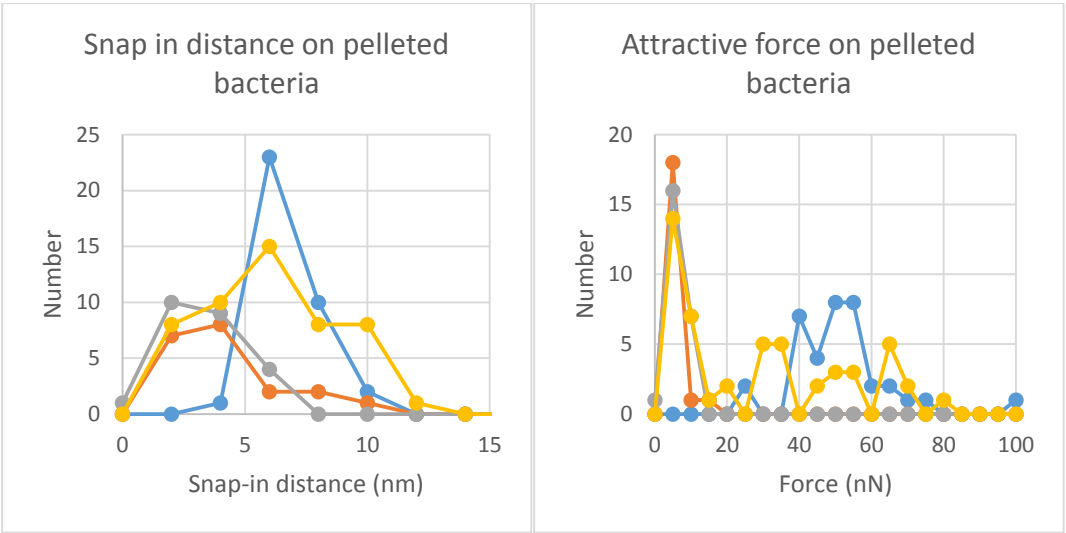

Figure 6.6 Frequency distribution plots of snap in distance and attractive force values, where yellow indicates autoclaved silicon, blue indicates TSB incubated silicon after 24 hours, grey indicates the NCC13360 pellet and orange indicates the *ATCC35984* pellet.

Snap in data showed similarities between bacterial strains with low values suggesting the depth the tip can penetrate was quite small and relates to the outer structure of the bacteria with a low level of hydrocarbons on the surface. Similarities to autoclaved material relate to the comparable depth the tip can penetrate on each sample, with the bacteria overall

showing a narrower range. On comparison to TSB incubated silicon, the depth the tip can penetrate bacteria was smaller, and relates to the repulsive nature of the outer layer of the bacteria.

Attractive force values were similar between bacterial strains and have some overlap with autoclaved silicon that can be assumed was related to a thin overlayer of atmospheric hydrocarbons. The difference between TSB incubated silicon and bacteria will be used to identify the difference in layer formed on incubation in later chapters and reflect the less adhesive nature of the bacteria.

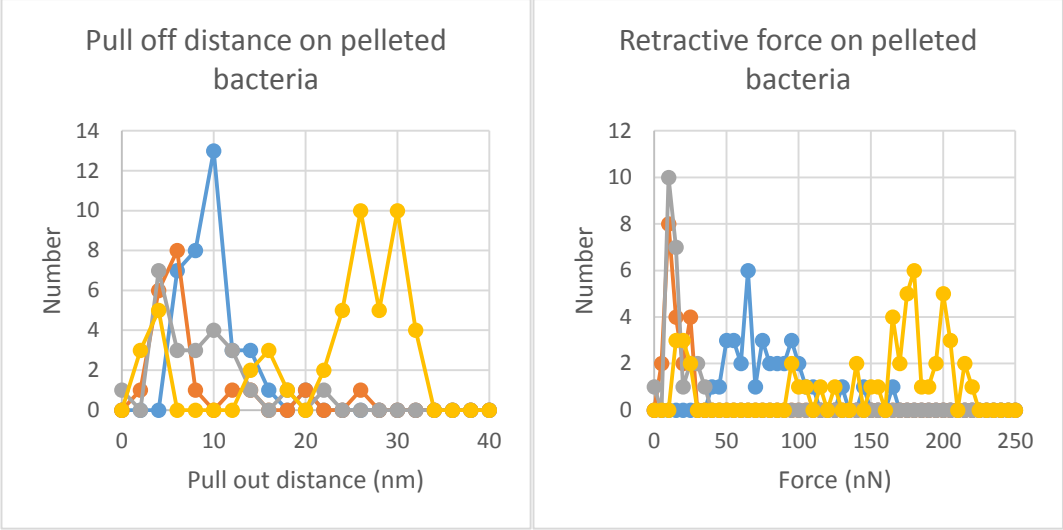

Figure 6.5 Frequency distribution plots of pull out distance and retractive force values, where yellow indicates autoclaved silicon, blue indicates TSB incubated silicon after 24 hours, grey indicates the NCC13360 pellet and orange indicates the *ATCC35984* pellet.

Pull out distances from the bacteria samples showed slight variation between the bacterial strains. Similarities between strains relate to the similarities of the structure of both strains, with variations indicated the outer structure was not identical. Both strains showed similarities to TSB incubated silicon indicating the structures probed on both samples were of similar complexity.

Retractive forces were similar across both bacteria, with a slight variation between the two. The low value for adhesion reflects the outer layer of the bacteria to having a predominance to no adhesion to the tip in this state. Adhesion values on bacteria were significantly lower than that of TSB incubated silicon and autoclaved silicon, which was indicative that the original contamination layer and TSB had a more adhesive nature than bacteria, potentially contributing to attractive force incubation experiments.

6.3 Conclusions

Chemical analysis by XPS showed both pellet and lawn bacteria, while having slight differences were similar in composition. Both bacteria showed the outer layer composition of teichoic acids and peptidoglycan predominantly. Differences between the lawn and pellet sample were due to sample preparation.

Variations in the technique used to prepare the bacterial sample played a small role in the chemical analysis of the bacteria surface. This is related to the level of stress endured by the bacteria during preparation. Centrifugation has the potential to damage cells, in particular by rinsing the cells in water. This issue was overcome by lawn samples, which were kept in saline solution. The similarities in results confirmed there was little damage to cells on centrifugation, so results by AFM were comparable with the data on biofilms presented in Chapters 7 and 8. Variations between pelleted and lawn samples by XPS also came from approximations made about the substrate. In the case of silicon, there a small possibility for error in the organic oxygen calculations, discussed further in Chapter 3.

Images of the bacteria acquired by AFM showed the structure of the bacteria as approximately spherical with a diameter of in the region of 500 nm. In comparison to the structures seen on the surfaces presented in Chapters 4 and 5, the bacteria were significantly larger and so should be easily identifiable on analysis of bacterial films in subsequent chapters.

The structure of the bacteria can be clearly defined by AFM, with force curves showing a range of information. Typically, both bacterial strains showed similar characteristics, reflecting the structure of the bacteria to be inelastic and non-adhesive in comparison to the TSB layer on silicon. The force curve data showed sufficient differences in values to identify the presence of bacteria in comparison to TSB and autoclaved substrate, which all have the potential to be present on incubating substrates with bacteria.

Analyses of lawn sample of these strains in liquid were presented by Hu (2011). Forces measured were found to be 206 ±66pN for *ATCC35984* and 181 ±64pN for *NCTC13360* compared to 11 ±7nN and 13 ±8nN respectively for samples analysed in these experiments. The difference was assumed to be a result of preservation of the samples and analysis under water by Hu (2011), where measured forces may be expected to more reliably describe the true nature of the adhesion forces on the bacteria surface. This is due to the bacteria changing structure on drying. While attempts were made in the work reported in this thesis

to keep cells in a moist, physiologic state in AFM analysis, there was inevitably some drying out of the samples during the time the measurements were carried out. Some work was carried out to investigate the possibility of analysis under water using the liquid mode capability of the NT-MDT AFM, but these were not pursued due to technical difficulties. Further discussion of the effects of AFM analysis in liquids was included in Chapter 2. Additionally, the trapping of bacteria may result in additional forces from the membrane acting on the bacteria, which was also explored further in Chapter 2.

Overall, this chapter clarifies the chemical and physical properties of the bacteria without the presence of media. Information gained about the bacteria in this chapter contributed to understanding the analysis of incubated samples and the consequences of attractive force in the films formed on several substrate materials on incubation.

Chapter 7 Analysis of *NCTC13360* Bacterial Films on Silicon (111), Glass, Mica, Silver and Titanium Surfaces

NCTC13360 is a non-biofilm forming strain of *Staphylococcus epidermidis*, a pathogenic bacterium with the potential to cause infection in the human body. The initial adhesion of bacteria to the film substrate is believed to occur in the first few hours of incubation. The analyses by AFM and XPS of the initial adhesion of *S. epidermidis NCTC13360* (*ATCC12228*) is described in this chapter. The analysis of this non-film forming strain is contrasted with the growth of a second, film-forming, strain in the following chapter.

Samples were prepared as described in Chapter 3. Results of analyses of the substrates after incubation of bacteria were compared and modelled against equivalent results from the analyses of TSB incubated samples and bacterial pellets as described in the previous chapters.

7.1 Modelling bacterial coverage

To fully understand information gained from XPS, several assumptions and considerations about the sample must be made to analyse XPS data in terms of bacterial coverage.

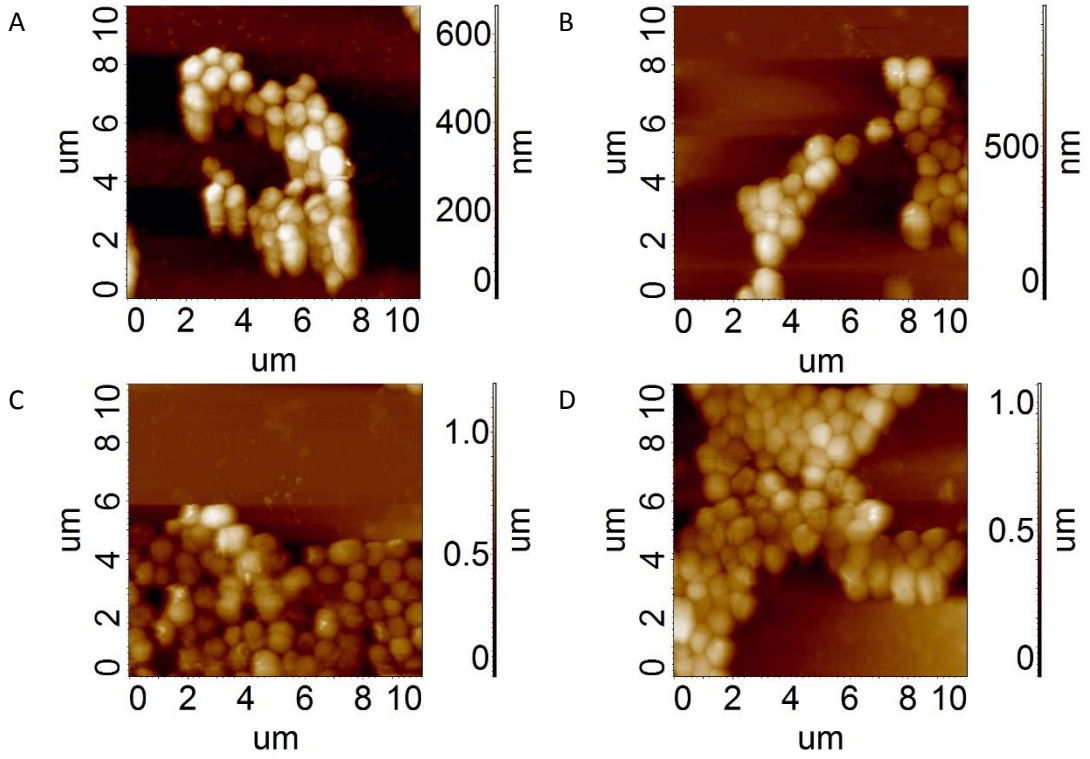

Figure 7.1 AFM images of samples incubated with *NCTC13360* after 24 hours. A is incubated with glass, B is incubated with mica, C is incubated with titanium and D is incubated with silver.

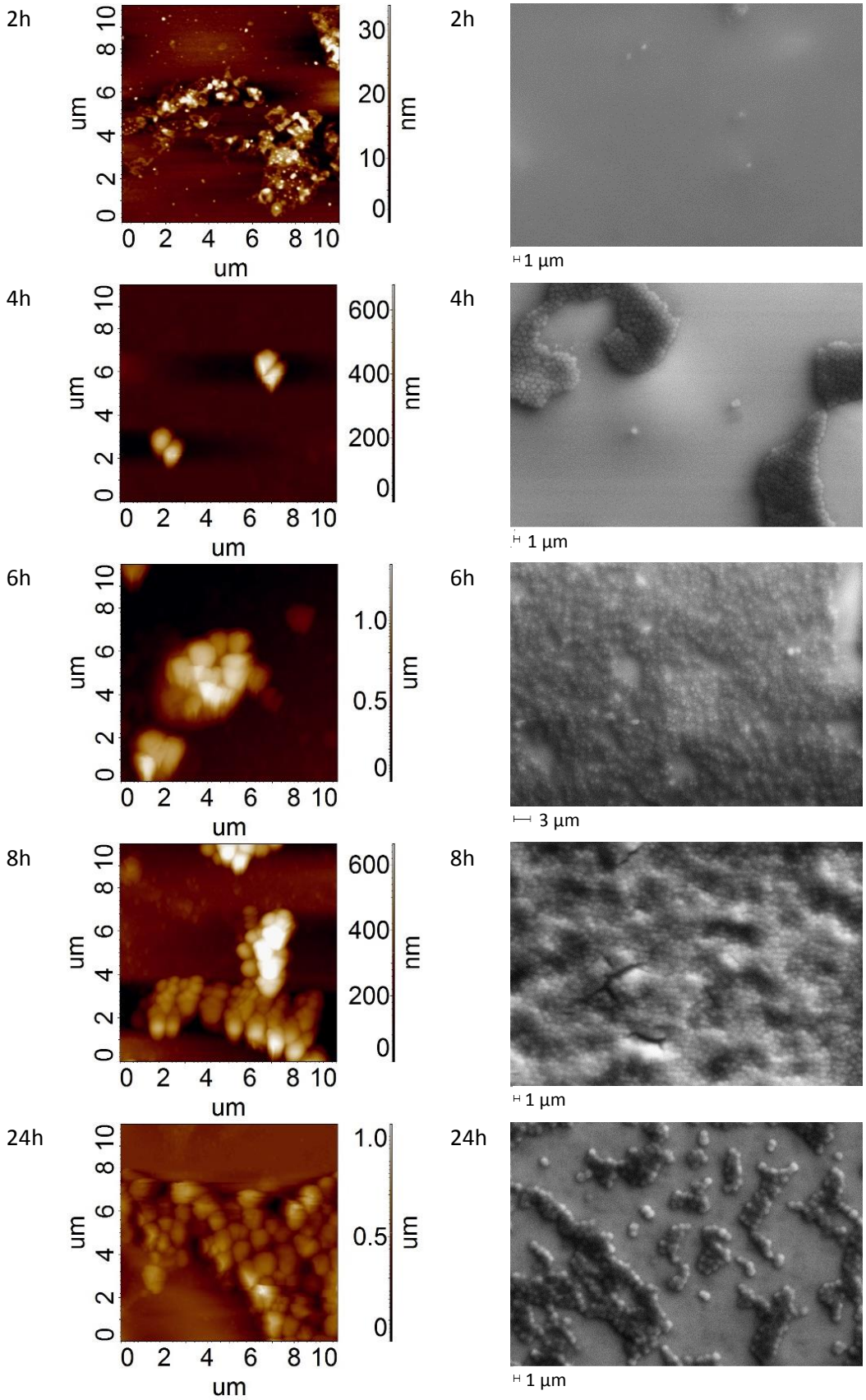

Figure 7.2 AFM and SEM images of silicon incubated samples as a function of time.

The bacteria were determined to have a diameter of 500 nm, from images shown in Chapter 6. As described in Chapter 3, the depth that can be analysed by XPS is approximately 10 nm.

This therefore means any material under the bacteria is undetectable, so any signal that is detected from the substrate is from uncovered material and therefore the bacterial coverage on the sample can be determined by comparing the substrate signal intensity with that from the as-received or autoclaved substrate. The method has limited accuracy as a result of neglect of other compounds bound to the surface on the incubated sample that may also attenuate the substrate signal. As an alternative to using the XPS signal intensities, the coverage can be estimated from AFM images. AFM images were processed through the NT-MDT Nova Px software, filtering images based on height from the sample. Heights were selected through the height of features. The feature height chosen was that of the size of bacteria observed in AFM images in Figures 7.1 and 7.2. For the average coverage estimated by AFM, 3 squares each of 10 x 10µm were used to estimate the bacterial coverage. For timed samples this was not possible, as AFM images were not taken for all timed samples that were taken for XPS analysis. Instead a model was formed using average coverage of known samples.

Using estimated coverages from both the XPS model and AFM model above, along with the chemical composition data from the bacterial pellet surface described in Chapter 6, it was possible to estimate the bacterial contribution to the surface composition. The variation between the calculated bacterial contribution, defined as *proportion pellet*, and the measured value of the incubated sample was used to determine the nature of the residual layer. This was then compared to that of the TSB media assumed to be in the sample in the first instance.

$$Proportion\ pellet = pellet\ \times coverage$$

$$Total\ incubated - proportion\ pellet = residual\ layer$$

While the composition of this layer could be determined as described above, the structure of the surface film on the surface could not. Figure 7.3 shows schematically the range of potential variations the bacteria can have with the residual layer. In the first instance, model A was selected for analysis. This model assumes that the residue covers the entire sample, including any bacteria present. Model G also assumes the same principle but ignores the possibility that the layer is not TSB. Models B and F both assume only the substrate is covered and the bacterial surface composition is therefore similar to that of the pellet. In models C and E, the layer only covers the bacteria, leaving the substrate in the same condition as before adhesion of any bacteria. In these cases, the defining peak signal should relate to that of the autoclaved material. D models a complex system, in which it would be difficult to

separate the two layers, as one is of unknown composition. Comparing the residual layer to that of TSB incubated sample and pelleted bacteria should indicate the true model.

Figure 7.3 Potential models of sample coverage in incubated samples, where the substrate or bacteria (yellow) is interacting with TSB (green) or bacteria excreted compound (purple).

In previous chapters, calculations were made to the thickness of the layer. In the case of bacterial samples, this was not possible. The composition of the residual layers by either model can only be an estimate. Further, the elemental composition of the surface of the bacteria may be very similar to the elemental composition of the residual layer, and therefore calculating accurate electron attenuation lengths becomes very difficult. Attempts to use the layer thickness model including the bacteria also gave errors, as the calculation assumes an even layer of less than approximately 10 nm, significantly smaller than the size of a bacteria.

One of the limitations with the use of the XPS technique is that the coverage of bacteria on the substrates may be variable, and sub-sampling of substrates during incubation was necessary. Subsampling is required as it was not possible to remove a sample from incubation for analysis, carry out the XPS analysis, and then return the sample to the growth medium for further incubation. Once a sample had been removed for analysis, external factors such as the effect of drying or of the XPS vacuum may have affected its composition or structure. Therefore, to minimise contamination and disruption of film growth, separate samples were used for each measurement. Sample coverage may have been different from sample to sample, and evidence for this was seen in the XPS results

7.2 XPS data analysis

7.2.1 Silicon timed data

Silicon samples were incubated with *NCTC13360* in tryptic soy broth and were removed at frequent times in relation to the growth of bacteria. Figure 7.4 shows the growth curve of the bacteria.

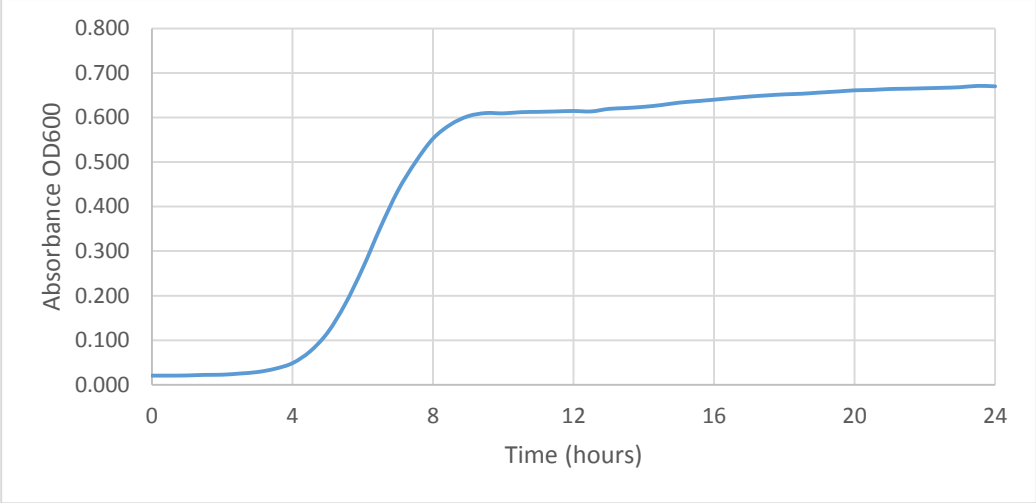

Figure 7.4 Growth curve of *NCTC13360* over 24 hours, as measured by absorbance at 600 nm.

Generally, samples were taken at alternate hours, increasing to hourly during the high growth period, and every 4 hours once the stationary phase was reached at approximately 16 hours. Results of analyses of the samples were compared to those from the timed TSB incubation, the proportioned pellet and the residual layer.

Results of analysis of timed samples on silicon (111) with regards to XPS survey spectrum and C 1s peak with calculations of the pellet and residue are shown in Tables 7.1 to Table 7.6. Figure 7.5 shows the survey spectrum and C 1s peak fit for the silicon incubated with *NCTC13360* after 24 hours. XPS spectra and C 1s peak fits for other timed samples can be found in the Appendix.

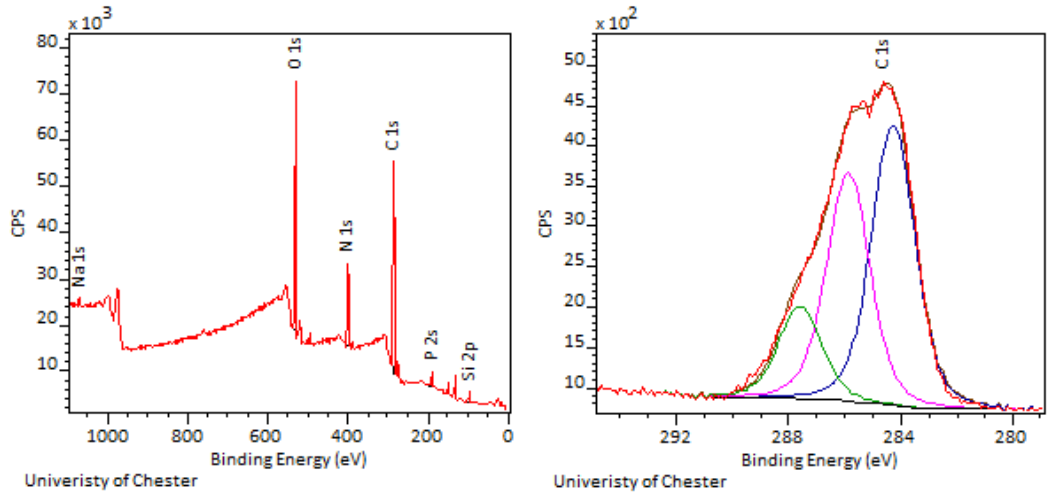

Figure 7.5 XPS survey and C 1s peak fit for silicon incubated in *NCTC13360* after 24 hours

	0h	1h	2h	3h	4h	5h	6h	7h	7h	8h	9h	10h	12h	12h	14h	16h	18h	20h	22h	24h
C 1s	21.1		30.0	23.0	38.8	37.2	60.6	44.5	57.1	60.8	62.0	60.1	62.2	57.2	56.8	59.1	48.9	52.5	59.6	60.8
O 1s	22.6		22.0	23.8	22.9	23.0	19.8	21.5	20.5	21.3	21.0	23.3	21.0	19.5	22.7	22.2	21.6	19.8	23.7	24.2
O_{org}	3.0		3.0	5.8	5.8	12.3	10.9	17.7	12.2	17.9	21.3	20.0	22.6	21.0	15.3	18.5	18.7	14.7	14.3	23.0
N 1s	0.0		3.5	3.6	6.3	6.9	13.6	8.4	12.8	13.2	11.4	12.1	13.2	11.2	8.8	10.2	9.9	9.9	10.6	10.6
Si 2p	56.3		56.3	44.6	49.6	31.7	32.7	5.6	24.3	6.6	0.0	2.7	1.4	0.3	11.2	9.2	6.9	19.2	16.1	2.9
P 2s	0.0		0.0	0.0	0.0	0.0	0.0	0.0	0.0	0.7	0.7	1.3	2.0	0.7	0.5	2.3	1.4	0.0	0.0	1.9
Na 1s	0.0		0.0	0.0	0.0	0.3	0.3	0.4	0.4	1.0	1.5	0.9	0.6	1.0	0.4	0.1	0.3	0.4	0.9	0.6
Ca 2s	0.0		0.0	0.0	0.0	0.0	0.0	0.0	0.0	0.0	0.0	0.0	0.0	0.0	0.0	0.0	0.0	0.0	0.0	0.0
Cl 2p	0.0		0.0	0.0	0.0	0.0	0.0	0.0	0.9	1.5	2.5	0.8	0.5	1.7	0.0	0.0	0.0	0.0	0.9	0.7
C285	87.9		70.8	59.7	55.3	46.1	43.9	50.5	46.1	39.8	47.9	47.4	47.1	53.2	49.5	51.0	52.1	50.9	48.0	47.7
C286.5	8.8		17.9	26.5	27.4	32.7	33.1	30.3	32.7	39.0	31.2	34.0	31.0	28.3	33.3	31.9	29.1	28.2	34.2	37.6
C288	3.3		11.4	13.8	17.3	21.1	23.0	19.2	21.1	21.2	20.9	18.5	21.8	18.6	17.2	17.1	18.8	20.9	17.8	14.8
O_{org}/C	0.00		0.14	0.20	0.25	0.32	0.29	0.29	0.27	0.31	0.35	0.32	0.38	0.34	0.27	0.33	0.32	0.30	0.24	0.39
N/C	0.00		0.00	0.12	0.16	0.16	0.19	0.22	0.19	0.22	0.22	0.18	0.20	0.21	0.20	0.15	0.17	0.20	0.18	0.18

Table 7.1 XPS surface composition data in atom % for *NCTC13360* incubated on Si (111) over time, as measured. Also shown are the relative % contributions of the 285.0, 286.5 and 288.0 eV contributions to the C 1s peak, and the O_{org}/C and N/C ratios.

	0h	1h	2h	3h	4h	5h	6h	7h	7h	8h	9h	10h	12h	12h	14h	16h	18h	20h	22h	24h
%			21%	12%	44%	42%	90%	57%	88%	100%	95%	98%	99%	80%	84%	88%	66%	71%	95%	95%
C 1s			12.5	7.1	26.3	25.2	54.2	34.2	53.2	60.2	57.3	58.7	59.8	48.2	50.3	52.7	39.6	43.0	57.1	57.4
O 1s			5.2	3.0	11.0	10.5	22.6	14.2	22.1	25.1	23.9	24.4	24.9	20.1	20.9	22.0	16.5	17.9	23.8	23.9
O_{org}			4.6	2.7	9.8	9.4	20.1	12.7	19.7	22.3	21.3	21.8	22.2	17.9	18.7	19.6	14.7	16.0	21.2	21.3
N 1s			1.9	1.1	4.1	3.9	8.4	5.3	8.2	9.3	8.9	9.1	9.3	7.5	7.8	8.2	6.1	6.7	8.8	8.9
Si 2p			0.3	0.2	0.6	0.6	1.3	0.8	1.2	1.4	1.3	1.4	1.4	1.1	1.2	1.2	0.9	1.0	1.3	1.3
P 2s			0.8	0.4	1.6	1.5	3.3	2.1	3.3	3.7	3.5	3.6	3.7	2.9	3.1	3.2	2.4	2.6	3.5	3.5
Na 1s			0.0	0.0	0.0	0.0	0.0	0.0	0.0	0.0	0.0	0.0	0.0	0.0	0.0	0.0	0.0	0.0	0.0	0.0
Ca 2s			0.1	0.0	0.1	0.1	0.3	0.2	0.3	0.3	0.3	0.3	0.3	0.3	0.3	0.3	0.2	0.2	0.3	0.3
Cl 2p			0.0	0.0	0.0	0.0	0.0	0.0	0.0	0.0	0.0	0.0	0.0	0.0	0.0	0.0	0.0	0.0	0.0	0.0
C285			10.3	5.9	21.6	20.7	44.5	28.1	43.6	49.4	47.0	48.2	49.1	39.5	41.3	43.3	32.5	35.3	46.8	47.1
C286.5			7.2	4.1	15.3	14.6	31.4	19.8	30.8	34.8	33.2	34.0	34.7	27.9	29.1	30.6	22.9	24.9	33.0	33.2
C288			3.3	1.9	6.9	6.6	14.2	9.0	14.0	15.8	15.0	15.4	15.7	12.6	13.2	13.8	10.4	11.3	15.0	15.1
O_{org}/C			0.37	0.37	0.37	0.37	0.37	0.37	0.37	0.37	0.37	0.37	0.37	0.37	0.37	0.37	0.37	0.37	0.37	0.37
N/C			0.15	0.15	0.15	0.15	0.15	0.15	0.15	0.15	0.15	0.15	0.15	0.15	0.15	0.15	0.15	0.15	0.15	0.15

Table 7.2 Contribution to measured composition from bacteria on the substrate surface, estimated using the surface composition of the pellet sample as reference and the bacterial coverage estimated from the reduction in the Si 2p signal compared to the autoclaved Si (111) wafer.

	0h	1h	2h	3h	4h	5h	6h	7h	7h	8h	9h	10h	12h	12h	14h	16h	18h	20h	22h	24h
C 1s	21.1		17.5	15.8	12.4	11.9	6.5	10.4	4.0	0.6	4.7	1.4	2.3	9.0	6.5	6.3	9.3	9.5	2.5	3.4
O 1s	22.6		16.8	20.8	12.0	12.5	-2.8	7.3	-1.7	-3.8	-2.9	-1.1	-4.0	-0.5	1.8	0.2	5.1	1.9	0.0	0.3
O_{org}	3.0		1.2	3.1	2.5	1.5	-2.4	-0.5	-1.9	-1.0	-1.3	0.8	-1.3	-2.5	-0.2	-0.9	0.0	-1.7	1.8	1.7
N 1s	0.0		1.5	2.5	2.2	3.0	5.2	3.1	4.5	3.9	2.5	3.0	3.9	3.8	1.0	2.0	3.7	3.2	1.8	1.0
Si 2p	56.3		44.3	49.4	31.0	32.1	4.3	23.5	5.3	-1.4	1.3	0.0	-1.1	10.1	8.1	5.7	18.3	15.1	1.6	1.3
P 2s	0.0		-0.8	-0.4	-1.6	-1.5	-3.3	-2.1	-2.6	-3.0	-2.2	-1.6	-3.0	-2.5	-0.8	-1.9	-2.4	-2.6	-1.6	-1.3
Na 1s	0.0		0.0	0.0	0.3	0.3	0.4	0.4	1.0	1.5	0.9	0.6	1.0	0.4	0.1	0.3	0.4	0.9	0.6	0.4
Ca 2s	0.0		-0.1	0.0	-0.1	-0.1	-0.3	-0.2	-0.3	-0.3	-0.3	-0.3	-0.3	-0.3	-0.3	-0.3	-0.2	-0.2	-0.3	-0.3
Cl 2p	0.0		0.0	0.0	0.0	0.0	0.0	0.9	1.5	2.5	0.8	0.5	1.7	0.0	0.0	0.0	0.0	0.9	0.7	0.0
C285	87.9		60.5	53.8	33.7	25.4	-0.6	22.5	2.5	-9.6	0.9	-0.7	-2.0	13.7	8.3	7.7	19.6	15.6	1.2	0.6
C286.5	8.8		10.6	22.3	12.1	18.1	1.7	10.5	2.0	4.1	-2.0	0.0	-3.6	0.3	4.1	1.4	6.1	3.3	1.1	4.3
C288	3.3		8.1	12.0	10.4	14.5	8.8	10.2	7.2	5.5	5.9	3.1	6.1	5.9	4.0	3.3	8.4	9.6	2.8	-0.3
O_{org}/C	0.00		0.07	0.20	0.20	0.13	-0.37	-0.05	-0.47	-1.60	-0.28	0.58	-0.55	-0.28	-0.03	-0.14	0.00	-0.18	0.73	0.49
N/C	0.00		0.09	0.16	0.18	0.25	0.81	0.30	1.15	5.98	0.54	2.07	1.70	0.42	0.15	0.31	0.40	0.34	0.72	0.31

Table 7.3 Approximate composition of non-bacterial material (residue) on the surface, estimated by subtracting values in Table 7.2 from values in Table 7.1. The occasional apparently-negative values arise from inadequacies of the model used, see text.

	0h	1h	2h	3h	4h	5h	6h	7h	7h	8h	9h	10h	12h	12h	14h	16h	18h	20h	22h	24h
C 1s	21.1	58.6	34.1	30.5		34.3	38.8			30.4	56.9									41.2
O 1s	22.6	19.3	22.3	21.1		24.7	22.1			22.3	20.6									23.5
O_{org}	3.0	13.0	4.4	3.8		5.2	8.1			7.6	16.2									11.0
N 1s	0.0	6.5	3.7	3.1		4.2	4.8			5.3	9.5									3.8
Si 2p	56.3	12.8	39.4	44.8		36.6	32.7			41.9	10.8									31.5
P 2s	0.0	0.0	0.0	0.0		0.0	0.0			0.0	0.3									0.0
Na 1s	0.0	0.9	0.1	0.0		0.2	0.7			0.1	0.9									0.0
K 2s	0.0	0.0	0.0	0.0		0.0	0.0			0.0	0.0									0.0
Ca 2s	0.0	0.6	0.5	0.6		0.0	0.0			0.0	0.0									0.0
Mg 2p	0.0	0.0	0.0	0.0		0.0	0.0			0.0	0.0									0.0
Cl 2p	0.0	1.4	0.0	0.0		0.0	0.9			0.0	1.1									0.0
C285	87.9	69.0	73.7	69.6		68.0	68.4			54.8	49.7									72.9
C286.5	8.8	17.9	13.6	19.4		19.8	18.5			27.5	30.7									16.6
C288	3.3	13.1	12.7	11.0		12.2	13.2			17.7	19.6									10.6
O_{org}/C	0.14	0.23	0.13	0.13		0.15	0.21			0.25	0.28									0.27
N/C	0.00	0.17	0.11	0.10		0.12	0.12			0.17	0.17									0.09

Table 7.4 XPS surface composition data from media-incubated Si, from Chapter 5, reproduced here for reference.

	0h	1h	2h	3h	4h	5h	6h	7h	7h	8h	9h	10h	12h	12h	14h	16h	18h	20h	22h	24h
%	0%	0%	5%	10%	15%	21%	26%	31%	31%	36%	41%	46%	56%	56%	56%	56%	56%	56%	56%	56%
C 1s			3.1	6.2	9.3	12.3	15.4	18.5	18.5	21.6	24.7	27.8	34.0	34.0	34.0	34.0	34.0	34.0	34.0	34.0
O 1s			1.3	2.6	3.9	5.1	6.4	7.7	7.7	9.0	10.3	11.6	14.1	14.1	14.1	14.1	14.1	14.1	14.1	14.1
O_{org}			1.1	2.3	3.4	4.6	5.7	6.9	6.9	8.0	9.2	10.3	12.6	12.6	12.6	12.6	12.6	12.6	12.6	12.6
N 1s			0.5	1.0	1.4	1.9	2.4	2.9	2.9	3.3	3.8	4.3	5.3	5.3	5.3	5.3	5.3	5.3	5.3	5.3
Si 2p			0.1	0.1	0.2	0.3	0.4	0.4	0.4	0.5	0.6	0.6	0.8	0.8	0.8	0.8	0.8	0.8	0.8	0.8
P 2s			0.2	0.4	0.6	0.8	0.9	1.1	1.1	1.3	1.5	1.7	2.1	2.1	2.1	2.1	2.1	2.1	2.1	2.1
Na 1s			0.0	0.0	0.0	0.0	0.0	0.0	0.0	0.0	0.0	0.0	0.0	0.0	0.0	0.0	0.0	0.0	0.0	0.0
K 2s			0.0	0.0	0.0	0.0	0.0	0.0	0.0	0.0	0.0	0.0	0.0	0.0	0.0	0.0	0.0	0.0	0.0	0.0
Ca 2s			0.0	0.0	0.0	0.1	0.1	0.1	0.1	0.1	0.1	0.1	0.2	0.2	0.2	0.2	0.2	0.2	0.2	0.2
Mg 2p			0.0	0.0	0.0	0.0	0.0	0.0	0.0	0.0	0.0	0.0	0.0	0.0	0.0	0.0	0.0	0.0	0.0	0.0
Cl 2p			0.0	0.0	0.0	0.0	0.0	0.0	0.0	0.0	0.0	0.0	0.0	0.0	0.0	0.0	0.0	0.0	0.0	0.0
C285			2.5	5.1	7.6	10.1	12.7	15.2	15.2	17.7	20.3	22.8	27.9	27.9	27.9	27.9	27.9	27.9	27.9	27.9
C286.5			1.8	3.6	5.4	7.2	8.9	10.7	10.7	12.5	14.3	16.1	19.7	19.7	19.7	19.7	19.7	19.7	19.7	19.7
C288.8			0.8	1.6	2.4	3.2	4.1	4.9	4.9	5.7	6.5	7.3	8.9	8.9	8.9	8.9	8.9	8.9	8.9	8.9
O_{org}/C			0.37	0.37	0.37	0.37	0.37	0.37	0.37	0.37	0.37	0.37	0.37	0.37	0.37	0.37	0.37	0.37	0.37	0.37
N/C			0.15	0.15	0.15	0.15	0.15	0.15	0.15	0.15	0.15	0.15	0.15	0.15	0.15	0.15	0.15	0.15	0.15	0.15

Table 7.5 Contribution to measured composition from bacteria on the substrate surface, estimated using the surface composition of the pellet sample as reference and the bacterial coverage estimated from the analysis of the AFM images.

	0h	1h	2h	3h	4h	5h	6h	7h	7h	8h	9h	10h	12h	12h	14h	16h	18h	20h	22h	24h
C 1s	21.1		26.9	16.8	29.5	24.8	45.2	26.0	38.6	39.2	37.3	32.3	28.2	23.2	22.9	25.1	14.9	18.5	25.6	26.8
O 1s	22.6		20.7	21.2	19.1	17.8	13.3	13.8	12.7	12.3	10.7	11.7	6.8	5.4	8.6	8.1	7.4	5.6	9.6	10.0
O_{org}	3.0		1.8	3.6	2.4	7.7	5.2	10.8	5.3	9.9	12.1	9.6	10.0	8.3	2.7	5.9	6.1	2.1	1.6	10.4
N 1s	0.0		3.0	2.6	4.9	5.0	11.2	5.5	9.9	9.9	7.6	7.8	7.9	6.0	3.5	4.9	4.6	4.6	5.4	5.4
Si 2p	56.3		56.2	44.5	49.4	31.4	32.3	5.2	23.9	6.0	-0.6	2.0	0.6	-0.5	10.4	8.4	6.1	18.4	15.3	2.1
P 2s	0.0		-0.2	-0.4	-0.6	-0.8	-0.9	-1.1	-1.1	-0.7	-0.8	-0.4	-0.1	-1.4	-1.6	0.2	-0.7	-2.1	-2.1	-0.2
Na 1s	0.0		0.0	0.0	0.0	0.3	0.2	0.4	0.3	1.0	1.5	0.8	0.6	1.0	0.3	0.1	0.2	0.4	0.9	0.6
K 2s	0.0		0.0	0.0	0.0	0.0	0.0	0.0	0.0	0.0	0.0	0.0	0.0	0.0	0.0	0.0	0.0	0.0	0.0	0.0
Ca 2s	0.0		0.0	0.0	0.0	-0.1	-0.1	-0.1	0.8	1.4	2.4	0.7	0.3	1.5	-0.2	-0.2	-0.2	-0.2	0.7	0.5
Mg 2p	87.9		70.8	59.7	55.3	46.1	43.9	50.5	46.1	39.8	47.9	47.4	47.1	53.2	49.5	51.0	52.1	50.9	48.0	47.7
Cl 2p	8.8		17.9	26.5	27.4	32.7	33.1	30.3	32.7	39.0	31.2	34.0	31.0	28.3	33.3	31.9	29.1	28.2	34.2	37.6
C285	87.9		68.2	54.6	47.7	36.0	31.2	35.3	30.9	22.1	27.7	24.6	19.3	25.3	21.7	23.1	24.2	23.0	20.1	19.8
C286.5	8.8		16.1	22.9	22.0	25.6	24.2	19.6	22.0	26.4	16.8	17.9	11.4	8.6	13.6	12.2	9.4	8.6	14.5	17.9
C288	3.3		10.5	12.2	14.9	17.9	19.0	14.3	16.2	15.6	14.4	11.2	12.9	9.6	8.3	8.2	9.9	12.0	8.9	5.9
O_{org}/C	0.14		0.07	0.21	0.08	0.31	0.11	0.42	0.14	0.25	0.33	0.30	0.36	0.36	0.12	0.23	0.41	0.11	0.06	0.39
N/C	0.00		0.11	0.16	0.17	0.20	0.25	0.21	0.26	0.25	0.20	0.24	0.28	0.26	0.15	0.19	0.31	0.25	0.21	0.20

Table 7.6Approximate composition of non-bacterial material (residue) on the surface, estimated by subtracting values in Table 7.5 from values in Table 7.1.

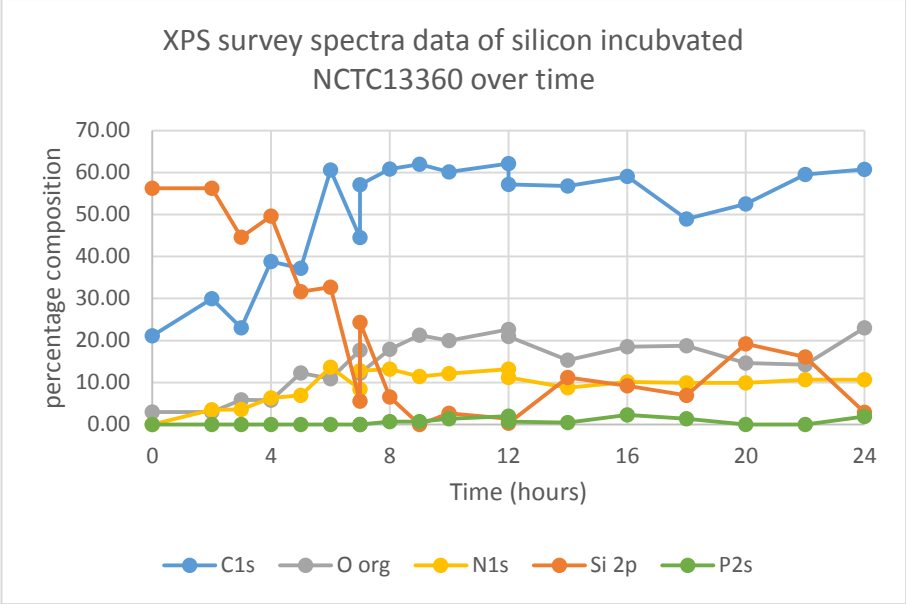

Figure 7.6 XPS analysis of survey spectrum data of *NCTC13360* over time.

As shown in Figure 7.6, the changes in surface composition as determined by XPS spectra over time showed an anti-correlation between silicon and carbon. As the silicon decreased in intensity the C 1s signal increases, indicating the increase in C 1s relates to coverage of the silicon substrate. The C 1s increased over the first 7 hours after which the carbon content stabilised at between 50 and 65%. This indicated the bacteria attaches to the surface within the first 7 hours, after which the amount of bacteria attached to the surface was approximately stable. After 7 hours the changes in relative C 1s and Si 2p intensities are thought to be primarily due to variations as a result of subsampling leading to variations in the area on the sample analysed.

Nitrogen in the sample was detected after 2 hours, after which it slowly increased until 7 hours. Subsequently the amount of N 1s signal detected became more stable. The organic oxygen followed a similar trend to the N 1s signal, where there was a steady increase until 9 hours after which the organic oxygen level remained approximately constant, with variations in the range between 15 and 25%.

Although the AFM and SEM images showed the presence of bacteria within 4 hours, P 2s was not detected until 8 hours. The presence of P 2s is indicative of bacteria, however there must be sufficient amount of bacteria on the surface to give a detectable P 2s signal. The minimum detection of level of P 2s is approximately 0.5% and anything less than this will not be detected due to signal-to-noise considerations. As discussed previously, the P 2s signal was used instead of the P 2p signal due to the sloping background arising from second plasmon

loss peak on the high binding energy side of the Si 2s peak making it difficult to identify the P 2p peak on silicon based samples.

As shown in Figure 7.7, The C 1s peak fit showed the relative proportion of the C285 signal decreased for the first 7 hours and stabilised. This followed a similar trend to that of the Si 2p peak, indicating that some of the hydrocarbon content was associated with the exposed silicon surface. The remainder of the carbon intensity was therefore associated with the bacteria, which also showed hydrocarbon content. The relative proportion of C286.5 and C288 was found to increase for the first 7 hours and then stabilise. This followed a similar trend to that shown by the organic oxygen and by the nitrogen, indicating this change relates to biological compounds on the surface.

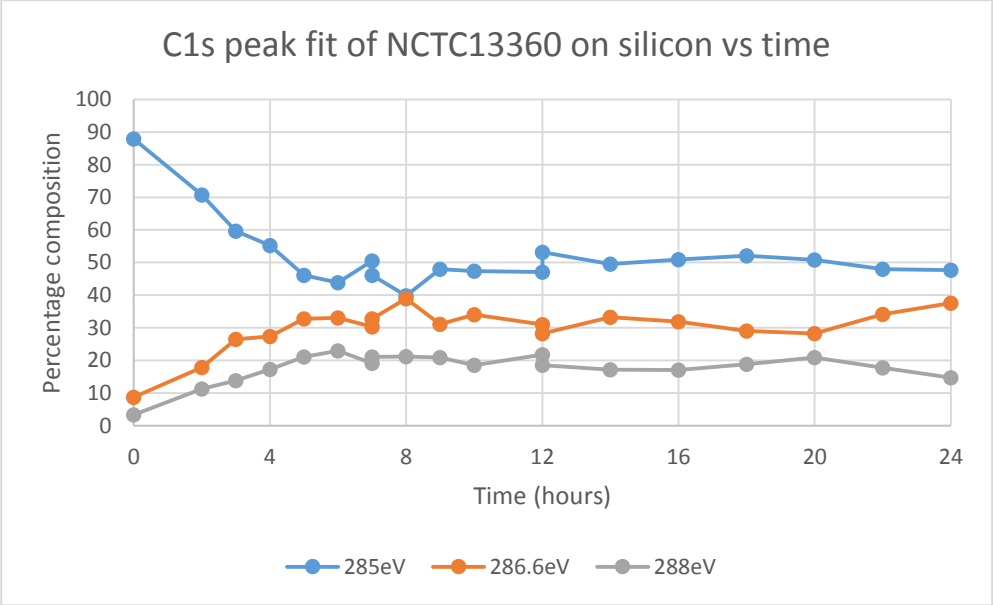

Figure 7.7 C 1s peak fit against time for silicon incubated in *NCTC13360.*

Comparisons made between results from the calculated data and measured data are shown in the Figures below based on their individual measurement for ease of analysis. The chemical composition of bacterial incubated silicon relative to that of media incubated silicon, the pelleted ratio of bacteria calculated from the change in Si 2p from autoclaved material, and the calculated residual layer for both models is discussed below.

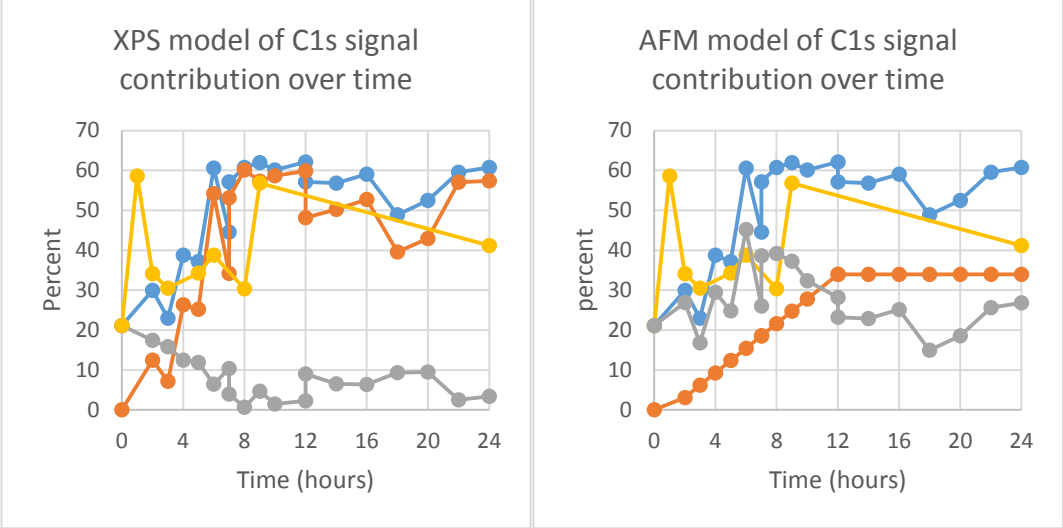

Figure 7.8 Graphs comparing models of C1s signal within overlayer composition models against time, calculated from estimating the coverage from XPS data (left) and AFM (right), taken from Tables 7.1-7.6.Calculations of the bacterial contribution to signal (red) and the resulting non-bacterial residue (grey) are compared to the original incubation data of silicon incubated with *NCTC13360* (blue) and silicon incubated with TSB over time (yellow).

On analysis of bacteria coverage model by XPS by time, the estimated pelleted contribution to signal showed similarities to the incubated sample, with the first 5 hours of incubation showing a wider difference (Figure 7.8, left hand panel). The pelleted bacterial contribution to signal was lower than that of the incubated sample. The wider range during the first hours was possibly due to the residual hydrocarbon layer on the substrate contributing to the C 1s signal. During this time more of the silicon was exposed and from media incubated data, where initial adhesion of proteins and polysaccharides to the substrate take place. The residual layer decreased in signal over the first 8 hours and then remained low, at less than 10 % of the total contribution to signal intensity. This showed that the residual layer in this stage was not a dominant feature, with the first few hours relating to the decrease in atmospheric carbon bound to the surface, and being replaced by other compounds, either bacteria or proteins and polysaccharides.

Analysis of the C 1s using the AFM model of coverage (Figure 7.8, right hand panel) showed a lower carbon content than that of the incubated sample, with some similarities observed in trend of C 1s increase over the first 8 hours. The residual layer showed similarities to the incubated sample for the first 8 hours with the carbon signal decreasing after 8 hours, with a similar trend to the incubated sample. The similarity with the first 8 hours indicated the possibility that the residual layer consisted of components of the atmospheric layer as well as the gradually increasing contribution to the signal from bacterial adhesion. The trend after

8 hours relates to the unknown coverage of samples by AFM and the model used to determine the bacterial coverage at this time was assumed to be linear.

Typically, the pelleted bacteria ratio fell below that of the incubated sample, thereby indicating the presence of an organic residual layer. From this result it is important to note the calculated coverage is an estimate of bacteria and does not take into account that some of the apparent coverage may be due to the suppression of the silicon signal by a non-bacterial organic compound, as observed in Chapter 5 on incubation with the media. Before 7 hours there appears to be a larger difference between pelleted sample and incubated sample. This may be related to variations in coverage, along with the possible presence of alternate compounds bound on the surface. Comparing the calculated residue to that of the timed media samples for these times, the values for the calculated residue are significantly lower than those of media. This suggests that although there may be low coverage, less media was bound to the surface at this stage, and this may potentially be related to a higher level of bacterial excreted compounds.

The biological model described in Chapters 2 and 3 were applied to the XPS data. Analysis of C 1s peak fit data with regards to the biological model determined by XPS showed similarities with the C285 peak of the *ATCC35984* incubated sample for the first few hours, confirming differences observed in the first few hours of the C 1s signal. After this time the model showed inconsistencies at various points in modelling the carbon peak fit signals, as evidenced by apparent negative calculated values in the residual layer. This was due to the estimated bacterial pellet giving a higher value than that of the incubated samples, indiating the potential for errors in the biological model determined by XPS.

The signal of the incubated sample at C286.5 showed similarities to the XPS pellet contibution after 6 hours, indicating that the bacteria was the main contribution to the signal. The C288 signal followed a similar trend to the C286.5 signal, with the C288 signal showing a wider difference between the incubated sample and the XPS calculated pellet contribution than was observed for C286.5. The wider gap observed for the C288 signal relates to the potential presence of more complex compounds of non-bacterial origin on the surface. Comparing the XPS calculated residual layer to media incubated silicon, the C288 peak showed some similarites to TSB after 8 hours, indicating the residual layer had a similar carbon content to TSB. Overall, the carbon peak fit data for the first few hours showed a dominance of hydrocarbons, likely originating from the exposed silicon substrate. After 5 hours the C286.5 and C288 signals become closer to the XPS estimated bacterial pellet, which was the main contribution to the carbon signal. The gap in C288 relates to the residual layer and overall

difference in C 1s peak between the incubated bacteria and expected pelleted bacteria. The similarties between the residual layer calculated from the XPS model and the TSB incubated silicon model gave an indiation they may be composed of similar complexes of components on the surface.

On analysis of the AFM model of bacterial coverage, the contribution of bacteria calculated as originating from the overall incubated signal was lower than that estimated by XPS, giving a different model of signal contribution to the sample. The C285 signal of the incubated sample showed a similar trend to that of the residual layer, with the first 5 hours having a closer similarity. Similarities in the first 5 hours relate to the atmospheric contamination carbon bound to the exposed silicon, with later times relating to both atmospheric hydrocarbon and hydrocarbons from bacteria obsevered in the pelleted bacteria.The C286.5 and C288 signals followed a similar trend to that seen for the C285, indicating the sample consisted of a combination of hydrocarbons from exposed material and more complex compounds as a result of the presence of the pelleted bacteria and the residual layer on the sample.

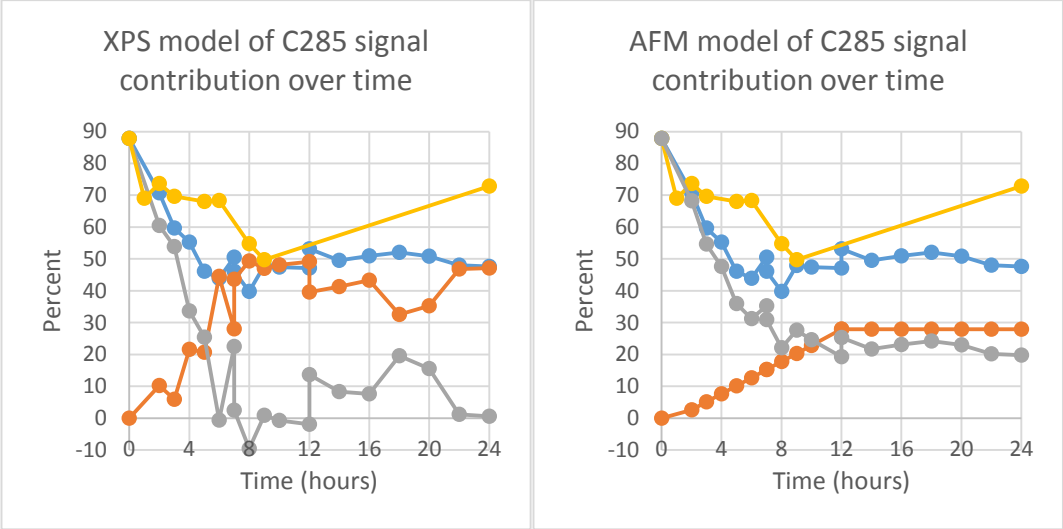

Figure 7.9 Graphs comparing models of C285 signal within overlayer composition models against time, calculated from estimating the coverage from XPS data (left) and AFM (right), taken from Tables 7.1-7.6.Calculations of the bacterial contribution to signal (orange) and the resulting non-bacterial residue (grey) are compared to the original incubation data of silicon incubated with *NCTC13360* (blue) and silicon incubated with TSB over time (yellow).

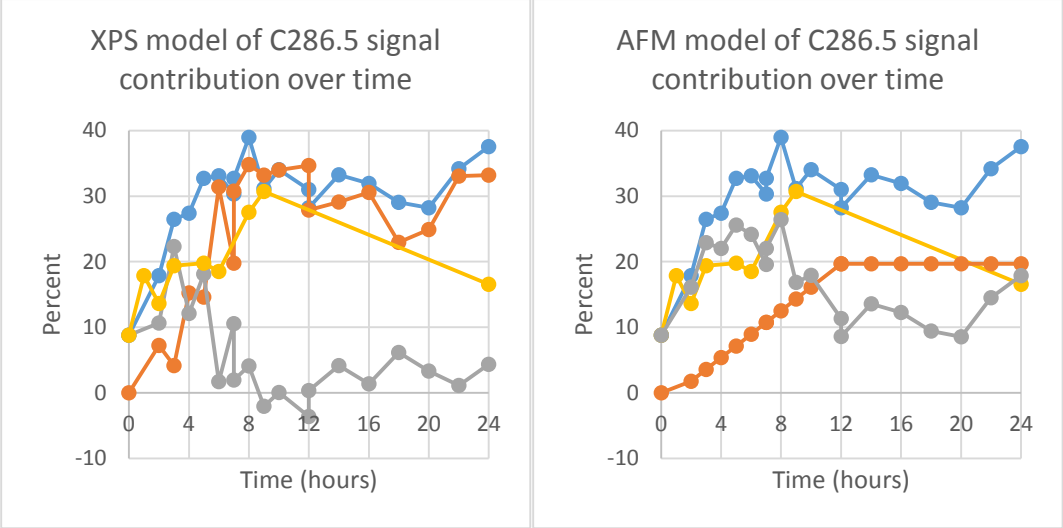

Figure 7.10 Graphs comparing models of C286.5 signal within overlayer composition models against time, calculated from estimating the coverage from XPS data (left) and AFM (right), taken from Tables 7.1-7.6.Calculations of the bacterial contribution to signal (orange) and the resulting non-bacterial residue (grey) are compared to the original incubation data of silicon incubated with *NCTC13360* (blue) and silicon incubated with TSB over time (yellow).

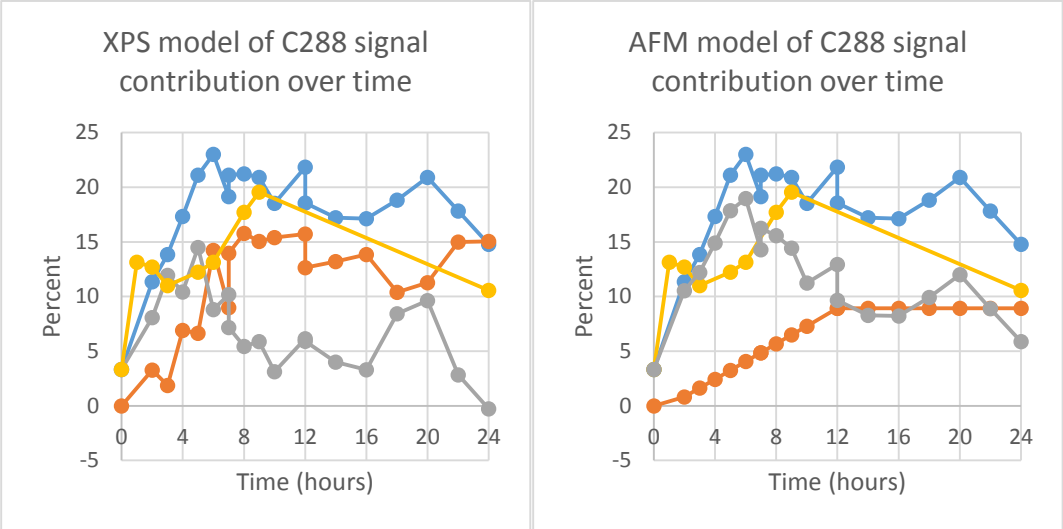

Figure 7.11 Graphs comparing models of C288 signal within overlayer composition models against time, calculated from estimating the coverage from XPS data (left) and AFM (right), taken from Tables 7.1-7.6.Calculations of the bacterial contribution to signal (orange) and the resulting non-bacterial residue (grey) are compared to the original incubation data of silicon incubated with NCTC13360 (blue) and silicon incubated with TSB over time (yellow).

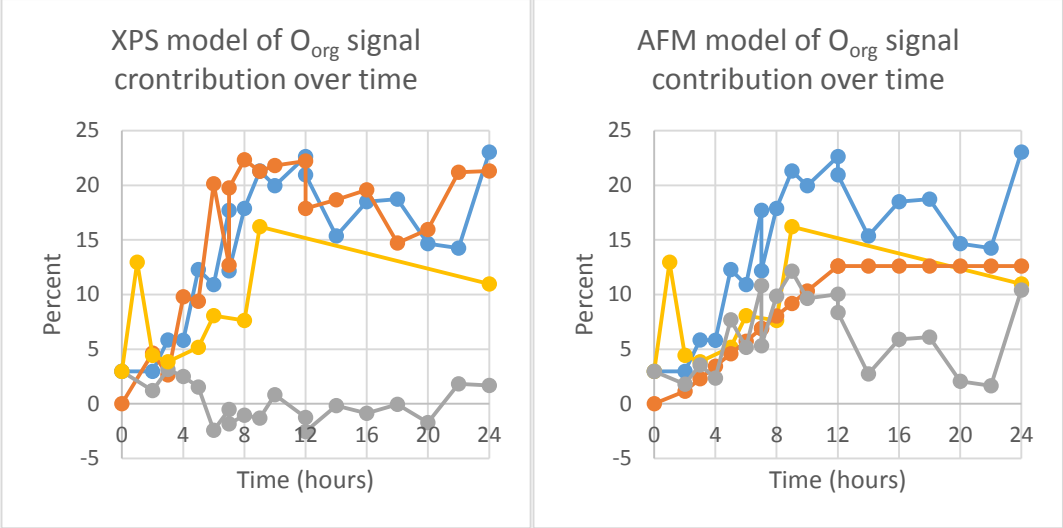

Figure 7.12: Graphs comparing models of calculated organic oxygen signal within overlayer composition models against time, calculated from estimating the coverage from XPS data (left) and AFM (right), taken from Tables 7.1-7.6.Calculations of the bacterial contribution to signal (orange) and the resulting non-bacterial residue (grey) are compared to the original incubation data of silicon incubated with *NCTC13360* (blue) and silicon incubated with TSB over time (yellow).

Analysis of the organic oxygen signal using the XPS model showed the incubated sample and the proportioned pellet calculated by XPS to have similar values, where in some cases the model for the bacterial coverage overestimated the bacterial contribution of organic oxygen, leading to negative values for the residual layer. For the first 5 hours there was some organic oxygen detected in the sample that is not related to the bacterial pellet. This was assumed to be low amounts of oxygen detected in the atmospheric hydrocarbon layer, the detection of which decreases over the first few hours.

Analysis of organic oxygen according to the AFM model for bacterial coverage showed the pelleted bacteria contribution to signal to be lower than that of the incubated sample, indicating the potential presence of a residual layer on the surface. The residual layer estimated by AFM showed similarities to the incubated sample for the first 9 hours after which the organic oxygen began to fall. Similarities seen in the first 9 hours of incubation relate to a low amount of oxygen in the atmospheric carbon layer along with the adhesion of other biological compounds to the surface. The residual layer estimated by AFM showed similarities to that of TSB in this time, indicating similarities in the residual layer, and the potential presence of TSB bound to the surface. The change in organic oxygen after 9 hours was related to the changes in residual layer, following a different trend to that of the TSB incubated sample. While there is the possibility that the organic oxygen originated from a TSB layer in the sample, it is not possible to eliminate the possibility of the organic oxygen alone coming from an alternate source.

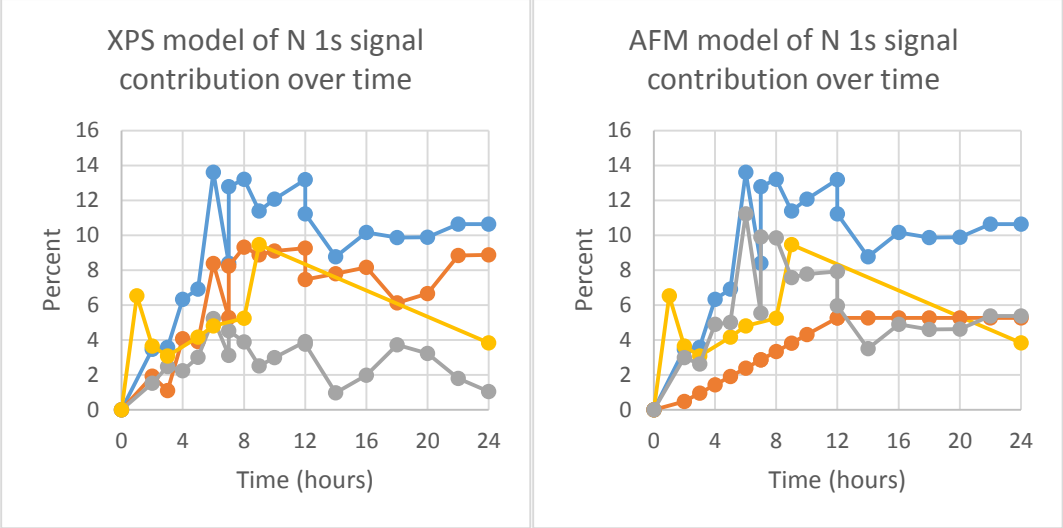

Figure 7.13 Graphs comparing models of N 1s signal within overlayer composition models against time, calculated from estimating the coverage from XPS data (left) and AFM (right), taken from Tables7.1-7.6.Calculations of the bacterial contribution to signal (orange) and the resulting non-bacterial residue (grey) are compared to the original incubation data of silicon incubated with *NCTC13360* (blue) and silicon incubated with TSB over time (yellow).

Analysis of the nitrogen signal using the XPS model led to similarities in the nitrogen content between the calculated bacterial contribution and incubated sample being observed, with the bacterial contribution to the signal having a lower nitrogen content. Similarities in trends between the calculated residual layer and incubated sample indicated the influence of bacterial adhesion on the residual layer. Similarities in trends between the residue and the TSB incubated silicon were observed during the first 8 hours after which the differences in N 1s became greater, indicating the potential influence TSB may have had on the residual layer. The residual layer cannot be determined as TSB alone, as the TSB layer is a complex mixture. The organic oxygen and the carbon signals may be interpreted in terms of the possible presence of proteins; this is discussed further below.

Analysis of the nitrogen signal in terms of the AFM model of coverage, showed the residual layer to closely follow a similar trend to that seen for the incubated sample for the first 9 hours. After this, the nitrogen content of the sample showed some similarities to the incubated sample, with a wider difference observed. In comparison to the TSB incubated silicon, the residual layer showed a higher amount of nitrogen between 4 and 9 hours, indicating the calculated residual layer was more than just media bound to the exposed material at this stage.

The trend of the calculated AFM residue showed that the first 3 hours may be related to media adhesion on the surface, after which there was evidence for an additional amount of nitrogen in the residual layer, possibly from bacteria-excreted compounds. After 8 hours the

nitrogen content of the bacteria became more apparent, affecting the signal of the calculated residual layer. Variations after 8 hours may have occurred as a result of changes in the residual layer or as a result of subsampling.

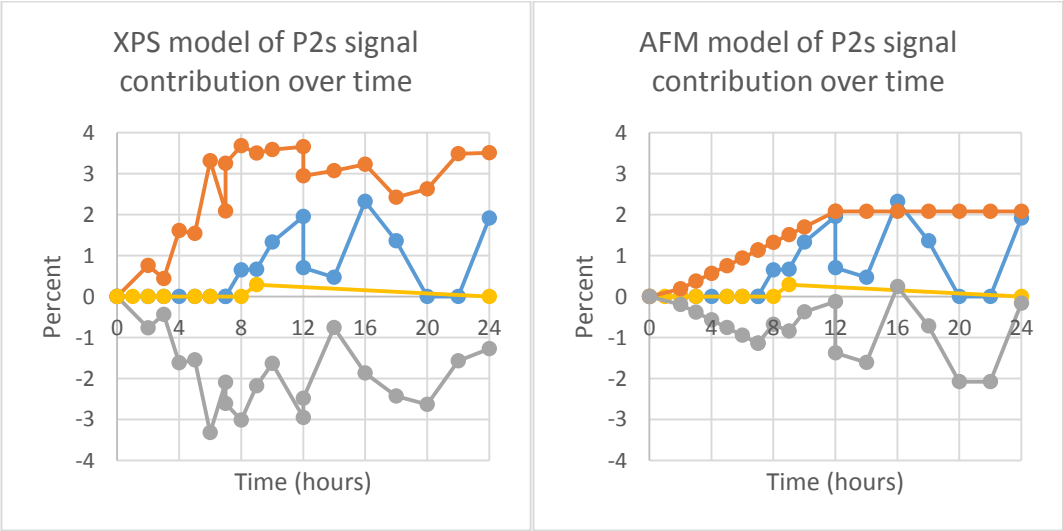

Figure 7.14 Graphs comparing models of P 2s signal within overlayer composition models against time, calculated from estimating the coverage from XPS data (left) and AFM (right), taken from Tables 7.1-7.6.Calculations of the bacterial contribution to signal (orange) and the resulting non-bacterial residue (grey) are compared to the original incubation data of silicon incubated with *NCTC13360* (blue) and silicon incubated with TSB over time (yellow).

The amount of P 2s in the sample was used to determine whether the bacterial coverage calculation was acceptable, and if so then the residual layer estimated on the surface indicated the composition of the residue covering the bacteria. As discussed earlier there is a limit to the amount of P 2s needed to be present on the sample before the signal is detected. This led to potential discrepancies in estimating the P 2s signal from the bacteria to the sample. The XPS model continuously overestimated the P 2s peak, suggesting that in combination with other signals in the model, the model overestimated the bacterial coverage. This was due to the residue layer on the surface contributing to the suppression of the silicon signal from the underlying substrate. Analysis of the AFM model showed the model overestimates the P 2s signal. The AFM model showed a lower coverage of bacteria than the XPS model. From this it can be assumed that while there was a possibility of error in bacterial coverage, the error partially came from limit of detection of P 2s signal along with the possibility that the bacteria may be covered with the residual layer. The potential presence of a residual layer was seen through the modelling of other bacteria-related signals using the bacterial coverage estimated by AFM.

To determine the biological composition of the potential residual layer the O_{org}/C and N/C ratios were analysed and compared to ideal results of the model proposed in Chapter 3. The

model was not used to directly determine the composition of the residual layer, as the model is only valid for systems with ideal compound structures, where the structure of the compounds is known and well-defined. For more complex systems the biological component model is more likely to fail. Therefore, the values in the model are taken to be approximate models of proteins and polysaccharides.

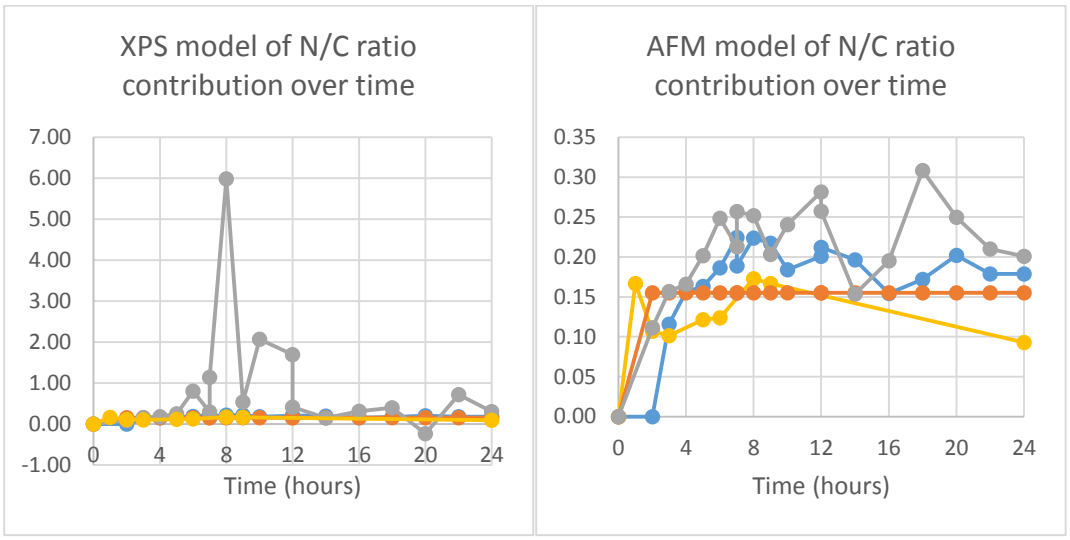

Figure 7.15 Graphs comparing models of N/C ratio within overlayer composition models against time, calculated from estimating the coverage from XPS data (left) and AFM (right), taken from Tables 7.1-7.6.Calculations of the bacterial contribution to signal (orange) and the resulting non-bacterial residue (grey) are compared to the original incubation data of silicon incubated with *NCTC13360* (blue) and silicon incubated with TSB over time (yellow).

For both models, the N/C ratio for the pelleted sample was constant at 0.15. Generally, the incubated sample had a higher N/C ratio than the incubated sample after 4 hours. On analysis of the XPS model, the residual layer showed a higher N/C ratio, with some values being greater than 1. This means the compounds on the surface are nitrogen heavy. While this may indicate the possibility of proteins, the high values indicated the more likely potential error in the calculations of N 1s and C 1s for these points as a result of the inadequacies of the model, leading to the N/C ratio for this model to be unreliable. The AFM model of bacterial coverage showed the composition of the residual layer to have a higher N/C ratio than the incubated sample and pelleted bacteria, indicating a larger amount of proteins on both. Chapter 5 showed the silicon substrates to have a dominance of proteins adhered to the surface, the N/C of the calculated residual layer was generally higher, indicating the presence of more proteins on the sample that are unrelated to bacteria. This leads to the conclusion that the residual layer was not just TSB bound to the exposed silicon, but contains additional proteins bound to the sample. The percentage of proteins bound to the surface varied between samples, indicating the layer was not constant.

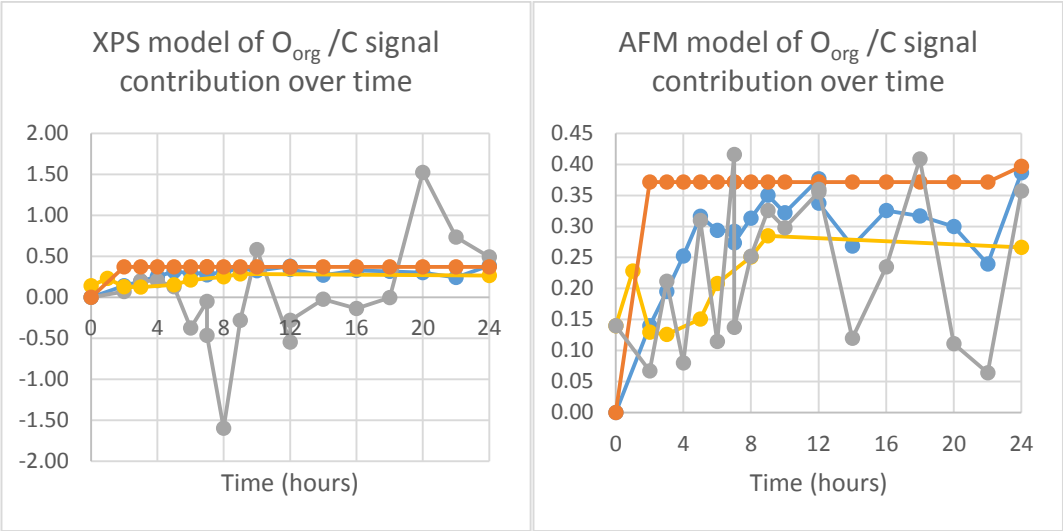

Figure 7.16 Graphs comparing models of O_{org}/C ratio within overlayer composition models against time, calculated from estimating the coverage from XPS data (left) and AFM (right), taken from Tables 7.1-7.6. Calculations of the bacterial contribution to signal (orange) and the resulting non-bacterial residue (grey) are compared to the original incubation data of silicon incubated with *NCTC13360* (blue) and silicon incubated with TSB over time (yellow).

Analysis of the O_{org}/C ratio showed the pellet to have a ratio of 0.37, which was higher than that of most points measured on the incubated sample. The XPS model showed a wide range of O_{org}/C across time, with those below zero indicating errors in the model. As with N/C, the error came from the low carbon in the residual layer calculated. While this model cannot be used to determine the potential polysaccharides in the sample, it showed there is a range in composition of the sample over time, and the layer was not of a consistent composition. The AFM model had a larger C 1s peak estimation, leading to the potential of a lower level of errors in the calculation of O_{org}/C. The O_{org}/C ratio varied over time, with values varying between 0.05 and 0.45. No distinct trend can be seen, indicating that while protein content contributing to the O_{org}/C was also not consistent, the lack of similarity in trend between the N/C and O_{org}/C indicated the amount of polysaccharide on the surface varied from sample to sample.

Overall, the timed silicon incubated samples showed the limitations of modelling bacteria based on the bacterial coverage. One of the main issues was the limit of the calculations of the residual layer. This was seen more through the XPS modelled bacteria coverage, where results of bacterial coverage above 90% have a higher tendency to estimate errors in the calculated residual layer.

However, this was not the only source of error in calculations. Additionally, the XPS model was more prone to error in the model. This was due to the use of the Si 2p peak as an estimate of coverage. While this is an indication of bacterial coverage, the model does not take into account any substances on the substrate supressing the signal. As seen in Chapter 5, the organic layer not from a source of bacteria has the ability to supress the silicon signal and AFM images shown in Chapter 5 confirmed this was due to a patchy layer on the surface. Due to the size of bacteria compared to the thickness of these patches, AFM images do not show these features, however errors in the XPS model showed this to still be the case.

The AFM model predicted a lower coverage compared to the XPS model, giving a more reasonable composition of residual layer. The AFM model is limited through the number of areas the average coverage was taken over, as well as the limited number of timed points used to estimate the coverage of other timed points. In reality, if AFM coverage was taken at more points, the model would show a variation in coverage at these points, which may account for changes in chemical composition between samples.

One of the main sources of error for both models was the P 2s signal, which showed a negative apparent phosphorus composition for all samples. While this may possibly have been due to the error in the bacterial coverage or the bacteria covered in the residual layer, there was also the issue with the detection limit of P 2s signal. This can be seen through the incubated samples where bacteria can be seen in AFM images within 4 hours but the P 2s signal was only detected by XPS after 8 hours of incubation. In this case, using the pelleted bacteria as an approximation of P 2s signal resulting from bacteria was inaccurate, and rather significant numbers of bacteria must be bound to the surface before the P 2s signal can be detected. This needs to be considered when analysing the P 2s peak in terms of determining if the bacterial layer was covered by a residual layer.

Both models predicted the presence of a residual layer with the detection of C 1s that was not related to the calculated coverage of bacteria. The composition of this layer varies between models. Both models predicted the presence of proteins in the model, with the amount of proteins varying between samples. The XPS model had a higher tendency to fail, however the N/C signal in the residual layer indicated the presence of proteins, with the lower O_{org}/C ratio, despite showing errors for organic oxygen, indicating that the layer is potentially protein dominant, with some samples showing traces of polysaccharide and hydrocarbons. The AFM model of coverage also showed the presence of proteins varied from sample to sample. The detection of O_{org}/C and C285 indicated the sample contained a mixture

of proteins, polysaccharides and hydrocarbons, varying between each point and indicating that the residual layer was in flux and the determination of its composition was limited to the area analysed.

Considering the concerns about P 2s peak in terms of a sample coverage model, the XPS model was assumed to overestimate the bacterial coverage. However, there is also the possibility that the overlayer covers the bacteria resulting in the P 2s signal being negative.

7.2.2 Glass

Glass was incubated with *NCTC13360* and TSB for 24 hours before analysis with XPS, Figure 7.17 shows the survey spectra and C 1s peak fit of the sample. The incubated glass with *NCTC13360* after 24 hours compared to TSB incubated glass after 24 hours and bacterial pelleted bacteria in Table 7.7.

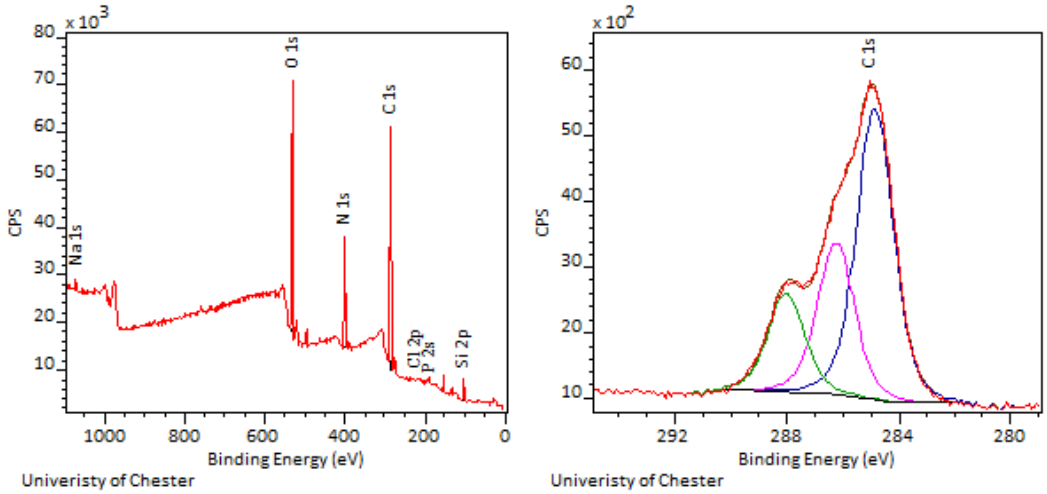

Figure 7.17 XPS survey spectrum and C 1s peak fit of glass incubated with *NCTC13360* after 24 hours.

The glass incubated with *NCTC13360* showed bacterial adhesion through the introduction of P 2p. Increases in C 1s, N 1s and O_{org} compared to TSB incubated glass supported the possibility of an additional organic substance on the surface. The presence of bacteria was confirmed through AFM images (Figure 7.1). The decrease in Si 2p showed the bacterial coverage of the sample to be at approximately 74%. The slight increase in carbon and nitrogen compared to the pellet indicated the sample was covered with an additional substance. As the organic oxygen level decreased, this layer was likely to be protein dominant. The C 1s peak fit showed the presence of the C285 peak in the sample, indicating the presence of hydrocarbons in the sample.

	TSB incubated Glass 24h	*NCTC13360* Pellet	*NCTC13360* incubated Glass 24h	XPS model		AFM model	
				Bacterial contribution	Calculated residue	Bacterial contribution	Calculated residue
C 1s	30.6	60.2	60.8	44.7	16.0	18.0	42.8
O 1s	41.0	25.1	21.9	18.6	3.3	7.5	14.4
O_{org}	4.4	22.3	14.5	17.7	3.7	7.1	7.4
N 1s	2.8	9.3	11.3	6.9	4.4	2.8	8.5
Si 2p	22.1	1.4	4.4	1.0	3.4	0.4	4.0
P 2s	0.0	3.7	0.9	2.7	-1.9	1.1	-0.2
Na 1s	0.3	0.1	0.5	0.1	0.5	0.0	0.4
Al 2p	1.6	0.0	0.0	0.0	0.0	0.0	0.0
Ca 2s	0.3	0.3	0.0	0.2	-0.2	0.1	-0.1
Mg 2p	1.3	0.0	0.2	0.0	0.2	0.0	0.2
C285	66.7	49.4	53.8	36.7	17.1	14.7	39.1
C286.5	26.1	34.8	28.1	25.9	2.2	10.4	17.7
C288	7.2	15.8	18.1	11.7	6.3	4.7	13.4
O_{org}/C	0.14	0.37	0.24	0.37	0.23	0.37	0.17
N/C	0.09	0.15	0.19	0.15	0.27	0.15	0.20
Model coverage				74%		30%	

Table 7.7 XPS analysis of the *NCTC13360* incubated glass after 24 hours compared to pelleted *NCTC13360* and media incubated glass after 24 hours. XPS data was analysed in terms of bacterial coverage estimated by XPS and AFM, and calculated residue on the surface.

On modelling the bacterial coverage through XPS data, the phosphorus level on the surface was found to decrease indicating the potential of the residue covering the bacteria. The composition of the residual layer showed the O_{org}/C was lower than that of N/C indicating the residue was predominantly protein. The residual layer calculated through the XPS model is TSB like, which had a dominance of polysaccharides as opposed to proteins. The calculated C285 signal of the residue was higher than that of C286.5 and C288, indicating the presence of hydrocarbon in the sample was high.

AFM images were also used to estimate the bacterial coverage. In comparison to the XPS model, the bacterial coverage by AFM was lower, however the P 2s peak is still negative. This indicated the bacteria was covered. As the P 2s was smaller than in the XPS model, it can be assumed the layer was either as a thin layer or in patches over the bacteria, which cannot be determined from XPS data. However, the low P 2s signal indicates the residual layer was predominantly bound to the glass, which was confirmed by the decrease in the silicon composition.

The composition of the residue showed the N/C was higher than O_{org}/C indicating the layer was protein dominant. The C285 peak indicates the presence of hydrocarbons in the sample. Comparing the residual layer to the TSB layer on the glass, the composition of the residual

layer changes from polysaccharides-dominant to protein-dominant, as seen through the change increase in N/C with a slight increase in O_{org}/C overall.

While estimating the bacterial coverage at different levels, both models predicted the residual layer to be protein dominant. This implied the residual layer was not TSB bound to glass. In terms of the AFM model, this indicated the residual layer was not TSB bound to the surface, with a small amount bound to the bacteria. The XPS model also assumed the layer bound to the glass was not TSB alone, however the layer was potentially covering the bacteria, making the interactions between bacteria and residue more complex to model.

7.2.3 Mica

After 24 hours mica incubated with *NCTC13360* was analysed by XPS and compared to pelleted *NCTC13360* and TSB incubated mica after 24 hours in Table 7.8 XPS analysis of the *NCTC13360* incubated mica after 24 hours compared to pelleted *NCTC13360* and media incubated glass after 24 hours. XPS data was analysed in terms of bacterial coverage estimated by XPS and AFM, and calculated residue on the surface.. Figure 7.18 shows the survey spectrum and C 1s peak fit of the 24-hour sample incubated with *NCTC13360*. Figure 7.1 in section 7.1 shows AFM images of the bacteria adhered to the 24 hour incubated mica with *NCTC13360*.

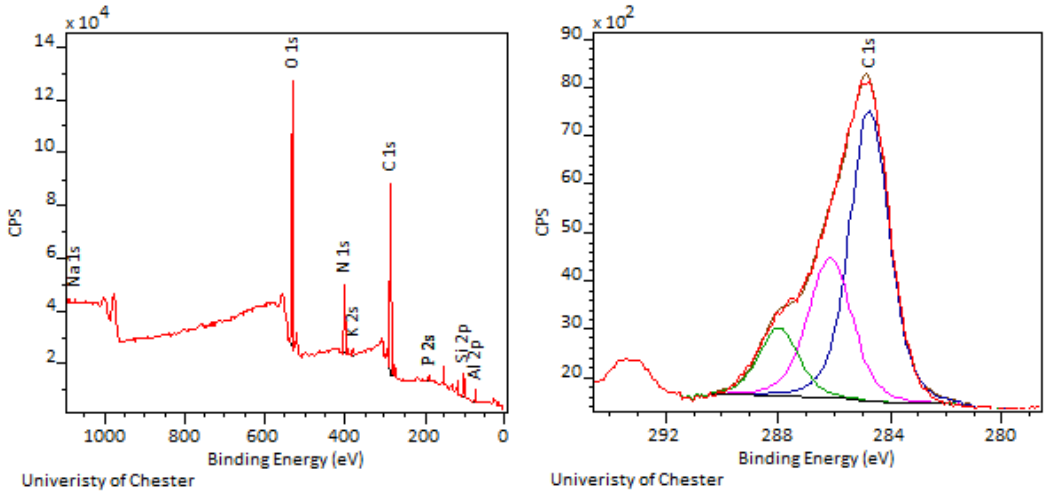

Figure 7.18 XPS survey spectrum and C 1s peak fit of mica incubated with *NCTC13360* after 24 hours.

In comparison to the TSB incubated mica and bacterial incubated sample, there was an increase in C 1s, N 1s and O 1s relating to an increase in organic content. The introduction of P 2s indicated the potential presence of bacteria, confirmed by AFM images.

	TSB incubated mica 24 h	*NCTC13360* Pellet	*NCTC13360* incubated mica 24h	XPS model		AFM model	
				Bacterial contribution	Calculated residue	Bacterial contribution	Calculated residue
C 1s	17.6	60.2	53.1	42.4	10.8	5.9	47.2
O 1s	45.0	25.1	25.8	17.6	8.1	2.5	23.3
O_{org}	6.0	22.3	12.7	16.8	3.7	2.3	10.3
N 1s	2.9	9.3	8.6	6.6	2.0	0.9	7.7
Si 2p	18.8	1.4	6.3	1.0	5.3	0.1	6.2
P 2s	0.0	3.7	0.9	2.6	-1.7	0.4	0.6
Na 1s	0.2	0.1	0.3	0.1	0.3	0.0	0.3
K 2s	2.9	0.0	0.9	0.0	0.9	0.0	0.9
Al 2p	12.7	0.0	4.1	0.0	4.1	0.0	4.1
Ca 2s	0.0	0.3	0.0	0.2	-0.2	0.0	0.0
C285	62.7	49.4	56.7	34.8	22.0	4.8	51.9
C286.5	27.9	34.8	30.0	24.5	5.5	3.4	26.6
C288	9.5	15.8	13.2	11.1	2.1	1.5	11.7
O_{org}/C	0.34	0.37	0.24	0.37	0.38	0.37	0.22
N/C	0.16	0.15	0.16	0.15	0.19	0.15	0.16
Model coverage				70%		10%	

Table 7.8 XPS analysis of the *NCTC13360* incubated mica after 24 hours compared to pelleted *NCTC13360* and media incubated glass after 24 hours. XPS data was analysed in terms of bacterial coverage estimated by XPS and AFM, and calculated residue on the surface.

In comparison to the pelleted bacteria, there was a decrease in C 1s, N 1s and P 2s indicating the sample wasn't covered completely with bacteria, which was confirmed in AFM images

After 24 hours of incubation mica with *NCTC13360*, the decrease in silicon compared to autoclaved material was used to determine the coverage of the sample, by XPS, to be 72%. Modelling the bacterial coverage, the phosphorus decreases, relating potentially to the bacteria covered in the residual layer calculated.

From the XPS model, there was a decrease in P 2s to negative values after calculating the residual layer, indicates the bacteria was potentially covered by the residual layer. The composition of the residual layer showed a higher O_{org}/C ratio to N/C ratio but showed similarities to TSB incubated mica. On analysis in Chapter 5, the composition of the TSB incubated mica showed a high level of proteins. Considering the formulas used to calculate the biological content, the value of N/C compared to O_{org}/C indicated a dominance of protein content, slightly higher than TSB layer.

The coverage calculated through AFM images was significantly lower than that calculated through XPS data. The AFM model showed the P 2s signal to be positive, indicating the bacteria was unlikely to be covered with a residual layer, and the potential the AFM model underestimated bacterial coverage. The composition of the residual layer showed the O_{org}/C ratio to be higher than N/C, but as the N/C was similar to that of O_{org}/C, the residual layer is

predominantly protein. The composition of the residual layer compared to the XPS model showed the O_{org}/C and N/C ratio was lower in the AFM model, indicating the AFM model has a higher hydrocarbon content, as confirmed by the carbon peak fit, through the larger C285 peak.

Both models showed a wide range of coverage, however both showed protein content dominance. The AFM model showed a higher hydrocarbon content.

7.2.4 Titanium

Sputter-coated titanium was removed from incubation with *NCTC13360* after 24 hours and analysed by XPS. Figure 7.19 shows the survey spectra and C 1s peak fit. The XPS data of the *NCTC13360* incubated sample was compared to TSB incubated titanium after 24 hours and the pelleted bacteria in Table 7.9.

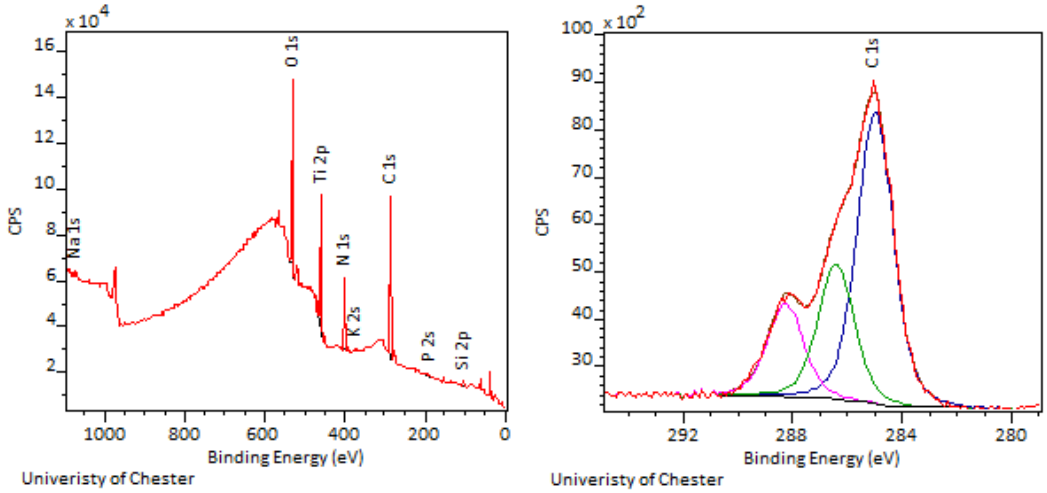

Figure 7.19 XPS survey spectrum and C 1s peak fit of titanium incubated with *NCTC13360* after 24 hours.

After 24 hours, the comparison between TSB incubation and bacterial incubation showed an increase in C 1s, N 1s, P 2s and O_{org} indicating an increase of biological content. The AFM image (

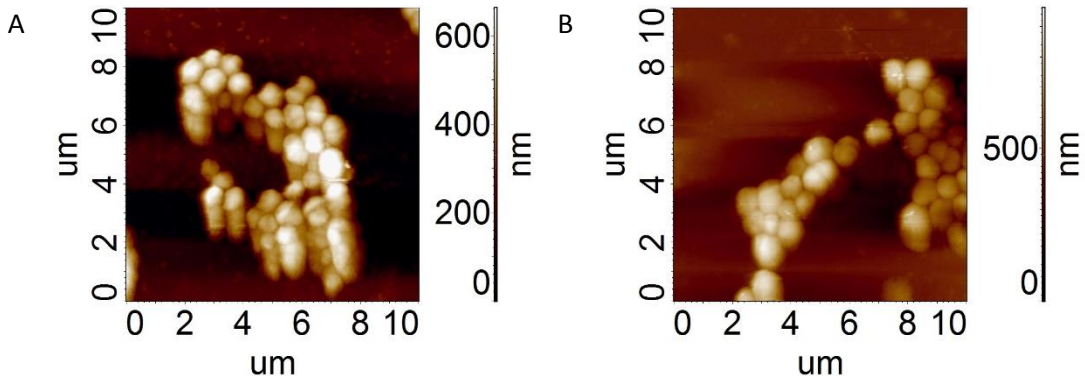

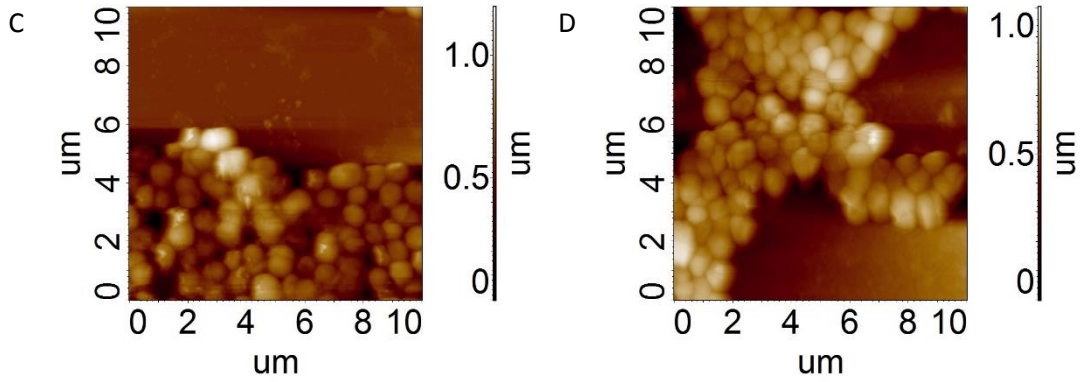

Figure 7.1) indicated a proportion of the increase relates to the presence of bacteria. After incubation with *NCTC13360* the silicon detected in the sample increased in intensity and the titanium decreased in intensity. This indicated that there was potentially some deterioration of the titanium layer, however this may also reflect the difference in titanium layer thickness between samples. The AFM images did not show any deterioration of the titanium layer, however as there were multiple changes occurring at the surface on incubation, it was difficult to isolate whether there was a change in the roughness or other parameter of the sample alone.

	TSB incubated titanium 24h	*NCTC13360* Pellet	*NCTC13360* incubated titanium 24h	XPS model		AFM model	
				Bacterial contribution	Calculated residue	Bacterial contribution	Calculated residue
C 1s	45.7	60.2	53.5	33.6	19.9	12.3	41.2
O 1s	36.0	25.1	28.2	14.0	14.2	5.1	23.1
O_{org}	24.7	22.3	14.4	12.5	6.4	4.6	9.9
N 1s	5.4	9.3	9.7	5.2	4.5	1.9	7.8
Si 2p	1.1	1.4	1.7	0.8	0.9	0.3	1.4
P 2s	0.6	3.7	0.9	2.1	-1.2	0.8	0.1
Na 1s	0.9	0.1	0.5	0.0	0.5	0.0	0.5
K 2s	0.0	0.0	0.2	0.0	0.2	0.0	0.2
Ti 2p	10.4	0.0	5.5	0.0	5.5	0.0	5.5
Ca 2s	0.0	0.3	0.0	0.2	-0.2	0.1	-0.1
C285	0.0	49.4	56.3	27.6	28.6	10.1	46.2
C286.5	22.7	34.8	26.0	19.5	6.5	7.1	18.9
C288	10.0	15.8	17.8	8.8	9.0	3.2	14.6
O_{org}/C	0.54	0.37	0.27	0.37	0.32	0.37	0.24
N/C	0.12	0.15	0.18	0.15	0.23	0.15	0.19
Model coverage				56%		20%	

Table 7.9 XPS analysis of the *NCTC13360* incubated titanium after 24 hours compared to pelleted *NCTC13360* and media incubated glass after 24 hours. XPS data was analysed in terms of bacterial coverage estimated by XPS and AFM, and calculated residue on the surface.

To model the coverage of the sample using XPS data, the change in titanium 2p peak was used as a first approximation. Although there was the potential of titanium layer deterioration on incubation, this was indeterminable and therefore ignored in any further interpretation.

Analysis of residual layer after bacterial modelling by XPS indicated that the bacteria were covered with the residual material. This was demonstrated by the decrease in P 2s. Increases in nitrogen, oxygen and carbon indicated the layer consisted of proteins and polysaccharides. The N/C ratio was lower than that of O_{org}/C however as they were similar in value there was a dominance of protein content. The calculated presence of the C285 peak indicated that the layer also contained hydrocarbons. From the AFM model, the P 2s signal was large enough to suggest the bacteria was not covered by the residual layer. However, the TSB incubated titanium also showed the presence of phosphorus, this was not a clear method of determining if the bacteria was covered. The composition of the residual layer was predominantly protein. Although the N/C ratio was smaller than the O_{org}/C ratio, there was a similarity in value, indicative of protein adhesion. The change in C 1s peak fit suggested there was a reasonable amount of hydrocarbon bound to the surface through the C285 peak. Compared to the TSB layer, there was more protein bound to the surface, and a decrease in polysaccharides bound to the surface

Both models showed the presence of high levels proteins in the residual layer, with hydrocarbons bound to the surface. There was a difference in the bacterial coverage calculated by XPS. This sample showed the limit of both models on using P 2s as an indication of bacterial coverage, as there was potentially P 2s as a residue of phosphates from media.

7.2.5 Silver

Sputtercoated silver was analysed after 24 hours of incubation on *NCTC13360* and compared to TSB incubated silver after 24 hours and the pelleted bacteria in Table 7.10. Figure 7.20 shows the survey spectrum and C 1s peak fit of the sample.

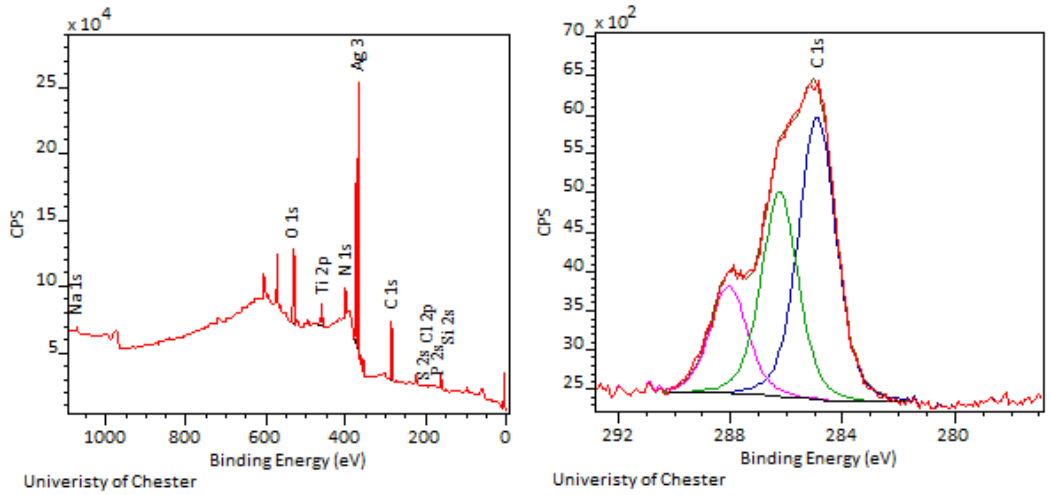

Figure 7.20 XPS survey spectrum and C 1s peak fit of silver inubated with *NCTC13360* after 24 hours.

After 24 hours of bacterial incubation, an increase in O 1s, C 1s and N 1s compared to TSB incubated silver was observed, indicating an increase in organic compounds on the surface, with the introduction of P 2p indicating the organic layer to be bacterial. The AFM images indicate an average bacterial coverage of approximately 39% on the areas of the sample investigated.

The decrease in Ag 3d showed a bacterial coverage of 73% however the observed Ti 2p and Si 2p peak in the sample indicates sample erosion, so coverage data estimated by XPS was potentially unreliable. Low levels of sulphur were detected on the surface, potentially due to contamination.

The detection of Ti 2p indicated the need to recalculate the organic oxygen component of the sample, using the equations presented in Chapters 2 and 3 to estimate the inorganic oxygen content of the sample due to the titanium/silicon underlayer.

	TSB incubated silver 24h	Pellet	*NCTC13360* incubated silver 24h	XPS model		AFM model	
				Bacterial contribution	Calculated residue	Bacterial contribution	Calculated residue
C 1s	43.1	60.2	46.2	44.5	1.7	24.0	22.2
O 1s	11.8	25.1	21.6	18.5	3.1	10.0	11.6
O_{org}	8.4	22.3	16.5	16.5	0.00	8.90	7.61
N 1s	6.9	9.3	8.0	6.9	1.1	3.7	4.3
Si 2p	0.0	1.4	5.0	1.0	4.0	0.6	4.5
P 2s	0.0	3.7	1.0	2.7	-1.7	1.5	-0.5
Na 1s	0.6	0.1	0.6	0.1	0.6	0.0	0.6
Ti 2p	0.0	0.0	2.2	0.0	2.2	0.0	2.2
Ag 3d	37.5	0.0	11.1	0.0	11.1	0.0	11.1
Cl 2p	0.0	0.0	0.5	0.0	0.5	0.0	0.5
S 2s	0.0	0.0	3.8	0.0	3.8	0.1	3.8
Ca 2s	0.0	0.3	0.0	0.2	-0.2	19.7	-0.1

C285	65.7	49.4	47.6	36.5	11.0	13.9	27.9
C286.5	20.3	34.8	34.4	25.8	8.6	6.3	20.5
C288	14.0	15.8	18.1	11.7	6.4	0.4	11.8
O_{org}/C	0.19	0.37	0.36	0.37	0.00	0.15	0.34
N/C	0.16	0.15	0.17	0.15	0.64	0.06	0.19
Model Coverage				72%		40%	

Table 7.10 XPS analysis of the *NCTC13360* incubated silver after 24 hours compared to pelleted *NCTC13360* and media incubated glass after 24 hours. XPS data was analysed in terms of bacterial coverage estimated by XPS and AFM, and calculated residue on the surface.

On modelling the surface coverage on the assumed bacterial coverage by XPS, the overall organic oxygen was zero. This implied any residual layer consisted of nitrogen and carbon only, which does not relate to any biological compounds expected on the surface. As P 2s was also negative, it can be assumed there was a significant overestimation of bacterial coverage according to this model and this was related to inadequacies in the calculation of the residual layer. It can be assumed that the overestimated bacterial coverage was due to the neglect of the residue supressing the silver signal along with the erosion of the silver layer, giving a lower silicon signal.

The coverage determined by AFM was lower than that estimated by the XPS model. In comparison to the XPS model of bacteria coverage, the residual layer gives more reasonable results, including an N 1s and an organic oxygen contribution to the signal. The P 2s signal was still below zero indicating the potential covering of bacteria by the calculated residue. The residual layer had a significantly higher O_{org}/C compared to N/C indicating it consisted of polysaccharides as well as proteins.

7.2.6 Conclusions from the XPS analyses

The two models proposed to estimate coverage gave different results for coverage, with XPS giving higher coverages than AFM model. This was due to XPS model potentially overestimating the bacterial coverage, by neglecting the effect of the residue bound to the surface on the defining peak. In addition to this, in some cases layer erosion also occurred, leading to further errors in bacterial coverage calculations. AFM theoretically miscalculates the coverage, as it was calculated by average area on 10 µm squares, which is insufficient to give an overall accurate estimate of coverage of the sample.

Generally, this led to the XPS model estimating the P 2s to be below zero. While this can imply that the bacteria are covered by the residual layer, it was more likely due to the overestimate of bacterial coverage. This can be seen through AFM samples, where there

some which estimate the P 2s to be positive or close to zero, consistent with typical detection limits for the P 2s peak.

The composition of the residue varied between samples. In general, the overall composition of the residual layer was found to be dominated by protein. The carbon 285eV for each sample varied, as an indication of hydrocarbon in the sample. In some cases, there was a loose correlation between substrate coverage and hydrocarbon content, indicating the residual layer was not thick to supress this and is potentially an uneven layer.

In comparison to the TSB incubated samples, the protein and sugar content differ from the residual layer. This indicated the residual layer is not TSB alone. The difficulty lies in determining the composition of the new layer in terms of it the substances are TSB based or a result of bacteria excreting substances. The model also does not consider if there are preferential binding locations of compounds to the sample and how that affects bacterial adhesion.

7.3 AFM Force curve analysis

Force curve measurements were taken at 9 points on 3 squares of 10 x 10 µm. Force distance curves were correlated to position on the AFM image and treated separately depending on whether the force curve was taken on or off a bacterium in Table 7.11 and through histograms in Figures 7.21, 7.23, 7.25 and 7.27. Large standard deviations were observed within force curve data and consequently frequency distributions were used to clarify key features, these are included in Figures 7.21 -7.28 and in the appendix.

Material	TSB incubated 24 hours				*NCTC13360* incubated substrate 24 hours							
					Bacterial points				Non-bacterial points			
	Snap in (nm)	Attractive force (nN)	Pull out (nm)	Retractive force (nN)	Snap in (nm)	Attractive force (nN)	Pull out (nm)	Retractive force (nN)	Snap in (nm)	Attractive force (nN)	Pull out (nm)	Retractive force (nN)
Glass	7.9	50.9	9.3	73	3.2	7.5	8.1	42	4.6	7.8	12.7	92
	3.0	25.4	4.9	40	1.8	7.7	5.9	40	1.5	10.3	8.9	70
Mica	1.2	11.3	3.0	47	3.7	9.2	6.6	25	2.9	6.4	9.4	32
	0.4	6.6	0.7	12	2.2	7.2	3.8	12	1.1	6.3	9.3	18
Titanium	3.3	23.7	9.1	76	3.6	6.2	9.5	24	2.3	6.4	8.0	40
	1.5	15.7	4.2	29	3.0	5.3	9.8	13	1.5	7.7	2.2	15
Silver	3.9	26.7	6.2	44	3.8	16.2	7.9	52	3.2	10.6	7.7	59
	1.2	13.2	1.6	13	1.8	12.6	4.5	23	1.6	6.7	2.2	22
Pelleted *NCTC13360*					2.5	3.4	7.8	14				
					1.4	2.4	4.7	8				

Table 7.11 AFM force curve comparison of substrates incubated with TSB after 24 hours and *NCTC13360* incubated substrates after 24 hours, divided into points on and off the bacteria. The first row for each material shows the mean value and the second row for the material shows standard deviation.

	TSB incubated silicon time				*NCTC13360* incubated silicon timed							
					Bacterial				Non-bacterial			
	Snap in (nm)	Attractive force (nN)	Pull out (nm)	Retractive force (nN)	Snap in (nm)	Attractive force (nN)	Pull out (nm)	Retractive force (nN)	Snap in (nm)	Attractive force (nN)	Pull out (nm)	Retractive force (nN)
2 hours									4.0	18.8	14.6	112
									2.2	19.4	7.8	63
4 hours					4.5	8.3	21.2	71	3.0	11.7	7.5	55
					3.0	11.1	12.7	56	1.5	12.8	4.5	18
6 hours					2.7	8.5	8.9	54	2.8	15.3	10.8	95
					2.5	11.6	7.0	38	1.3	14.2	7.2	58
8 hours					2.4	6.1	16.1	91	3.0	8.2	10.9	85
					1.3	6.9	10.4	62	2.7	8.4	4.4	39
24 hours	6.0	49.1	8.8	77	4.0	19.1	12.5	83	4.4	12.4	12.4	77
	1.1	13.4	3.2	28	1.6	15.0	3.2	39	1.6	3.7	3.7	30
Pelleted *NCTC13360*					2.5	3.4	7.8	14				
					1.4	2.4	4.7	8				

Table 7.12AFM force curve comparison of silicon incubated with TSB over time and *NCTC13360* incubated substrates over time, divided into points on and off the bacteria. The first row for each material shows the mean value and the second row for the material shows stand ard deviation.

7.3.1 Snap in distance

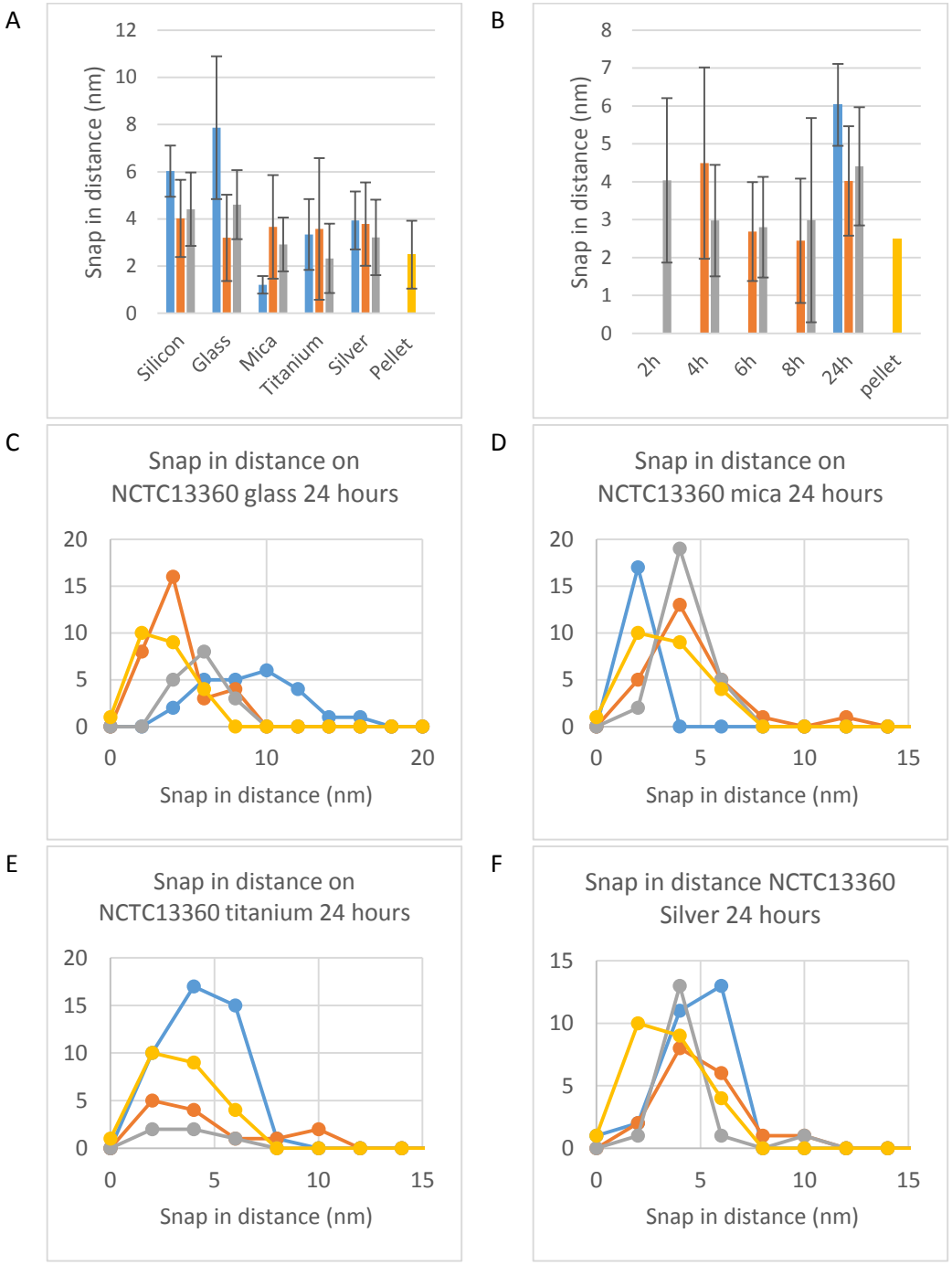

Figure 7.21 Histograms showing the snap in distance of the substrates after 24 hours(A) and of silicon during the first 8 hours (B). In both cases, data are shown for measurements on and off individual bacteria, and for the 24 hour data the equivalent data for the substrate incubated in TSB alone is also shown. Below images of frequency distributions are included for glass(C), silicon(D), titanium(E) and silver(F). Blue is TSB incubated sample, orange is *NCTC13360* incubated bacterial points, grey relates to non bacterial points on *NCTC13360* and yellow is the *NCTC13360* bacterial pellet.

Snap in distance frequency distributions for the timed data after incubation of *NCTC13360* bacteria on Si (111) substrates are shown in Figure 7.21 for data both on and off individual

bacteria. The timed bacterial points on incubated silicon overlap with range of 0 - 8 nm with 4 hours showing a wider range. All bacterial points showed overlap with the pelleted bacteria. Non-bacterial points showed a wide range of 0-8nm for all non-bacterial points that all overlap. The timed 2 hour sample showed non-bacterial points have a slightly wider range, covering the lower end of the range of 24 hour TSB incubated silicon. 24 hour sample bacterial incubated sample had a smaller range (3-8nm).

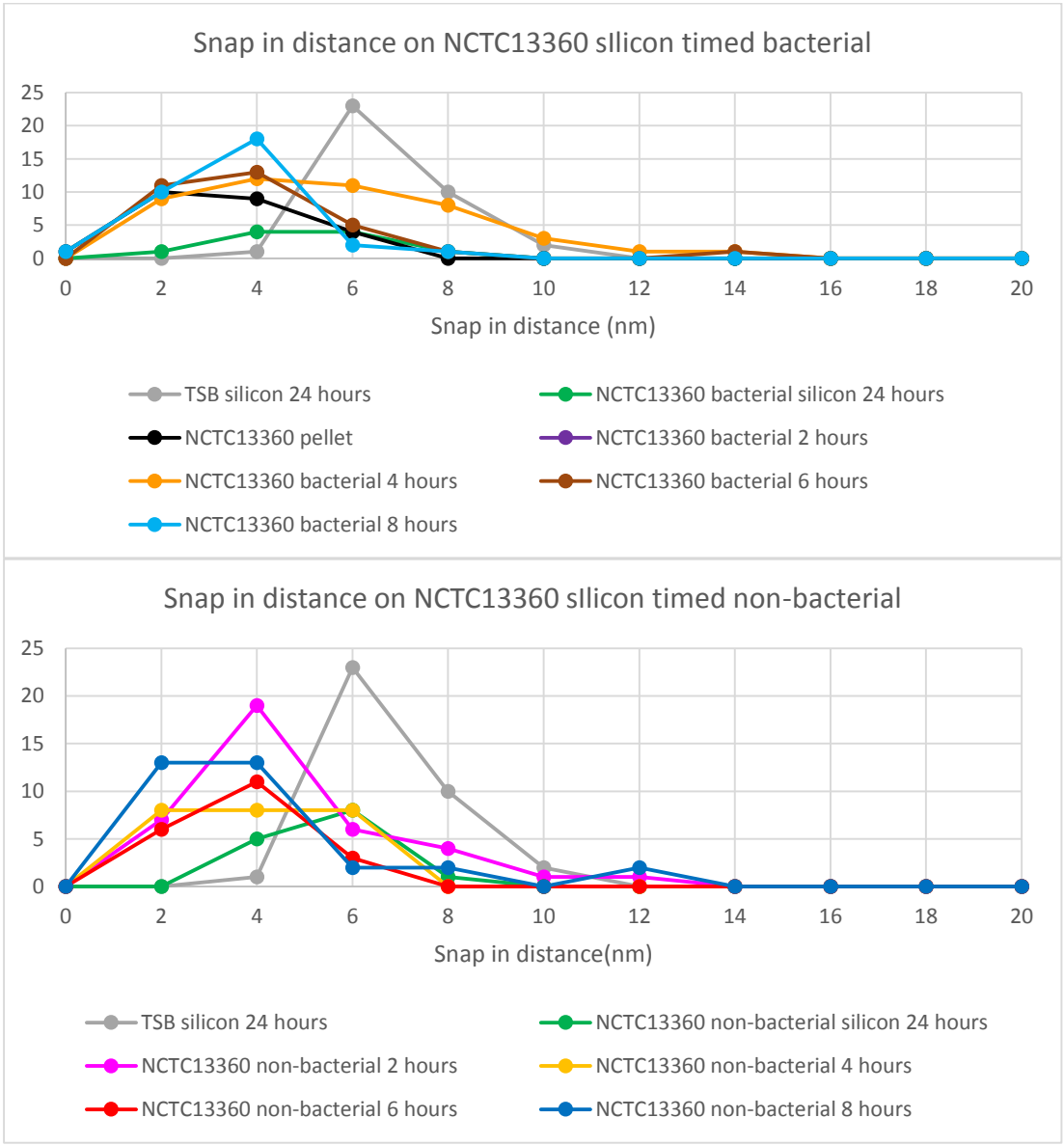

Figure 7.22 Frequency distributions of snap in values on *NCTC13360* on silicon over time, including TSB incubated silicon after 24 hours and pelleted bacteria.

Analysis of 24 hour TSB incubated substrates showed similarities between points on and off the bacteria as well as other 24 hour bacterial incubated samples. Silver and titanium showed similarities to that of the relevant 24 hour TSB incubated substrates. Mica showed the 24 hour media incubated sample had a lower snap in distance than that of the bacterial sample. Silicon

and glass showed a higher snap in value for the relevant 24 hour media sample than bacterial samples.

Frequency distributions showed there was generally a degree of overlap between bacterial and non-bacterial data points. Glass and titanium had wider ranges on bacterial points compared to non-bacterial points, but as observed in the histograms glass showed a shift to higher values for non-incubated points compared to non-incubated points. All samples showed overlay of points on and off the bacteria. In addition, analysis of non-bacterial points on the glass sample over overlapped with the lower end of the range TSB incubated glass after 24 hours. Titanium and silver showed overlap of the relevant TSB incubated sample with points on and off the bacteria.

7.3.2 Attractive force

On analysis of frequency distributions of timed samples, bacterial points were more frequently observed between 0 - 10 nN, with points of higher forces having less frequency. Attractive force measurements of early stage bacterial points showed some similarities to that of the pelleted sample. The 24 hour incubated sample on silicon showed similarities to other incubated silicon incubated samples but were not as intense between 0 - 10 nN. This indicates the potential change in the composition of the overlayer. All timed bacterial points overlap with data from the pelleted samples and had a slight overlap with the wide range of data from TSB incubated silicon. All non-bacterial points followed the same trend as the bacterial points.

Data from the incubated samples on glass, silicon, mica and titanium showed overlap of bacterial and non-bacterial points. Silver showed bacterial points having higher adhesion values on bacteria compared to off the bacteria. Mica also showed similarities to that of TSB, with all other incubated samples showing a decrease. Titanium, glass and mica were similar in value both on and off the bacteria. Silver and silicon also showed similarities in bacterial measured points. Analysis of frequency distributions indicated all bacterial incubated samples showed similarities to the bacterial pellet. Analysis of silver showed that the distribution of bacterial points had 2 peak bi-modal distribution, giving a wider range and explaining the high standard deviations seen for this substrate. One of the peaks of the distribution on silver overlapped with data from the non-incubated points and pelleted bacteria. The other peak of the distribution showed similarities to the distribution measured for TSB incubated silicon.

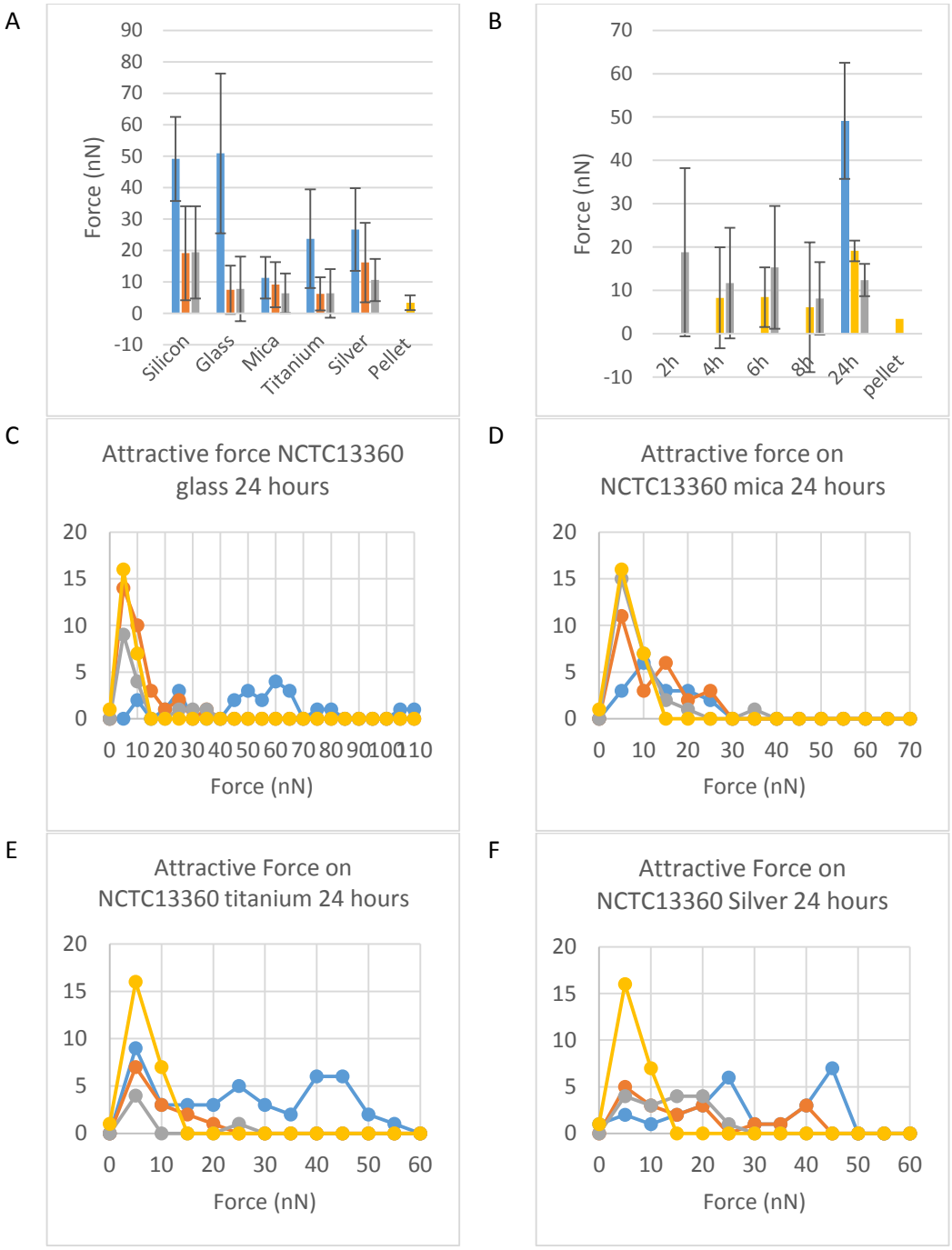

Figure 7.23 Histograms showing the attractive force of the substrates after 24 hours(A) and of silicon during the first 8 hours (B). In both cases, data are shown for measurements on and off individual bacteria, and for the 24 hour data the equivalent data for the substrate incubated in TSB alone is also shown. Below images of frequency distributions are included for glass(C), silicon(D), titanium(E) and silver(F). Blue is TSB incubated sample, orange is *NCTC13360* incubated bacterial points, grey relates to non bacterial points on *NCTC13360* and yellow is the *NCTC13360* bacterial pellet.

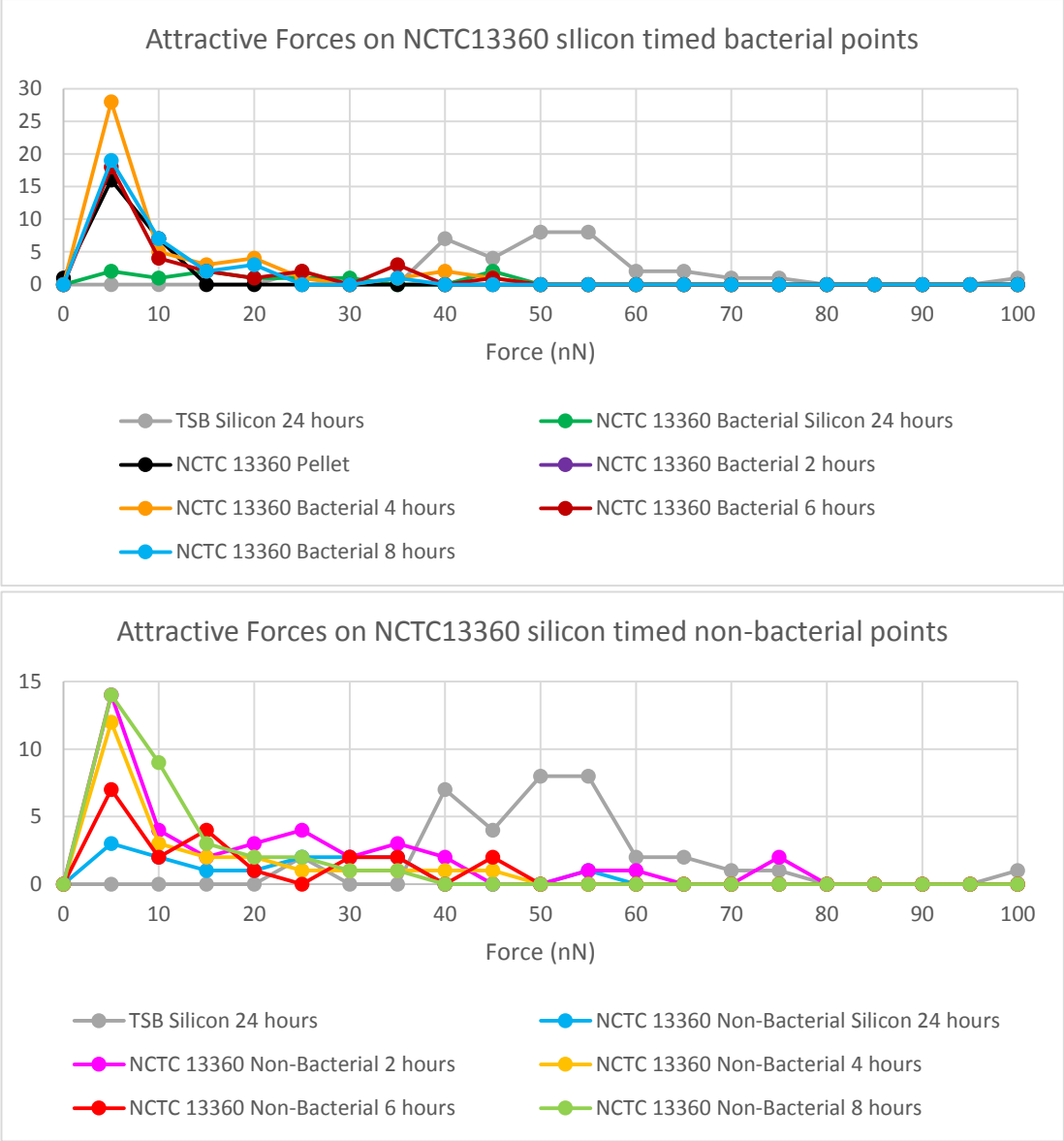

Figure 7.24 Frequency distributions of attractive forces on *NCTC13360* on silicon over time, including TSB incubated silicon after 24 hours and pelleted bacteria.

Data from the 24 hour samples on silicon and silver showed similarities between points on and off the bacteria. Glass and mica showed adhesive force values to be slightly higher on non-bacterial points while titanium showed a decrease in adhesion force values on comparison to non-bacterial points. Silicon, mica and silver showed an increase in adhesive force after incubation with bacteria, whereas glass and titanium incubated TSB sample were similar to those of incubated bacterial samples.

Glass and mica showed direct overlap of bacterial and non-bacterial points. Glass also showed similarities TSB and pelleted bacteria, with bacterial incubated samples showing a wider range covering both. Mica showed a direct overlap between bacterial sample and pelleted bacteria

and overlap with media, where the range on media being tighter and average lower than that of pellet and incubated mica with bacteria.

Data from the titanium substrate showed overlap of bacterial, non-bacterial and pelleted bacteria. TSB incubated bacteria also overlapped but with a wider range.

Silver showed overlap of data from the TSB, pellet and incubated bacterial sample with non-bacterial points having a higher range than bacterial points.

7.3.3 Pull out distances

Average pull out distances measured on bacterial samples range from 7 nm to 22 nm with wide ranges measured on timed samples, with the exception of the 24 hour incubated sample. Some similarities between data recorded on or off the bacteria and the TSB sample were observed, however, differences were revealed using the frequency distributions plots. All points showed a wide range from 0 – 40 nm, with the most frequent points being between 10 - 20 nm. In comparison to the pelleted sample, bacterial points were typically higher. In comparison to TSB, both bacterial and non-bacterial points had a wider range.

Inspection of data from the 24 hour samples showed overlap on points on and off the bacteria, indicating the potential formation of an overlayer covering the entire sample.

The TSB incubated glass showed similarities to points both on and off the bacteria. On titanium the data measured on bacteria showed a smaller range than non-bacterial points. Force curves on silver samples showed the pull out distance to have a very slightly higher average value on the bacteria than on non-bacterial points.

Analysis of bacterial points on several samples showed overlap with data from the pelleted bacteria. Incubated titanium and silver showed direct overlap, whereas glass showed pelleted bacteria to have a lower average value and mica to have a higher average value.

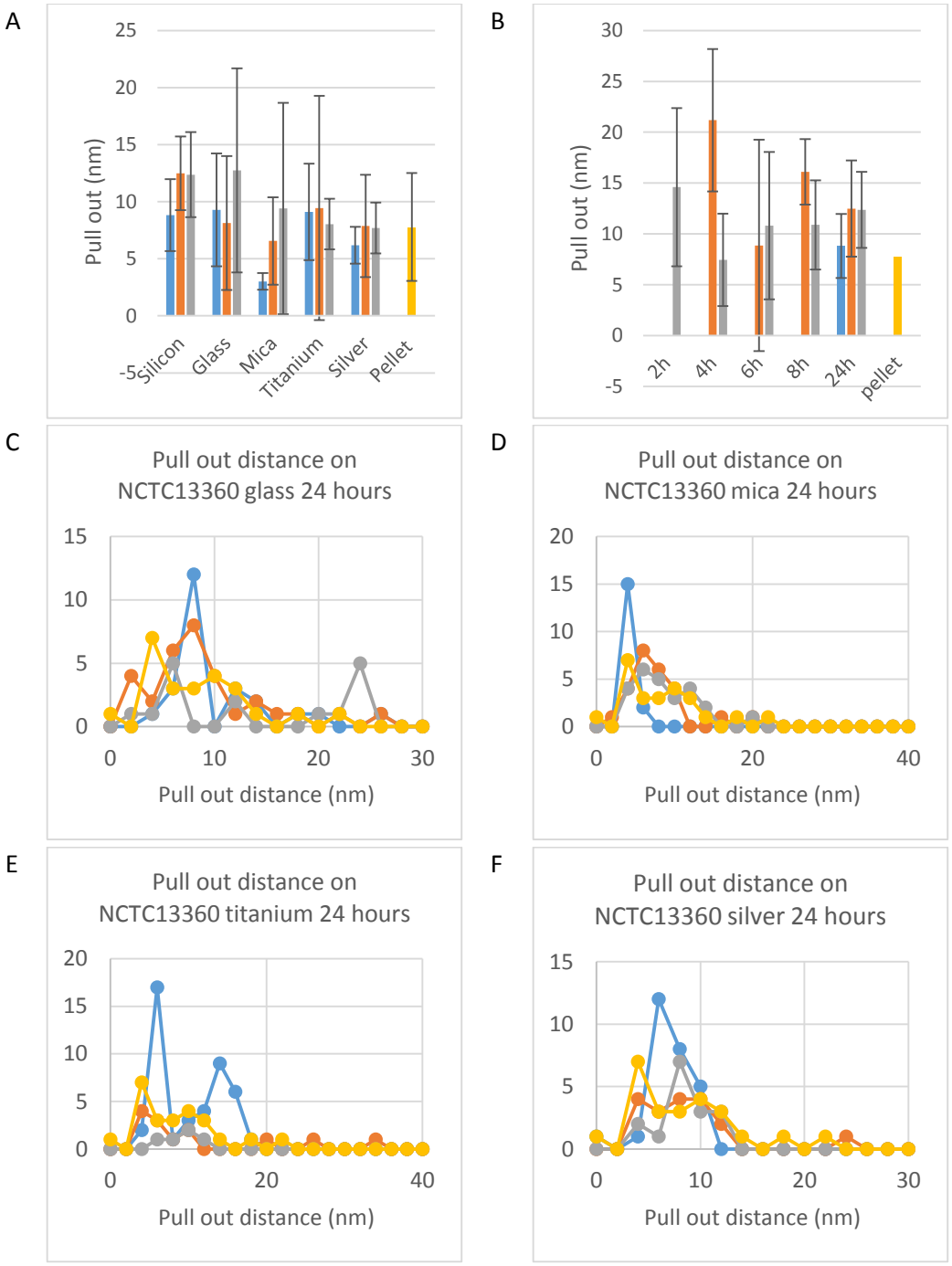

Figure 7.25 Histograms showing the pull out distance of the substrates after 24 hours(top left) and of silicon during the first 8 hours (top right). In both cases, data are shown for measurements on and off individual bacteria, and for the 24 hour data the equivalent data for the substrate incubated in TSB alone is also shown. Below images of frequency distributions are included for glass(C), silicon(D), titanium(E) and silver(F). Blue is TSB incubated sample, orange is *NCTC13360* incubated bacterial points, grey relates to non bacterial points on *NCTC13360* and yellow is the *NCTC13360* bacterial pellet.

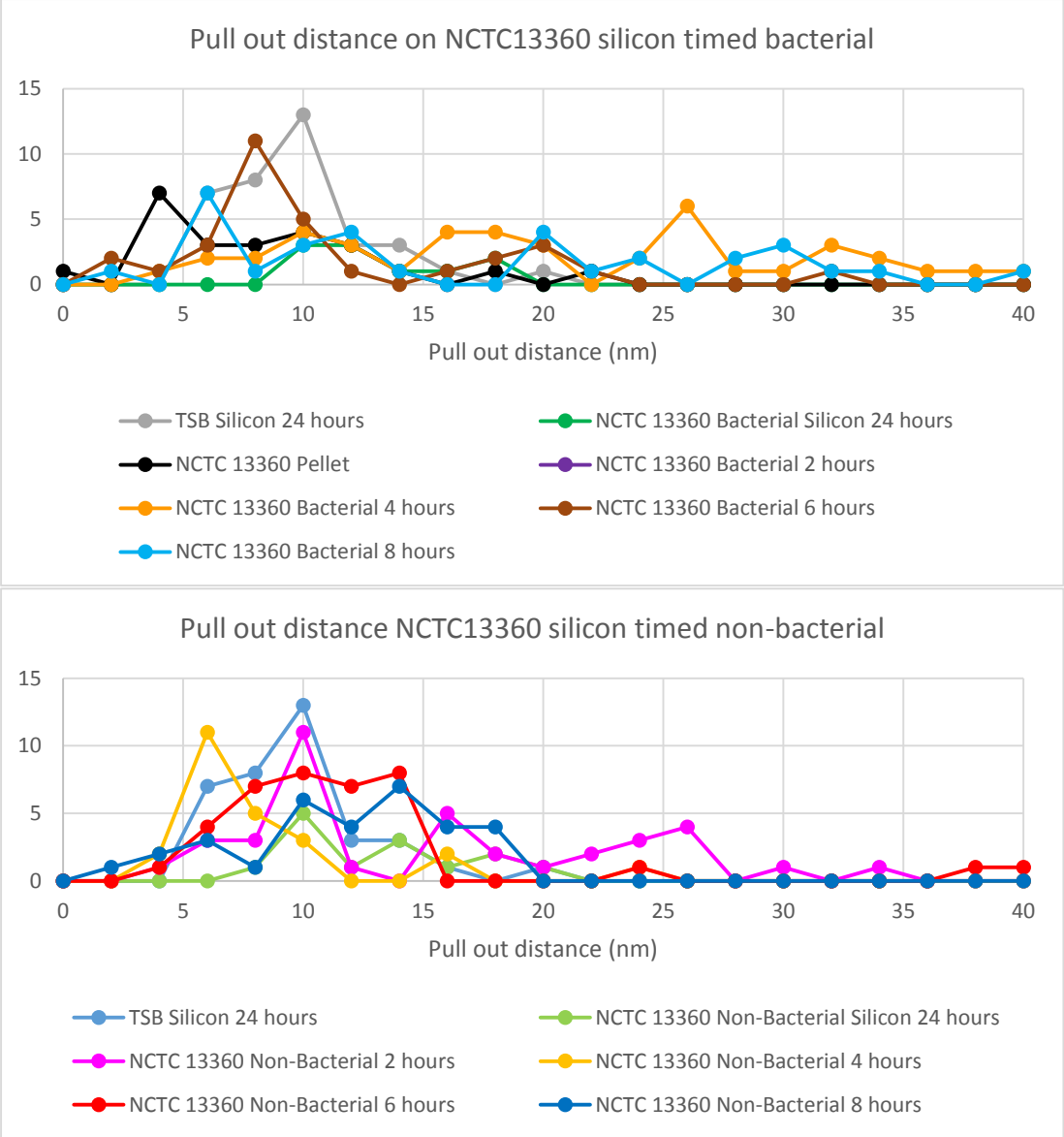

Figure 7.26 Frequency distributions of pull out distances on *NCTC13360* on silicon over time, including TSB incubated silicon after 24 hours and pelleted bacteria.

7.3.4 Retractive forces

Retractive forces values on timed samples showed variation over 50 to 100 nN with wide ranges recorded in the data. In comparison to pellet samples all data recorded on bacteria were on average higher than those of the pelleted bacteria, indicating additional levels of adhesiveness.

Both points on and off the bacteria fall in the same range as found for the TSB-incubated samples. On analysis of frequency distributions, all bacterial points overlapped with TSB, with broader distributions to overlap with measures of pelleted sample.

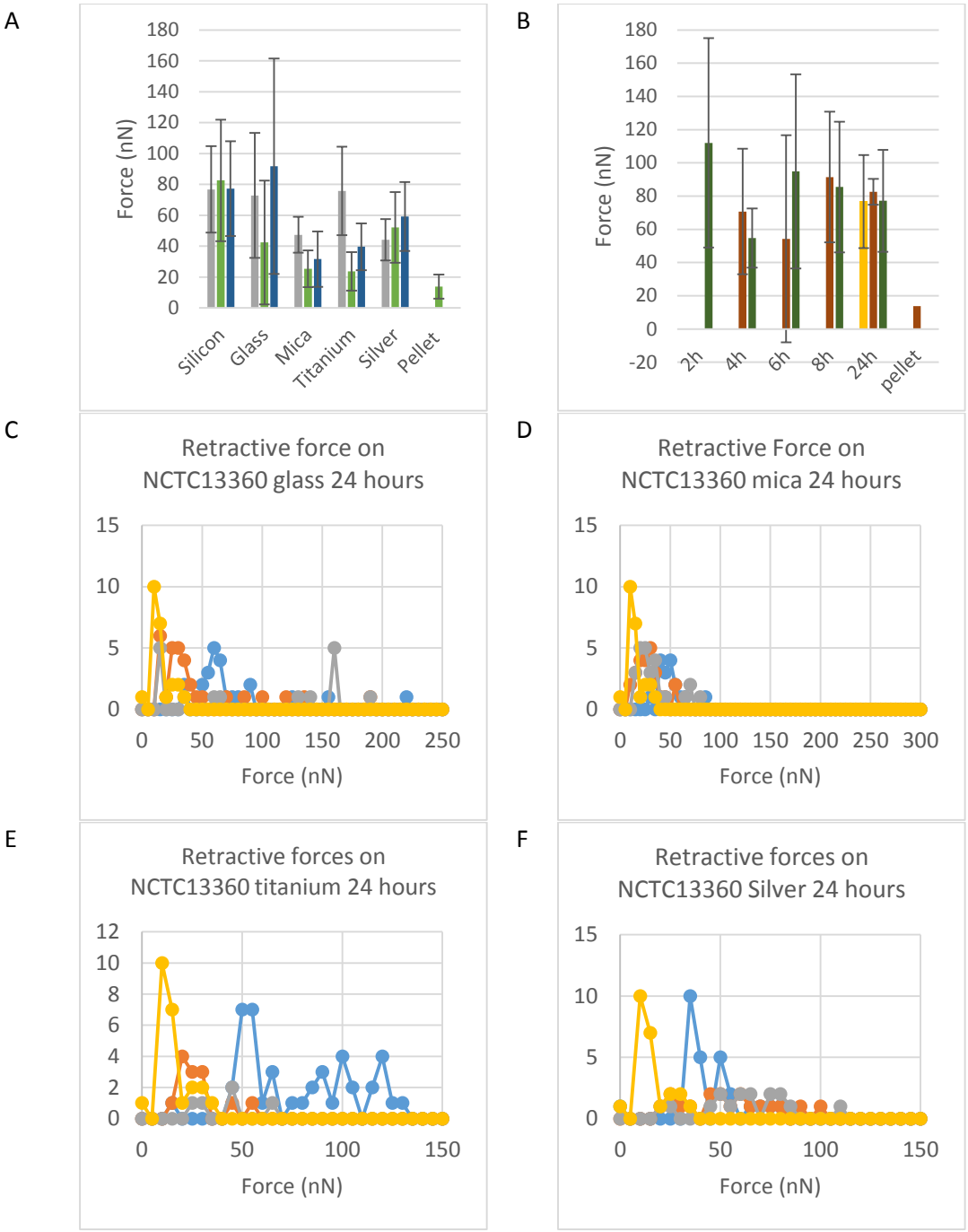

Figure 7.27 Figure 7.28 Histograms showing the retractive force of the substrates after 24 hours(top left) and of silicon during the first 8 hours (top right). In both cases, data are shown for measurements on and off individual bacteria, and for the 24 hour data the equivalent data for the substrate incubated in TSB alone is also shown. Below images of frequency distributions are included for glass(C), silicon(D), titanium(E) and silver(F). Blue is TSB incubated sample, orange is *NCTC13360* incubated bacterial points, grey relates to non bacterial points on *NCTC13360* and yellow is the *NCTC13360* bacterial pellet.

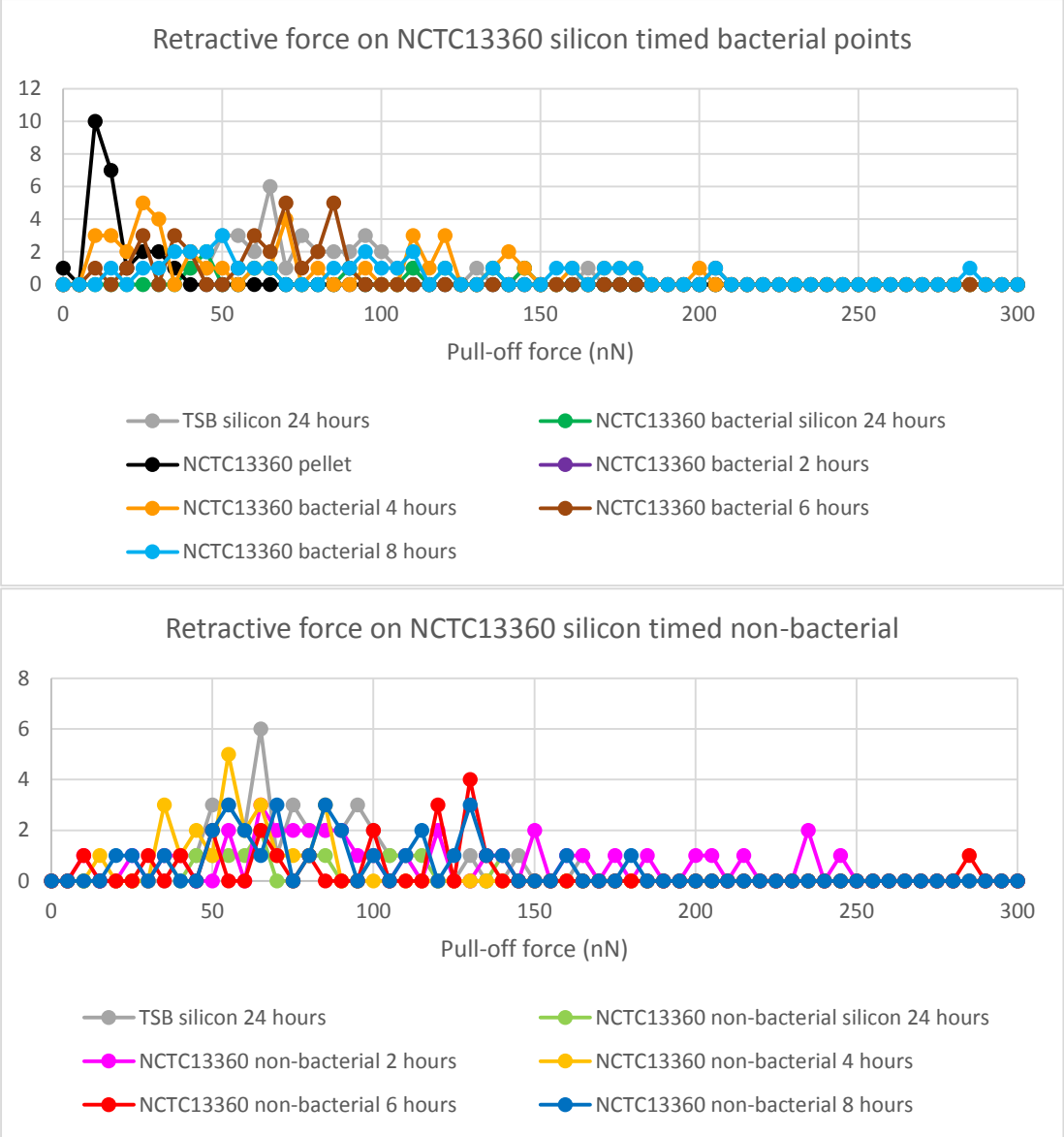

Figure 7.29 Frequency distributions of retractive forces on *NCTC13360* on silicon over time, including TSB incubated silicon after 24 hours and pelleted bacteria.

For 24 hours samples, most materials showed some degree of change between points on and off the bacteria, with non-bacterial points having lower values. Mica and titanium substrates showed an observable decrease between the TSB and bacterial incubated sample, whereas glass and silver showed an increase. On analysis of frequency distributions, non-bacterial points were found to have generally 2 peaks of intensity, one at approximately 15 nN and one at approximately 160 nN. This accounts for the large values of apparent standard deviation. The lower peak, at 15 nN, overlaps with pelleted bacterial points, whereas the incubated bacterial points generally occurred in the higher range. In comparison to TSB, bacterial points were generally lower in value, whereas non-bacterial points showed values either side of the range of TSB values. The pelleted bacteria showed some overlap to bacterial points but were generally smaller.

For mica, bacterial and non-bacterial points were found to have direct overlap, with outliers skewing the average in some cases. Both bacterial and non-bacterial points showed a smaller range than in the data recorded for TSB. The TSB-incubated data overlapped data from the bacterial points at the higher end of the range of the TSB data. In comparison to pelleted bacteria, both showed overlap but fall within a higher range than pellets.

7.3.5 Overall AFM force curve analysis

Analysis of force-distance curves for all samples showed similarities between points on and off the bacteria, indicating the potential formation of an overlayer over the entire sample. Variations between points on and off the bacteria in this case indicated the uneven thickness of the overlayer as well as an uneven distribution of organic compounds. Additionally, this could also indicate the preferential binding of some organic compounds to the surface of the bacteria. The nature of the organic compounds bound to bacteria cannot be unambiguously determined from the XPS data.

Analysis of force distance curves for these samples becomes more difficult with the prospect of tip contamination. The tip can be contaminated with organic compounds or with bacteria. During experiments, tip contamination was minimised through minimal tip- sample contact. The potential for bacterial contamination of the tip was also minimised through shaking the tip between each image analysis by running a high frequency scan away from the sample.

Comparing the bacterial points on incubated samples to pelleted bacteria showed similarities, indicating the presence of bacteria, the slight variation may indicate the presence of an overlayer. Alternatively, as bacterial points also showed similarities to the pelleted bacteria, the organic residue may have been of a similar nature to the bacteria cells. This case indicates that the overlayer may not cover the bacteria. Evidence for the presence of an overlayer on the bacteria is seen through the analysis of retractive forces, where results from the pelleted bacteria are lower than the incubated bacteria

Comparing to TSB incubated samples showed some overlap with bacteria incubated samples, with some degree of variation. This indicates the nature of the residue is similar to TSB. The non-bacterial points differed slightly from TSB samples, indicating that the residual layer is not TSB bound material seen in Chapter 5. This could be due to the preferential binding of bacteria to media bound substrates or to additional compounds on the surface as a consequence of the bacteria excreting compounds. Determination of this was difficult from AFM data, due to the similarities in measurements for all organic compounds so far. Potential ways around this are discussed in Chapter 9.

Overall, the potential presence of the residual organic compounds covering the bacteria is feasible, due to similarities between points on and off the bacteria. This agrees with retractive force data of bacteria incubated samples being typically higher than the bacterial pellet.

7.4 Conclusions

XPS raw data showed that the *NCTC13360* incubated samples, are not only bacteria alone. Therefore, models were built on the theory that the bacteria adhered to the sample was of the same composition as the pelleted bacteria, and the remaining is what is covering the non-bacterial covered substrate. Two methods were used to estimate the coverage of the bacteria. The first was using the XPS data on the change of the defining peak (Si 2p, Ti 2p or Ag 3d) as a guide to bacterial coverage. This model was limited, as it does not consider the suppression of the defining peak on points where the residual layer is in excess of 10nm. The second model used AFM data, where the coverage was estimated from AFM images for most samples. As all timed samples were not analysed by AFM, a model was created using information from known samples to estimate the coverage at these times. The limits of using AFM images is the size of the area scanned, which averages the area of 3 randomly chosen points of 10 x 10 µm for each sample, leading to estimates that may not characterise the total coverage of the sample. Further the estimation of unknown timed samples was also limited by the error in AFM coverage of known samples, as well as knowing whether any additional adhesion events took place. Both models give different models of coverage as seen in the graph. The use of SEM images for coverage was considered however only a small subset of samples were analysed by SEM and therefore not considered as a useable technique for the model.

Variations in calculation of bacterial coverage led to 2 different set of values calculated for the residual uncovered bacteria. While XPS models showed the suppression of P 2s of the bacterial samples, the AFM model showed a smaller change in P 2s. This indicated that XPS assumed the bacteria were covered with an overlayer, whereas AFM model showed only a small, or potentially uncovered bacteria (image limit). The limitations of both models suggest that XPS data is an overestimate of bacterial coverage whereas AFM may show an underestimate in bacterial coverage. As it is uncertain which model is correct, we can assume the average is somewhere in the middle, and the bacteria is potentially covered with an overlayer.

The results of both models gave different assumptions of coverage, and therefore calculated the residual layer had different compositions. The composition of overlayer showed the overlayer is not just the residual TSB on the surface alone, and therefore must have its own composition. Some material effect must also play a role in this overlayer as the composition varied between

materials. This effect can also be seen in Chapter 5, where each material showed variation in the adhesion of TSB compounds to the surface.

The overall model is limited in samples which had a bacterial coverage above 90%. These samples were the most likely to calculate negative signal contributions for the residual layer, which is not possible. In most cases, this was found on XPS sample, which has been shown to be an overestimate of bacterial coverage of the sample. The estimation of a bacterial coverage above 90% is feasible, as seen in Figure 7.2 where the 8 hour sample analysed by SEM appeared to have a 100% coverage. The error calculated by high coverage samples, is therefore not just due to the overestimation of bacterial coverage, but also due the limit of measuring the sample composition accurately from one point on the sample. As previously discussed, the coverage of the sample was not an even layer, which results in a change in chemical composition depending on the location the sample is analysed. Additionally, the effect of an overlayer on the bacteria was not explored, in terms of effect on the suppression of signal from the bacteria. Determination of this is difficult due to the unknown composition of the overlayer as due to uncertainties in bacterial coverage, as well as the unknown location and thickness of the organic layer.

Overall, limits in the bacterial model lead to difficulties in determining the true composition and location of the residual layer. AFM analysis was used in addition to the model to determine the location of the residual layer as well as its effect on adhesion of the sample.

AFM analysis of force curves give a range information about the incubated samples. Overall, similarities between bacterial and non-bacterial points on the sample were found, indicating both have the same characteristics, potentially implying that the overlayer covers the entire sample. The presence of the overlayer is confirmed through variations in retractive forces.

In comparison to TSB there were some samples which showed some overlap, but overall there was enough difference between the two to suggest the overlayer was not just TSB alone. Both bacterial and non-bacterial points showed wider ranges than that of TSB and, in some cases, pelleted bacteria, indicating that the overlayer is a complex composition of materials which varies in thickness and composition across the material.

Analysis of XPS and AFM data together indicated the potential of the residual layer covering both the bacteria and substrate material. Calculations of the chemical composition of the residual layer from both XPS models did not necessarily correlate to data obtained by AFM. While the XPS data showed variation between samples, AFM data showed very little changes between

materials, indicating the layer is a complex dynamic of substances that interact with the AFM tip in a similar manner.

Ideally, being able to model the biological composition of the residual layer may help to give a clearer picture to the composition of the sample, but as discussed in Chapter 6 the biological model was not used, due to limits of the model. If the biological model could have been used, the protein and polysaccharide content of the residual layer may indicate the slight variations between samples relate to adhesion values, as seen in Chapter 5, where TSB interactions analysed with the substrate showed variations in both AFM and XPS data depending on substrate material and overlayer composition.

Overall the analysis of the *NCTC13360* bacterial incubated sample showed evidence for the presence of signals from a layer that was not present on the lawn or pellet samples. This residual layer is shown to potentially cover the entire sample.

Chapter 8 Analysis of *ATCC35984* Bacterial Films on Si (111), Glass, Mica, Silver and Titanium Surfaces

Staphylococcus epidermidis is pathogenic bacteria with the potential to cause infection, in the human body. The ability of some strains to form a biofilm makes treatment harder, due to the protection a biofilm can provide. The initial stages of bacterial adhesion play a crucial role in biofilm formation, so is considered a better target than an established biofilm, which is when the bacteria is more vulnerable.

In this chapter the initial stages of adhesion of a model strain of *S. epidermidis ATCC35984* was analysed by AFM and XPS, chosen for its potential to form biofilms, as discussed in literature *ATCC35984* (Ista et al., 2009; Méndez-Vilas et al., 2004). Samples were prepared as described in Chapter 3 and analysis of the substrate on incubation of bacteria was compared and modelled against analysis at TSB incubated samples and bacterial pellet samples from previous chapters.

8.1 Bacterial modelling

To be able to properly interpret the XPS data, several assumptions and considerations about the sample must be made. These were discussed in Chapter 7 and are briefly summarised here.

Firstly, the size of the bacteria was determined in Chapter 6, to have a diameter of approximately 500 nm. As the size of the bacteria is greater than the 10nm maximum depth measured by XPS, any material from under the bacteria is undetectable. This means that any signal from the substrate is theoretically from material that is not covered by bacteria. Measurement of the relative strength of this signal compared to that from the reference sample therefore allows the bacterial coverage of the sample to be estimated. However, this model is limited in accuracy, as the calculation neglects the presence of compounds bound to the sample that may also attenuate the substrate signal.

Alternatively, AFM images can be used to estimate the coverage of the sample using the AFM software and information based on the size of the bacteria observed in Figures 8.1 and 8.2, to calculate the area of coverage of areas on the sample that are similar or higher than the size of a bacteria.

The estimated coverage can be used to determine if any material that is not bacterial is bound to the substrate, by assuming the bacteria covering the substrate is of the same composition as the bacterial pellet analysed in Chapter 6, and any remaining substance is non-bacterial, described as the residual layer. The residual layer can be compared to the TSB incubated substrate, to identify the nature of the residual layer, whether the layer is TSB bound to the

substrate or bacteria excreted compounds.

$$proportion\ pellet = pellet\ \times coverage$$

$$Total\ incubated - proportioned\ pellet = residual\ layer$$

The discussion of possible structural models A – G shown in Figure 7.3 and described in Chapter 7 also applies here and is not repeated. As was the case for the non-biofilm forming bacteria described in Chapter 7, separate samples were used for each measurement here also, and the methods used to correct for this as described in Chapter 7 were also used here.

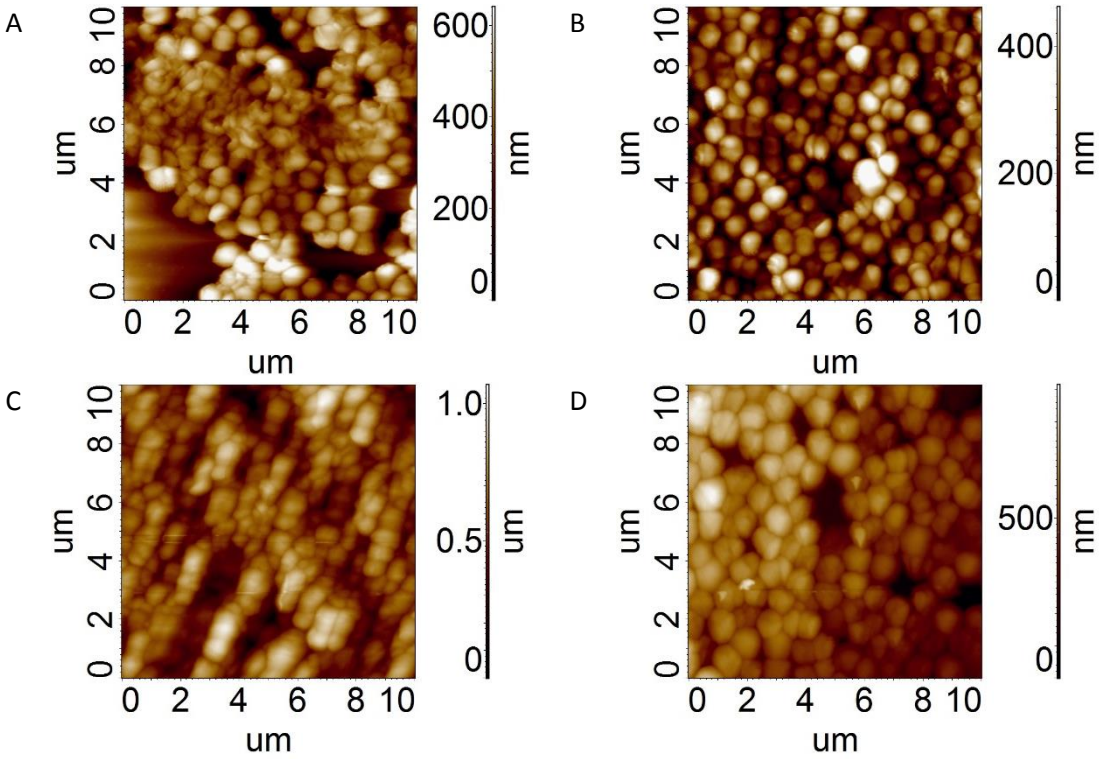

Figure 8.1 AFM images of samples incubated with *ATCC35984* after 24 hours. A is incubated on glass, B is incubated on mica, C is incubated on titanium and D is incubated on silver.

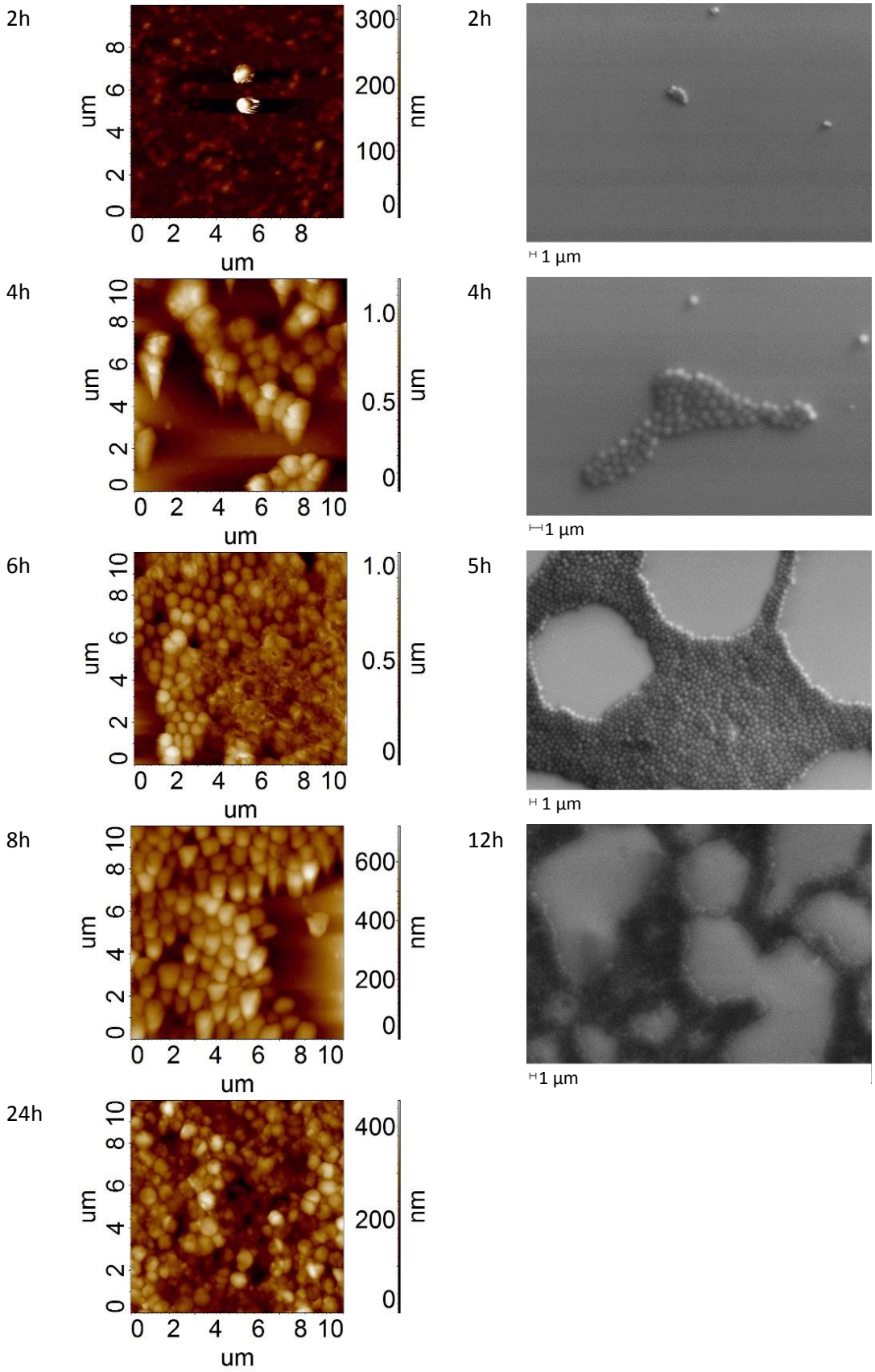

Figure 8.2 AFM and SEM images of silicon incubated with *ATCC35984* over time.

8.1.1 Silicon timed data

Samples of silicon incubated with *ATCC35984* in tryptic soy broth were removed at frequent times in relation to the growth of bacteria. Figure 8.3 shows the growth curve of the bacteria. Generally, samples were taken at alternate hours, increasing to hourly during high growth period, and every 4 hours, once stationary phase was reached, at 16 hours.

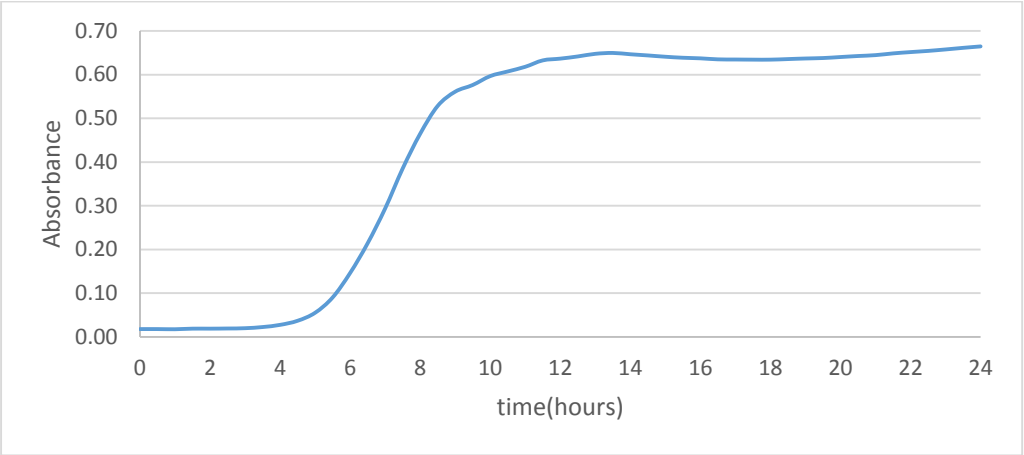

Figure 8.3 Growth curve of *ATCC35984* over 24 hours

Samples were compared to samples prepared after timed TSB incubation, to the proportioned pellet and residual layer data. Results of analysis of the XPS survey spectra and C 1s peak fits from the samples removed from incubation at timed intervals are listed below. Results of calculations of the pellet and residue are included in the table. Comparisons made between results from the measured data and calculated data are graphed in Figures 8.7 to 8.15 based on their individual measurement for ease of analysis. The XPS survey spectra and C1s peak fit of the 24 hour incubated silicon with *ATCC35984* sample and other time data spectra can be found in the appendix.

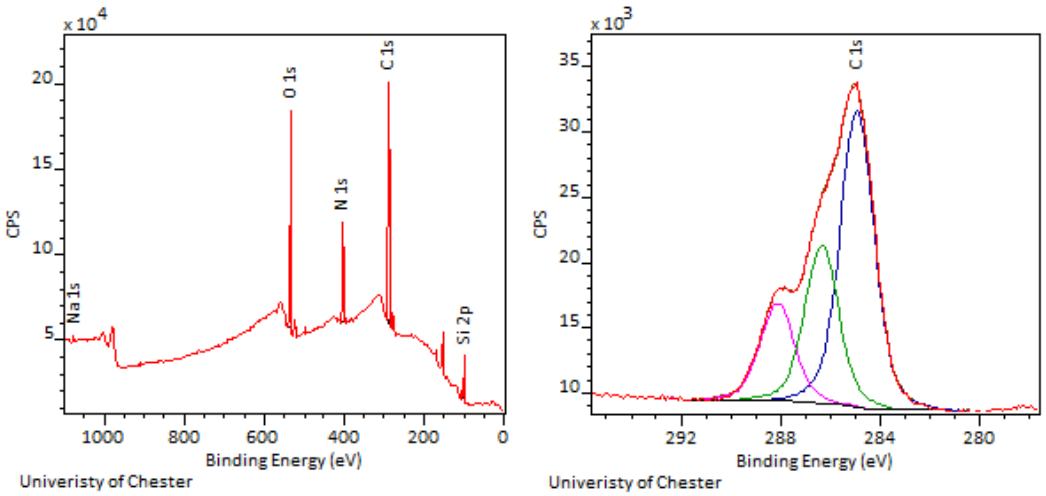

Figure 8.4 XPS survey and C 1s peak fit of silicon incubated in *ATCC35984* after 24 hours.

	0h	1h	2h	3h	4h	5h	6h	7h	8h	9h	12h	14h	16h	20h	22h	24h
C 1s	21.1		34.4		41.2	58.4	58.4	60.1	61.4	57.4	59.5	59.1	57.5	61.6	62.2	62.4
O 1s	22.6		23.3		22.2	20.5	20.8	23.9	22.3	22.4	24.8	20.3	22.3	21.8	24.6	17.6
O_{org}	3.0		7.8		11.5	17.6	17.4	22.4	22.3	19.2	23.4	20.3	19.0	21.8	24.3	13.7
N 1s	0.0		4.9		7.5	12.8	11.4	11.0	11.3	11.2	11.4	12.7	11.2	12.1	10.9	10.5
Si 2p	56.3		37.2		27.1	6.4	7.6	2.8	0.0	7.2	2.6	0.0	6.7	0.0	0.2	9.4
P 2s	0.0		0.0		0.0	0.7	0.6	1.1	1.3	0.6	1.3	1.1	0.8	1.0	1.5	0.0
Na 1s	0.0		0.2		0.5	0.8	0.7	0.6	1.7	0.8	0.4	2.6	0.6	1.6	0.6	0.2
Ca2p	0.0		0.0		0.0	0.0	0.0	0.0	0.0	0.0	0.0	0.0	0.0	0.0	0.0	0.0
Cl 2p	0.0		0.0		1.6	0.6	0.4	0.6	2.1	0.5	0.0	4.2	0.9	1.9	0.0	0.0
C285	87.9		65.6		52.1	41.9	48.5	37.1	44.2	42.3	36.2	43.6	42.3	42.1	37.6	53.8
C286.5	8.8		13.9		29.5	34.6	28.5	40.4	34.5	35.1	42.5	33.5	35.8	35.2	42.1	28.5
C288	3.3		20.5		18.4	23.5	23.0	22.6	21.3	22.7	21.4	23.0	21.9	22.7	20.3	17.7
O_{org}/C	0.14		0.23		0.28	0.30	0.30	0.37	0.36	0.33	0.39	0.34	0.33	0.35	0.39	0.22
N/C	0.00		0.14		0.18	0.22	0.20	0.18	0.18	0.19	0.19	0.22	0.19	0.20	0.17	0.17

Table 8.1 Raw XPS data of silicon (111) incubated with *ATCC35984* over time as measured.

	0h	1h	2h	3h	4h	5h	6h	7h	8h	9h	12h	14h	16h	20h	22h	24h
C 1s	21.1	58.6	34.1	30.5		34.3	38.8		30.4	56.9						21.1
O 1s	22.6	19.3	22.3	21.1		24.7	22.1		22.3	20.6						22.6
O_{org}	3.0	13.0	4.4	3.8		5.2	8.1		7.6	16.2						3.0
N 1s	0.0	6.5	3.7	3.1		4.2	4.8		5.3	9.5						0.0
Si 2p	56.3	12.8	39.4	44.8		36.6	32.7		41.9	10.8						56.3
P 2s	0.0	0.0	0.0	0.0		0.0	0.0		0.0	0.3						0.0
Na 1s	0.0	0.9	0.1	0.0		0.2	0.7		0.1	0.9						0.0
Ca 2s	0.0	0.6	0.5	0.6		0.0	0.0		0.0	0.0						0.0
Cl 2p	0.0	1.4	0.0	0.0		0.0	0.9		0.0	1.1						0.0
C285	87.9	69.0	73.7	69.6		68.0	68.4		54.8	49.7						72.9
C286.5	8.8	17.9	13.6	19.4		19.8	18.5		27.5	30.7						16.6
C288	3.3	13.1	12.7	11.0		12.2	13.2		17.7	19.6						10.6
O_{org} /C	0.14	0.23	0.13	0.13		0.15	0.21		0.25	0.28						0.27
N/C	0.00	0.17	0.11	0.10		0.12	0.12		0.17	0.17						0.09

Table 8.2 XPS surface composition data from media-incubated Si, from Chapter 5, reproduced here for reference.

	0h	1h	2h	3h	4h	5h	6h	7h	8h	9h	12h	14h	16h	20h	22h	24h
%			34%		52%	89%	87%	95%	100%	80%	95%	100%	88%	100%	100%	83%
C 1s			20.4		31.1	53.2	51.9	57.0	60.0	48.1	57.1	60.0	52.8	60.0	59.8	50.0
O 1s			8.7		13.4	22.8	22.3	24.5	25.8	20.6	24.5	25.8	22.7	25.8	25.7	21.5
O_{org}			8.6		13.1	22.4	21.8	24.0	25.2	20.2	24.1	25.2	22.2	25.2	25.2	21.0
N 1s			2.9		4.4	7.6	7.4	8.1	8.5	6.8	8.1	8.5	7.5	8.5	8.5	7.1
Si 2p			1.0		1.5	2.5	2.5	2.7	2.9	2.3	2.7	2.9	2.5	2.9	2.8	2.4
P 2s			0.9		1.3	2.2	2.2	2.4	2.5	2.0	2.4	2.5	2.2	2.5	2.5	2.1
Na 1s			0.1		0.2	0.4	0.3	0.4	0.4	0.3	0.4	0.4	0.4	0.4	0.4	0.3
Ca2p			0.0		0.0	0.0	0.0	0.0	0.0	0.0	0.0	0.0	0.0	0.0	0.0	0.0
Cl 2p			0.0		0.0	0.0	0.0	0.0	0.0	0.0	0.0	0.0	0.0	0.0	0.0	0.0
C285			13.0		19.9	34	33.1	36.4	38.3	30.7	36.5	38.3	33.7	38.3	38.2	31.9
C286.5			15.1		23.0	39.6	38.3	42.2	44.5	35.6	42.3	44.4	39.1	44.4	44.2	37.0
C288			5.9		9.0	15.4	15.0	16.5	17.4	13.9	16.6	17.4	15.3	17.4	17.3	14.5
O_{org}/C			0.42		0.42	0.42	0.42	0.42	0.42	0.42	0.42	0.42	0.42	0.42	0.42	0.42
N/C			0.14		0.14	0.14	0.14	0.14	0.14	0.14	0.14	0.14	0.14	0.14	0.14	0.14

Table 8.3 Contribution to measured composition from bacteria on the substrate surface, estimated using the surface composition of the pellet sample as reference and the bacterial coverage estimated from the reduction in the Si 2p signal compared to the autoclaved Si (111) wafer.

	0h	1h	2h	3h	4h	5h	6h	7h	8h	9h	12h	14h	16h	20h	22h	24h
C 1s	21.1		14.0		10.1	5.2	6.6	3.1	1.4	9.3	2.4	-0.9	4.7	1.7	2.4	12.4
O 1s	22.6		14.6		8.8	-2.4	-1.4	-0.6	-3.4	1.8	0.2	-5.4	-0.4	-3.9	-1.0	-3.8
O_{org}	3.0		-0.8		-1.6	-4.8	-4.5	-1.6	-2.9	-1.1	-0.6	-4.9	-3.2	-3.4	-0.9	-7.3
N 1s	0.0		2.0		3.0	5.2	4.0	2.9	2.8	4.3	3.3	4.2	3.7	3.6	2.4	3.4
Si 2p	56.3		36.2		25.6	3.8	5.1	0.1	-2.9	4.9	-0.1	-2.9	4.2	-2.9	-2.7	7.0
P 2s	0.0		-0.9		-1.3	-1.6	-1.6	-1.3	-1.2	-1.5	-1.1	-1.5	-1.5	-1.6	-1.0	-2.1
Na 1s	0.0		0.1		0.3	0.4	0.4	0.2	1.3	0.5	0.0	2.2	0.2	1.2	0.2	-0.2
Ca 2s	0.0		0.0		0.0	0.0	0.0	0.0	0.0	0.0	0.0	0.0	0.0	0.0	0.0	0.0
Cl 2p	0.0		0.0		1.6	0.6	0.4	0.6	2.1	0.5	0.0	4.2	0.9	1.9	0.0	0.0
C285	87.9		52.5		32.2	8.0	15.3	0.7	5.9	11.6	-0.3	5.3	8.6	3.8	-0.6	21.9
C286.5	8.8		-1.1		6.5	-4.7	-9.9	-1.8	-9.9	-0.5	0.2	-10.9	-3.2	-9.2	-2.1	-8.4
C288	3.3		14.6		9.4	8.1	8.0	6.1	3.9	8.8	4.8	5.6	6.6	5.4	3.0	3.2
O_{org}/C	0.14		-0.05		-0.16	-0.92	-0.68	-0.51	-2.05	-0.11	-0.27	5.79	-0.69	-2.04	-0.38	-0.59
N/C	0.00		0.14		0.30	1.00	0.62	0.95	1.92	0.46	1.38	-4.96	0.79	2.13	0.98	0.27

Table 8.4 XPS residue Approximate composition of non-bacterial material (residue) on the surface, estimated by subtracting values in Table 8.3 from values in Table 8.1.

	0h	1h	2h	3h	4h	5h	6h	7h	8h	9h	12h	14h	16h	20h	22h	24h
			16%		35%	45%	54%	63%	73%	73%	73%	73%	73%	73%	73%	73%
C 1s			9.9		21.1	26.7	32.3	37.9	43.6	43.6	43.6	43.6	43.6	43.6	43.6	43.6
O 1s			4.2		9.1	11.5	13.9	16.3	18.7	18.7	18.7	18.7	18.7	18.7	18.7	18.7
O_{org}			4.2		8.9	11.2	13.6	16.0	18.3	18.3	18.3	18.3	18.3	18.3	18.3	18.3
N 1s			1.4		3.0	3.8	4.6	5.4	6.2	6.2	6.2	6.2	6.2	6.2	6.2	6.2
Si 2p			0.5		1.0	1.3	1.5	1.8	2.1	2.1	2.1	2.1	2.1	2.1	2.1	2.1
P 2s			0.4		0.9	1.1	1.4	1.6	1.8	1.8	1.8	1.8	1.8	1.8	1.8	1.8
Na 1s			0.1		0.1	0.2	0.2	0.3	0.3	0.3	0.3	0.3	0.3	0.3	0.3	0.3
Ca2p			0.0		0.0	0.0	0.0	0.0	0.0	0.0	0.0	0.0	0.0	0.0	0.0	0.0
Cl 2p			0.0		0.0	0.0	0.0	0.0	0.0	0.0	0.0	0.0	0.0	0.0	0.0	0.0
C285			0.0		0.0	0.0	0.0	0.0	0.0	0.0	0.0	0.0	0.0	0.0	0.0	0.0
C286.5			0.0		0.0	0.0	0.0	0.0	0.0	0.0	0.0	0.0	0.0	0.0	0.0	0.0
C288			0.0		0.0	0.0	0.0	0.0	0.0	0.0	0.0	0.0	0.0	0.0	0.0	0.0
O_{org}/C			0.42		0.33	0.33	0.33	0.33	0.33	0.33	0.33	0.33	0.33	0.33	0.33	0.33
N/C			0.14		0.11	0.11	0.11	0.11	0.11	0.11	0.11	0.11	0.11	0.11	0.11	0.11

Table 8.5 Contribution to measured composition from bacteria on the substrate surface, estimated using the surface composition of the pellet sample as reference and the bacterial coverage estimated from the analysis of the AFM images.

	0h	1h	2h	3h	4h	5h	6h	7h	8h	9h	12h	14h	16h	20h	22h	24h
C 1s	21.1		30.1		32.2	46.9	44.5	43.8	42.7	38.7	40.8	40.4	38.8	42.9	43.5	43.7
O 1s	22.6		19.2		13.3	9.2	7.2	7.9	4.0	4.1	6.4	2.0	4.0	3.5	6.3	-0.7
O_{org}	3.0		6.4		8.5	13.8	12.8	17.0	16.1	13.0	17.3	14.1	12.8	15.6	18.1	7.6
N 1s	0.0		4.4		6.4	11.5	9.9	9.2	9.2	9.1	9.3	10.7	9.1	10.0	8.8	8.4
Si 2p	56.3		36.8		26.2	5.2	6.2	1.2	-1.8	5.3	0.8	-1.8	4.9	-1.8	-1.7	7.6
P 2 s	0.0		-0.1		-0.1	0.5	0.4	0.8	1.0	0.3	1.0	0.8	0.5	0.7	1.2	-0.3
Na 1s	0.0		0.2		0.5	0.8	0.7	0.6	1.7	0.8	0.4	2.6	0.6	1.6	0.6	0.2
Ca 2s	0.0		0.0		0.0	0.0	0.0	0.0	0.0	0.0	0.0	0.0	0.0	0.0	0.0	0.0
Cl 2p	0.0		0.0		1.6	0.6	0.4	0.6	2.1	0.5	0.0	4.2	0.9	1.9	0.0	0.0
C285	87.9		65.6		52.1	41.9	48.5	37.1	44.2	42.3	36.2	43.6	42.3	42.1	37.6	53.8
C286.5	8.8		13.9		29.5	34.6	28.5	40.4	34.5	35.1	42.5	33.5	35.8	35.2	42.1	28.5
C288	3.3		20.5		18.4	23.5	23.0	22.6	21.3	22.7	21.4	23.0	21.9	22.7	20.3	17.7
O_{org}/C	0.14		0.21		0.26	0.29	0.29	0.39	0.38	0.34	0.42	0.35	0.33	0.36	0.42	0.17
N/C	0.00		0.15		0.20	0.25	0.22	0.21	0.22	0.23	0.23	0.26	0.24	0.23	0.20	0.19

Table 8.6 Approximate composition of non-bacterial material (residue) on the surface, estimated by subtracting values in Table 8.5 from values in Table 8.1.

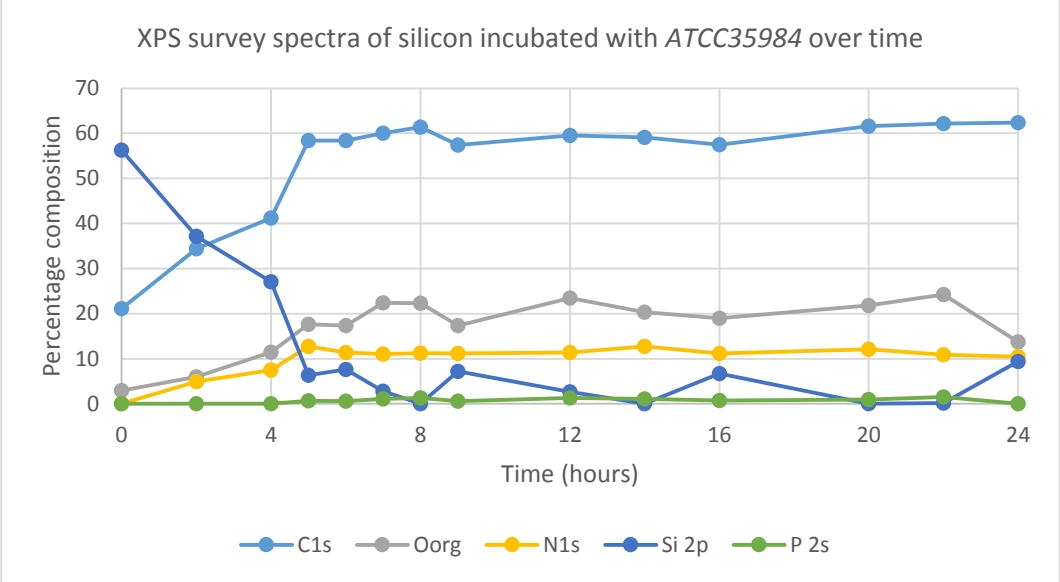

Figure 8.5 XPS survey spectra analysis of *ATCC35984* on silicon (111) over time.

Analysis of XPS spectra over time showed the C 1s signal increasing steadily over the first 5 hours, at the same time Si 2p decreased. The anti-correlation between the two indicated samples was covered by an organic substance, which on analysis of AFM and SEM images (Figure 8.2) was assumed to be partially due to the increase in bacterial adhesion during this time. After 5 hours the C 1s signal stabilised around 55-65%. The silicon signal reaches zero at 8 hours, after which the Si 2p peak remains below 10%. Variations seen after 5 hours, where Si 2p drops below 10%, was thought to be related to variations due to subsampling and area of sample analysed.

After 2 hours the N 1s and organic oxygen showed signs of an increase to 5 hours, after which the N 1s signal began to stabilise between 10-15%. The organic oxygen continues to increase until 7 hours, after which measurements become more stable, between 15 and 25%. Increases in nitrogen and organic oxygen were consistent with that of the increase of C 1s, relating to the presence of more complex organic substance, changing from atmospheric hydrocarbon layer to proteins and polysaccharides.

The lack of P 2s in early samples may be due to the low levels of bacteria on the surface, leading to the low definition of the P 2s peak. The P 2p peaks occur on a rapidly-changing background due to the presence of the second plasmon resonance peak behind the Si 2p peak. This was responsible for difficulties in measuring low level phosphorus at the surface using the P 2p. To overcome this the P 2s peak was chosen over the P 2p peak, as the P 2s peak has less overlap with the resonance peak. Phosphorus was initially detected at 5 hours, where the surface coverage was calculated to be above 80%.

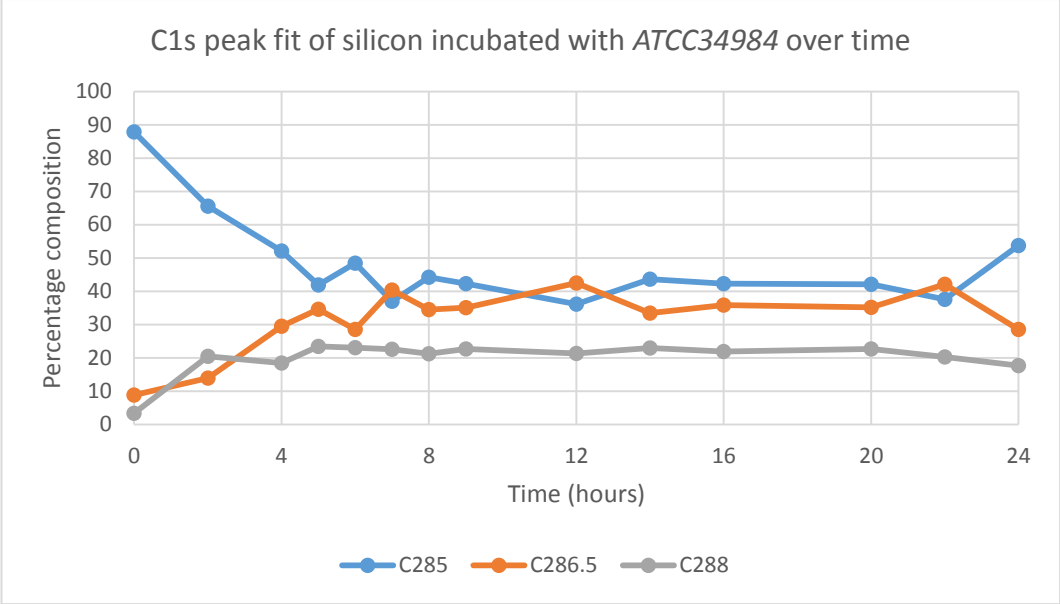

Figure 8.6 C 1s peak fit data of silicon (111) incubated with *ATCC35984* over time.

The C 1s peak fit showed the C285 signal decreased over the first 7 hours, which showed an anti-correlation to the silicon signal, indicating the hydrocarbons detected partially relate to the atmospheric hydrocarbons bound to the silicon substrate, with the remaining belonging to the adhered bacteria. The increase in peaks at 286.5eV and 288eV over the first few hours relate to the increase in complex organic compounds as seen with the increase of N 1s and organic oxygen within the first 7 hours.

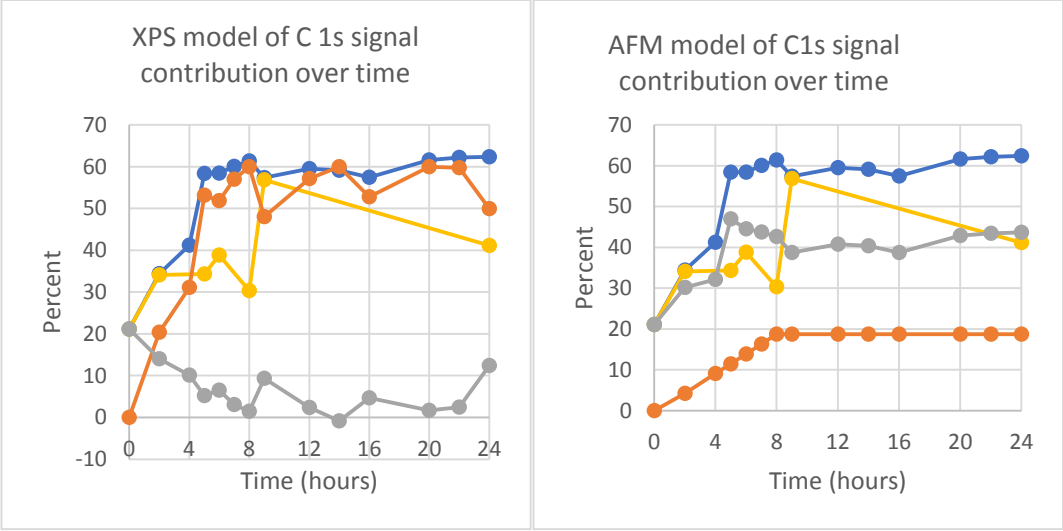

Figure 8.7 Graphs comparing models of C1s signal within overlayer composition models against time, calculated from estimating the coverage from XPS data (left) and AFM (right), taken from Tables 8.1-8.6.Calculations of the bacterial contribution to signal (orange) and the resulting non-bacterial residue (grey) are compared to the original incubation data of silicon incubated with *ATCC35984* (blue) and silicon incubated with TSB over time (yellow).

As discussed in Chapter 7, variable coverage due to sub-sampling led to some variability in the results. However, trends were observed and issues with variable coverage were minimised by considering (i) the organic layer only, and (ii) how bacterial adhesion to the surface contributes to the overall model of the structures present.

Using the bacterial coverage estimated by XPS, the pelleted bacteria showed similarities in composition to the incubated sample, with the points after 5 hours showing a closer similarity to the incubated sample. The first few hours had a lower bacterial coverage, so the remaining difference could relate to additional compounds bound to the surface, including atmospheric carbon on exposed silicon, as well as proteins and polysaccharides from either media or excreted from the bacteria. Analysing the non-bacterial contribution to signal, the layer decreased over the first 7 hours, relating potentially to the reduction of exposed silicon. Beyond 7 hours, there were variations in carbon in the residual layer, however the XPS model shows the possibility of over calculating, as seen by the negative C 1s estimate at 14 hours. The amount of carbon in the residual layer showed similarities to the Si 2p peak, indicating the possibility the residual layer was substrate bound only.

Analysing the C 1s using the AFM data to estimate the bacterial coverage, a lower carbon content was observed in the pelleted samples compared to the incubated sample. Some similarities in trend were seen between the incubated and bacterial contribution, however the residual layer showed a closer similarity to the incubated sample. The residual layer was closer to the incubated sample for the first 5 hours and showed some similarities to that of the TSB incubated sample. From this, the residual layer was similar to TSB bound to the substrate for the first few hours, as bacterial adhesion takes place. Once the bacterial growth starts to slow down the similarities between the residual and incubated sample indicated the amount of signal contributed by the residual layer was dominant in the sample.

The peak fit data can be used to highlight the chemical changes on the surface. Analysis of the XPS model of bacterial coverage showed similarities with the C285 signal for the bacteria contribution to signal and bacteria incubated silicon after 8 hours, indicating the bacteria was the main source of hydrocarbons after 8 hours. During the first 8hours, the residue decreased, which was similar to that of Si 2p, indicating the residual layer during early stages still contained a layer of atmospheric hydrocarbons.

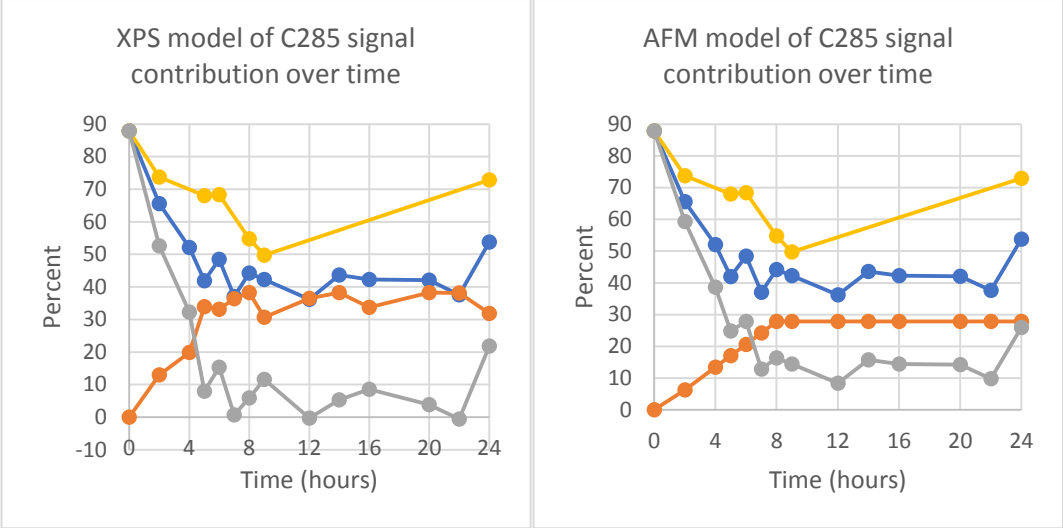

Figure 8.8 Graphs comparing models of C285 signal within overlayer composition models against time, calculated from estimating the coverage from XPS data (left) and AFM (right), taken from Tables 8.1-8.6.Calculations of the bacterial contribution to signal (orange) and the resulting non-bacterial residue (grey) are compared to the original incubation data of silicon incubated with *ATCC35984* (blue) and silicon incubated with TSB over time (yellow).

The AFM model indicated a slightly lower amount of C285 contributed to the incubated sample from the bacteria. The AFM model appears to be more reliable in terms of estimating bacterial coverage. The AFM model showed, after 8 hours most the C285 signal comes from the bacteria, with a small amount coming from another source, potentially exposed silicon.

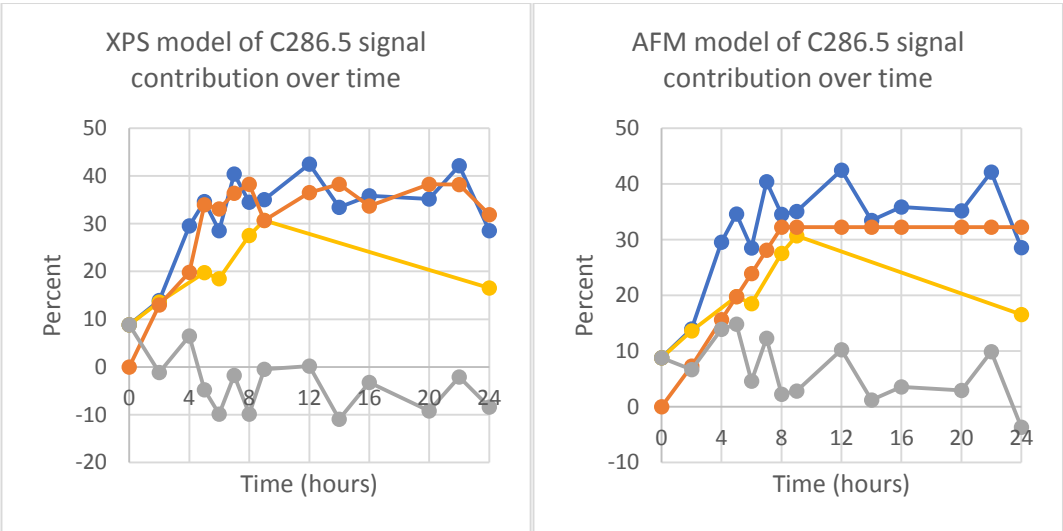

Figure 8.9 Graphs comparing models of C286.5 signal within overlayer composition models against time, calculated from estimating the coverage from XPS data (left) and AFM (right), taken from Tables 8.1-8.6.Calculations of the bacterial contribution to signal (orange) and the resulting non-bacterial residue (grey) are compared to the original incubation data of silicon incubated with *ATCC35984* (blue) and silicon incubated with TSB over time (yellow).

The signal at C286.5 in the XPS bacterial coverage model indicated similarities to the bacterial contribution to signal, however as the residue gave negative results, the model was assumed

to overestimate bacterial coverage. In comparison, the AFM model assumed a lower bacterial coverage and was less prone to error. The only sample to estimate an error was the 24 hour sample, which was assumed to error due to limits of estimating the bacterial coverage by AFM rather than an error in determining the composition of the residual layer. Other samples showed similarities between the incubated sample and bacteria contributed signal, indicating it was the main contributor to signal. Some similarity between the TSB incubated sample and the residue during the first 5 hours indicated the non-bacterial contribution to signal was similar to TSB bound to exposed silicon.

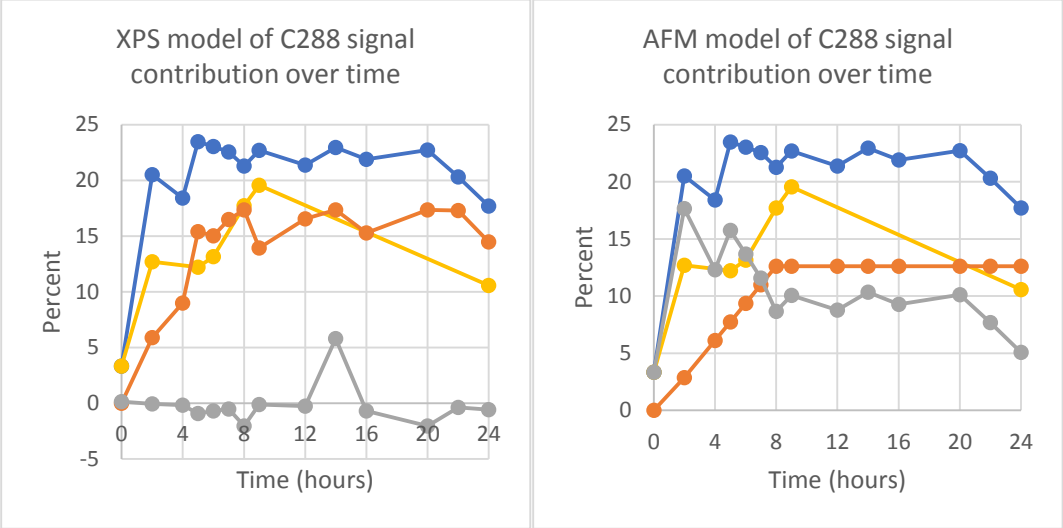

Figure 8.10 Graphs comparing models of C288 signal within overlayer composition models against time, calculated from estimating the coverage from XPS data (left) and AFM (right), taken from Tables 8.1-8.6.Calculations of the bacterial contribution to signal (orange) and the resulting non-bacterial residue (grey) are compared to the original incubation data of silicon incubated with *ATCC35984* (blue) and silicon incubated with TSB over time (yellow).

Analysis of the bacterial contribution to signal from bacterial coverage estimated by XPS, the model showed the pelleted bacteria have a similar trend to the incubated sample. The residual layer also showed the presence of C285 indicating the residual layer contained complex organic compounds. However as both C285 and C286.5 showed points of error, the C288 signal calculated in this model also must be taken as an overestimate, and not a true reflection of the sample.

Analysis of the C288 signal using the AFM model showed less error. The signal contribution of bacteria assumed from AFM coverage was lower than that by XPS but showed a similar trend to the XPS calculated model. The residual layer initially increased in C288 signal then subsequently decreased. This showed the initial adhesion of more complex organic

compounds to the surface initially, but then replaced by bacteria which has more complicated compounds.

The carbon peak fit showed the contribution to the signal at 285eV was influenced mostly by media adhesion for the first 5 hours, after which bacterial influences dominated. This relates to the bacterial coverage of the sample, where the first few hours showed the surface to have more uncovered substrate allowing the hydrocarbons bound to the surface to be detected. Influences to peaks at C286.5 and C288 were more difficult to determine due to similarities in values for the first few hours for the proportioned pellet and media for the first few hours. Considering other influences on the surface, these signals were indicative of the bacteria and potential over layer of protein.

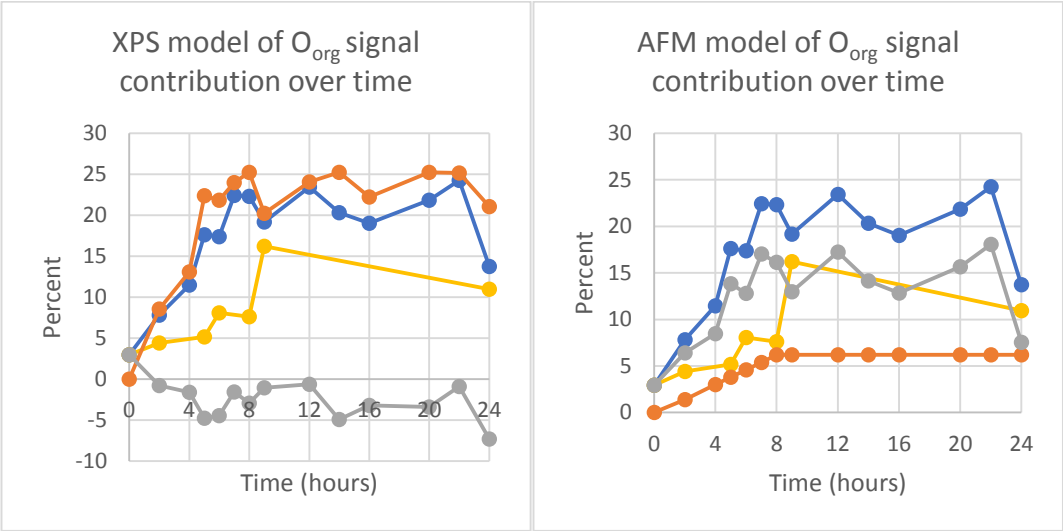

Figure 8.11 Graphs comparing models of organic oxygen calculation within overlayer composition models against time, calculated from estimating the coverage from XPS data (left) and AFM (right), taken from Tables 8.1-8.6.Calculations of the bacterial contribution to signal (orange) and the resulting non-bacterial residue (grey) are compared to the original incubation data of silicon incubated with *ATCC35984* (blue) and silicon incubated with TSB over time (yellow).

Analysis of the organic oxygen contribution of the bacteria, as determined by XPS, showed a higher organic oxygen content than in the incubated sample which was assumed to be a result of overestimate of bacterial coverage. The AFM model showed the bacterial contribution to organic oxygen was lower than the incubated sample, indicating the sample consists of a layer of organic compounds not associated with bacteria. The residual layer showed only a small similarity to the TSB incubated silicon within the first few hours, indicating that the residual layer at this stage relates to organic compounds binding to the surface along with bacterial adhesion. After initial stages of bacterial adhesion, the residual

layer still showed signs of organic oxygen, which relate to the potential polysaccharides and protein bound to the surface.

Analysis of the N 1s signal using the XPS model for bacterial coverage showed the bacterial pellet followed a similar trend to the incubated sample, with the bacterial pellet showing a lower nitrogen content. The remaining nitrogen was assumed to be part of an organic layer. Analysis of the organic layer showed an initial increase, relating to potential binding of organic compounds to the substrate, with the slight decrease after 5 hours assumed to be associated with bacteria binding to the substrate in place of organic compounds on the surface.

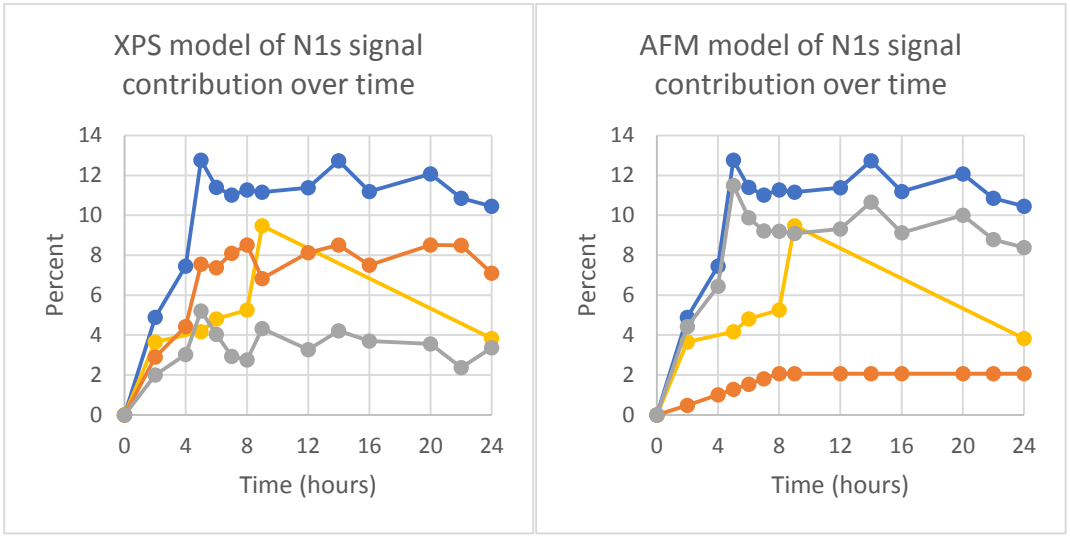

Figure 8.12 Graphs comparing models of N 1s signal within overlayer composition models against time, calculated from estimating the coverage from XPS data (left) and AFM (right), taken from Tables 8.1-8.6. Calculations of the bacterial contribution to signal (orange) and the resulting non-bacterial residue (grey) are compared to the original incubation data of silicon incubated with *ATCC35984* (blue) and silicon incubated with TSB over time (yellow).

Analysis of the nitrogen signal using the AFM model showed a low nitrogen contribution from the bacteria, resulting in similarities between the non-bacterial contribution to signal and the incubated sample. This indicated the presence of a nitrogen dominant residue, potentially as a result of proteins in the layer, due to the low phosphorus content. In comparison to the silicon incubated in TSB, the composition of the residual layer was significantly higher, indicating the proteins may not be from media alone, and as a result of bacteria excreting compounds.

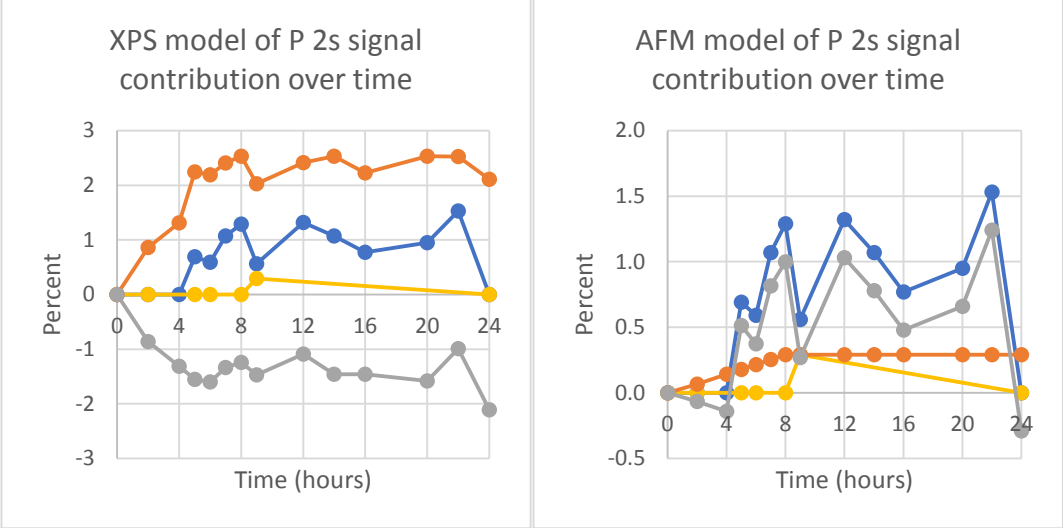

Figure 8.13 Graphs comparing models of P 2s signal within overlayer composition models against time, calculated from estimating the coverage from XPS data (left) and AFM (right), taken from Tables 8.1-8.6.Calculations of the bacterial contribution to signal (orange) and the resulting non-bacterial residue (grey) are compared to the original incubation data of silicon incubated with *ATCC35984* (blue) and silicon incubated with TSB over time (yellow).

Analysis of the P 2s signal was used to predict if the bacterial coverage was reliable and if any residue calculated was covered the bacteria. Using the P 2s signal is only an estimate as the limit of P 2s of 0.5% may result in the lack of P 2s in early samples which may have bacteria present. Additionally, P 2s may be a result of phosphates in the media, however earlier chapters show it is unlikely to affect results for silicon samples. The XPS model continuously overestimated the P 2s greatly, as a result of overestimation of bacterial coverage, as seen with other elemental analysis. The error in the XPS samples comes from the neglect of compounds supressing the silicon signal on the surface that were not bacteria. Analysis of the AFM model predicts a lower bacterial coverage, leading only the first few hours giving negative results, however this was within the limit of P 2s measurable, so was an expected result. The P 2s peak followed a similar trend to the incubated sample, indicating the bacterial coverage by AFM was an underestimate of bacterial coverage. In this case it was difficult to determine if the P 2s signal related to the bacteria covered in an additional organic layer, as the model incorrectly estimated the bacterial coverage. Alternatively, the positive P 2s signal may relate to the prospect of phosphate containing biological compounds, such as DNA, as well as phosphates from the media.

Analysing the potential residue in terms of O_{org}/C and N/C allows assumptions to be made with regards to the biological components of any non-bacterial contributions to signal, similar to analysis in Chapter 7.

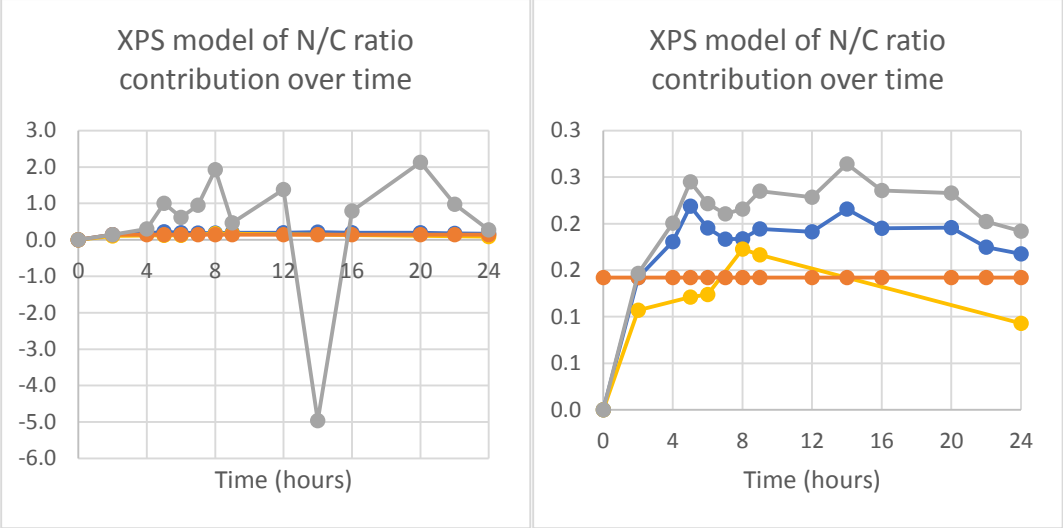

Figure 8.14 Graphs comparing models of N/C ratio within overlayer composition models against time, calculated from estimating the coverage from XPS data (left) and AFM (right), taken from Tables 8.1-8.6.Calculations of the bacterial contribution to signal (orange) and the resulting non-bacterial residue (grey) are compared to the original incubation data of silicon incubated with *ATCC35984* (blue) and silicon incubated with TSB over time (yellow).

Analysis of the XPS model showed large errors in the N/C content with values larger than ±1. This was due to the low amounts of carbon estimated from this model, which was a result of overestimation of bacterial coverage, along with other limiting factors of these models discussed in Chapter 7. Overall, it can be assumed the sample was protein dominant, as the lack of P 2s indicated the layer doesn't consist of DNA or teichoic acid like structures. The 14 hour sample showed a strongly negative N/C ratio due the lack of carbon in the residual layer with the presence of nitrogen. In reality this is a sign of the misestimation of bacterial coverage by XPS, and not due to the lack of carbon in the residual layer, as the source of nitrogen compounds without the presence of carbon is not realistic for these samples.

The AFM model estimated the residual layer to have a higher N/C ratio than the incubated sample and TSB incubated silicon, indicating the presence of protein or DNA like structures on the sample. As the residual layer estimated by AFM was higher than that of the TSB incubated sample, it can be assumed the layer was not of TSB alone. Variation in N/C between samples indicated the additional layer was not of consistent composition.

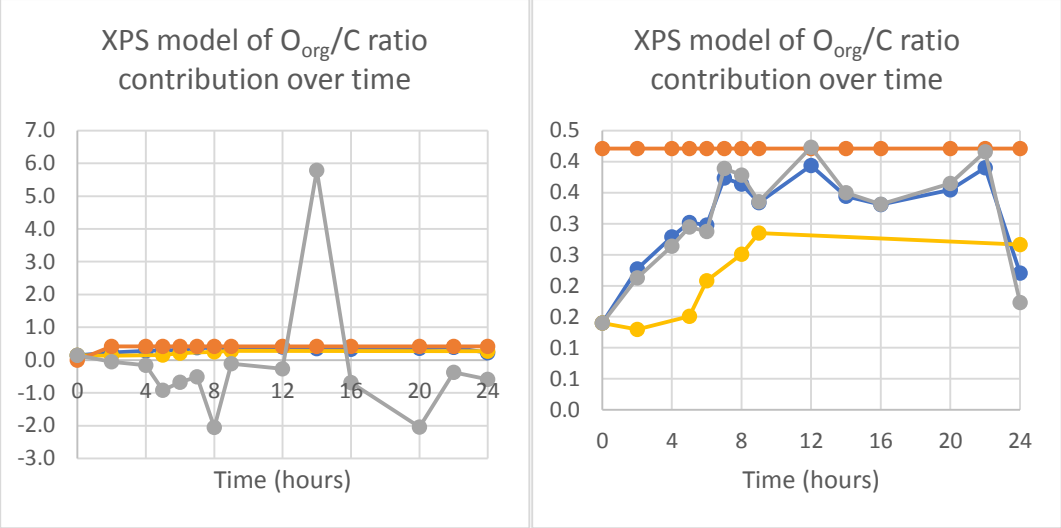

Figure 8.15 Graphs comparing models of O_{org}/C ratio within overlayer composition models against time, calculated from estimating the coverage from XPS data (left) and AFM (right), taken from Tables 8.1-8.6.Calculations of the bacterial contribution to signal (orange) and the resulting non-bacterial residue (grey) are compared to the original incubation data of silicon incubated with *ATCC35984* (blue) and silicon incubated with TSB over time (yellow).

Analysis of the XPS model showed errors in the O_{org}/C with negative values consistently. This is a result of the organic oxygen overestimation, due to overestimating the bacterial coverage. The 14 hour sample showed a positive value, due to the error in both organic oxygen and carbon within the residue giving negative values. High ratio of O_{org}/C across all samples were assumed to be due to overestimation in bacterial coverage, giving small values of organic oxygen and carbon. The low O_{org}/C ratio in relation to N/C indicated the possibility of a protein dominant system, with little to no polysaccharides on the surface.

Analysis of the AFM model showed the residue to have a similar O_{org}/C ratio to the incubated sample, indicating similarities in composition, potentially due to the underestimate of bacterial coverage. Variations in O_{org}/C indicated the change in composition between each sample, indicating the layer was not evenly covering the sample.

A slight trend in N/C and O_{org}/C ratio over time can be seen, indicating the change in O_{org}/C relates predominantly to protein based compounds, with some polysaccharides contributing to the ratio.

Overall, modelling the bacteria showed 2 different interpretation of results. The XPS sample has a higher tendency to overestimate the bacterial coverage. This was an overall error in the model, which neglected other compounds on the substrate. The AFM model predicted a lower bacteria coverage; however, analysis of the residual layer indicated the potential of underestimation, with the residual layer showing similarities in composition to bacteria. The

assumption of an underestimation was taken from the calculation of P 2s of the residual layer. The residual layer in the AFM model was calculated to have a P 2s signal, which although possible, the high value indicated a source of phosphorus that does not belong to TSB based phosphates. The other sources of phosphorus that are possible are bacterial teichoic acids and DNA, of which the former is more feasible as other chemical signals calculated by the AFM model were close to that of incubated sample. As previously discussed, there were a limited amount of samples from which the bacterial coverage can be determined, which limits the reliability of the AFM model estimating the bacterial coverage for samples that were not measured by AFM.

If the model of AFM coverage is assumed to be correct, the presence of the overlayer is assumed, due to have high levels of oxygen, nitrogen and carbon, which when considering O_{org}/C and N/C indicated the sample was protein dominant, with little to no polysaccharides on the surface. The presence of phosphorus should also be taken into account, which may be phosphate salts from TSB or phosphates from DNA, which also contains nitrogen, oxygen and carbon. The residual layer calculated from the proportioned pellet showed no similarities to that of media, suggesting this layer was influenced by the bacteria. Potentially, any media influence with the surface in the first few hours are the initial points the bacteria adherers to, and once initial adhesion has taken place, the bacteria influences both the surface and layer over itself for further adhesion.

8.1.2 Glass

Glass substrates were analysed after 24 hours of incubation with *S. epidermidis ATCC35984* and compared to TSB and pellet samples in Table 8.7. Figure 8.16 shows the survey spectrum and C 1s peak fit of glass incubated in *ATCC35984*. AFM images in Figure 8.1 showed the incubated sample was covered in bacteria. The average coverage of bacteria of *ATCC35984* incubated glass from AFM images was 52%.

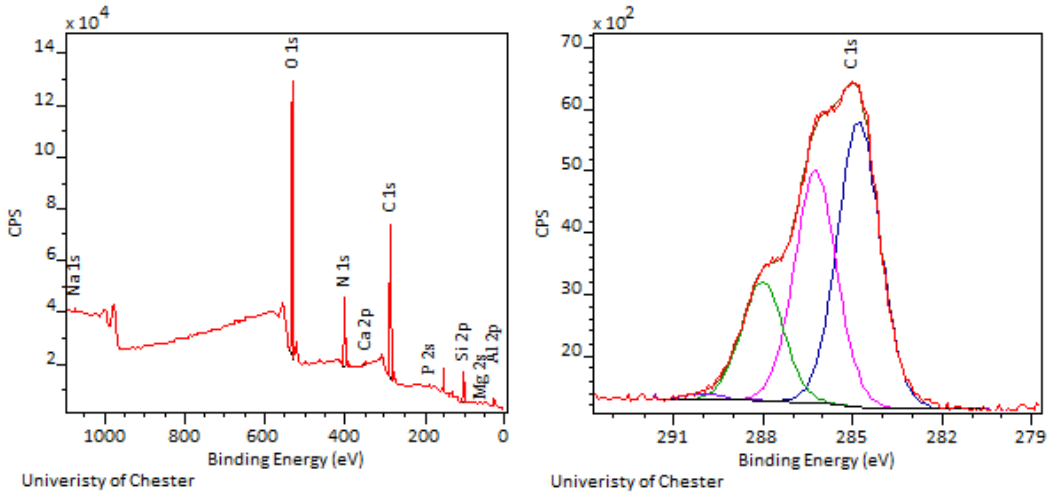

Figure 8.16 XPS survey and C 1s peak fit of glass incubated with *ATCC35984* after 24 hours.

	TSB incubated Glass 24h	*ATCC35984* pellet	ATCC35985 incubated Glass 24h	XPS model Bacterial contribution	XPS model Calculated residue	AFM model Bacterial contribution	AFM model Calculated residue
C 1s	30.6	60.2	52.7	30.8	21.9	31.4	21.3
O 1s	41.0	25.1	27.0	12.8	14.2	13.1	14.0
O_{org}	4.4	22.3	13.2	11.4	1.8	11.7	1.6
N 1s	2.8	9.3	9.2	4.8	4.5	4.9	4.4
Si 2p	22.1	1.4	8.5	0.7	7.7	0.7	7.7
P 2s	0.0	3.7	0.5	1.9	-1.4	1.9	-1.4
Na 1s	0.3	0.1	0.1	0.0	0.0	0.0	0.0
Al 2p	1.6	0.0	0.5	0.0	0.5	0.0	0.5
Ca 2s	0.3	0.3	0.3	0.2	0.1	0.2	0.1
Mg 2p	1.3	0.0	1.3	0.0	1.3	0.0	1.3
C285.0	66.7	49.4	44.4	25.3	19.1	25.8	18.6
C286.5	26.1	34.8	36.2	17.8	18.4	18.2	18.0
C288	7.2	15.8	18.6	8.1	10.5	8.2	10.3
C289	0.0	0.0	0.9	0.0	0.9	0.0	0.9
O_{org}/C	0.14	0.37	0.25	0.37	0.08	0.37	0.07
N/C	0.09	0.16	0.18	0.16	0.20	0.16	0.20
Model coverage				51%		52%	

Table 8.7 XPS analysis of glass incubated with *ATCC35984* compared to pelleted *ATCC35984* and media incubated glass after 24 hours. XPS data was analysed in terms of bacterial coverage estimated by XPS and AFM, and calculated residue on the surface.

Analysis of the survey spectrum showed the P 2s peak indicative of bacteria on the sample, through the detection of teichoic acids. Similarities between the *ATCC35984* glass and the pelleted bacteria were observed. The increase in C 1s and O_{org} relative to TSB relate to the increase in biological compounds on the surface. Further the C286.5 and C288 relate to the increase in oxygen and nitrogen based structures. The decrease in silicon relative to the TSB incubated sample is indicative of bacterial coverage calculated to be 51%.

Analysis of both the XPS and AFM model for estimating the bacterial coverage gave similar results, within 1%. Analysis of the residual layer gave a negative P 2s signal indicating either an error in bacterial coverage or the bacteria was partially covered with the residual layer. As both models estimate the bacterial coverage the same, it is more likely the bacteria were covered in a residual layer.

The composition of the residual layer showed a higher N/C than O_{org}/C indicative of a protein dominant layer. The calculated C 1s peak fit indicated there was hydrocarbons, as observed by the presence of C285, however as C286.5 and C288 combined were higher, this was likely to be only a fraction of the sample. The calculated residual layer showed a higher N/C and lower O_{org}/C compared to TSB, showing the residual layer was not similar to TSB bound to uncovered substrate material.

8.1.3 Mica

Mica incubated in *S. epidermidis ATCC35984* for 24 hours was analysed by XPS and AFM. Figure 8.17 shows the survey spectrum and C 1s peak fit for the 24 hour incubated mica in *ATCC35984*. Comparisons were made to the pelleted *ATCC35984* sample and mica incubated in TSB for 24 hours in Table 8.8.

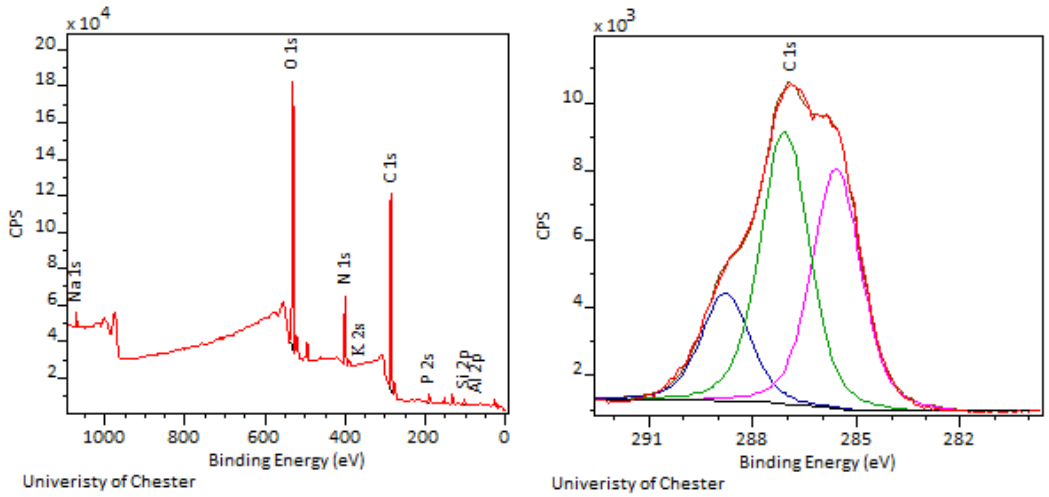

Figure 8.17 XPS survey and C 1s peak fit of mica incubated with *ATCC35984* after 24 hours.

	Mica incubated in TSB 24 h	*ATCC35984* pellet	Mica incubated in ATCC 35985 24h	XPS model		AFM model	
				Bacterial contribution	Calculated residue	Bacterial contribution	Calculated residue
C 1s	17.6	60.2	61.0	55.2	5.8	54.7	6.3
O 1s	45.0	25.1	25.7	23.0	2.7	22.8	2.9
O_{org}	6.0	22.3	20.8	20.5	0.3	20.3	0.5
N 1s	2.9	9.3	8.5	8.6	-0.1	8.5	0.0
Si 2p	18.8	1.4	1.8	1.3	0.5	1.3	0.5
P 2s	0.0	3.7	1.6	3.4	-1.8	3.4	-1.7
Na 1s	0.2	0.1	0.6	0.1	0.5	0.2	0.5
K 2s	2.9	0.0	0.6	0.0	0.6	0.0	0.6
Al 2p	12.7	0.0	0.3	0.0	0.3	0.0	0.3
Ca 2s	0.0	0.3	0.0	0.29	-0.3	0.3	-0.3
C285	62.7	49.4	38.6	45.3	-6.7	44.9	-6.3
C286.5	27.9	34.8	44.0	32.0	12.1	31.7	12.4
C288	9.5	15.8	17.3	14.5	2.8	14.4	3.0
O_{org}/C	0.34	0.37	0.34	0.37	0.06	0.37	0.08
N/C	0.16	0.16	0.14	0.16	-0.02	0.16	0.01
Model coverage				92%		91%	

Table 8.8 XPS analysis of mica incubated with *ATCC35984* compared to pelleted *ATCC35984* and media incubated glass after 24 hours. XPS data was analysed in terms of bacterial coverage estimated by XPS and AFM, and calculated residue on the surface.

XPS analysis of incubated mica with *ATCC35984* showed a significant decrease in silicon compared to the autoclaved sample relating to a 91.7 % coverage. From AFM (Figure 8.1) the coverage can be assumed to be bacterial. This was supported by decreases in K 2s and Al 2p signals from within the mica structure, when compared to the 24 hour TSB incubated mica sample. Further evidence for bacterial coverage was given by the increase in C 1s, N 1s and organic oxygen as well as introduction of P 2s.

With an estimated coverage of 90% bacteria on the surface as determined by XPS, the composition of the incubated sample should in principle be similar to that of the pellet. Carbon was measured to be at a slightly higher level compared to the pellet, whereas oxygen and nitrogen were at slightly lower levels. However, differences were relatively small compared to the pellet. The carbon 1s peak fit showed a decrease in peaks at 285 eV and increases in those at 286.5 eV and 288 eV.

Modelling the bacterial coverage based on AFM and XPS data gave similar results, indicating the coverage of the sample estimated to be close to the true value. Both models gave a negative P 2s signal for the residual layer, indicating the residual layer covers the bacteria. The sensitivity of the measurements can be seen through the N 1s signal, where a difference

of 1% alters the residual nitrogen signal form positive the AFM model to negative in the XPS model. As the values of N 1s were relatively small, it can be assumed zero. The composition of the residual layer was shown to have a small O_{org}/C ratio indicative of polysaccharide content the resulting layer showed a negative C285 signal, indicating the resulting layer lacks hydrocarbon content, and therefore the layer was likely to consist of polysaccharides only.

8.1.4 Titanium

Sputtercoated titanium was removed from incubation with *ATCC35984* after 24 hours. The XPS sample showed a visible difference in the adhered layer across the sample, with an area of relatively thick film and an area of relatively thin film. Both areas were analysed and compared to each other as well as pelleted *ATCC35984* and titanium incubated with TSB for 24 hours in Table 8.9. Figure 8.18 shows the XPS survey spectrum and C 1s peak fit for both points.

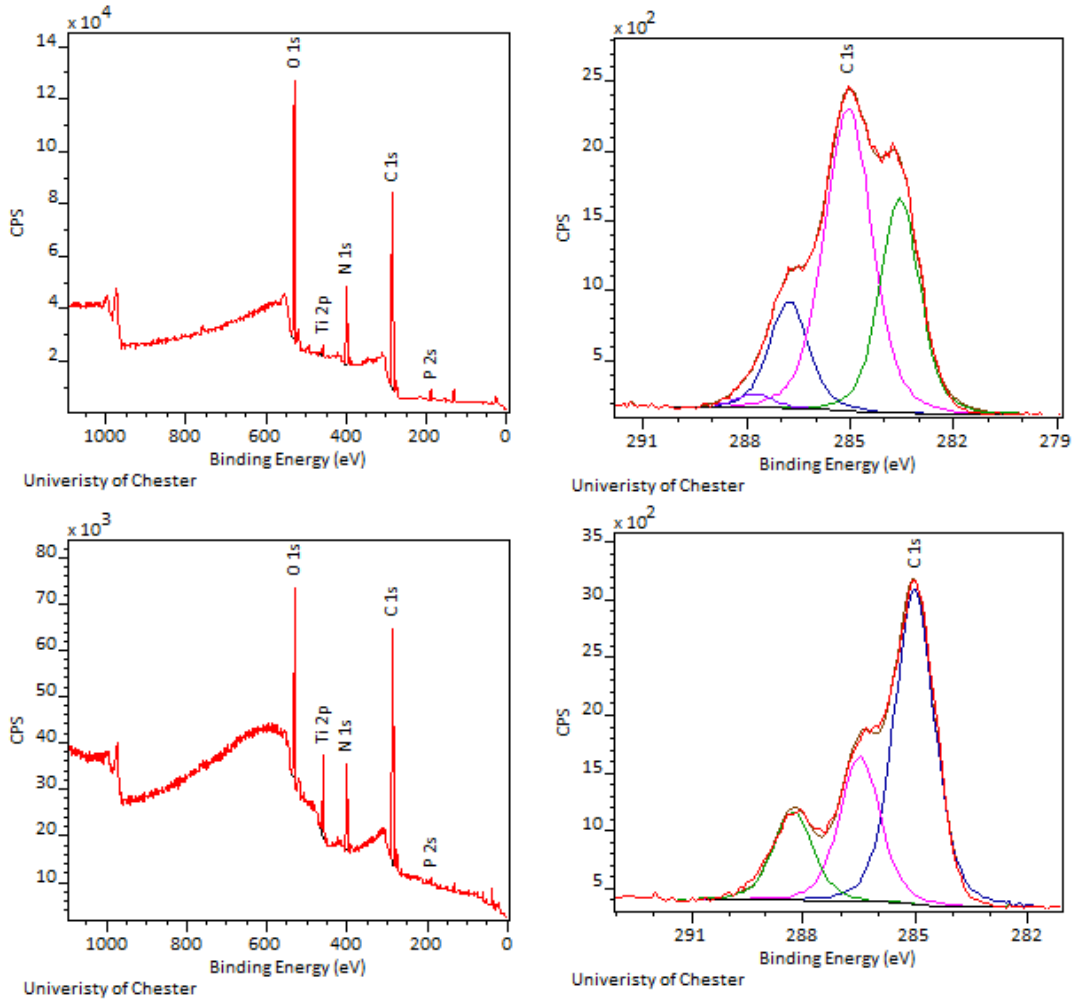

Figure 8.18 XPS survey and C 1s peak fit of titanium incubated with *ATCC35984* after 24 hours. The above relates to the thicker biofilm layer and the below images relate to the thin layer.

	Titanium incubated TSB 24h	*ATCC35984* Pellet	*ATCC35984* Incubated titanium 24h		XPS model				AFM model		
					Thick		Thin			Thick	Thin
			Thick	Thin	Bacterial contribution	Calculated residue	Bacterial contribution	Calculated residue	Bacterial contribution	Calculated residue	Calculated residue
C 1s	45.7	60.2	61.2	64.7	57.8	3.4	46.5	18.1	12.3	48.9	52.4
O 1s	36.0	25.1	26.5	21.8	24.1	2.4	19.4	2.4	5.1	21.4	16.7
O_{org}	24.7	22.3	22.5	18.7	21.5	1.0	17.3	1.4	4.6	17.9	14.2
N 1s	5.4	9.3	9.8	10.1	9.0	0.9	7.2	2.8	1.9	7.9	8.2
Si 2p	1.1	1.4	0.0	0.0	1.4	-1.4	1.1	-1.1	0.3	-0.3	-0.3
P 2s	0.6	3.7	2.0	0.7	3.5	-1.6	2.8	-2.2	0.8	1.2	-0.1
Na 1s	0.9	0.1	0.0	0.0	0.1	-0.1	0.1	-0.1	0.0	0.0	0.0
Ti 2p	10.4	000	0.5	2.8	0.0	0.5	0.0	2.8	0.0	0.5	2.8
Ca 2s	0.0	0.3	0.0	0.0	0.3	-0.3	0.3	-0.3	0.1	-0.1	0.1
C285.00	67.3	49.4	37.3	57.5	47.5	-10.1	38.2	19.3	10.1	27.3	47.4
C286.5.00	22.7	34.8	33.7	26.6	33.5	0.2	27.0	-0.4	7.1	26.6	19.4
C288.00	10.0	15.8	18.3	16.0	15.2	3.1	12.2	3.8	3.2	15.0	12.7
C289	0.0	0.0	11.0	0.0	0.0	11.0	0.0	0.0	0.0	0.0	0.00
O_{org}/C	0.54	0.37	0.37	0.29	0.37	0.30	0.37	0.08	0.37	0.37	0.27
N/C	0.12	0.16	0.16	0.16	0.16	0.26	0.16	0.16	0.16	0.16	0.16
Model coverage					96%		77%		20%		

Table 8.9 XPS analysis of titanium incubated with *ATCC35984* compared to pelleted *ATCC35984* and media incubated glass after 24 hours. XPS data was analysed in terms of bacterial coverage estimated by XPS and AFM, and calculated residue on the surface.

Analysis of the samples at both points showed similar properties. The decrease in Ti 2p with the suppression of the Si 2p observed on incubation indicated coverage. The observed increase in P 2p indicated the potential of bacterial adhesion, as observed through AFM imagining (Figure 8.3). Both areas on the sample showed an increase in C 1s and N 1s compared to pelleted bacteria. The O_{org} increased in the 'thick' layer and decreased in the 'thin' layer indicating differences in the residual layer.

The variation in coverage determined by the change in Ti 2p signal gave a different coverage value each point. On analysis of the residual layer both showed a negative P 2s signal indicating the residual layer covers the bacteria. Analysis of the 'thick' layer gave an O_{org}/C ratio slightly higher than N/C indicative of a protein dominant coating, with the potential of polysaccharide binding. The C285 had a resulting negative value, indicating the layer doesn't contain hydrocarbon. The 'thin' layer, in comparison, showed the residual C285 indicative of hydrocarbon. It is potentially related to the exposed titanium calculated, which was higher than in the 'thick' layer. The residual layer also consists of protein, as seen by the N/C ratio being higher than O_{org}/C ratio, with a lower probability of polysaccharide binding.

Compared to the TSB layer bound to titanium, both points analysed by XPS showed a lower O_{org}/C and slightly higher N/C ratio indicative of the dominance of proteins and lack of polysaccharides on the surface on bacterial incubation, indicating the possibility the residual layer was not TSB alone on the surface.

In comparison, the AFM model indicated a lower coverage of 20%, which was applied to both points on the sample. The 'thick' layer showed the potential of bacteria not covered by the residual layer, as P 2s was calculated as positive in the residual layer. The composition of the layer showed O_{org}/C was twice as big as N/C indicative of polysaccharides and proteins on the surface, with the dominance of polysaccharides on the surface. The presence of hydrocarbons in the residual layer was indicated through the presence of C 285 in the calculated residual layer. The 'thin' layer indicated the potential of the bacteria partially covered by the residual layer shown through a negative P 2s calculated signal. The composition of the residual layer contains proteins and polysaccharides as shown through the O_{org}/C being higher than N/C such that O_{org}/C ratio was 1.5 times larger than N/C. The presence of hydrocarbons was seen through the calculated C285 signal.

One of the limitations with analysis of the P 2s peak as an indication of whether there were bacteria present is the presence of P 2s on the surface on incubation with TSB. In the case of TSB

incubated titanium, it was assumed to be phosphates from the media bound to the surface. As the titanium incubated with bacteria in TSB, there is still the possibility of the exposed titanium having phosphates bound to the surface. In modelling the surface, the only residue layer this is more relevant to is the 'thick' layer on the sample analysed using the AFM model, as the only model not to estimate the suppression of P 2s by the residual layer. In this sample, the resulting P 2s signal was higher than that of the titanium incubated in TSB alone sample, indicating that, while there was a possibility of phosphates bound to the exposed titanium, there was also some P 2s signal remaining, indicating the bacteria was not covered completely by the residual layer.

Overall, the composition of the titanium incubated sample at different points on the XPS sample gave different composition, and different bacterial coverage, by XPS. Modelling through XPS, the composition of the residual layer changes between points. The 'thick' layer indicated the potential for polysaccharides in the residual layer whereas ' thin' layer doesn't. Both points modelled on the AFM showed different compositions, however both indicated the residual layer contained both proteins and polysaccharides. The carbon C285 signal varied between points on the sample, potentially relating to the hydrocarbon lap on the exposed substrates. The composition of the layer differed between each model indication of variation of bacterial composition leads to a change in biological composition of the layer.

8.1.5 Silver

Sputtercoated silver was incubated with *ATCC35984* and analysed by XPS after 24 hours. Figure 8.19 shows the survey spectrum and C 1s peak fit of the sample, with the Table 8.10 showing the XPS analysis of the sample and comparing it to the TSB incubated silver and pelleted *ATCC35984*. Figure 8.1 shows the AFM image of silver incubated with *ATCC35984* after 24 hours, confirming the presence of bacteria.

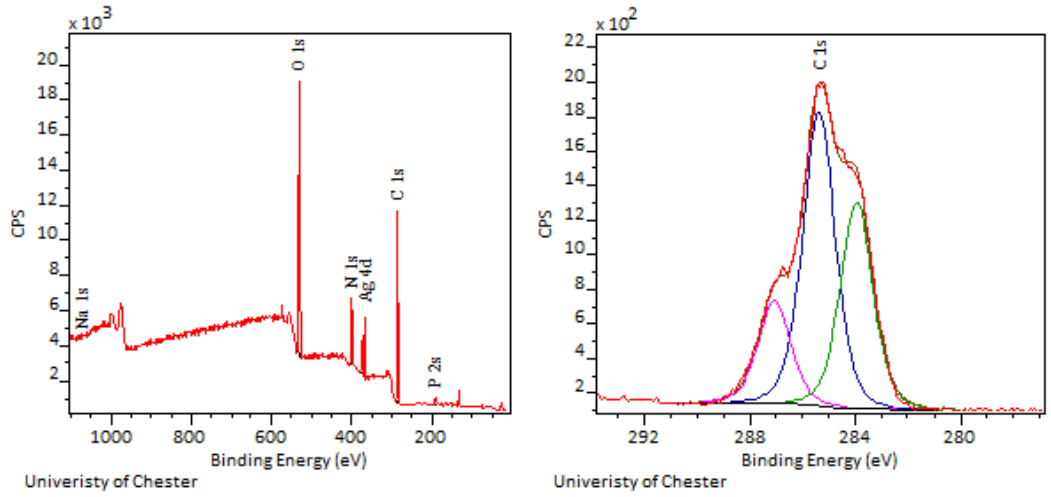

Figure 8.19 XPS survey and C 1s peak fit of glass incubated with *ATCC35984* after 24 hours.

	TSB incubated silver 24h	*ATCC35984* Pellet	*ATCC35984* incubated Silver 24h	XPS model		AFM model	
				Bacterial contribution	Calculated residue	Bacterial contribution	Calculated residue
C 1s	43.1	60.2	65.0	59.1	5.9	56.4	8.6
O 1s	11.8	25.1	23.9	24.6	-0.8	23.5	0.4
O_{org}	8.4	22.3	21.9	22.0	-0.1	20.9	0.9
N 1s	6.9	9.3	8.1	9.2	-1.0	8.7	-0.6
Si 2p	0.0	1.4	0.0	1.4	-1.4	1.3	-1.3
P 2s	0.0	3.7	2.3	3.6	-1.3	3.5	-1.2
Na 1s	0.6	0.1	0.0	0.1	-0.1	0.1	-0.1
Ag 3d	37.5	0.0	0.7	0.0	0.7	0.0	0.7
Ca 2s	0.0	0.3	0.0	0.3	-0.3	0.3	-0.3
C285	65.7	49.4	34.2	48.5	-14.3	46.3	-12.1
C286.5	20.3	34.8	48.8	34.2	14.6	32.7	16.1
C288	14.0	15.8	17.0	15.5	1.5	14.8	2.2
O_{org}/C	0.20	0.37	0.33	0.37	-0.02	0.37	0.11
N/C	0.16	0.16	0.13	0.16	-0.17	0.16	-0.07
Model coverage				98%		94%	

Table 8.10 XPS analysis of silver incubated with *ATCC35984* compared to pelleted *ATCC35984* and media incubated glass after 24 hours. XPS data was analysed in terms of bacterial coverage estimated by XPS and AFM, and calculated residue on the surface.

On calculation of coverage using the change in Ag 3d signal, the sample was found to have a 98% coverage, so should have a similar composition to pellet samples. On comparison to the pellet, there was an increase in carbon. Slight changes in nitrogen and oxygen were observed, but the differences were likely to be within the measurement error and therefore not significant.

Taking into account the effect of coverage estimated by XPS, the formula results in error, giving negative values for O_{org}, N 1s and C 285, making analysis of the layer in terms of biological composition difficult. It can be assumed, that in this case the bacterial coverage of the sample is over calculated.

Analysis of AFM images gave an estimated coverage of 93.7%. The residual layer still gave negative values for P 2s, N 1s and C285. The P 2s signal may be attributed to the coverage of bacteria, with the presence of O_{org} and C 1s indicating the layer was polysaccharides based, with no hydrocarbon. However, unlike the mica sample incubated with *ATCC35984* which showed only a slight negative N 1s signal calculated for the residual layer (-0.1) the N 1s signal of the silver residual layer was high enough to assume the model was still overestimating the bacterial coverage.

8.1.6 Summary of XPS analysis

Overall, both XPS and AFM models were used to estimate the coverage of bacteria. Interestingly, glass, mica and silver gave similar estimates for bacterial coverage in both models. Theoretically, this should lead to the proof that the XPS model estimates the bacterial coverage correctly. However, the XPS model overestimated the bacterial coverage due to the neglect of the residual layer, indicating the AFM coverage must also overestimate the coverage. The overestimation of bacterial coverage of both samples can be seen through the presence of the residual layer. While this alone is not proof of overestimation, the proof can be seen in the modelling of the residual layer of these some of samples, calculating the chemical signals as very small or below zero. The limitation of the AFM model has been discussed previously and attributed to the limited amount of areas analysed on the sample. Additionally, for this model, there is a limit to bacterial coverage of about 90%, after which calculations have a higher tendency to miscalculate the chemical composition of the residual layer due to errors in analysis.

Analysis of these models were limited, however the samples which have a coverage of lower than 90% showed a dominance of proteins, with little to no polysaccharide content. The amount of polysaccharide isn't consistent in these samples, as seen by the change in O_{org}/C relative to the N/C. Mica and silver both calculated the bacterial coverage as over 90%, which limits the use of this model, however the low amount of O_{org}/C is higher than the N/C ratio measured showing the residual layer to have a low polysaccharide residue.

Assessing P 2s signal in the model was used to determine the potential of the residue covering the bacteria. For samples which have been assumed to be an overestimate were not assessed as they have a higher probability to miscalculate the P 2s signal. For the AFM model of silicon, the high P 2s signal was assumed to be a result of potential underestimate of bacterial coverage. Ignoring this, the model would assume the bacteria in this sample would not be covered by the residual layer. Analysis of the glass sample showed a similar coverage for both models and estimate bacterial coverage. For titanium, the model assumes the XPS calculated coverage to have the bacteria covered in the residual layer, whereas the AFM model assumes a lower coverage, resulting in the P 2s signal to be estimated as -0.3 which is within the limit of detection of P 2s for these samples and indicating the bacteria may not be covered by the residue. On average the model assumes the bacteria to be covered by a residue, however the samples will be considered separately for comparison to the AFM force curve data.

8.2 AFM Data

AFM images of 10um squares were taken at 3 randomly selected points, with force curves taken at several points on each image. Force curves were divided depending on if the measurement was taken on or off a bacteria in Tables 8.13 and 8.14 and through histograms in Figure 8.20, 8.22, 8.24 and 8.26. Large standard deviations were observed within force curve data and resulted in frequency distributions being used to clarify key features, key examples of which can be seen in Figures 8.20-8.26 and remaining can be found in the Appendix. Comparisons to the *ATCC35984* incubated samples were compared to pelleted *ATCC35984* and relevant 24 hour incubated sample with TSB.

As previously noted in Chapter 6 a larger standard deviation on AFM samples relate to the weak adhesion forces between bacteria with the potential to pick bacteria up on the tip between force curves on the same sample. The was overcome between samples by removing the tip from the surface and running a high speed scan, effective shaking any loosely adhered matter to the tip off.

	TSB incubated sample 24 hours				*ATCC35984* incubated substrates 24 hours Bacterial points				Non-bacterial points			
	Snap in (nm)	Adhesive force (nN)	Pull out (nm)	Retractive force (nN)	Snap in (nm)	Adhesive force (nN)	Pull out (nm)	Retractive force (nN)	Snap in (nm)	Adhesive force (nN)	Pull out (nm)	Retractive force (nN)
Glass	7.9	50.9	9.3	73	3.2	4.4	11.7	50	2.1	7.6	10.7	50
	3.0	25.4	4.9	40	3.0	3.8	3.4	20	0.8	6.9	7.3	20
Mica	1.2	11.3	3.0	47	1.4	5.1	2.8	16	1.6	5.8	2.3	16
	0.4	6.6	0.7	12	0.9	2.0	1.3	5	1.0	2.8	1.5	6
Titanium	3.3	23.7	9.1	76	1.4	4.2	3.3	22	1.0	5.3	1.9	24
	1.5	15.7	4.2	29	0.6	2.4	1.7	8	0.3	3.0	2.1	6
Silver	3.9	26.7	6.2	44	4.4	21.1	7.9	54	3.0	10.7	10.0	41
	1.2	13.2	1.6	13	1.9	13.1	3.0	24	1.1	10.3	5.3	18
Pellet					3.1	2.8	6.8	11				
					2.2	2.5	6.2	6				

Table 8.11 AFM force curve comparison of substrates incubated with TSB after 24 hours and *ATCC35984* incubated substrates after 24 hours, divided into points on and off the bacteria. The first value in the table relates to the mean value and the second to the standard deviation

	Timed TSB incubated silicon sample				*ATCC35984* incubated silicon time samples							
					Bacterial				Non-bacterial			
	Snap in (nm)	Adhesive force (nN)	Pull out (nm)	Retractive force (nN)	Snap in (nm)	Adhesive force (nN)	Pull out (nm)	Retractive force (nN)	Snap in (nm)	Adhesive force (nN)	Pull out (nm)	Retractive force (nN)
2 hours					16.6	20.1	19.4	118	5.9	11.7	10.7	70
					18.5	23.2	19.6	135	5.7	12.6	7.3	75
4 hours					3.6	6.2	8.7	28	3.7	4.1	10.9	31
					3.3	5.5	4.3	7	4.5	3.3	7.4	18
6 hours					4.1	7.0	16.7	29	3.2	4.9	11.2	29
					3.3	8.1	40.4	21	1.6	2.5	7.9	19
8 hours					4.1	5.3	11.2	30	3.2	3.9	9.4	22
					2.7	5.5	6.3	30	1.4	3.0	3.7	7
24 hours	6.0	49.1	8.8	77	3.2	2.4	14.1	39	2.8	2.7	12.4	39
	1.1	13.4	3.2	28	2.8	1.8	8.0	24	2.1	2.3	5.5	16
Pellet					3.1	2.8	6.8	11				
					2.2	2.5	6.1	6				

Table 8.12AFM force curve comparison of silicon incubated with TSB over time and *ATCC35984* incubated substrates over time, divided into points on and off the bacteria. The first value in the table relates to the mean value and the second to the standard deviation

8.2.1 Snap in distance

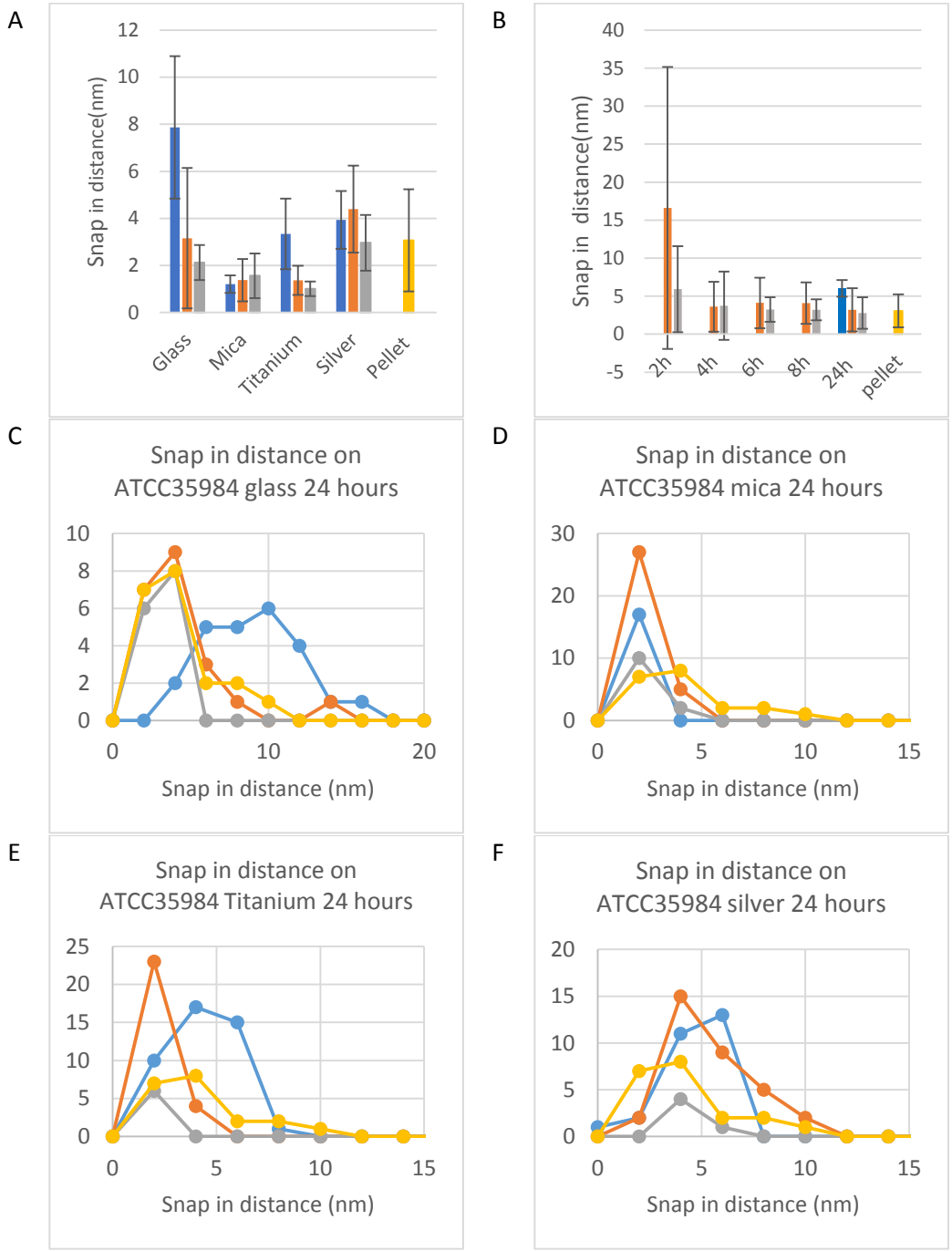

Figure 8.20 Histograms showing the snap in distance of the substrates after 24 hours(A) and of silicon during the first 8 hours (B). In both cases, data are shown for measurements on and off individual bacteria, and for the 24 hour data the equivalent data for the substrate incubated in TSB alone is also shown. Below images of frequency distributions are included for glass(C), silicon(D), titanium(E) and silver(F). Blue is TSB incubated sample, orange is *ATCC35984* incubated bacterial points, grey relates to non bacterial points on *ATCC35984* and yellow is the *ATCC35984* bacterial pellet.

Analysis of frequency distributions showed direct overlap of all timed bacteria between 0-15nm with a few outliers falling out of this range. The average value for timed samples varied

between samples, as seen in the histograms, but these fall between 2-4nm. All bacterial points overlapped directly with pelleted bacteria.

Likewise, all non-bacterial points mostly showed direct overlap, with 2 and 4 hours showing a wider range to shifting the average to larger values, narrowing as a function of time. Some overlap with bulk values with TSB was observed, with 2 and 4 hours showing more overlap due to the wider ranges. Most values fall between 0-8nm. As a function of time, direct overlap between points on and off the bacteria was observed, with the range of the 2 hours non-bacterial sample showing the widest range.

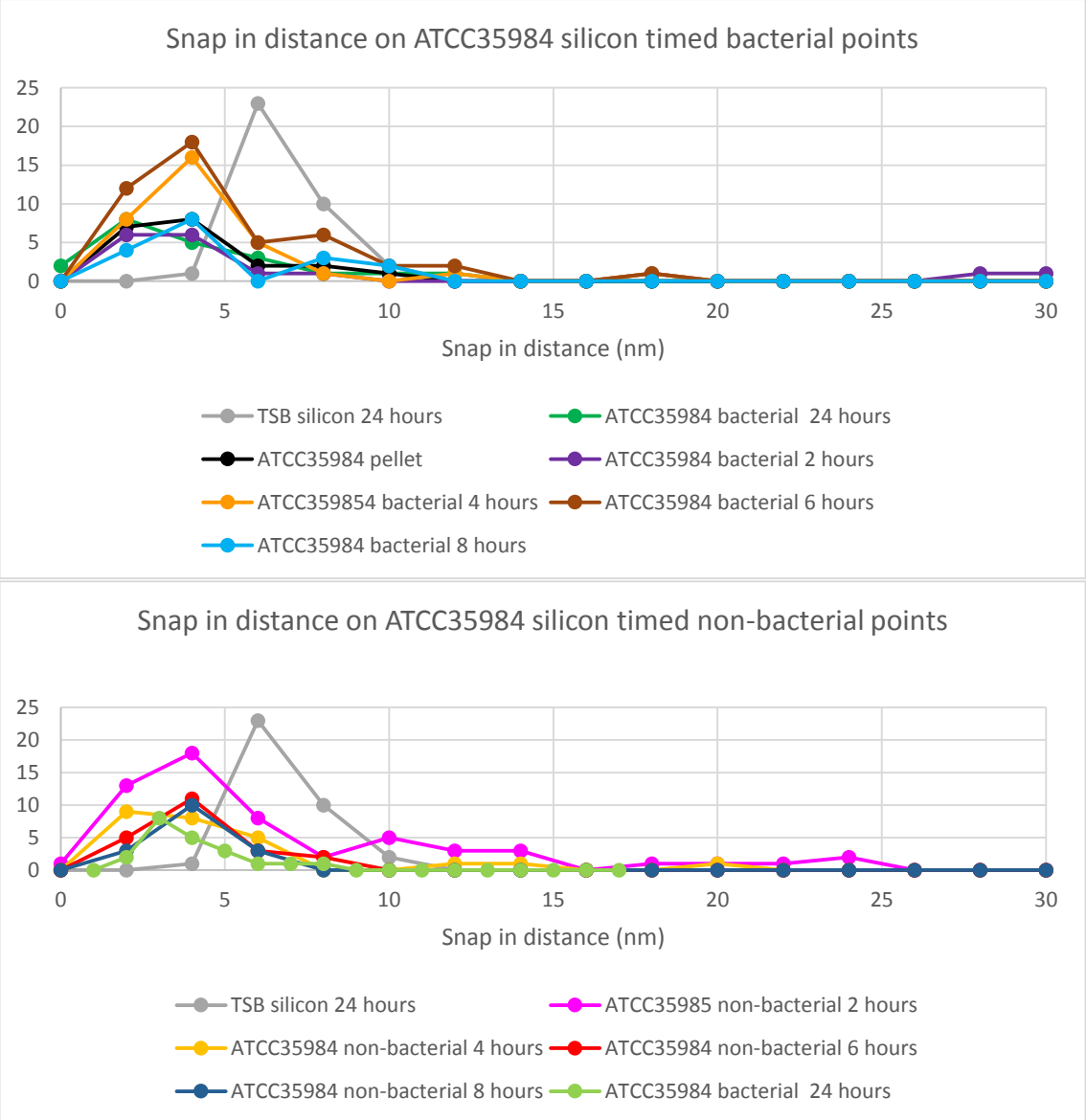

Figure 8.21 Frequency distributions of snap in values on *ATCC35984* on silicon over time, including TSB incubated silicon after 24 hours and pelleted bacteria.

Bacterial points on silicon, glass and titanium after 24 hours of incubation showed a decrease in snap in distance compared to that of TSB regardless of location on the sample. Bacterial

points on silver higher had a higher snap in value than that of the relevant media incubated sample, as well as bacteria on other samples. Mica showed a small increase in snap in values within its standard deviation showing little variation between points on and off the bacteria. Bacterial samples incubated with silicon and glass showed the most likeness to the bacterial pellet.

Analysis of frequency distributions showed more detailed information about overlap of high standard deviations measured. Glass showed direct overlap between points on and off bacteria as well as pelleted bacteria. Some overlap was observed with TSB, but TSB was shifted to higher values points on the bacteria showed outlier above main range. On mica, frequency distributions showed direct overlap of points on and off a bacteria and TSB, overlap of bacterial points and pelleted bacteria was also observed, however pelleted bacteria had a wider range. Titanium showed direct overlap between points on and off the bacteria pelleted bacteria has a wider range and overlap with bacterial points. TSB incubated silicon had a larger range skewed to higher values but showed overlap with non-bacterial points and bacterial points. Silver showed direct overlap between bacterial and non-bacterial points, with bacterial points having a wider range. Pelleted bacteria overlapped with bacterial points, but pelleted bacteria were skewed to lower values.

8.2.2 Attractive force

Analysis of frequency distributions on timed samples showed that all bacterial points overlapped directly, and all overlapped with pelleted *ATCC35984*. Bacterial points of timed samples showed some overlap with TSB incubated silicon; however, these were found to be with values that did not fall within the main range of 0-20nN. Non-bacterial points also showed direct overlap of points measured at different times within the range of 0-30nN, with the 2 hour sample having a wider range of 0-80nN and higher average value. The 2 hour sample was the only sample to show some overlap with TSB, due to the wider range.

Analysis of 24 hour samples of glass, mica and titanium showed the adhesion values of samples incubated in TSB to be significantly higher than those incubated with *ATCC35984*. Analysis of frequency distributions showed direct overlap with points on and off the bacteria, as well as with attractive forces on bacterial pellet of *ATCC35984*. Comparing the range, points off the bacteria showed a wider range. Comparisons between the attractive forces between substrates showed similarities in attractive forces between glass, silicon, mica and titanium. Analysis of silver showed a different trend compared to other samples. Silver

showed bacterial points have a larger range than non-bacterial, with an average value on bacterial points shifted to higher values.

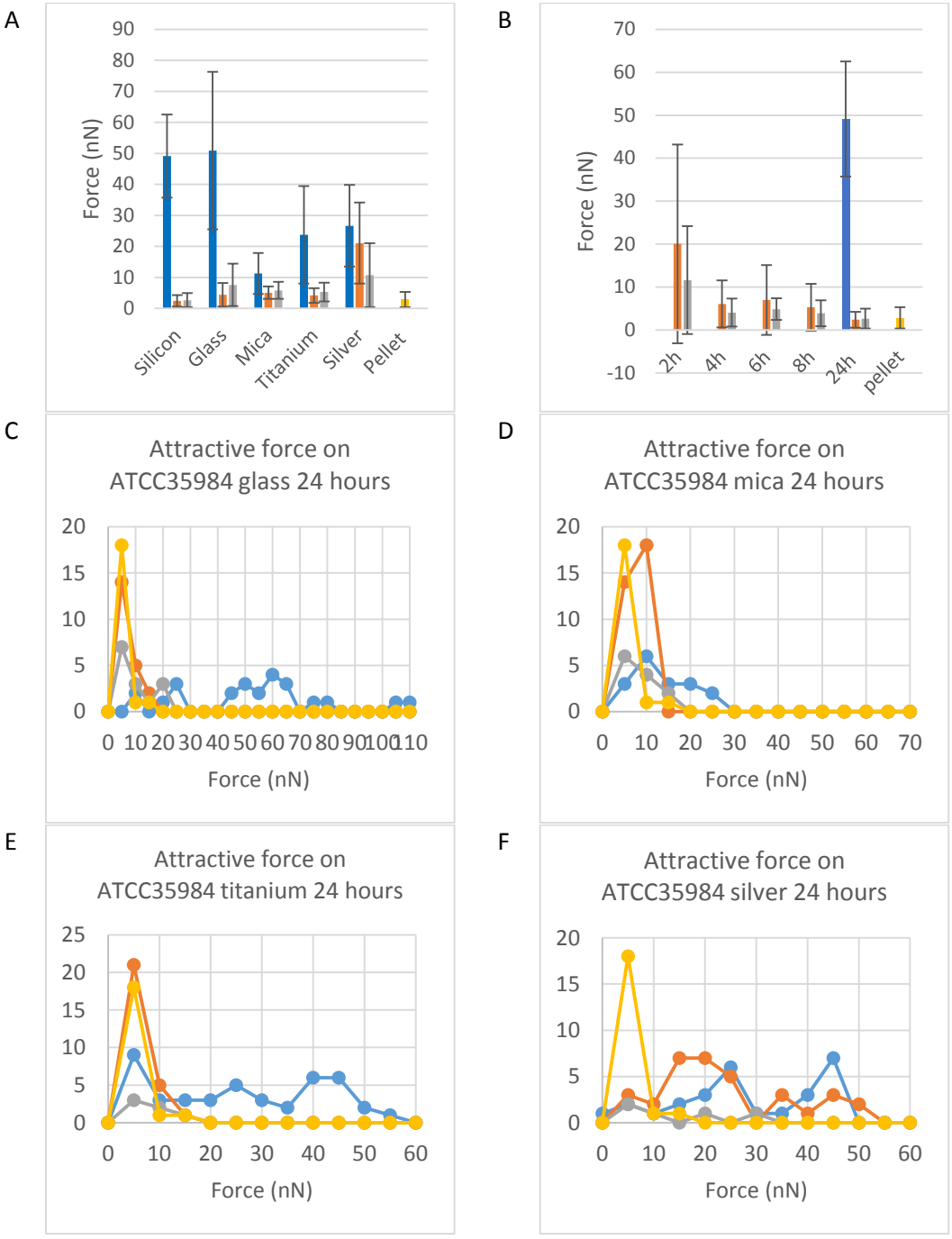

Figure 8.22 Histograms showing the attractive force the substrates after 24 hours(top left) and of silicon during the first 8 hours (top right). In both cases, data are shown for measurements on and off individual bacteria, and for the 24 hour data the equivalent data for the substrate incubated in TSB alone is also shown. Below images of frequency distributions are included for glass(C), silicon(D), titanium(E) and silver(F). Blue is TSB incubated sample, orange is *ATCC35984* incubated bacterial points, grey relates to non bacterial points on *ATCC35984* and yellow is the *ATCC35984* bacterial pellet.

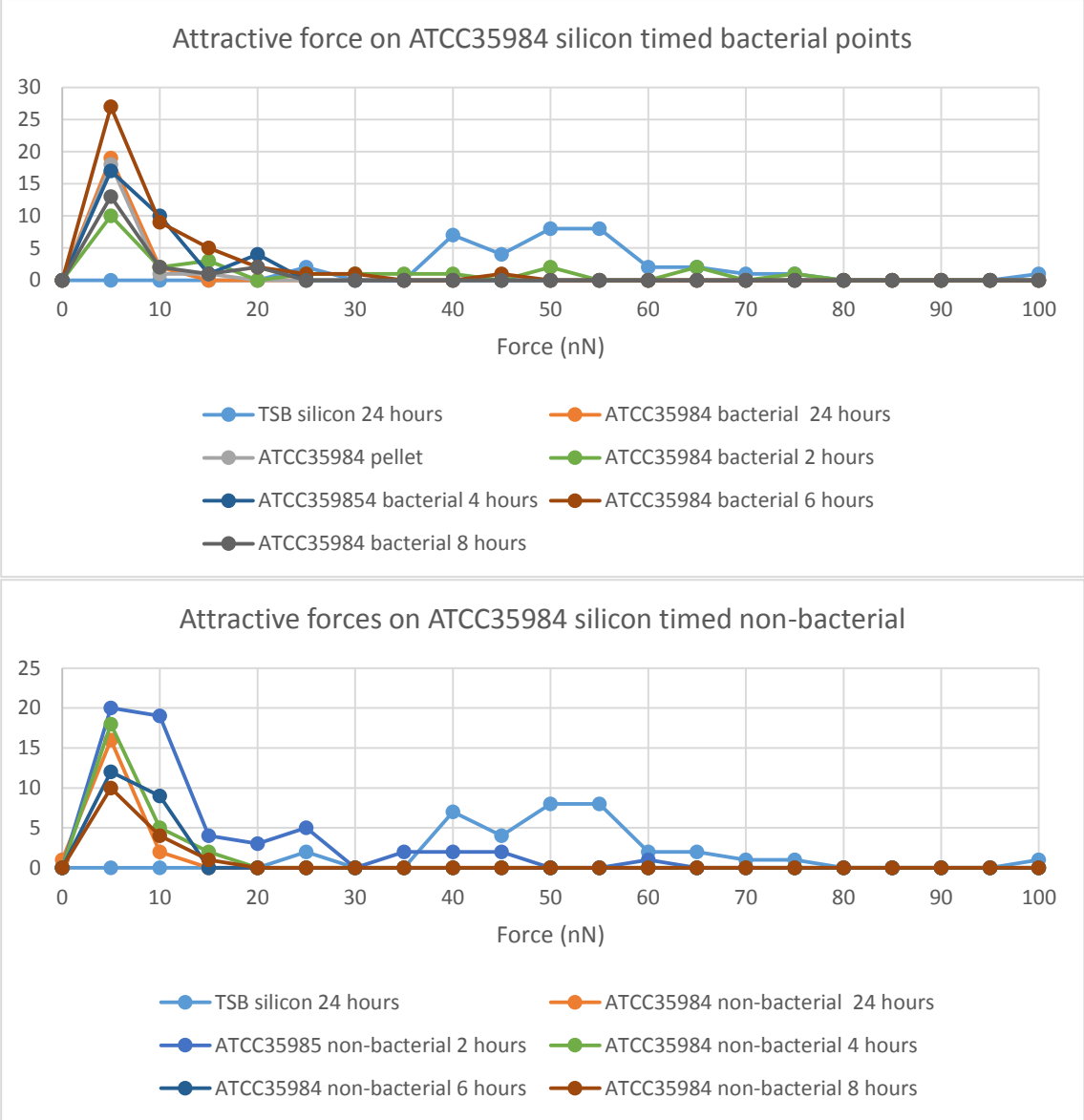

Figure 8.23 Frequency distributions of attractive forces on *ATCC35984* on silicon over time, including TSB incubated silicon after 24 hours and pelleted bacteria.

Overlap of attractive forces points on and off the bacteria showed similarities, indicating the potential similarities in adhesion properties. This was an indication that the residual layer calculated in Section 8.2 may cover the entire sample, including the bacteria. The difference between the bacterial samples and TSB incubated samples indicated the overlayer does not consist of TSB compound but of a less tip attracting substance. Similarities to the pelleted bacteria showed that there was the potential that the overlayer may not be covering the bacteria, and that the residual layer relates to a substance of similar nature to adhesion forces on the pelleted bacteria. Analysis of timed samples indicated this may occur at the same time as TSB adhesion to the substrate, as seen by the 2 hour sample, however the adhesion of TSB substrates to the surface was not seen beyond this sample, indicating that by 4 hours the overlayer was no longer showing signs of TSB bound substances.

Analysis of the silver sample indicated that this sample does not act the same way as other bacteria incubated samples. The analysis of the silver sample showed differences between points on and off the bacteria, indicating that the residual layer on and off the bacteria was not the same. Differences between the pellet and bacterial points on the silver sample showed that the tip is not analysing bacteria alone, and the potential the bacteria is covered by an additional substance.

8.2.3 Pull out distance

Analysis of timed samples showed that pull out distances of bacterial points on incubated samples shifted to larger distances as time progressed. On comparisons to the pelleted bacteria, all bacterial points on samples showed some overlap with bacterial pellets. The 2 and 4 hour sample overlapped with the lower values of the pelleted bacteria, whereas the 6 and 8 hours shifted to higher values. Overlap was also observed with the TSB incubated silicon, as the TSB incubated silicon had a wide range. Non-bacterial points varied between samples, where overlaps were observed between 0-20nm. A decrease in range of pull out distance on non- bacterial points over time was observed. Comparisons between points on and off the bacteria for each timed sample showed there was an overlap between the two, which varied over time, as a change in pull out distances of bacterial points were observed. Overall, this indicated the potential overlayer covered the whole sample, however the interaction of the overlayer with bacteria and substrate vary. There were also the additional changes observed as a function of time. As time progressed the increase in pull out distances indicated the nature of the overlayer interactions with the tip changes and becomes more adhesive in nature over time. This is an indication of the overlayer interaction with the bacteria changing with an increase of bacterial adhesion. Analysis of non-bacterial points confirmed there was a change in adhesive nature of the layer over time. The decrease in range was an indication of the residual layer changing over time, which may be a result of an additional layer forming alongside the TSB layer, which then covers or replaces the TSB layer and become the dominant layer probed.

Analysis of the 24 hour samples showed similarities between points on and off the bacteria, which were similar to that of the TSB alone, with the exception of titanium which showed the bacterial sample to have lower pull out distances than the TSB incubated titanium. Similarities between pellet and bacterial samples were observed on glass, silicon and silver. Similarities between the mica and titanium were also observed.

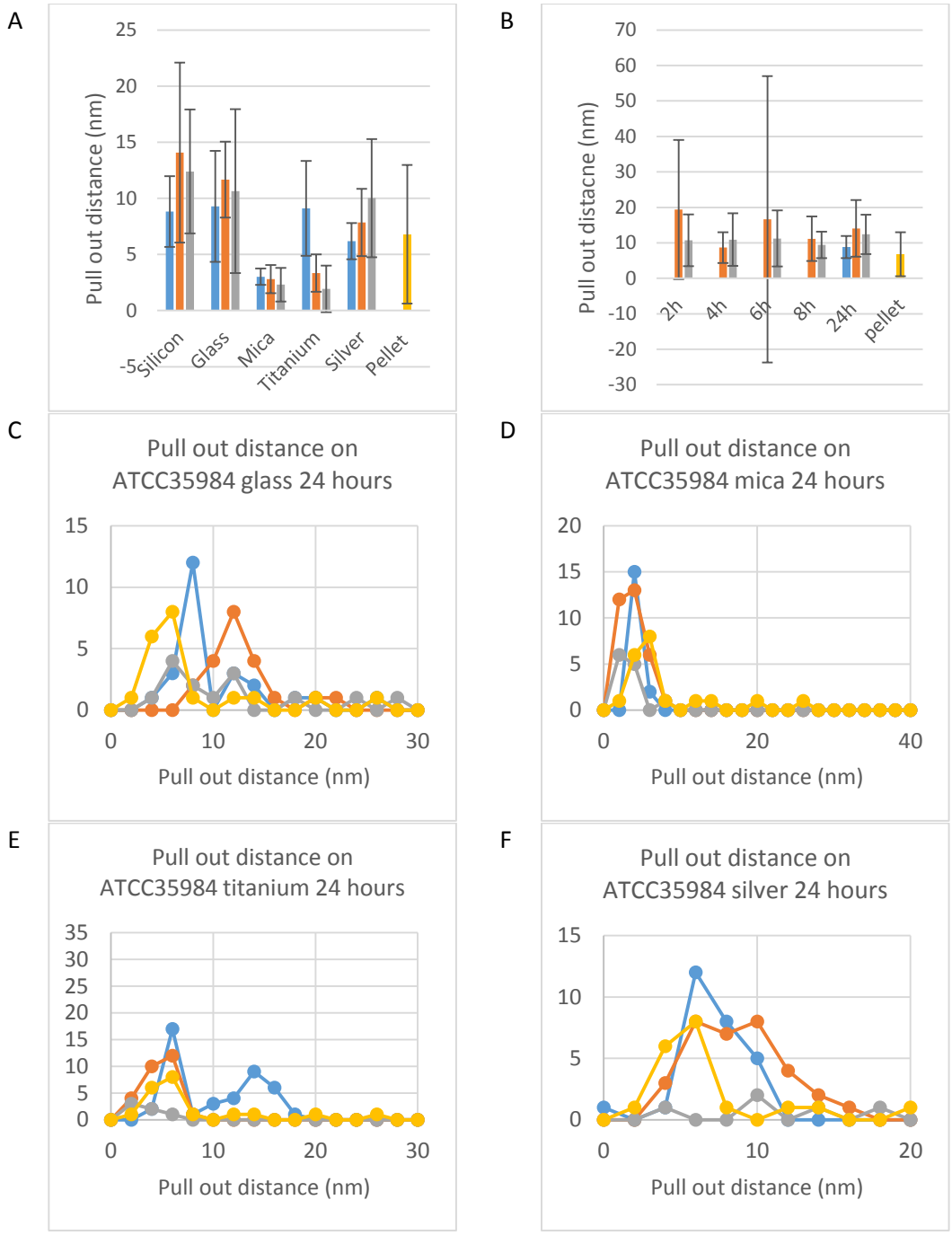

Figure 8.24 Histograms showing the snap in distance of the substrates after 24 hours(top left) and of silicon during the first 8 hours (top right). In both cases, data are shown for measurements on and off individual bacteria, and for the 24 hour data the equivalent data for the substrate incubated in TSB alone is also shown. Below images of frequency distributions are included for glass(C), silicon(D), titanium(E) and silver(F). Blue is TSB incubated sample, orange is *ATCC35984* incubated bacterial points, grey relates to non bacterial points on *ATCC35984* and yellow is the *ATCC35984* bacterial pellet.

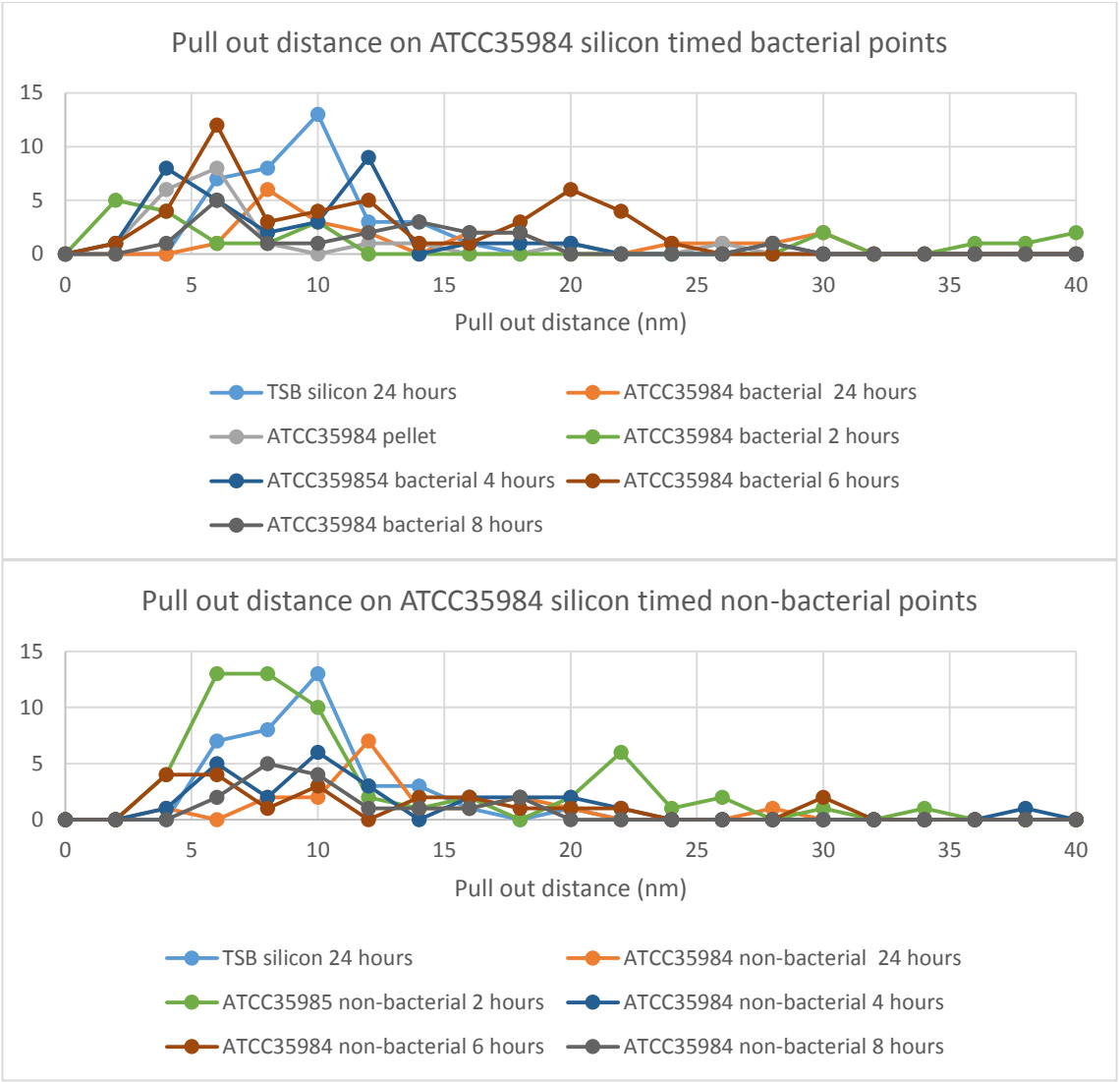

Figure 8.25 Frequency distributions of retractive forces of *ATCC35984* on silicon over time, including TSB incubated silicon after 24 hours and pelleted bacteria.

Analysis of frequency distributions of glass showed the non-bacterial points have a wider range than bacterial points, with the average value of non-bacterial points being lower than those of bacterial points. Overlap of TSB and bacterial samples were observed with TSB incubated glass and non-bacterial points were observed, with less overlap seen between the TSB sample and bacterial points. The bacterial points on glass showed some overlap with the pelleted bacteria, however the overlap was minimal. This indicated the potential that the bacteria were covered with an additional substance. The nature of the residual layer showed differences between points on and off the bacteria, and that the layer has some variance in interaction with the bacteria and substrate.

Analysis of mica and titanium showed direct overlap with points on and off the bacteria. On mica the bacterial points had a wider range. On titanium the average value on of non-bacterial points were smaller than bacterial points. Both samples showed overlap of bacterial

points and the pelleted *ATCC35984*, with mica showing bacterial points having a wider range and lower average value. TSB incubated mica also showed overlap of bacteria incubated mica. Analysis of titanium incubated with *ATCC35984* showed overlap of the lower peak TSB incubated titanium.

Analysis of silver showed overlap of bacterial and non-bacterial points, along with overlap with TSB incubated silver and pelleted *ATCC35984*. TSB incubated silver and bacterial points on silver had a wider range and a higher average value.

Overall, all 24 hour samples showed similarities in pull out distances on and off the bacteria indicating the potential of the overlayer. Similarities observed with TSB layer indicated the overlayer may consist of some TSB components. All samples showed similarities between bacterial pellet of *ATCC35984* and bacterial points indicating there was some bacteria interactions with the tip in these samples. Differences between mica and titanium compared to glass, silicon and silver indicated the potential of different bacterial adhesion systems, whereas titanium and mica showed the potential there was no additional layer of the bacteria. However, as bacterial and non-bacterial points were similar, it was more likely a different layer system has formed.

8.2.4 Retractive force

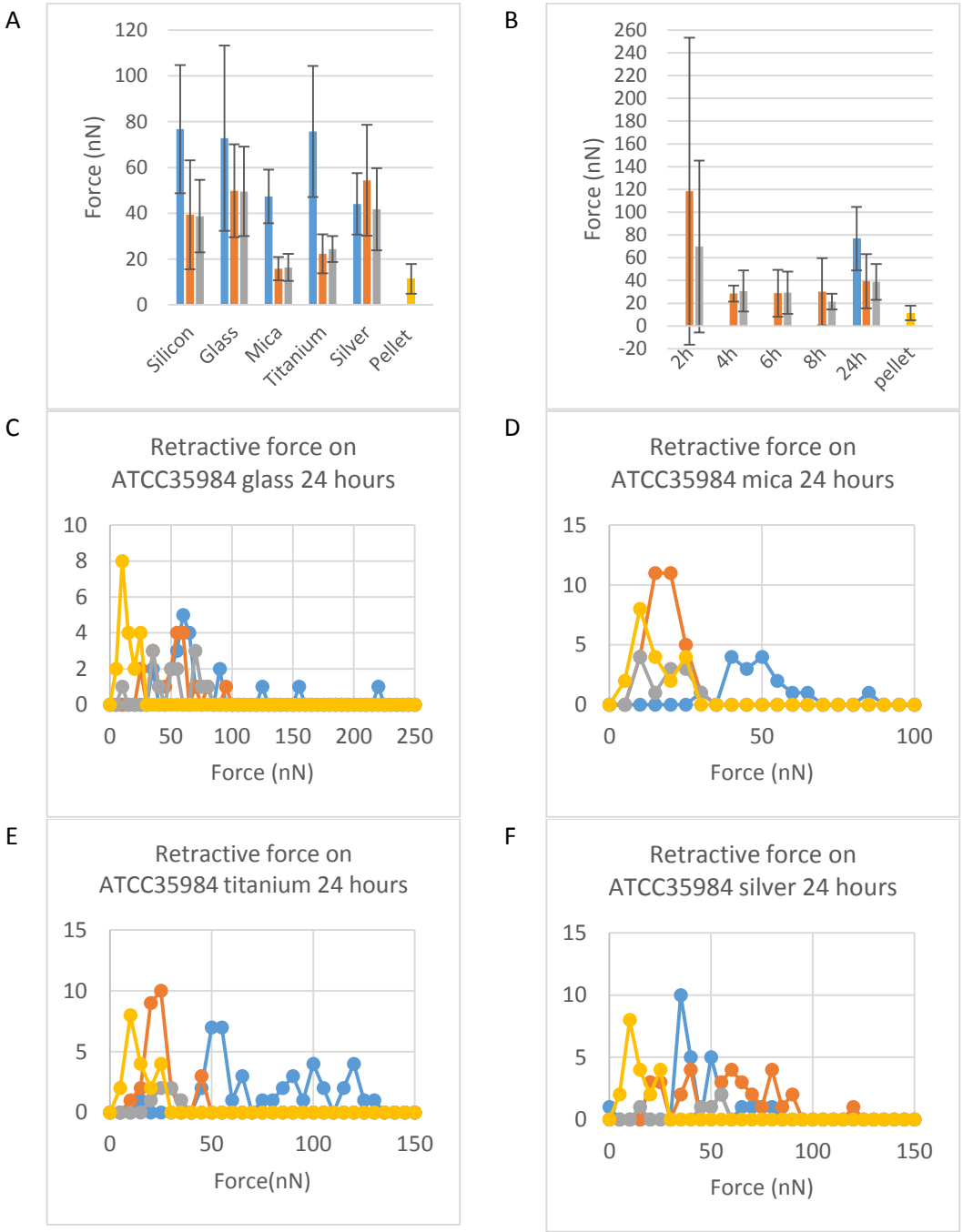

Figure 8.25 Histograms showing the retractive forces of the substrates after 24 hours(top left) and of silicon during the first 8 hours (top right). In both cases, data are shown for measurements on and off individual bacteria, and for the 24 hour data the equivalent data for the substrate incubated in TSB alone is also shown. Below images of frequency distributions are included for glass(C), silicon(D), titanium(E) and silver(F). Blue is TSB incubated sample, orange is *ATCC35984* incubated bacterial points, grey relates to non bacterial points on *ATCC35984* and yellow is the *ATCC35984* bacterial pellet.

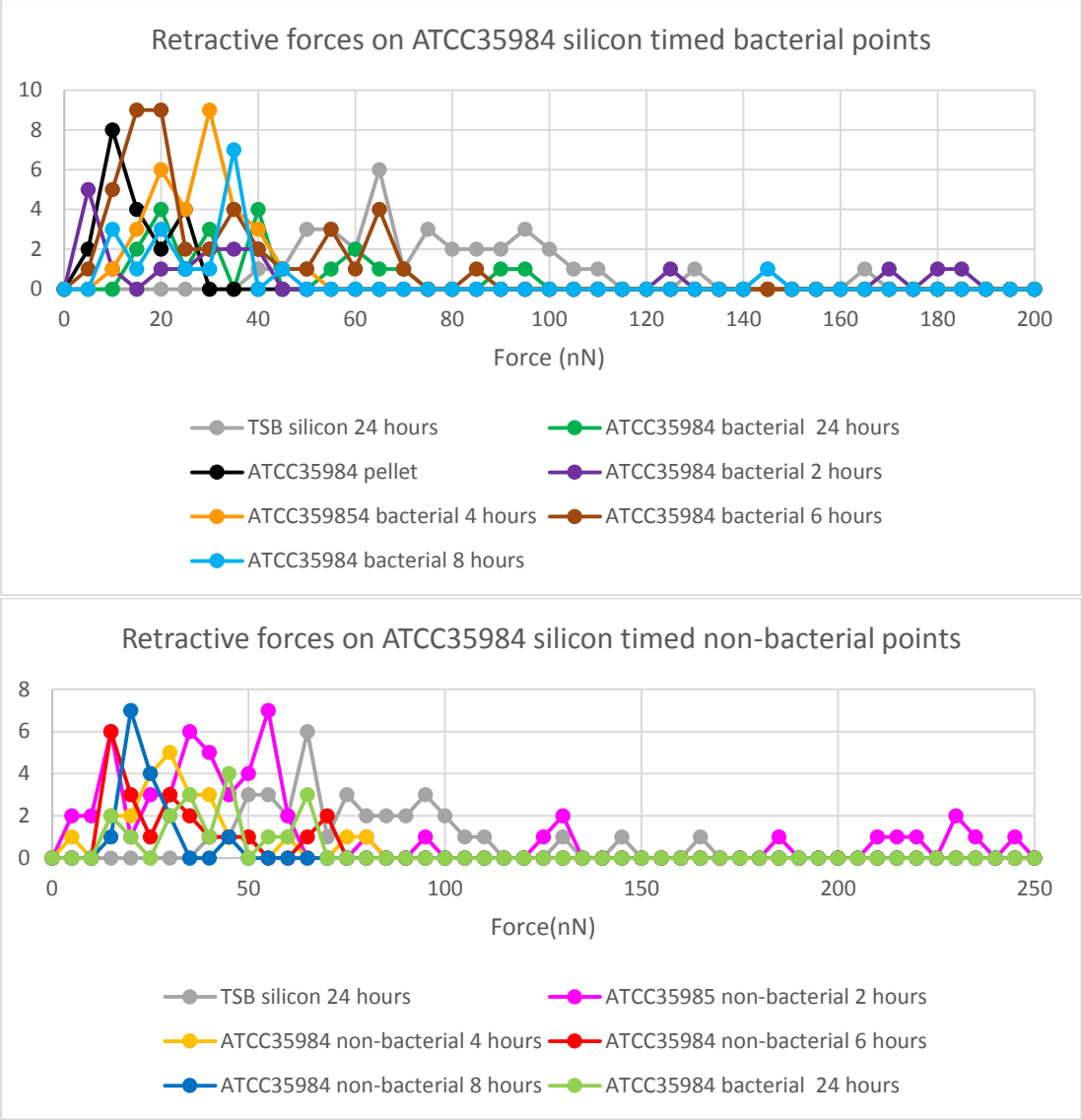

Figure 8.26 Frequency distributions of retractive forces on *NCTC13360* on silicon over time, including TSB incubated silicon after 24 hours and pelleted bacteria.

Frequency distributions of timed samples showed overlap, with a range of 0-50 for most predominant array of peaks, with 6 and 24 hours showed a range of 0-100nN. All bacterial points on timed samples showed some overlap with TSB, which has a range of 40-120nm. All bacterial points showed overlap with pelleted *ATCC35984* with a range of 0-30nN. Non-bacterial points on timed samples showed overlap with other timed samples, with the range narrowing over time, with 24 hour sample shifting to smaller value, indicating an additional change at longer incubation times. At 2 hours, bacterial points had a smaller range than non-bacterial points, with non-bacterial points showing overlap with TSB incubated silicon. Bacterial points showed direct overlap with the *ATCC35984* pellet, with the bacterial points of the 2 hour incubated sample showing outliers between 100-300nN. At 4 hours bacterial and non-bacterial points overlap with similar range and average was observed. Bacterial

points overlap with the pelleted bacteria and both bacterial and non-bacterial points overlap with TSB. At 6 hours overlap of bacterial and non-bacterial points was still observed, with a smaller range than earlier timed samples. The 6 hour sample showed a slight overlap with the TSB sample; however, this was less than in previous timed samples. The 8 hour sample still showed overlap of bacterial and non-bacterial points as well as with pelleted *ATCC35984*, however the previous overlap of with TSB incubated silicon seen in earlier samples were no longer observed.

Analysis of 24 hour incubated samples, with the exception of silver, showed similarities between points on and off the bacteria with TSB incubated sample having a higher adhesion value. Additionally, mica and titanium incubated with *ATCC35984* showed adhesion values that overlap and were closer to the pelleted bacteria than the glass, silicon and silver incubated samples.

Frequency distributions of glass incubated with *ATCC35984* showed direct overlap between bacterial and non-bacterial points with a range of 0-100nN. Some overlap with TSB incubated glass was observed, with the TSB incubated sample having a higher average. Comparisons to pelleted *ATCC35984* showed a slight overlap with the bacterial points of the incubated glass sample, however the pelleted bacteria were lower.

Mica incubated with *ATCC35984* showed direct overlap of points on and off the bacteria as well as with pelleted *ATCC35984*. TSB incubated mica did not show overlap with the *ATCC35984* incubated mica.

Analysis of titanium showed similarities between points on and of the bacteria, with bacterial points showing a wider range. In comparisons to TSB incubated titanium, bacteria incubated samples showed some overlap. The bacterial points on incubated titanium overlapped with pelleted *ATCC35984*, with the pelleted bacteria having a lower average.

Silver incubated with *ATCC35984* showed bacterial and non-bacterial points, however a wider range was observed with bacterial points. Overlap was also observed with TSB incubated silver, with the TSB sample having a smaller range. Some overlap of the *ATCC35984* incubated silver and the pellet was observed, with the pelleted bacteria having a lower range.

8.2.5 Analysis of AFM results

Glass and silicon showed similarities in AFM results, and mica and titanium showed similarities in AFM results. Typically, all samples showed similar trends. The lower snap in and

attractive force showed there was some repulsive nature to the tip-bacteria interaction, as a protective layer. The additional layer was reflected by difference in XPS data calculated. The slight variation between on and off the bacteria, suggested an even coating across all the sample. The pull out distance and retractive force information gained relate to the interactions of the tip with this layer, and with bacteria, which relate to the variation across points. However, there was no variation in adhesion values between points on and off bacteria. As the adhesion values relate to maximum pull out here, which relate to the additional layer formed.

Similarities between glass and silicon, as well as mica and titanium indicated the nature of the potential overlayer. Titanium and mica typically showed adhesion measurements closer to that of the pelleted bacteria compared to glass and silicon.

For each AFM measurement, silver showed different results compared to other substrates. This was an indication of a different type of residual layer measured on the sample compared to other samples. However, it should be noted that silver had a high bacterial coverage limiting the number of points available to analyse on non-bacterial points, limiting the reliability of the measurements off the bacteria, and its comparisons to bacterial points.

8.3 Conclusions

XPS data of incubated samples showed the attachment of bacteria to the surface, usually through the presence of low levels of P 2s signal, indicating teichoic acids. The samples which do not show P 2s signal relate to low level coverage as confirmed by SEM and AFM. Using the phosphorus signal to determine the presence of bacteria on silicon is tricky due to the phosphorus 2p peak overlapping with 2^{nd} plasmon resonance peak of silicon. To overcome this the P 2s peak was chosen over P 2p signal.

The bacterial coverage of the sample was calculated by considering the change in defining peak and used to model the bacteria on the surface. Alternatively, a model was also built using the coverage estimated though AFM. While some samples showed similarities between both models, attempts to model the bacterial coverage were shown to give limited results.

Sample	Bacterial coverage AFM	Bacterial coverage XPS
Silicon	73%	83%
Glass	51%	52%
Mica	92%	93%
Titanium	20%	96%/77%
Silver	93%	98%

Table 8.13 estimation of bacterial coverage by XPS and AFM compared

Generally, the XPS model overestimated the bacterial coverage leading to errors in the calculation of the residual layer. The only samples to give reasonable results were glass and titanium. The reason for this overestimation is a result of neglecting the effect the residual layer has on attenuating the substrate signal used when calculating the bacterial coverage.

The AFM model of bacterial coverage was shown to overestimate the coverage of mica and silver, whereas silicon was assumed to be an underestimate. The AFM model is limited in the size and number of areas analysed, leading to a miscalculation of bacterial coverage. Additionally, the coverage estimated on silicon samples were further limited by the number of samples used to estimate the bacterial coverage of samples not measured by AFM.

Attempts were made to use this model to determine the composition of non-bacterial contributions to XPS signal. For the remaining samples, a dominance of proteins was observed, with little to no polysaccharides detected. The amount of polysaccharides detected changed between samples. Using knowledge of bacterial coverage and the calculated residual layer, the samples were analysed to determine if the residual layer covered the bacteria.

Using the sample coverage models as an estimate of bacterial coverage, and composition of the calculated residual layer, the potential of the residual layer covering the bacteria can be determined. For samples that overestimate the bacterial coverage it is assumed the residual layer does not cover the bacteria, as the calculated values of other measured signals were low. Coverage calculated by XPS of glass and titanium were shown to estimate the coverage of the bacteria with the residual layer, whereas the AFM model of bacterial coverage indicated the residual layer doesn't cover the bacteria. Silicon was an interesting case, where the P 2s signal in the AFM model was large positive value in the residual layer, indicating the miscalculation of bacterial coverage, so therefore assumed the bacteria was not covered by the residual layer.

Analysis of AFM force curves gave a range of data regarding the sample. Points of bacteria incubated samples were divided into points on and off the bacteria. Generally, most samples showed similarities between points on and off the bacteria indicating similarities between the points may be a result of an overlayer covering the entire sample. Similarities between silicon and glass after 24 hours of incubation were observed as were similarities between titanium and mica. Silver showed some similarities to glass and silicon for pull out and retractive forces, but overall showed different results compared to other samples for each measurement.

Timed data showed standard deviations values higher than that of average values. While this may reduce the reliability of the results overall, it also reflects the variations of binding possible within the sample. This includes a range of factors including adhesive nature of bacteria to a surface, layer thickness, bacteria-layer interactions, bacteria- media interactions. At the resolution, along with the complexities of live biological sample, it was difficult to separate these possibilities out into AFM results. A way to potentially overcome this issue is the combination of AFM with other techniques such as in-situ infrared. Modelling each outcome is tricky, as each component is connected to each other. For example, the bacteria were covered by an additional layer as well as attached to the substrate material, with the potential of a layer formed between the substrate and bacteria, all situations contributing to adhesion measurements

Comparisons of force curve measurements and XPS data are limited, however an indication of correlation between force curve data and the assumed amount of polysaccharides on the surface may indicate the composition of the layer relates to force curve data. Generally, a higher polysaccharide content may be indicated by lower force curve values. This is based on the theory the proteins will show signs of unfolding leading to larger adhesion values overall. However, as calculating the composition of the layer in terms of biological compounds from XPS data have been shown to be tricky, it was difficult to determine if there was a true correlation between the two.

Chapter 9 Comparison of *S. epidermidis* analysis, discussion and future works

9.1 Comparison of bacterial data

Two different strains of *S. epidermidis* were analysed by XPS and AFM, one biofilm former (*ATCC35984*) and one non-biofilm formed (*NCTC13360*). Analysis was made in terms of coverage, potential composition of the residue layer and AFM results.

9.1.1 Coverage models

	NCTC13360		*ATCC35984*	
	XPS	AFM	XPS	AFM
Silicon	0-84%	0-56%	0-100%	0-73%
Glass	74%	29%	51%	52%
Mica	55%	9%	91%	90%
Titanium	55%	20%	96%/77%	20%
Silver	72%	39%	98%	93%

Table 9.1 Comparison of estimated coverage of *ATCC35984* and *NCTC13360* after 24 hours of incubation of different substrates analysed by XPS and AFM, results taken from chapters 7 and 8 and repeated here for ease.

As observed in Chapter 7 and 8, the AFM model of coverage usually predicts either a lower or equal coverage compared to XPS. This was due to the XPS model generally overestimating the bacterial coverage. Comparing both models between strains, *S. epidermidis* ATCC3594 generally has a higher substrate coverage than *NCTC13360*. This indicates *ATCC35984* is more likely to adhere to the surface of a material than *NCTC13360*.

9.1.2 Non-bacterial contribution to signal model

The calculation of the residue model has been discussed previously in Chapters 7 and 8. The model uses the bacterial coverage estimated by XPS and AFM to determine the bacterial contribution to signal, allowing the non-bacterial contribution, also described as residue, to be calculated. Analysis of the non-bacterial contribution to signal can identify the potential biological compounds on the surface and if the bacteria are covered by the residual layer.

Generally, the XPS model indicates the residual layer covers the bacteria, whereas the AFM model was likely to indicate the bacteria was not covered by the residue. This was determined through the P 2s signal, where a negative signal in the calculated residual layer was assumed to be due to the bacteria being covered, with some considerations to the potential of overestimating the coverage. The composition of the residual layer was more likely to be protein dominant, with some samples showing the presence of polysaccharides and hydrocarbons. A summary of the results in Chapters 7 and 8 can be seen in Table 9.1.

The detection of hydrocarbons was found to be partially due to the atmospheric layer on the exposed substrate. The composition of the residual layer was found to be different to that of TSB incubated substrates indicating that the bacteria is excreting parts of the residue as well as the potential that the bacteria has preferential binding to compounds bound to the substrate.

Bacteria	Model	Substrate	Residue composition			Residue details by XPS analysis	
			O_{org}/C	N/C	P 2s	Potential biological composition	Bacterial covered with residue?
NCTC13360	XPS	Silicon	0.49	0.31	-1.3	Protein dominant, some polysaccharides detected	Yes
		Glass	0.23	0.27	-1.9	Protein dominant, some hydrocarbon	Yes
		Mica	0.35	0.19	-1.7	Proteins and polysaccharide dominant, hydrocarbon detected	Yes
		Titanium	0.32	0.23	-1.2	Protein dominant, some hydrocarbons	Yes
		Silver	0.00	0.63	-1.7	Error in estimate of coverage, potential protein dominant	Yes
	AFM	Silicon	0.39	0.20	-0.2	Protein dominant, some polysaccharides and hydrocarbons detected	No
		Glass	0.17	0.20	-0.3	Protein dominant, hydrocarbon detected	No
		Mica	0.22	0.16	0.6	Protein dominant with some polysaccharides, hydrocarbon detected	No
		Titanium	0.34	0.19	0.1	Proteins and polysaccharides, hydrocarbon detected	No
		Silver	0.34	0.19	-0.5	Proteins and polysaccharides hydrocarbon detected	No
ATCC35984	XPS	Silicon	-0.58	0.27	-2.1	Error in calculation, possible protein dominant	Yes
		Glass	0.08	0.20	-1.9	Proteins and hydrocarbons	Yes
		Mica	0.06	-0.02	-1.8	Error in bacterial coverage, possible polysaccharides	Yes
		Titanium thin	0.08	0.16	-2.2	Protein dominant hydrocarbon detected	Yes
		Titanium thick	0.30	0.26	-1.8	Protein dominant, hydrocarbon detected	Yes
		Silver	-0.02	-0.17	-1.4	Error calculated	Yes
	AFM	Silicon	0.17	0.19	-0.3	Protein dominant, some hydrocarbon detected	No
		Glass	0.07	0.20	-0.3	Proteins and hydrocarbons	No
		Mica	0.08	0.01	-1.7	Error in bacterial coverage, potential proteins and polysaccharides	Yes
		Titanium thin	0.37	0.27	-0.1	Protein dominant, polysaccharides and hydrocarbon detected	No
		Titanium thick	0.16	0.16	1.2	Protein dominant, hydrocarbon detected	No
		Silver	0.11	-0.07	-1.2	Error calculated, potentially polysaccharide dominant	Yes

Table 9.2 Analysis of the non-bacterial contributions to signal for substrates incubated with *ATCC35984* and *NCTC13360* after 24 hours, results taken from Chapters 7 and 8 and repeated here for ease.

9.1.3 Force curve analysis

AFM analysis showed that the residue material may cover the entire sample, as similarities between points on and off the bacteria were observed for most AFM measurements. Specific differences between points on and off the bacteria for the same bacteria are explored in the relevant chapters. Silver was the only substrate shown to be an exception to the observed similarities between points on and off the bacteria seen with other substrates.

Comparison of silicon, glass, titanium, silver and mica incubated samples of both bacteria are below, grouped due to similarities between points on and off the bacteria.

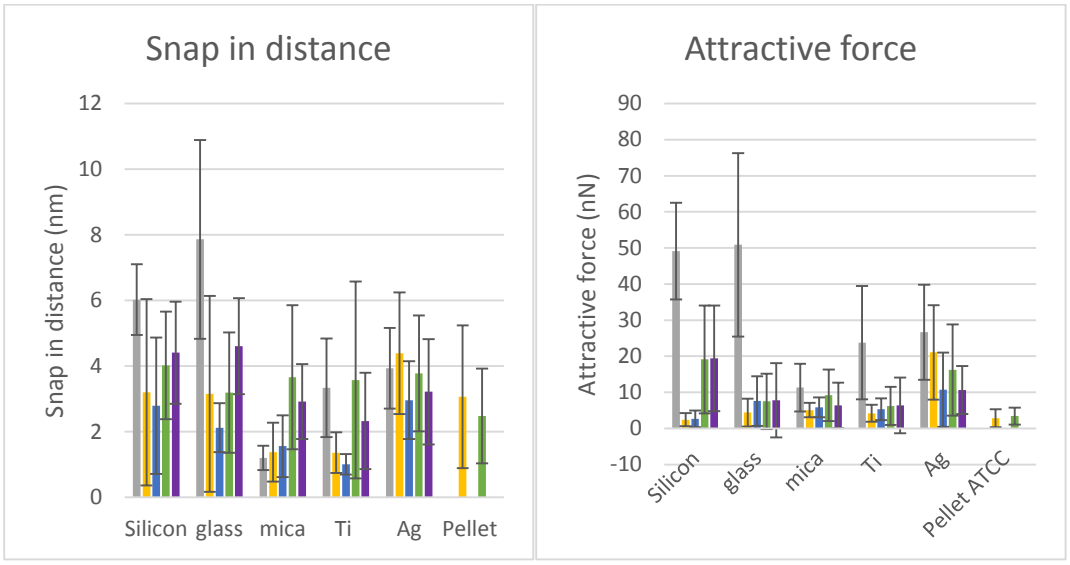

Figure 9.1 Comparisons of snap in (left) and attractive force (right) for substrates incubated with *S. epidermidis ATCC35984* and *NCTC13360* after 24 hours. Grey represents the TSB incubated sample, yellow represent the *ATCC35984* bacterial points, blue represents the *ATCC35984* nonbacterial points, green represents *NCTC13360* bacterial points and purple represent the *NCTC13360* nonbacterial points.

Analysis of snap in distances show a difference between the two strains, with the biofilm former *ATCC35984* showing lower snap in values and therefore a thinner surface layer. This indicates the overlayer on the sample was a different in thickness depending on the bacterial strain. The biofilm former having a thinner layer than the non-biofilm former indicates that the residual layer of the non-biofilm former *NCTC13360* is more loosely bound to the bacteria than that formed on the *ATCC35984*. The thinner layer on *ATCC35984* may be a result of the overlayer being closer to the bacteria to protect it from external influence, as seen within biofilm formation.

Attractive forces show the same trend across substrates, where the *NCTC13360* strain have a higher adhesion force. This indicates the nature of the residual layer differs between the two strains, which is possibly due the formation of a biofilm on the ATCC25984 strain.

The differences observed on snap in distance and attractive forces indicate the potential formation of a biofilm. The thinner layer observed on the *ATCC35984* strain may be due to the components of the overlayer being closely bound, as well as the high coverage leading to less residue measured. The potentially closer bound layer on *ATCC35984* was also less attracted to the tip, which may be a protective property of the overlayer.

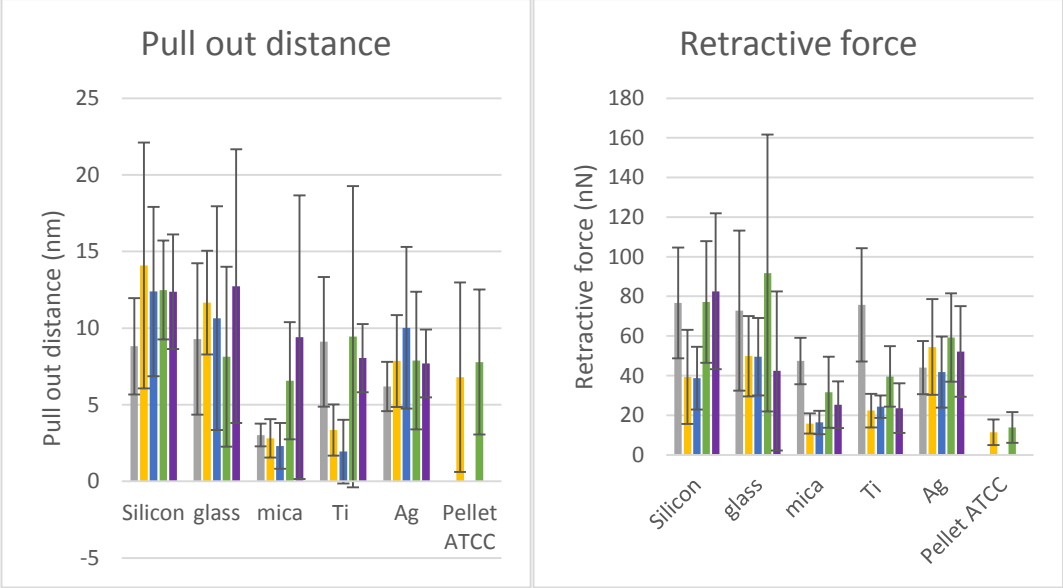

Figure 9.2 Comparisons of pull out (left) and retractive forces (right) for substrates incubated with *S. epidermidis ATCC35984* and *NCTC13360* after 24 hours. Grey represents the TSB incubated sample, yellow represent the *ATCC35984* bacterial points, blue represents the *ATCC35984* nonbacterial points, green represents *NCTC13360* bacterial points and purple represent the *NCTC13360* non-bacterial points.

Analysis of pull out distance between bacterial strains vary. Silicon and glass show similarities between the two strains, whereas mica and titanium show the non-biofilm former to have larger distances. This potentially relates to the composition of the residual layer, where mica and titanium were shown to be more likely to have polysaccharides in the residual layer for the *NCTC13360* strain. The complexity of the layer contributes to the higher pull out distances

Analysis of retractive forces show some differences between the two strains of *S. epidermidis*, with the *NCTC13360* strain having higher adhesion values. This confirms the theory that the overlayer, indicated by snap in distance and attractive forces, is a protective overlayer in the biofilm former strain *ATCC35984.*

9.1.4 Conclusions of bacterial analysis

Overall, analysis of both strains of bacteria after incubation showed characteristics of bacterial adhesion in AFM data, with some variations between the two strains observed.

Both XPS and AFM were used to estimate the coverage of the sample. While each model is limited in the estimates, both showed overall the *ATCC35984* strain was more likely to form bacterial adhesion. The difference between the two models was the calculated residual layer, which not only differed in composition between the two models, but also indicated different results in determination if the residual layer covered the bacteria. The XPS model assumed the layer covered the bacteria whereas the AFM model indicated the layer may not cover the sample, and if it did there was only a thin layer that was possibly uneven.

Analysis of AFM force curves indicated the overlayer covered the entire sample, through similarities in measurements on and off the bacteria. Analysis of the overlayers measured between strains showed the difference in overlayer properties. The overlayer for the *ATCC35984* strain reduces the interactions with external influences that may damage the bacteria, which is seen in attractive force values. The overlayer also showed resistance to tip interactions through observed low retractive forces. The thicker organic layer measured on *NCTC13360* does not protect the bacteria from tip interactions as much, indicating thickness of overlayer is not a contributing factor to adhesion to the tip.

It should be noted that while these results are found for the two strains of bacteria, that it is not an overall model for all types of bacteria. For the model to be applied more generally, analysis of more strains of *S. epidermidis* is needed to compare to the results here, and potentially expanded through measurements on other strains of bacteria.

9.2 Limitations of experiments and analysis

9.2.1 XPS

The raw XPS data was used in several models to assess the samples in terms of layer thickness, bacterial coverage, biological model compounds and organic oxygen determination

Evaluation of coverage models

To evaluate data obtained by XPS, models were formed to identify the coverage of the sample, using two models, one estimated from the XPS model of bacteria, and one estimated from AFM images. Both models are limited in the calculating of bacterial coverage.

XPS model used the defining peak (Si, Ti, and Ag) to estimate the bacterial coverage. The limit of this model is the overestimation of bacterial coverage by neglecting the presence of the residual layer.

One of the main issues is the limit of the calculations of the residual layer. This is seen more through XPS modelled bacteria, where results of bacterial coverage above 90% have a higher tendency to estimate errors in the calculated residual layer. This is due to the effect of variable coverage and reproducibility of XPS peak fittings.

However, this is not the only source of error in calculations. Additionally, the XPS model is more prone to error in the model. This is due to the use of the defining peak as an estimate of coverage. While this is an indication of bacterial coverage, the model does not consider any other substances on the substrate supressing the signal. As seen in Chapter 5, the organic layer not from a source of bacteria can supress the silicon signal and AFM images in Chapter 5 confirm this is due to a patchy layer on the surface. Due to the size of bacteria compared to the thickness of these patches' AFM images do not show these features, however errors in the XPS model show this to still be the case.

The AFM model predicts a lower coverage compared to the XPS model, giving a more reasonable composition of residual layer. The AFM model is limited by the number of areas the average coverage was taken as well as the limited number of timed points used to estimate the coverage of other timed points. In reality, if AFM coverage was taken at more points, the model would show a variation in coverage at these points, which may account for changes in chemical composition between samples.

One of the main sources of error for both models was the P 2s signal, which showed a negative result when calculated for the residual layer for all samples. While it was discussed that this could be due to the error in the bacterial coverage or as a result of the bacteria covering the residual layer, there is also the issue with the detection limit of P 2s signal. This can be seen through the incubated samples where bacteria can be seen in AFM images within 4 hours, P 2s signal is only detected after 8 hours of incubation. In this case, using the pelleted bacteria as an approximation of P 2s signal resulting from bacteria is inaccurate, and rather significant number of bacteria must be bound to the surface before P 2s is detected. This was considered when analysing the P 2s peak in terms of determining if the bacterial layer is covered by a residual layer.

Both models predict the presence of a residual layer with the detection of C 1s that is not related to the calculated coverage of bacteria. The composition of this layer varies between

models. Both models predicted the presence of proteins in the model, with the amount of proteins varying between samples. The XPS model had a higher tendency to fail, however the N/C signal in the residual layer indicates the presence of proteins, with the lower O_{org}/C ratio, despite showing errors for organic oxygen, indicate the potential the layer is protein dominant with some samples showing traces of polysaccharide and hydrocarbons. The AFM model also showed the presence of proteins varying from sample to sample, with the detection of O_{org}/C and C285 also detected the sample contains a mixture of proteins, polysaccharides and hydrocarbons, which varies between each point, indicating the residual layer is in flux and the determination of its composition is limited to the area analysed.

Considering the concerns about P 2s peak in terms of a sample coverage model, the XPS model is assumed to overestimate the bacterial coverage, however as the signs of a residue layer and the negative value of P 2s in the AFM model, there is a possibility the overlayer covers the bacteria resulting in the P 2s signal being negative.

Two models proposed to estimate coverage give different results for coverage, with XPS giving higher coverages than AFM model. This is due to XPS model potentially overestimating the bacterial coverage, by neglecting the effect of the residue bound to the surface on the defining peak. In addition to this, in some cases layer erosion of the sputtercoated materials occurred leading to further errors in bacterial coverage calculations. AFM theoretically miscalculates the coverage, as it is calculated by average area on 10µm squares, which is insufficient to give an overall accurate estimate of coverage of the sample.

Generally, this led to the XPS model estimating the P 2s to be below zero. While this can imply that the bacteria are covered by the residual layer, it is more likely due to the overestimate of bacterial coverage. This can be seen through AFM samples, where there some which estimate the P 2s to be positive or close to zero, consistent with typical detection limits for the P 2s peak.

The composition of the residue varies from sample to sample. In general, the overall composition of the residual layer was found to be dominated by protein. The carbon 285eV peak for each sample varied, indicating the hydrocarbon content varied between samples. In some cases, there is a loose correlation between substrate coverage and hydrocarbon content, indicating the residual layer is not thick enough to supress the original contamination layer and potentially uneven.

In comparison to the TSB, the protein and sugar content differ from the residual layer found on incubated samples. This indicates the residual layer is not TSB alone. The difficulty lies in

determining the composition of the new layer, in terms of it the substances are TSB based or a result of bacteria excreting substances. The model also does not consider if there are preferential binding locations of compounds to the sample and how that affects bacterial adhesion.

Organic oxygen

The first model applied to any sample was determining the organic oxygen. This was to ensure that subsequent models applied to XPS samples were considering the signals of the organic compounds on the substrate and not the substrate itself. Several models were applied to substrates to determine the organic oxygen content of the samples.

The organic oxygen of samples that detected the silicon wafer was calculated using the Si 2p peak. The signal of the Si 2p can be divided into pure silicon and silicon oxide, which was assumed to be in the form of SiO_2. While other forms of silicon oxides exist, SiO_2 is the most common. The identification of the layer as SiO_2 was shown in the as received substrate which had an oxygen to silicon ratio of approximately 2:1. The use of the Si 2p is an accurate determination of inorganic oxygen, and as a result a reliable method to determine the organic oxygen content.

For all other samples, the initial assumption made for most samples, was the determination of the organic oxygen of the as received material. Although, the layer was assumed to consist of atmospheric hydrocarbons, the layer potentially had organic oxygen in. The indication of organic oxygen was seen through the C 1s peak fit where signals at 286.5eV and 288eV were detected, and in most cases no nitrogen. To calculate organic oxygen of these samples the oxygen was assumed to be in simple structures, allowing the carbon peak fit to be used to calculate the organic oxygen, such that the 286.5eV and 288eV signal are bound one oxygen each. While this is a reasonable assumption, there is a low potential error of misinterpreting the type of bonding in this sample and miscalculating the organic oxygen. The error here may come from 2 places (i) the accuracy of the C 1s peak fit and (ii) the assumption that although the 288eV signal relates to carboxyl groups, which contain 2 oxygen. The second oxygen, for these samples, is likely to be detected by another carbon and therefore each carbon in the 288eV signal only measures as only one oxygen.

For single layered samples, the subsequent organic oxygen calculation was based on the ratio of defining peak to oxygen being consistent. For glass and silver, this is a reasonable assumption, however mica consists of layers, which may result in different oxygen

detection depending on the layer of the sample was cleaved. The effect of this should be minimal and not affect the organic oxygen calculation too significantly.

For multilayer samples, the calculations are more complex, this leads to additional sources of error. The error from the organic oxygen estimation of previous layers contribute to the overall error organic oxygen calculation of the sample.

For all samples, the organic oxygen calculations are limited by the neglect of the possibility of X-O-C bonding, where X is the substrate material. The level of this type of bonding is limited by the amount of free binding sites on the sample. Further, the amount of organic layer calculated for most samples is higher than the amount of binding points, so this effect is minimal.

Layer thickness

Layer thickness calculations were used on as received substrates, autoclaved substrates and substrates incubated in TSB. These calculations could not be used for bacteria incubated sample due to the thickness of bacteria, 500nm, is larger than the thickness detection limit of XPS of 10nm and therefore considered sufficiently thick to prevent any signal passing through.

Theoretically, the layer thickness model may be used on bacterial samples, if the composition of the residual layer is determined. However, the composition of the residual layer is only estimated from model calculations and its limits have been discussed previously. Additionally, the source of the constituents of the layer are unknown, therefore the average density of the layer is unknown, and so the layer thickness cannot be used due a lack of density. Attempts to use the layer thickness calculations on the residual layer alone assumes the layer is of even thickness and do not consider the potential that the layer may or may not cover the substrate.

As both the substrate and overlayer consist of oxygen containing compounds, the organic oxygen calculation was used when estimating the composition of the overlayer for the layer thickness calculations.

The density of the organic layer is a contributing factor to the layer thickness calculations. For autoclaved and as received materials, the density was assumed to be similar to that of low density hydrocarbons. For as received materials, this is a reasonable assumption as the layer consists of hydrocarbons from the atmosphere. For autoclaved materials, this may be

a source of error. While it is assumed that the organic layer is atmospheric hydrocarbons, the conditions the samples are subjected to may lead to a denser layer and or a more complex organic layer. As XPS data showed the layer to be hydrocarbon like, the density is assumed to be like that of atmospheric hydrocarbons, as the density of the layer is difficult to determine.

For TSB samples, the density was calculated to be an average of density of all components of tryptic soy broth. Although this is a reasonable assumption, XPS data shows the organic layer does not consist of all the components of TSB in the same ratio as the liquid TSB. A more accurate method of determining the density would involve the calculation of the density of biological components on the surface and using the combined density in these calculations. This would then also include the density of the hydrocarbon layer in the resultant density, which was neglected in the layer calculations used due to the amount of hydrocarbon on the surface being unknown.

Additionally, in Chapter 5, the AFM images show that the organic layer is found in patches across the surface. As the organic layer was found to not be a consistently even layer, the use of layer thickness calculations on TSB incubated samples was found to give inaccurate results. However, the layer thickness was found to be of some use in estimating the coverage of these patches across the sample.

Overall, the layer thickness calculations are of some use to simple, even layered organic layers. However, for more complex samples discussed, these may need additional analysis to estimate the layer thickness more accurately and have been shown to be an inaccurate portrayal of layer thickness for TSB samples.

Biological models

Biological models were found in literature (van der Mei, 2000, Rouxhet, 2011) and a modified model of Rouxhet was applied to media samples. Media samples consist of a simple mixture of sugars and proteins, which makes the application of biological model easy, as they follow the model structure of an ideal protein.

Bacteria samples are more difficult, the compounds on the surface are more complex. While other models such as van der Mei (van der Mei, 2000) are within literature, these are limited. The structures on bacteria vary between bacterial types making these models limited. Additionally, the van der Mei model is limited by assuming the peptidoglycan layer is a combination of protein and sugar.

Another factor is the sensitivity of signals. For phosphorus detection, the use of P 2p is a stronger signal than the P 2s signal used in this research. The sensitivity of P 2p is higher than that of P 2s, however as the P 2p overlaps with the 2nd plasmon resonance of the Si 2p peak, the accuracy of the measuring the phosphorus signal from the P 2p peak is questioned. Attempts to separate the signals detected were considered, however the strength of the plasmon resonance peak in relation to the Si 2p peak is unknown, leading to the use of P 2s as a measure of phosphorus. The Si 2s peak also show signs of plasmon resonance peaks, however the overlap between the 2nd plasmon resonance of Si 2s and P 2s is smaller and identification of each peak is possible, allowing the phosphorus signal to be measured from the P 2s signal. The samples which do not have a silicon contribution to signal are limited, and to allow comparison between all samples, the P 2s signal was used to determine the phosphorus content of all samples. As the sensitivity of the P 2s signal is different to that of the P 2p normally used, the atomic percent of other signals will vary in relation to this and affect the calculations of components calculated in the biological model.

Organic oxygen is also a consideration for the sensitivity of signals. As the organic oxygen is calculated from estimations of oxygen content detected from the substrate, the calculation is subject to error and may lead also lead to errors in estimating the biological composition of the samples.

One of the theoretical uses for the biological model was to apply these calculations to the model of bacterial coverage, to estimate the composition of the residual layer. This overall was not feasible due to the limits of both the biological model and the estimation of bacterial coverage.

Overall, the biological models are limited in determining the composition of the sample, leading to errors for calculation on bacterial samples. This led to the use of N/C and O_{org}/C to indicate the type of bonding detected on the surface using ideal models, but not to calculate the composition of the surface through these calculations. While the estimation of bacterial coverage and biological model may be improved, this requires additional work, which was not possible in the timeframe for this research. Additionally, for the biological model to work effectively, the signals need to be corrected for the bacteria used.

Alternate ways to detect the bacterial compounds can be used to confirm the composition of the surface such as FT-IR, Raman spectroscopy and mass spectrometry. Use of these

methods would support and confirm information gained through XPS and support theories formed using models.

9.2.2 AFM

To analyse force curves, the spring constant must first be calculated. There are several methods to calculate the spring constant each with its own limitations. The two methods used to determine the spring constant were Sader(Gibson et al., 2005) and thermal noise(Butt & Jaschke, 1995) Sader is limited by the degree of accuracy the measurements of the size of tips (Burnham et al., 2002). The average values of tip measurements were taken from NT-MDT website, which includes the accuracy of the tips. The thermo method is limited by the residual noise detected by the instrument. The accuracy of the spring constant, k, relates to the accuracy of adhesion forces measured in Chapters 4-8.

Overlap of peaks and non-Gaussian distributions made determining the nature of the binding complex. While the overlap of peaks was to be expected, the large range of overlaps indicate the complexities of system and limits the amount of information gained about the sample.

One of the ways AFM force curves have been analysed is through the shape of the curve. Due to the number of force curves measured and variations in force curves, this method of analysis was not explored.

One of the issues with working with live cells in AFM is the dynamic nature of the bacterial attachment. Literature explores methods of fixing the bacteria which are reviewed in Chapter 2. One of the methods of bacterial attachment explored was the effect of drying the bacteria (Meyer et al., 2010). For this work presented here, the aim was to analyse the bacteria without fixing, so measures were taken to prevent the samples drying when analysed in air. However, exposure to air over time will inevitably dry the sample, which resulted in a change in force curve analysis and is considered when analysing the sample. One of the ways bacterial drying can be prevented is to probe the samples in liquid mode. While attempts were made to analyse samples in liquid, additional problems arose and was not pursued further. One of the issues with liquid mode included the malleable nature of the bacteria.

An issue with working with soft samples, such as bacteria, in AFM is the potential of contaminating the tip. While running experiments, it is impossible to know if the tip is contaminated and changing the tip between scans is unfeasible. The issue with tip contamination is the interactions between the tip and sample give different results, limiting the reliability of the results. When analysing literature, no methods were found that could

fully overcome the issue of tip contamination. To prevent tip contamination affecting sample analysis, samples were run in Semi contact mode and shaken through the use of a high speed scan away from the sample after each scan, to remove any excess organic layer bound to the tip.

9.2.3 Experimental technique.

As well as limitations within the analytical techniques chosen, there is the additional limitations observed with experimental techniques. These include subsampling and variable coverage. Issues with subsampling and variable coverage in XPS samples were discussed in Chapters 5, 6 and 8. Subsampling and variable coverage cause variations between XPS samples depending on the distribution of organic matter across the substrate, that cannot be explained as part of organic layer growth. To overcome issues with variable coverage, analysis of multiple points on the sample would have confirmed outcomes in XPS analysis and analysis of multiple samples for each data set would reduce the effects of subsampling, however, due to time constraints this was not possible. Analysis of only one sample for each data point gives an overview of the sample composition and the potential uses of XPS data in forming biological models. Issues with variable coverage also effect the results of AFM samples, which can be overcome by analysing more points on the sample. However, the effects of sample drying must be taken into account, and therefore a better approach would be to analyse multiple samples for each AFM data set. An alternate approach is to use liquid AFM to overcome the effect of drying. However only short periods of time for analysis are feasible, to prevent the effect of bacterial growth affecting the results.

9.3 Conclusions and Future work

This work shows the analysis of 2 strains *of S. epidermidis* (ATCC35984 and NCTC 13360) by XPS and AFM on different substrates. Analysis of samples at points which have a potential influence on the chemical and adhesion involved in bacterial adhesion to a surface was used to model what is potentially happening on incubation on the surface. This included analysing bacterial pellet, analysing substrates after incubating with media and analysing substrates before and after autoclaving. The two strains used in this study were chosen to reflect the differences between a biofilm and non-biofilm former, to identify changes in adhesion properties and apply models to both systems.

Analysis of AFM images showed the change in topography between each treatment and the variation in coverage between samples and bacterial strains. Force curve analysis showed differences in measurements across samples, including between bacteria. Differences

between the bacteria was assumed to be due to ATCC35984 having a protective organic layer as a sign of early biofilm formation, whereas NCTC13360 does not, leading to lower approach tip measurements (snap in and attractive forces) on ATCC35984. Analysis of point on and off a bacteria suggest that organic layer is an even layer on both bacteria, which varied between substrates. Comparisons to media suggest that the overlayer was not TSB. Differences between substrates for both bacteria suggest there is an additional influence of substrate material in bacterial adhesion, which may be influenced by TSB or bacterial excretions, with the latter being more likely, as the layer on non-bacterial points was not TSB like.

Analysis of the organic layer using XPS showed differences composition across each treatment and substrate. This suggests there is some material-dependant physiochemical effect on the nature of bonding and adhesion of bacteria. Analysis of incubated spectra showed peaks of the original substrate, which was used to estimate bacterial coverage. Differences between the incubated bacterial sample and the pelleted bacteria indicated the presence of another source of organic substance, named residue in this research. Using XPS and AFM data to estimate the bacterial coverage of the sample, which was then used in models for determining the composition of the additional organic substance as well as indicating if the layer covers the bacteria or not. Analysis of this layer was found to be different to TSB and in most cases found to potentially cover the bacteria.

While it is discussed that the differences between strains are influenced by the early stages of biofilm adhesion, there is insufficient data to indicate this is the case for all *S. epidermidis* strains and other bacterial strains. The models are also limited in what each experimental technique indicate about the surface. However, these models show how both XPS and AFM can be used in bacterial analysis as well as forming a basic model that can be developed by increasing the number of strains, types of bacteria and the use of other complementary techniques such as mass spectrometry to determine the organic compounds or to use AFM-IR instruments to indicate the type of compounds the tip is interacting with. There are other potential experiments that could be carried out to develop the models and theories proposed here, these include:-

- Analysing TSB as a function of time on silicon
- Analyse other substrates included in this work as a function of incubated with TSB and bacteria over time
- Using an alternate technique of determining coverage such as SEM
- Analysing the effect of each TSB component on substrates

- Analysing the residual layer without the presence of bacteria
- Analyse longer time periods of growth to confirm biofilm formation
- Analyse other substrate materials

References

Al-Mailem, D. M., Kansour, M. K., & Radwan, S. S. (2014). Hydrocarbonoclastic biofilms based on sewage microorganisms and their application in hydrocarbon removal in liquid wastes. *Canadian Journal of Microbiology, 60*(7), 477-486. doi:10.1139/cjm-2014-0214

Antoci, V., Jr., Adams, C. S., Parvizi, J., Davidson, H. M., Composto, R. J., Freeman, T. A., . . . Hickok, N. J. (2008). The inhibition of Staphylococcus epidermidis biofilm formation by vancomycin-modified titanium alloy and implications for the treatment of periprosthetic infection. *Biomaterials, 29*(35), 4684-4690. doi:10.1016/j.biomaterials.2008.08.016

Arciola, C. R., Campoccia, D., Speziale, P., Montanaro, L., & Costerton, J. W. (2012). Biofilm formation in Staphylococcus implant infections. A review of molecular mechanisms and implications for biofilm-resistant materials. *Biomaterials, 33*(26), 5967-5982. doi:10.1016/j.biomaterials.2012.05.031

Auerbach, I. D., Sorensen, C., H.G., H., & Holden, P. A. (2000). Physical Morphology and Surface Properties of Unsaturated Pseudomonas putida Biofilm. *Journal of bacteriology, 182*(13), 3809-3815.

Beamson, G., & Briggs, D. (1992). *High resolution XPS of organic polymers*. Chitchester, West Sussex: John Whiley and sons ltd.

Bernstein, R., Freger, V., Lee, J. H., Kim, Y. G., Lee, J., & Herzberg, M. (2014). 'Should I stay or should I go?' Bacterial attachment vs biofilm formation on surface-modified membranes. *Biofouling, 30*(3), 367-376. doi:10.1080/08927014.2013.876011

Binnig, G., Quate, C. F., & Gerber, C. (1986). Atomic force microscope. *Physical review letters, 56*(9), 930-934.

Biosafety in microbiological and biomedical laboratories.

Bjarnsholt, T. (2013). The role of bacterial biofilms in chronic infections. *APMIS Suppl, 121*(136), 1-51. doi:10.1111/apm.12099

Braem, A., Van Mellaert, L., Mattheys, T., Hofmans, D., De Waelheyns, E., Geris, L., . . . Vleugels, J. (2014). Staphylococcal biofilm growth on smooth and porous titanium coatings for biomedical applications. *J Biomed Mater Res A, 102*(1), 215-224. doi:10.1002/jbm.a.34688

Briggs, B., & Grant, J. T. (2003). XPS: basic principles, spectral features and Qualitative analysis. In B. Briggs & J. T. Grant (Eds.), *Surface analysis by Auger and X-Ray Photoelectron Spectroscopy* (pp. 31-56). UK: IM Publications and SurfaceSpectra limited.

Burnham, N. A., chen, X., Hodges, C. S., Matei, G. A., Thorseson, E. J., Roberts, C. J., . . . Tendler, S. J. B. (2002). Comparision of calibration methods for atomic force microscopy cantilevers. *Nanotechnology, 14*(1), 1-6.

Butt, H., & Jaschke, M. (1995). Calculation of thermal noise in atomic force microscpy. *Nanotechnology, 6*(1), 1-7.

Campoccia, D., Montanaro, L., & Arciola, C. R. (2013). A review of the biomaterials technologies for infection-resistant surfaces. *Biomaterials, 34*(34), 8533-8554. doi:10.1016/j.biomaterials.2013.07.089

Carvalho, I., Henriques, M., Oliveira, J. C., Almeida Alves, C. F., Piedade, A. P., & Carvalho, S. (2013). Influence of surface features on the adhesion of Staphylococcus epidermidis to Ag-TiCN thin films. *Sci Technol Adv Mater, 14*(3), 035009. doi:10.1088/1468-6996/14/3/035009

. Casa XPS v2.3.17. (2015): Casa Software Ltd.

Cerca, N., Pier, G. B., Vilanova, M., Oliveira, R., & Azeredo, J. (2005). Quantitative analysis of adhesion and biofilm formation on hydrophilic and hydrophobic surfaces of clinical

isolates of Staphylococcus epidermidis. *Res Microbiol, 156*(4), 506-514. doi:10.1016/j.resmic.2005.01.007
Chen, M., Yu, Q., & Sun, H. (2013). Novel strategies for the prevention and treatment of biofilm related infections. *Int J Mol Sci, 14*(9), 18488-18501. doi:10.3390/ijms140918488
Chung, P. Y., & Toh, Y. S. (2014). Anti-biofilm agents: recent breakthrough against multi-drug resistant Staphylococcus aureus. *Pathog Dis, 70*(3), 231-239. doi:10.1111/2049-632X.12141
De Poel, W., Pintea, S., Drnec, J., Carla, F., & Felicic, R. (2014). Muscovite Mica: Flatter than a pancake. *Surface Science, 619*, 19-24.
Desrousseaux, C., Sautou, V., Descamps, S., & Traore, O. (2013). Modification of the surfaces of medical devices to prevent microbial adhesion and biofilm formation. *J Hosp Infect, 85*(2), 87-93. doi:10.1016/j.jhin.2013.06.015
Dickschat, J. S. (2010). Quorum sensing and bacterial biofilms. *Nat Prod Rep, 27*(3), 343-369. doi:10.1039/b804469b
Dufrene, Y. (2001). Application of atomic force microscopy to microbial surfaces:

from reconstituted cell surface layers to living cells. *Micron*, 153-165.
Dufrene, Y. F. (2014). Atomic Force Microscopy in Microbiology: New Structural and Functional Insights into the Microbial Cell Surface. *Mbio, 5*(4). doi:ARTN e01363-14

10.1128/mBio.01363-14
Dufrene, Y. F. (2015). Sticky microbes: forces in microbial cell adhesion. *Trends Microbiol, 23*(6), 376-382. doi:10.1016/j.tim.2015.01.011
England, P. H. (2016). Retrieved from https://www.phe-culturecollections.org.uk/products/bacteria/detail.jsp?refId=NCTC%2013360&collection=nctc
Ercan, B., Taylor, E., Alpaslan, E., & Webster, T. J. (2011). Diameter of titanium nanotubes influences anti-bacterial efficacy. *Nanotechnology, 22*(29), 295102. doi:10.1088/0957-4484/22/29/295102
Fairley, N. (2016). Casa XPS (Version 2.3.17).
Flemming, H. C., & Wingender, J. (2010). The biofilm matrix. *Nat Rev Microbiol, 8*(9), 623-633. doi:10.1038/nrmicro2415
Fournier, B., & Philpott, D. J. (2005). Recognition of Staphylococcus aureus by the innate immune system. *Clinical Microbiology Review, 18*(3), 521-540. doi:10.1128/CMR.18.3.521-540.2005
Friedrichs, J., Zieris, A., Prokoph, S., & Werner, C. (2012). Quantifying the effect of covalently immobilized enzymes on biofilm formation by atomic force microscopy-based single-cell force spectroscopy. *Macromol Rapid Commun, 33*(17), 1453-1458. doi:10.1002/marc.201200359
Germano, F., Bramanti, E., Arcuri, C., Cecchetti, F., & Cicciu, M. (2013). Atomic force microscopy of bacteria from periodontal subgingival biofilm: Preliminary study results. *Eur J Dent, 7*(2), 152-158. doi:10.4103/1305-7456.110155
Gibson, C. T., Smith, D. A., & Roberts, C. J. (2005). Calibration of silicon atomic force microscope cantilevers. *Nanotechnology, 16*(2), 234-238.
Gomes, F., Teixeira, P., & Oliveira, R. (2014). Mini-review: Staphylococcus epidermidis as the most frequent cause of nosocomial infections: old and new fighting strategies. *Biofouling, 30*(2), 131-141. doi:10.1080/08927014.2013.848858
Gries, W. H. (1996). A universal predictive equation for the inelastic mean free pathlengths of x-ray photoelectrons and Auger electrons. *Surface and Interface Analysis, 24*(1), 38-50.

Halder, P., Nasabi, M., Lopez, F. J., Jayasuriya, N., Bhattacharya, S., Deighton, M., . . . Bhuiyan, M. A. (2013). A novel approach to determine the efficacy of patterned surfaces for biofouling control in relation to its microfluidic environment. *Biofouling, 29*(6), 697-713. doi:10.1080/08927014.2013.800192

Harimawan, A., Zhong, S., Lim, C. T., & Ting, Y. P. (2013). Adhesion of B. subtilis spores and vegetative cells onto stainless steel--DLVO theories and AFM spectroscopy. *J Colloid Interface Sci, 405*, 233-241. doi:10.1016/j.jcis.2013.05.031

Hu, Y., Ulstrup, J., Zhang, J., Molin, S., & Dupres, V. (2011). Adhesive properties of Staphylococcus epidermidis probed by atomic force microscopy. *Phys Chem Chem Phys, 13*(21), 9995-10003. doi:10.1039/c0cp02800b

Ista, L. K., Mendez, S., Balamurugan, S. S., Balamurugan, S., Rama Rao, V. G., & Lopez, G. P. (2009). Smart Surfaces for the Control of Bacterial Attachment and Biofilm Accumulation. In T. Provder & J. Baghdachi (Eds.), *Smart Coatings Ii* (Vol. 1002, pp. 95-110).

Ivanov, I. E., Boyd, C. D., Newell, P. D., Schwartz, M. E., Turnbull, L., Johnson, M. S., . . . Camesano, T. A. (2012). Atomic force and super-resolution microscopy support a role for LapA as a cell-surface biofilm adhesin of Pseudomonas fluorescens. *Res Microbiol, 163*(9-10), 685-691. doi:10.1016/j.resmic.2012.10.001

Ivanova, E. P., Truong, V. K., Webb, H. K., Baulin, V. A., Wang, J. Y., Mohammodi, N., . . . Crawford, R. J. (2011). Differential attraction and repulsion of Staphylococcus aureus and Pseudomonas aeruginosa on molecularly smooth titanium films. *Sci Rep, 1*, 165. doi:10.1038/srep00165

Jena, P., Mohanty, S., Mallick, R., Jacob, B., & Sonawane, A. (2012). Toxicity and antibacterial assessment of chitosan-coated silver nanoparticles on human pathogens and macrophage cells. *Int J Nanomedicine, 7*, 1805-1818. doi:10.2147/IJN.S28077

Kalia, V. C. (2013). Quorum sensing inhibitors: an overview. *Biotechnol Adv, 31*(2), 224-245. doi:10.1016/j.biotechadv.2012.10.004

Kan, Y., Tan, Q., Wu, G., Si, W., & Chen, Y. (2015). Study of DNA adsorption on mica surfaces using a surface force apparatus. *Sci Rep, 5*, 8442. doi:10.1038/srep08442

Khalil, F., Franzmann, E., Ramcke, J., Dakischew, O., Lips, K. S., Reinhardt, A., . . . Maison, W. (2014). Biomimetic PEG-catecholates for stabile antifouling coatings on metal surfaces: applications on TiO2 and stainless steel. *Colloids Surf B Biointerfaces, 117*, 185-192. doi:10.1016/j.colsurfb.2014.02.022

Kim, M. T. (1996). Influences of substrates on the elastic reaction of films for microindentation tests. *thin solid films, 283*(1-2), 12-16.

Liu, Z. H., & Brown, N. M. D. (1998). XPS characterization of mica surfaces processed using a radio frequency(rf) argon plasma. *Journal of Physics D: Applied Physics, 31*(15), 1771-1781.

Ma, Y., Chen, M., Jones, J. E., Ritts, A. C., Yu, Q., & Sun, H. (2012). Inhibition of Staphylococcus epidermidis biofilm by trimethylsilane plasma coating. *Antimicrob Agents Chemother, 56*(11), 5923-5937. doi:10.1128/AAC.01739-12

McArthur, S. L., Mishra, G., & Easton, C. D. (2014). Applications of XPS in Biology and Biointerface Analysis *Surface Analysis and techniques in Biology* (pp. 9-36).

Méndez-Vilas, A., Gallardo-Moreno, A. M., González-Martín, M. L., Calzado-Montero, R., Nuevo, M. J., Bruque, J. M., & Pérez-Giraldo, C. (2004). Surface characterisation of two strains of Staphylococcus epidermidis with different slime-production by AFM. *Applied Surface Science, 238*(1-4), 18-23. doi:10.1016/j.apsusc.2004.05.183

Meyer, R., Zhou, X., Tang, L., Arpanaei, A., Kingshott, P., & Besenbacher, F. (2010). Immobilisation of living bacteria for AFM imaging under physiological conditions. *Ultramicroscopy, 110*(11), 1349-1357. doi:10.1016/j.ultramic.2010.06.010

Missirlis, Y. F., & Katsikogianni, M. (2007). Theoretical and experimental approaches of bacteria-biomaterial interactions. *Materialwissenschaft Und Werkstofftechnik, 38*(12), 983-994. doi:10.1002/mawe.200700240

Mitik-Dineva, N., Wang, J., Truong, V. K., Stoddart, P., Malherbe, F., Crawford, R. J., & Ivanova, E. P. (2009). Escherichia coli, Pseudomonas aeruginosa, and Staphylococcus aureus attachment patterns on glass surfaces with nanoscale roughness. *Curr Microbiol, 58*(3), 268-273. doi:10.1007/s00284-008-9320-8

Moreno-Herrero, F., Colchero, J., Gomez-Herrero, J., & Baro, A. M. (2004). Atomic force microscopy contact, tapping, and jumping modes for imaging biological samples in liquids. *Phys Rev E Stat Nonlin Soft Matter Phys, 69*(3 Pt 1), 031915. doi:10.1103/PhysRevE.69.031915

Muller, C., & Ziegler, C. (2013). The scanning force microscope in bacterial cell investigations. *Physica Status Solidi a-Applications and Materials Science, 210*(5), 846-852. doi:10.1002/pssa.201200768

Müller, R., Ruhl, S., Hiller, K. A., Schmalz, G., & Schweikl, H. (2007). Adhesion of eukaryotic cells and Staphylococcus aureus to silicon model surfaces. *Journal of Biomedical Materials Research Part A, 84*(3), 817-826.

Myszka, K., & Czaczyk, K. (2011). Bacterial Biofilms on Food Contact Surfaces - a Review. *Polish Journal of Food and Nutrition Sciences, 61*(3), 173-180. doi:10.2478/v10222-011-0018-4

Naz, I., Saroj, D. P., Mumtaz, S., Ali, N., & Ahmed, S. (2015). Assessment of biological trickling filter systems with various packing materials for improved wastewater treatment. *Environmental Technology, 36*(4), 424-434. doi:10.1080/09593330.2014.951400

Neumann, A. W., Good, R. J., Hope, C. J., & Sejpal, M. (1974). An equation-of-state approach to determine surface tensions of low-energy solids from contact angles. *J Colloid Interface Sci, 49*(2), 291-304.

Oliveira, C., Escobar Galindo, R., Palacio, C., Calderon, S. V., Almeida, B. G., Henriques, M., . . . Carvalho, S. (2011). Surface characterization of Ti-Si-C-ON coatings for orthopedic devices: XPS and Raman spectroscopy. *Solid State Sciences, 13*(1), 95-100. doi:10.1016/j.solidstatesciences.2010.10.015

Otto, M. (2009). Staphylococcus epidermidis--the 'accidental' pathogen. *Nat Rev Microbiol, 7*(8), 555-567. doi:10.1038/nrmicro2182

Ploszaj-Pyrek, J., Talik, E., & Piotrowska-Seget, Z. (2014). Studies of the Bacterial Surfaces by XPS and SEM Methods. *Acta Physica Polonica A, 125*(4), 929-931.

Powell, C. J., & Jablonski, A. (2011). NIST Electron Effective Attenuation Length Database (Version Version 1.3) [SRD 82]. Gaithersburg, MD National Institute of Standards and Technology.

Preedy, E., Perni, S., Nipic, D., Bohinc, K., & Prokopovich, P. (2014). Surface roughness mediated adhesion forces between borosilicate glass and gram-positive bacteria. *Langmuir, 30*(31), 9466-9476. doi:10.1021/la501711t

Qin, Z., Zhang, J., Hu, Y., Chi, Q., Mortensen, N. P., Qu, D., . . . Ulstrup, J. (2009). Organic compounds inhibiting *S. epidermidis* adhesion and biofilm formation. *Ultramicroscopy, 109*(8), 881-888. doi:10.1016/j.ultramic.2009.03.040

Robichon, D., Girard, J. C., Cenatiempo, Y., & Cavellier, J. F. (1999). Atomic force microscopy imaging of dried or living bacteria. *C R Acad Sci III, 322*(8), 687-693.

Rodriguez-Cano, A., Cintas, P., Fernandez-Calderon, M. C., Pacha-Olivenza, M. A., Crespo, L., Saldana, L., . . . Babiano, R. (2013). Controlled silanization-amination reactions on the Ti6Al4V surface for biomedical applications. *Colloids Surf B Biointerfaces, 106*, 248-257. doi:10.1016/j.colsurfb.2013.01.034

Romaniuk, J. A. H., & Cegelski, L. (2015). Bacterial cell wall composition and the influence of antibiotics by cell-wall and whole-cell NMR. *philosophical Transactions B, 370*(1679). doi:https://doi.org/10.1098/rstb.2015.0024

Rouxhet, P. G., & Genet, M. J. (2011). XPS analysis of bio-organic systems. *Surface and Interface Analysis, 43*(12), 1453-1470. doi:10.1002/sia.3831

Sadovskaya, I., Vinogradov, E., Li, J., & Jabbouri, S. (2004). Structural elucidation of the extracellular and cell-wall teichoic acids of Staphylococcus epidermidis RP62A, a reference biofilm-positive strain. *Carbohydr Res, 339*(8), 1467-1473. doi:10.1016/j.carres.2004.03.017

Sancet, M. P., Hanke, M., Wang, Z., Bauer, S., Azucena, C., Arslan, H. K., . . . Rosenhahn, A. (2013). Surface anchored metal-organic frameworks as stimulus responsive antifouling coatings. *Biointerphases, 8*(1), 29. doi:10.1186/1559-4106-8-29

Scofield, J. H. (1976). Hartree-Slater subshell photoionization cross-sections at 1254 and 1487 eV. *Journal of Electron Spectroscopy and Related Phenomena, 8*(2), 129-137.

Sharma, G., Rao, S., Bansal, A., Dang, S., Gupta, S., & Gabrani, R. (2014). Pseudomonas aeruginosa biofilm: potential therapeutic targets. *Biologicals, 42*(1), 1-7. doi:10.1016/j.biologicals.2013.11.001

Shirley, D. A. (1972). High-Resolution X-Ray Photoemission Spectrum of the Valence Bands of Gold. *Physical Review B, 5*(12), 4709-4714.

Smith, G. C. (2005). Evaluation of a simple correction for the hydrocarbon contamination layer in quantitative surface analysis by XPS. *Journal of Electron Spectroscopy and Related Phenomena, 148*(1), 21-28. doi:10.1016/j.elspec.2005.02.004

Supernak, M., & Świeczko-Żurek, B. (2010). Reactions on the Surface of the Implant Under the Influence of Biofilm. *Advances in Materials Sciences, 10*(4). doi:10.2478/v10077-010-0011-3

Tan, S. Y., Chew, S. C., Tan, S. Y., Givskov, M., & Yang, L. (2014). Emerging frontiers in detection and control of bacterial biofilms. *Curr Opin Biotechnol, 26*, 1-6. doi:10.1016/j.copbio.2013.08.002

Tanuma, S. (2003). Electron attenuation lengths *XPS: basic principles, spectral features and Qualitative analysis Surface analysis by Auger and X-Ray Photoelectron Spectroscopy* UK: IM Publications and SurfaceSpectra limited.

Taraszkiewicz, A., Fila, G., Grinholc, M., & Nakonieczna, J. (2013). Innovative strategies to overcome biofilm resistance. *Biomed Res Int, 2013*, 150653. doi:10.1155/2013/150653

Todar, K. (2008). Todar's online Textbook of Baccteriology. Retrieved from www.textbookofbacteriology.net

Trotsenko, O., Koestner, R., Roiter, Y., Tokarev, A., & Minko, S. (2016). Probing rough composite surfaces with atomic force microscopy: Nafion ionomer in fuel cell electrodes. *Polymer, 102*, 396-403.

Truong, V. K., Rundell, S., Lapovok, R., Estrin, Y., Wang, J. Y., Berndt, C. C., . . . Ivanova, E. P. (2009). Effect of ultrafine-grained titanium surfaces on adhesion of bacteria. *Appl Microbiol Biotechnol, 83*(5), 925-937. doi:10.1007/s00253-009-1944-5

Vadillo-Rodriguez, V., Busscher, H. J., Norde, W., De Vries, J., Dijkstra, R. J., Stokroos, I., & van Der Mei, H. C. (2004). Comparison of atomic force microscopy interaction forces between bacteria and silicon nitride substrata for three commonly used immobilization methods. *Appl Environ Microbiol, 70*(9), 5441-5446. doi:10.1128/AEM.70.9.5441-5446.2004

Van der Marel, C., Verheijen, M. A., Tamminga, Y., Pijnenburg, R. H. W., Tombros, N., & Cubaynes, F. (2004). Thickness and composition of ultrathin SiO2 layers on Si. *J. Vac. Sci. Technol*, 1572 - 1578.

van der Mei, H. C., de Vries, J., & Busscher, H. J. (2000). X-Ray Photoelectron spectroscopy for the study of microbial cell surfaces. *Surface science reports*.

van der Mei, H. C., van de Belt-Gritter, B., Reid, G., Bialkowska-Hobrzanska, H., & Busscher, H. J. (1997). Adhesion of coagulase-negative staphylococci grouped according to physico-chemical surface properties. *Microbiology, 143 (Pt 12)*, 3861-3870. doi:10.1099/00221287-143-12-3861

Wright, C. J., Burns, L. H., Jack, A. A., Back, C. R., Dutton, L. C., Nobbs, A. H., . . . Jenkinson, H. F. (2013). Microbial interactions in building of communities. *Mol Oral Microbiol, 28*(2), 83-101. doi:10.1111/omi.12012

Wright, C. J., Shah, M. K., Powell, L. C., & Armstrong, I. (2010). Application of AFM from microbial cell to biofilm. *Scanning, 32*(3), 134-149. doi:10.1002/sca.20193

Zenkiewicz, M. (2007). Methods for the calculation of surface free energy of solids. *Journal of Achievements in materials and Manufacturing Engineering, 24*(1), 137-145.

Appendix

Appendix A XPS spectrum

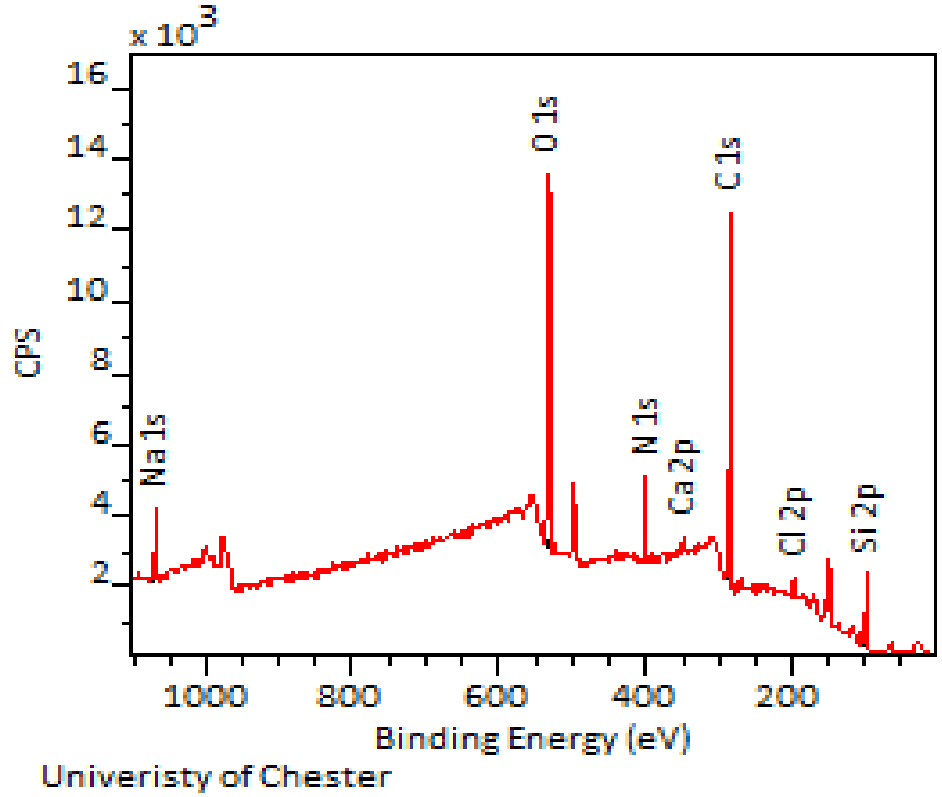

Figure A.1 Survey spectrum of silicon incubated with tryptic soy broth after 1 hour.

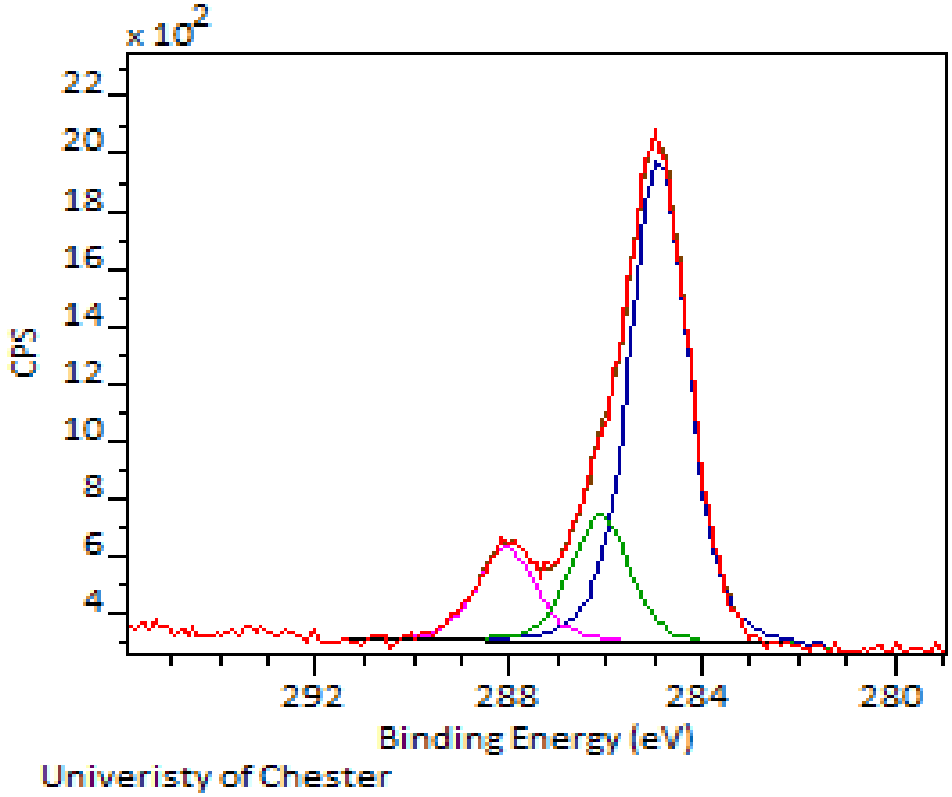

Figure A.2 C 1s peak fit of silicon incubated with tryptic soy broth after 1 hour.

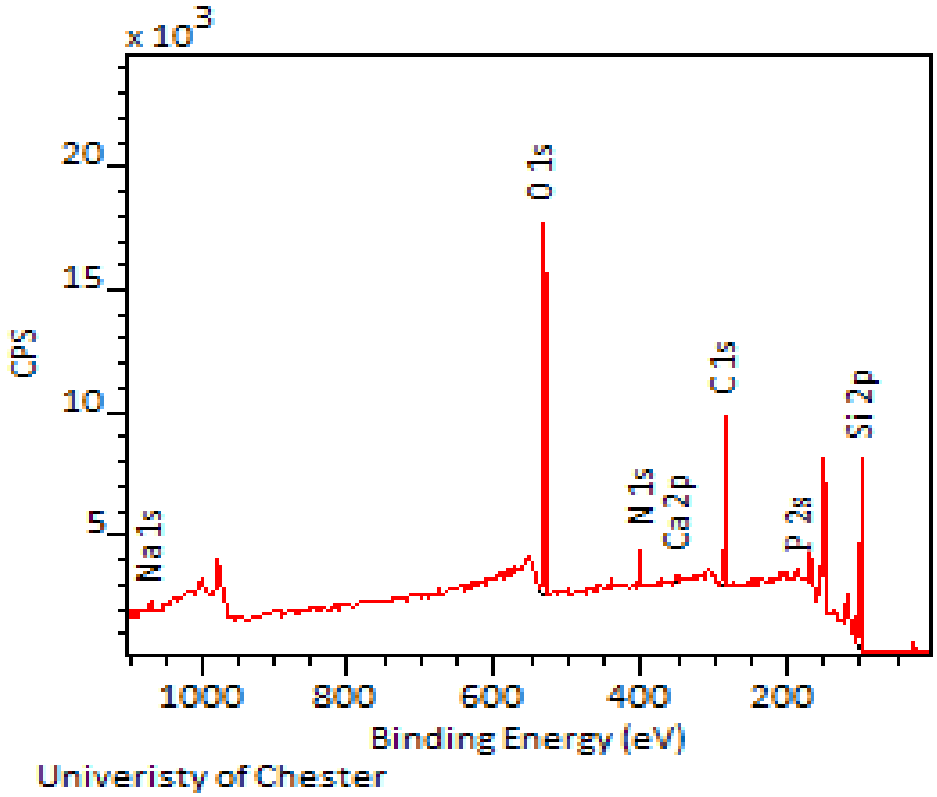

Figure A.3 Survey spectrum of silicon incubated with tryptic soy broth after 2 hours.

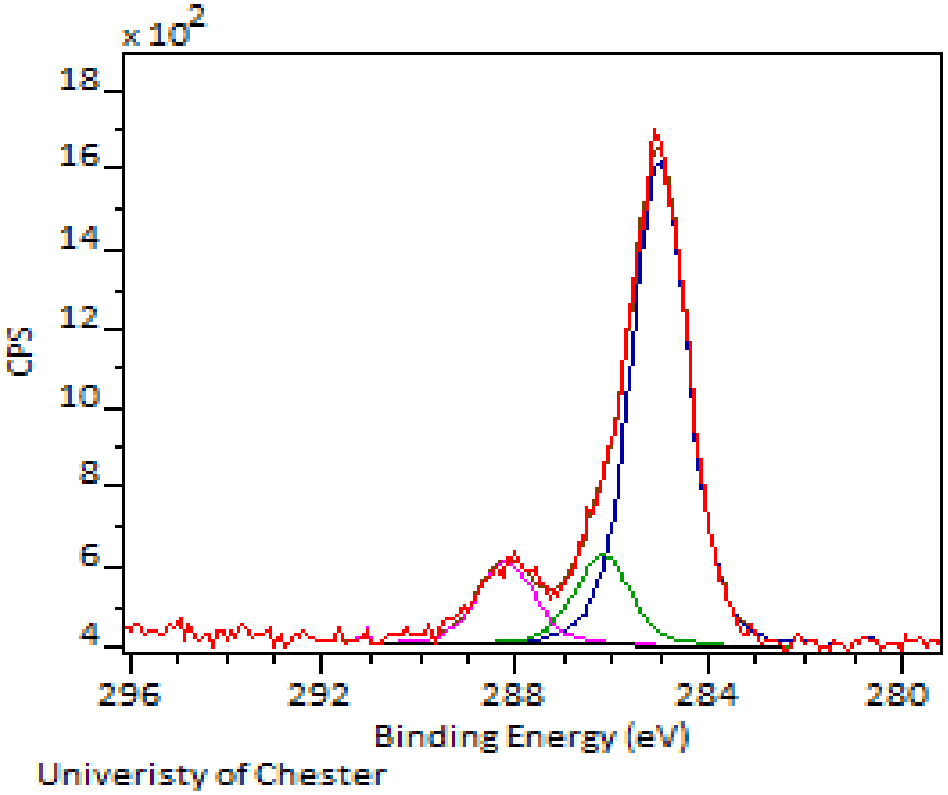

Figure A.4 C 1s peak fit of silicon incubated with tryptic soy broth after 2 hours.

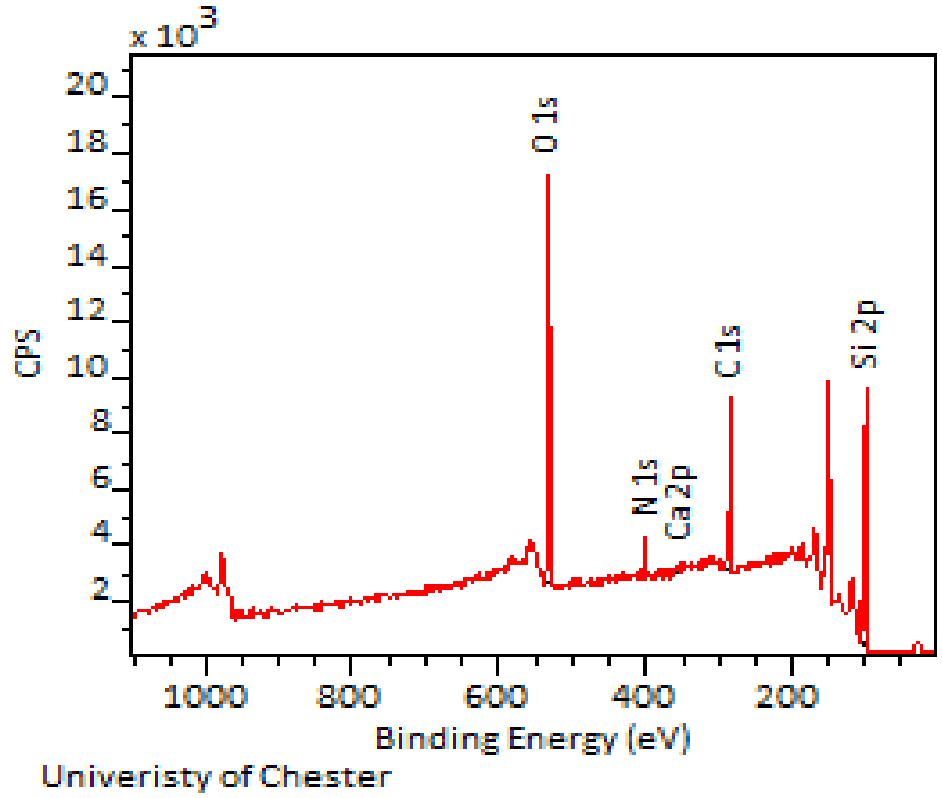

Figure A.5 Survey spectrum of silicon incubated with tryptic soy broth after 3 hours.

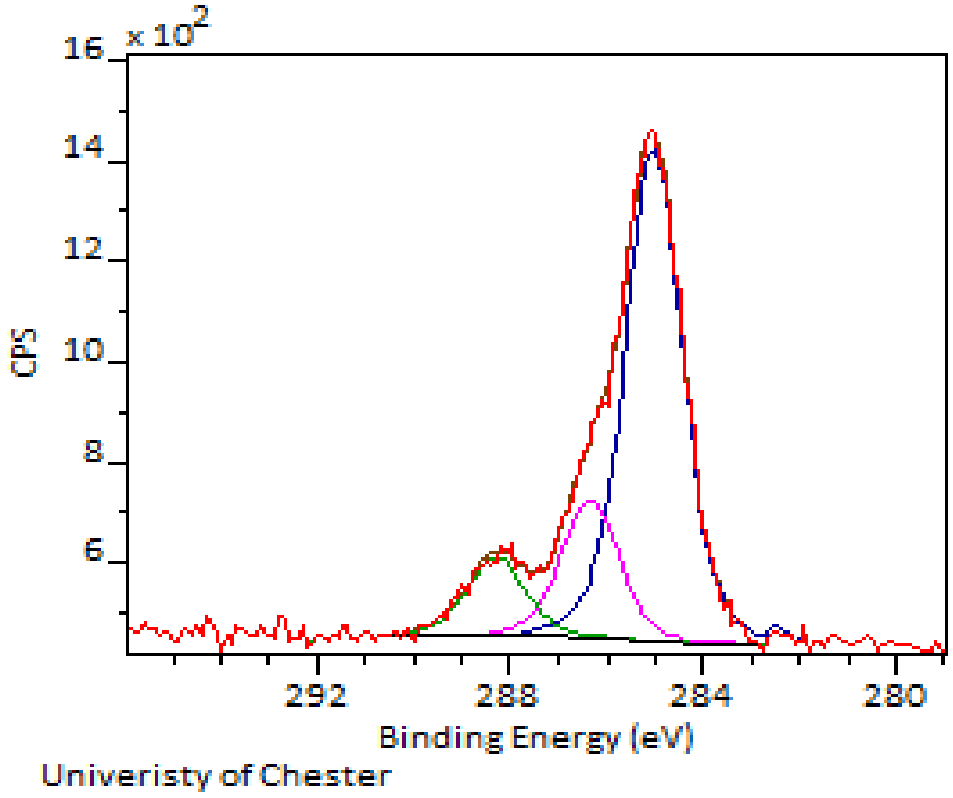

Figure A.6 C 1s peak fit of silicon incubated with tryptic soy broth after 3 hours.

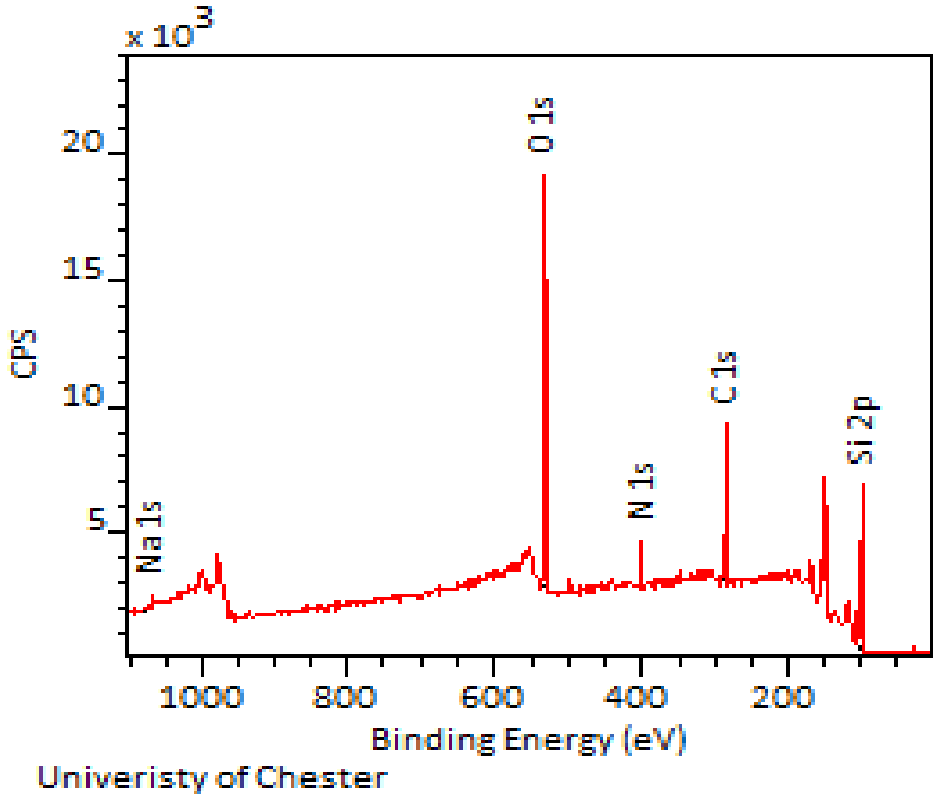

Figure A.7 Survey spectrum of silicon incubated with tryptic soy broth after 5 hours.

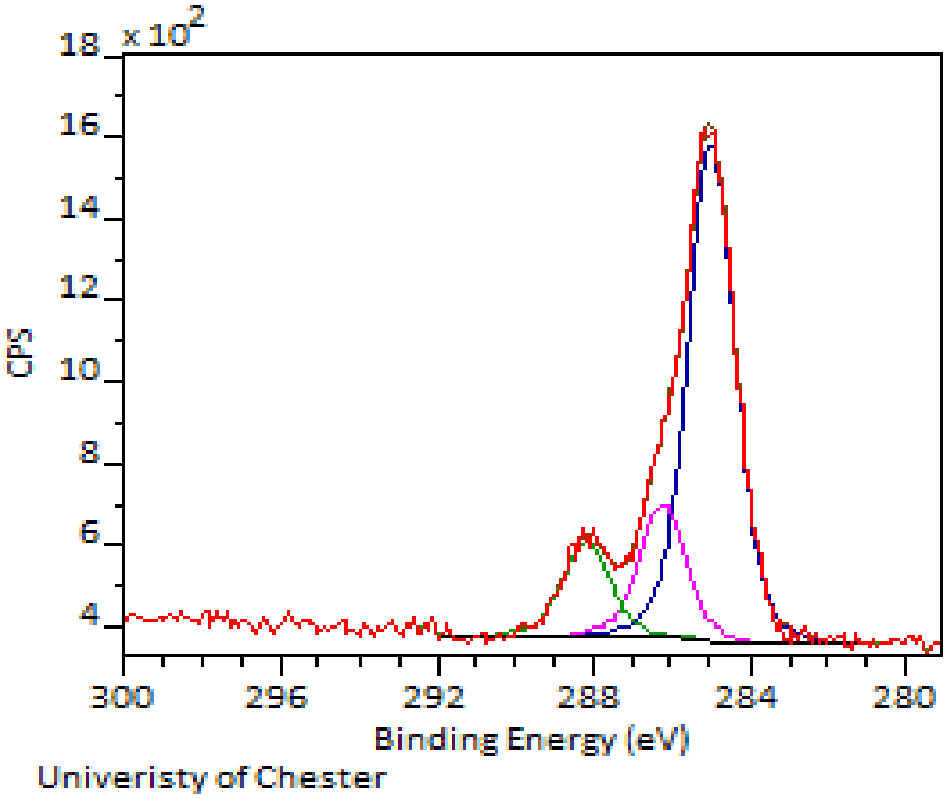

Figure A.8 C 1s peak fit of silicon incubated with tryptic soy broth after 5 hours.

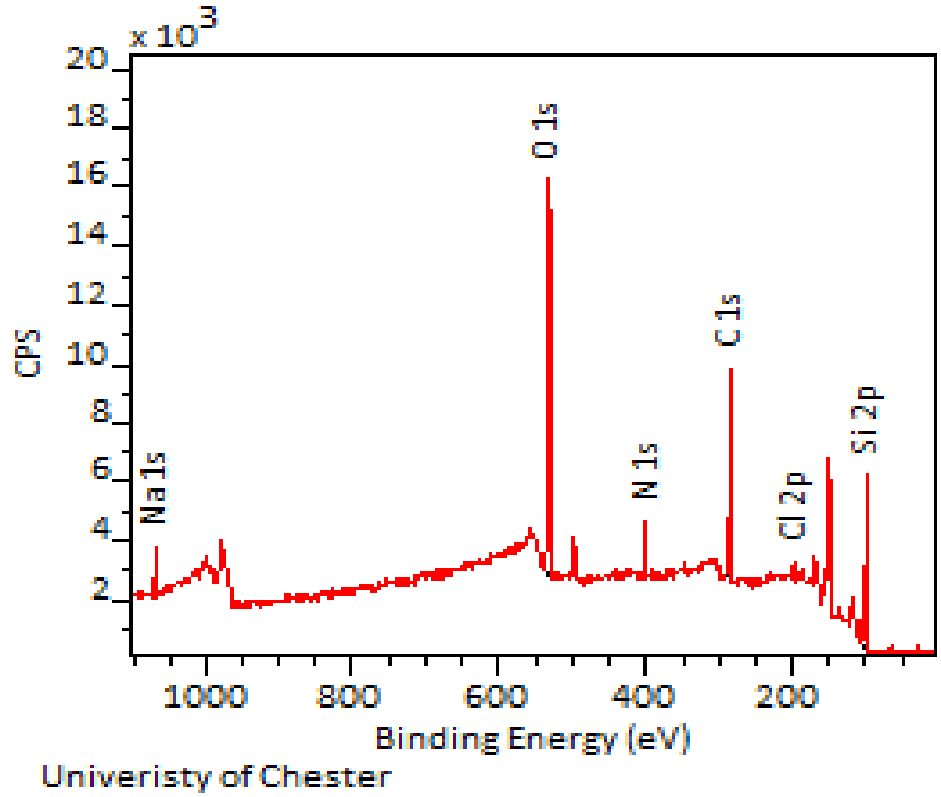

Figure A.9 Survey spectrum of silicon incubated with tryptic soy broth after 6 hours.

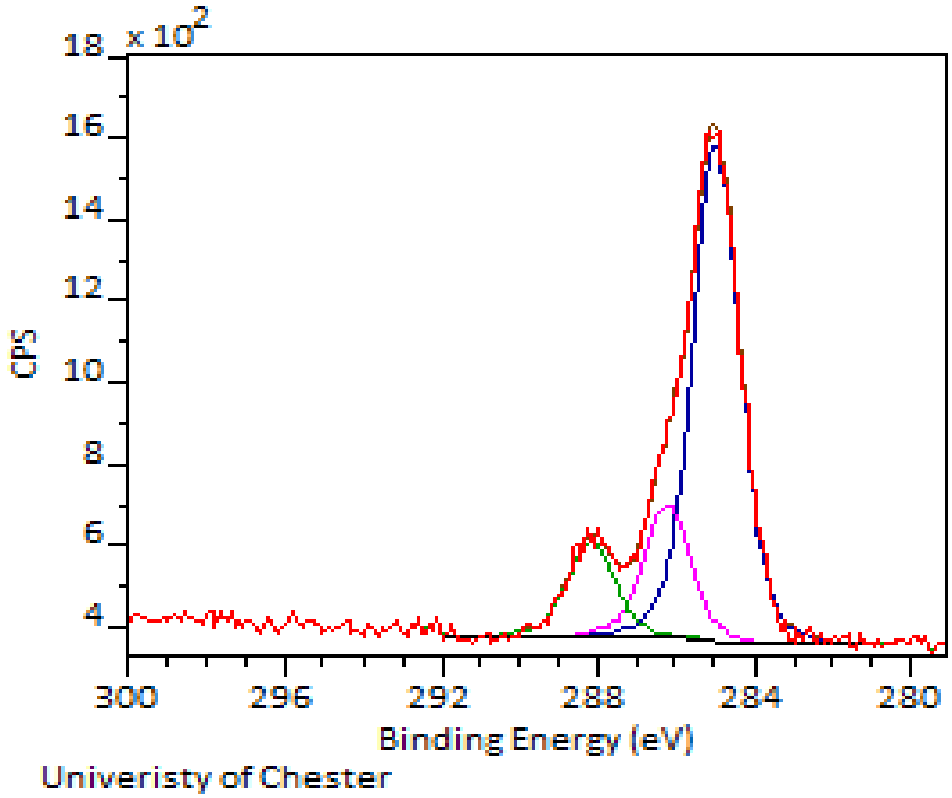

Figure A.10 C 1s peak fit of silicon incubated with tryptic soy broth after 6 hours.

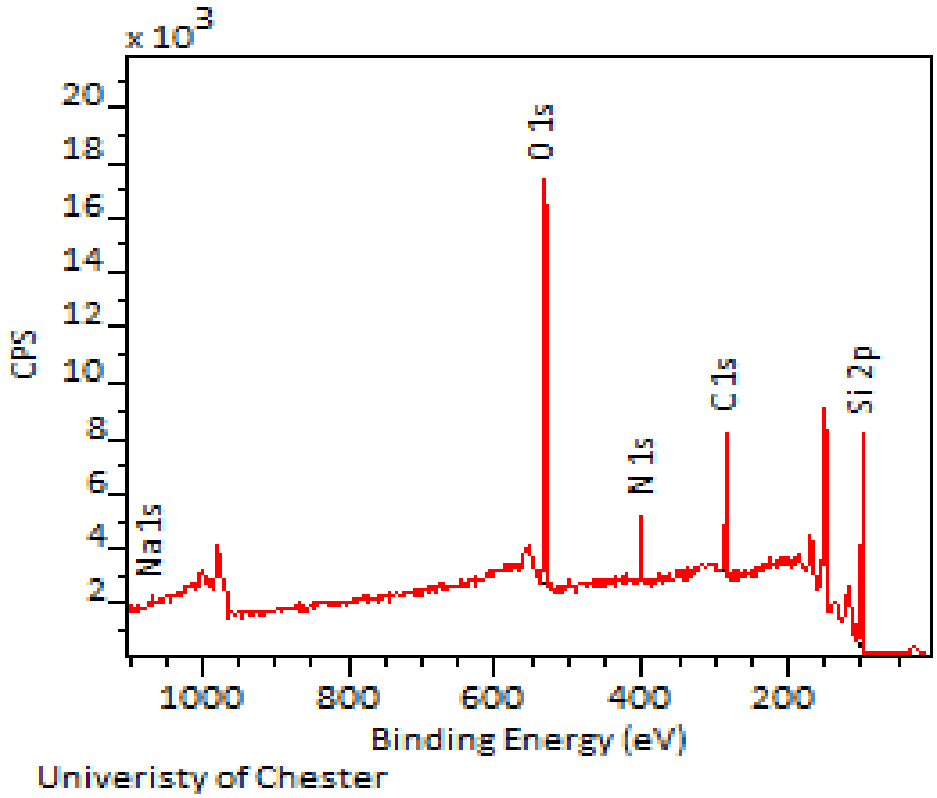

Figure A.11Survey spectrum of silicon incubated with tryptic soy broth after 8 hours.

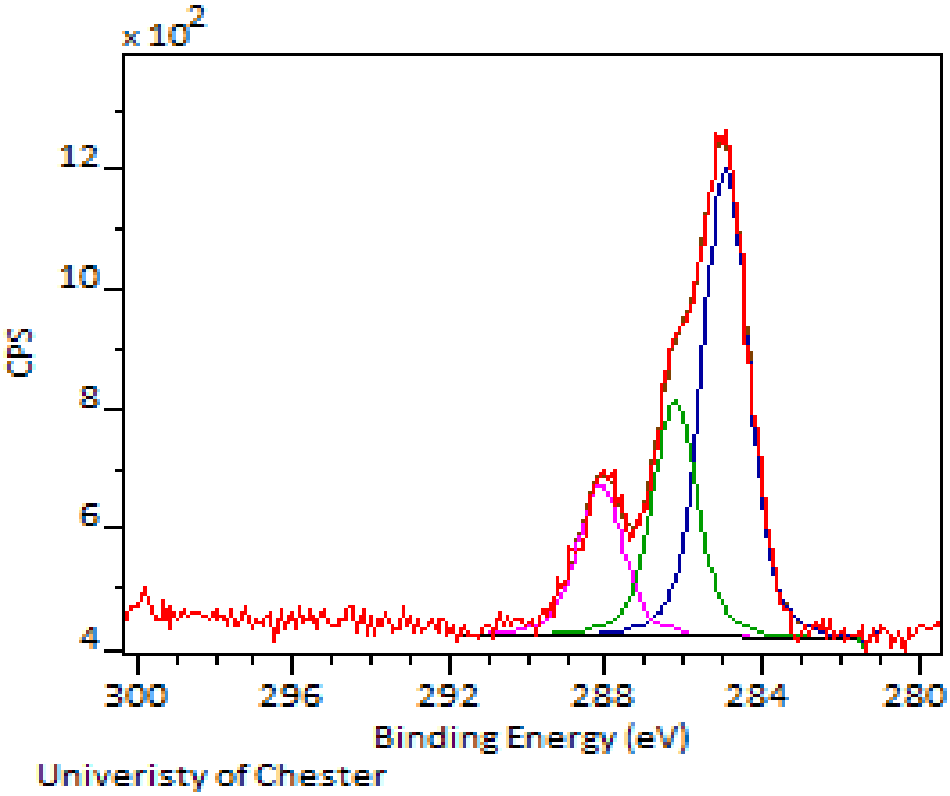

Figure A.12 C 1s peak fit of silicon incubated with tryptic soy broth after 8 hours.

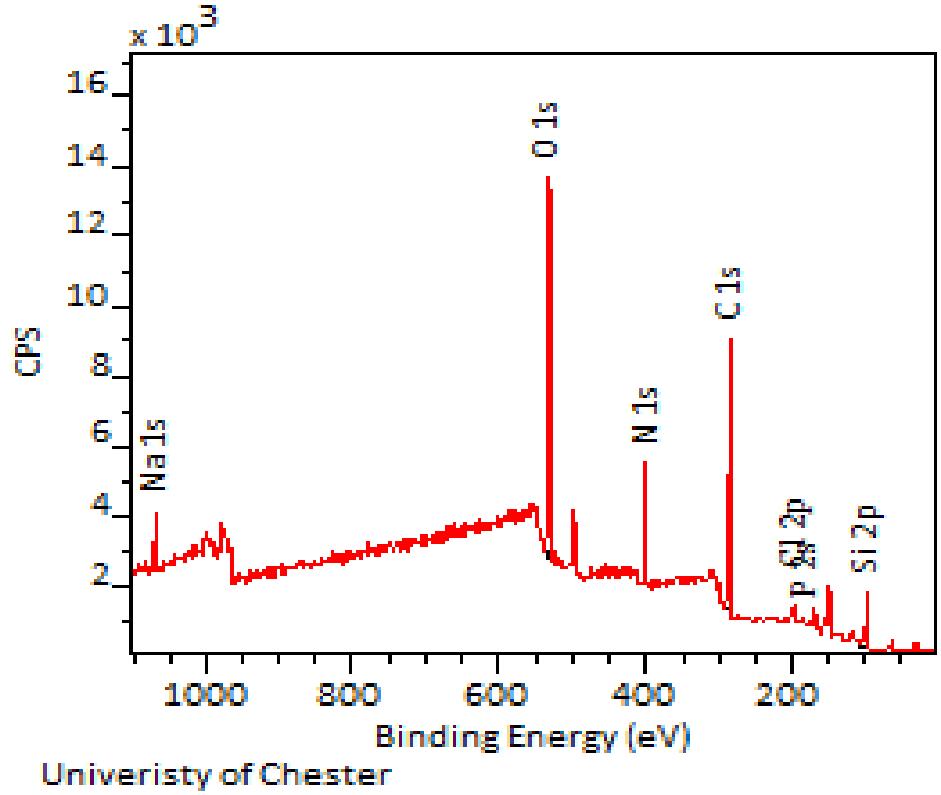

Figure A.13 Survey spectrum of silicon incubated with tryptic soy broth after 9 hours.

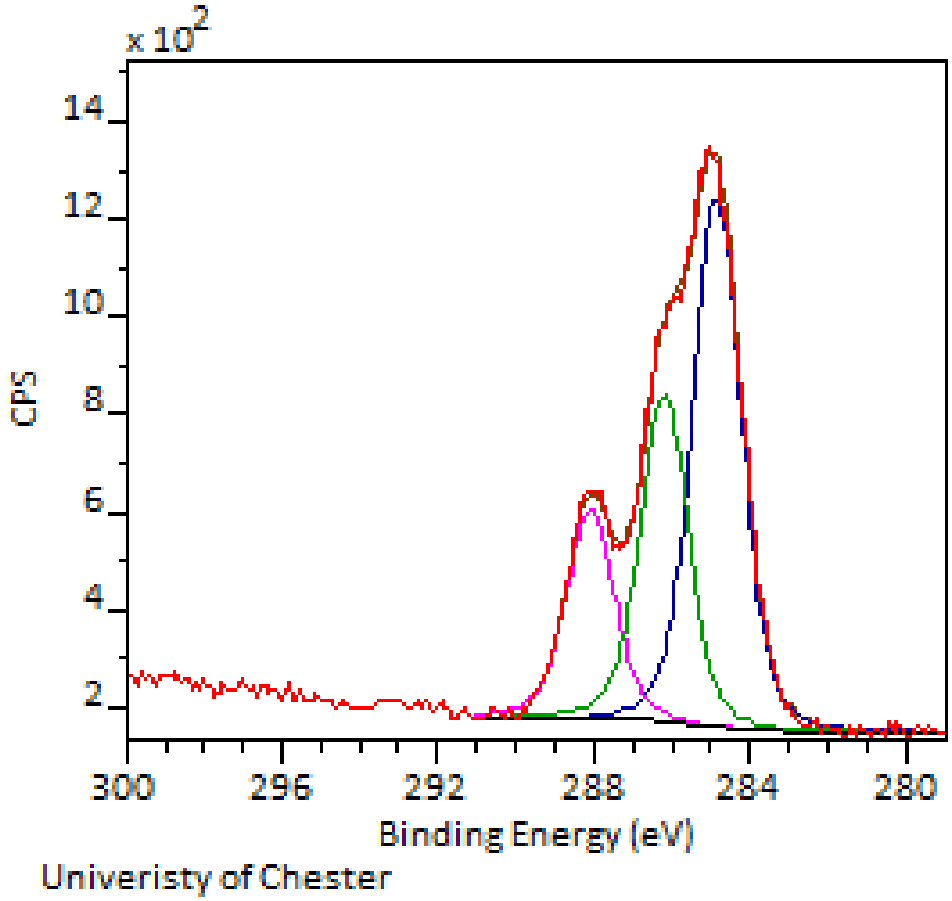

Figure A.14 C 1s peak fit of silicon incubated with tryptic soy broth after 9 hours.

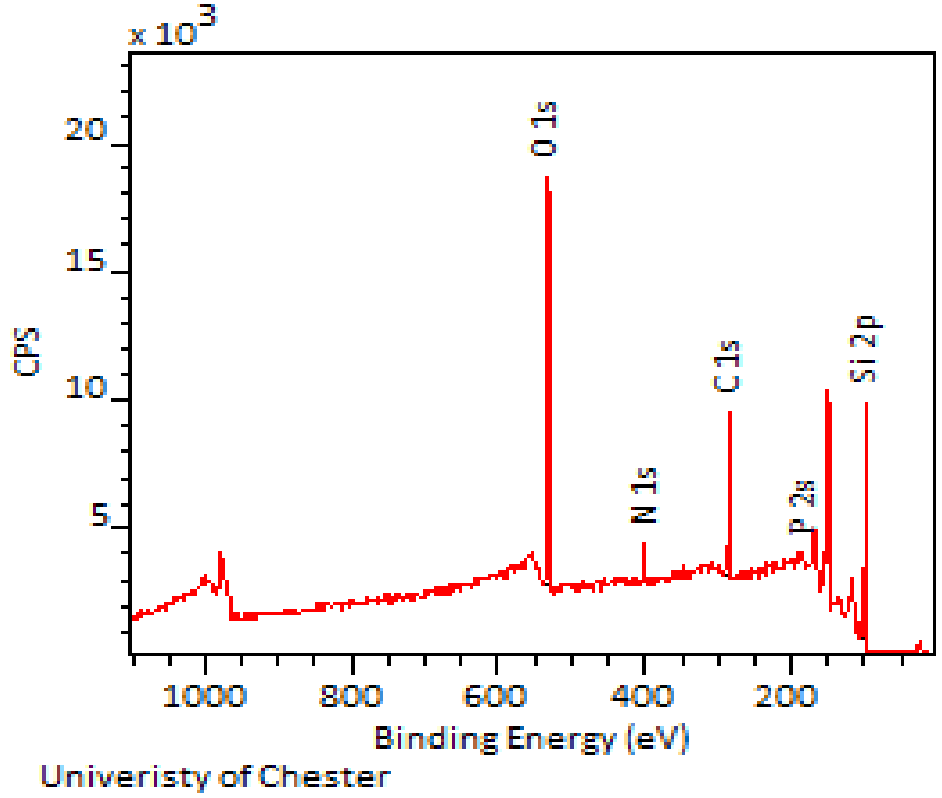

Figure A.15 Survey spectrum of silicon incubated with *NCTC13360* after 2 hours.

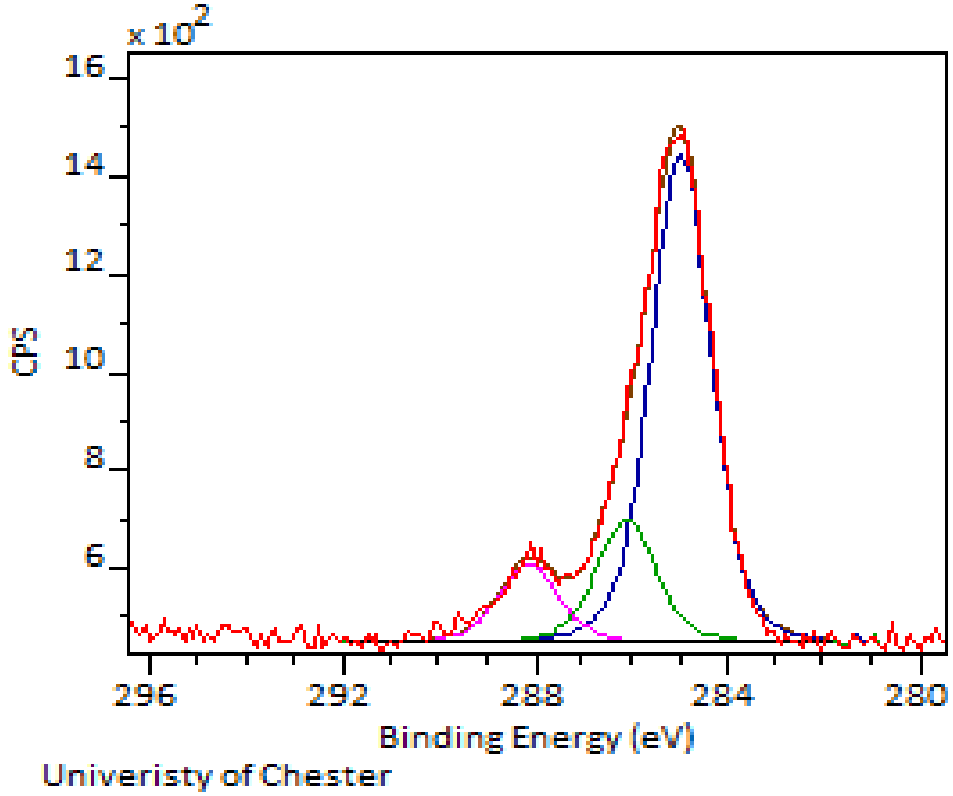

Figure A.16 C 1s peak fit of silicon incubated with *NCTC13360* after 2 hours.

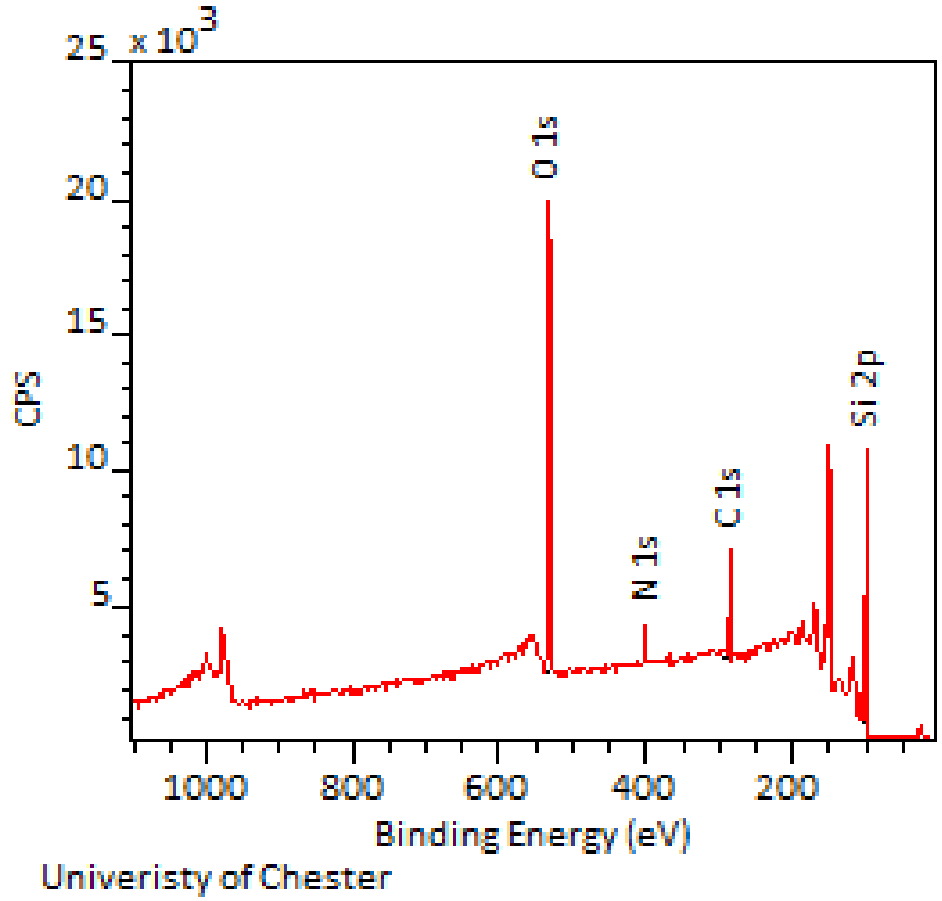

Figure A.17 Survey spectrum of silicon incubated with *NCTC13360* after 3 hours.

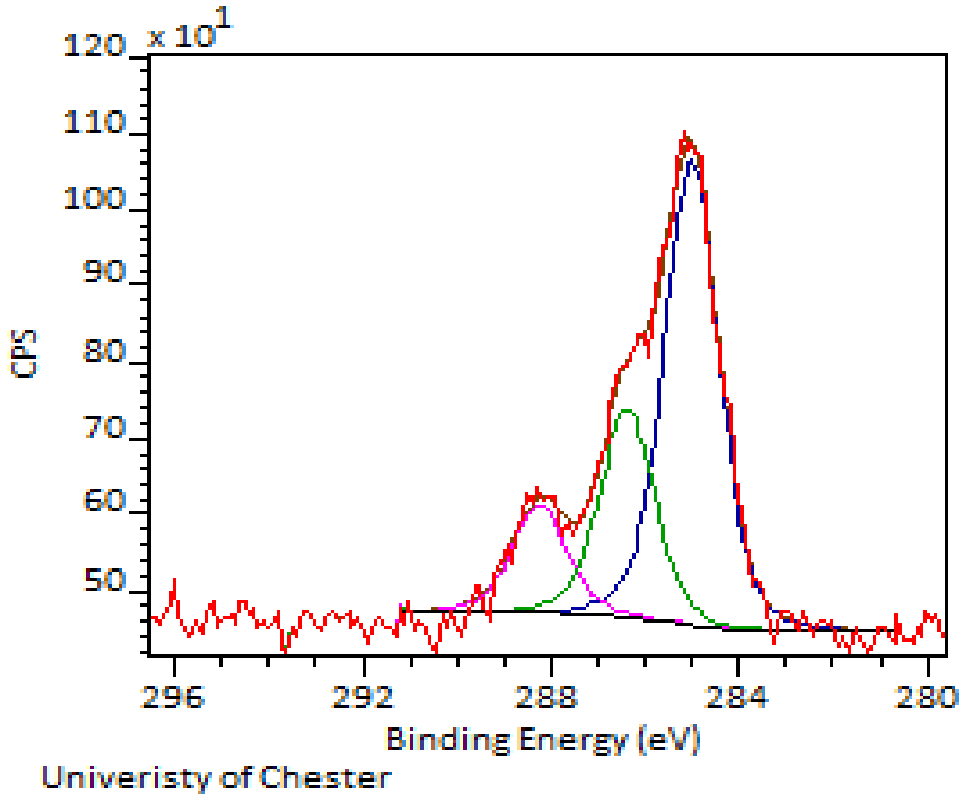

Figure A.18 C 1s peak fit of silicon incubated with *NCTC13360* after 3 hours.

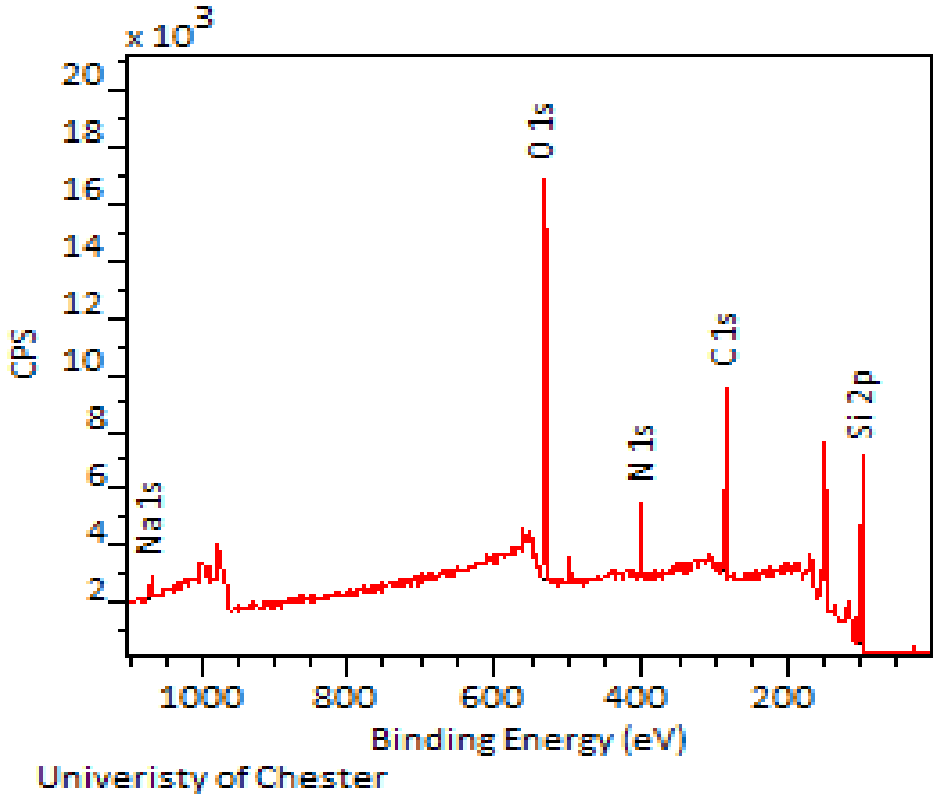

Figure A.19 Survey spectrum of silicon incubated with *NCTC13360* after 4 hours.

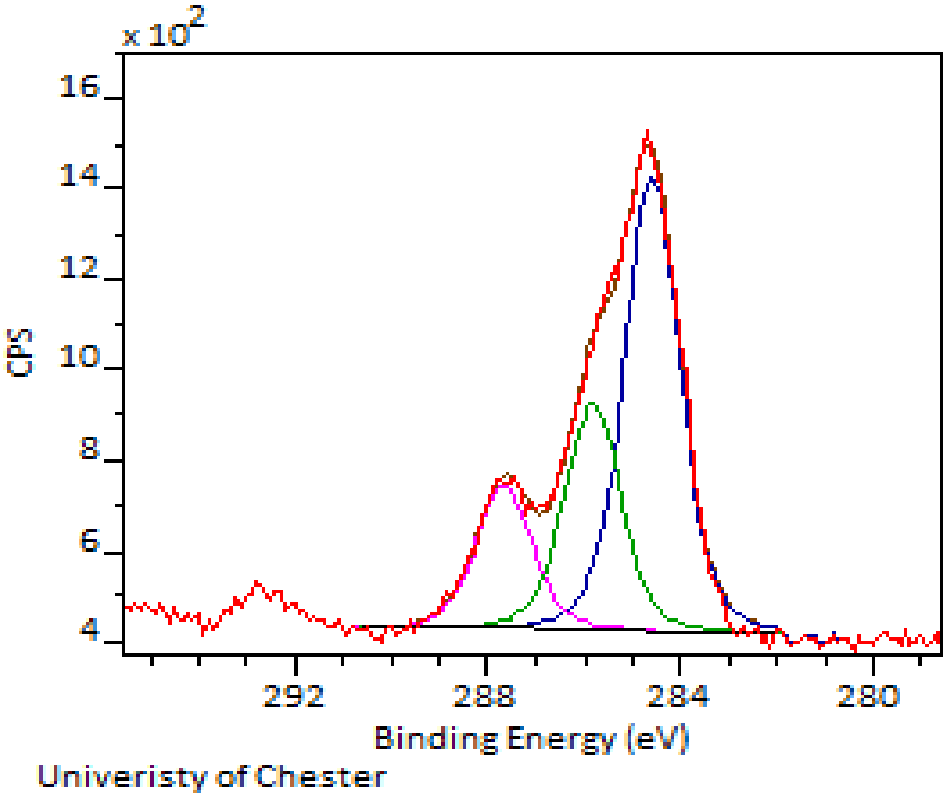

Figure A.20 C 1s peak fit of silicon incubated with *NCTC13360* after 4 hours.

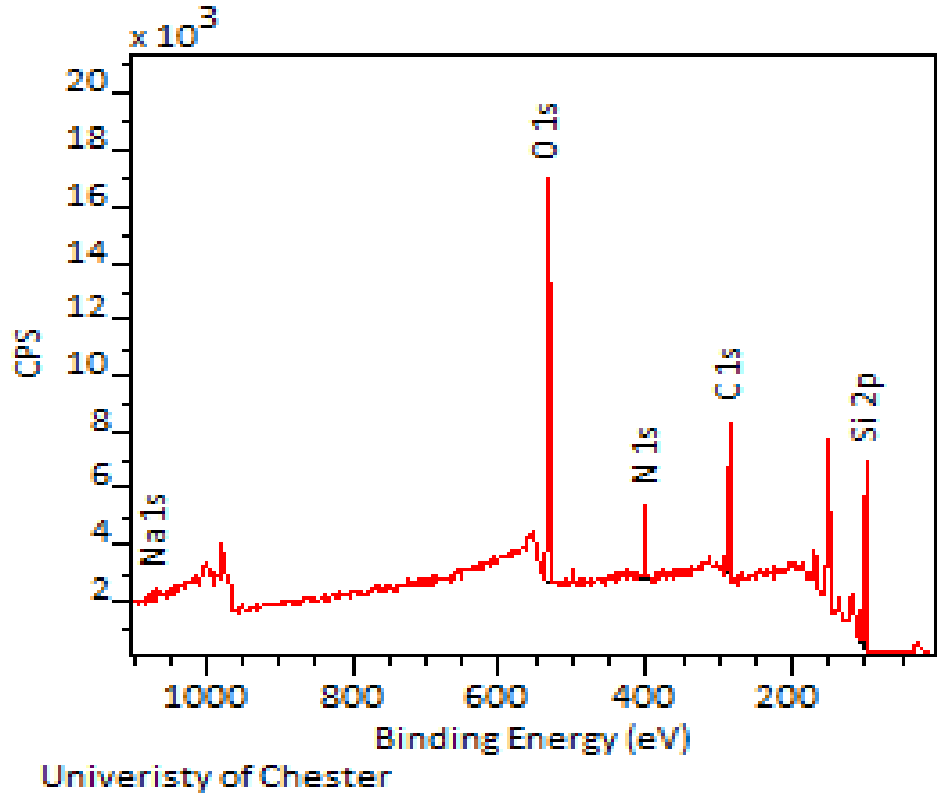

Figure A.21 Survey spectrum of silicon incubated with *NCTC13360* after 5 hours.

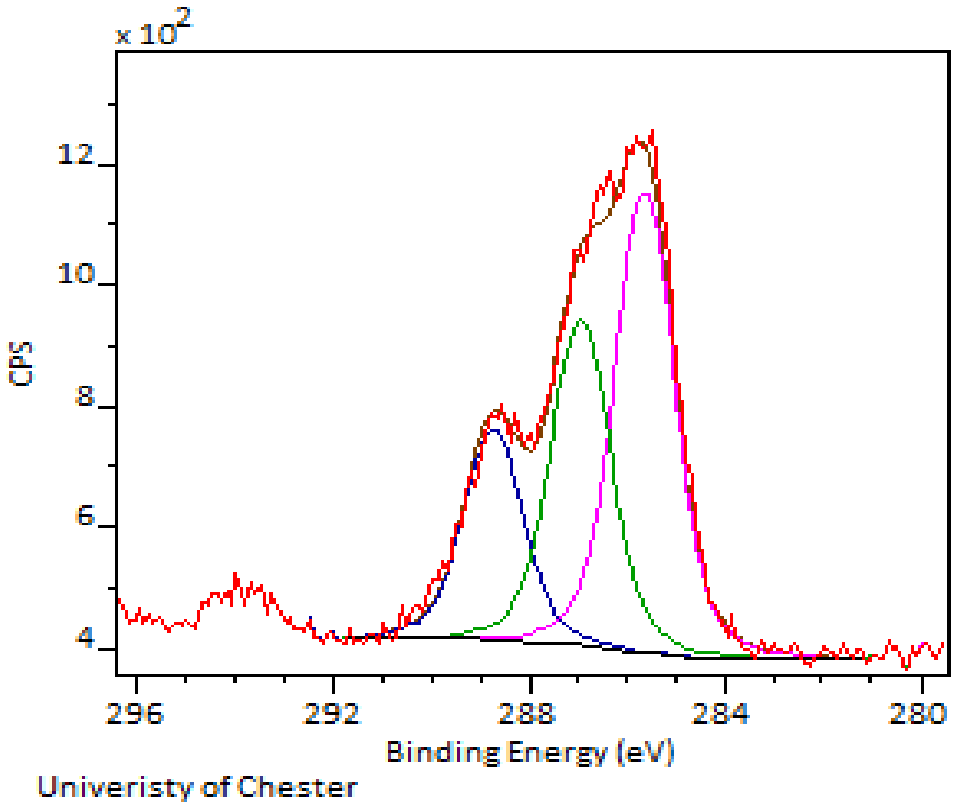

Figure A.22 C 1s peak fit of silicon incubated with *NCTC13360* after 5 hours.

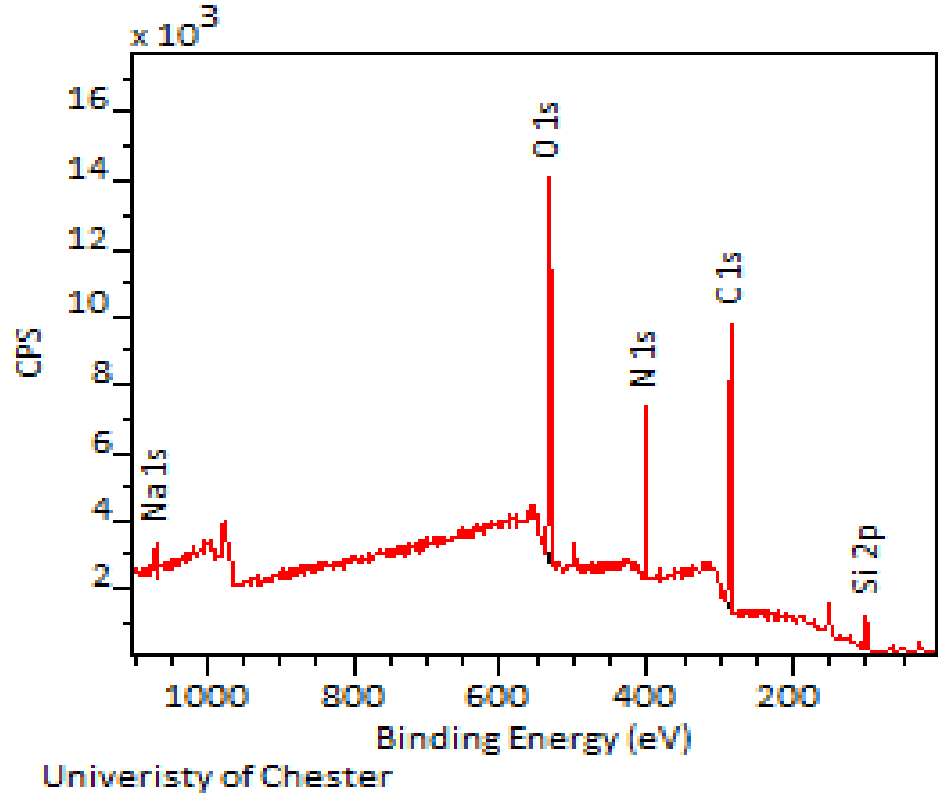

Figure A.23 Survey spectrum of silicon incubated with *NCTC13360* after 6 hours.

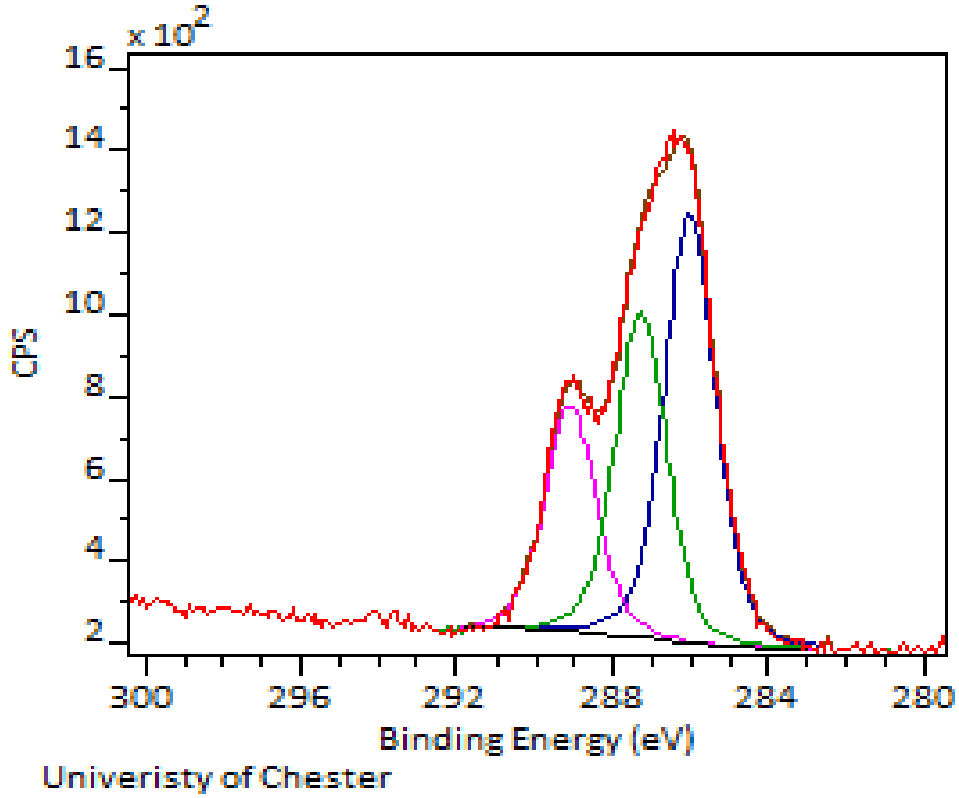

Figure A.24 C 1s peak fit of silicon incubated with *NCTC13360* after 6 hours.

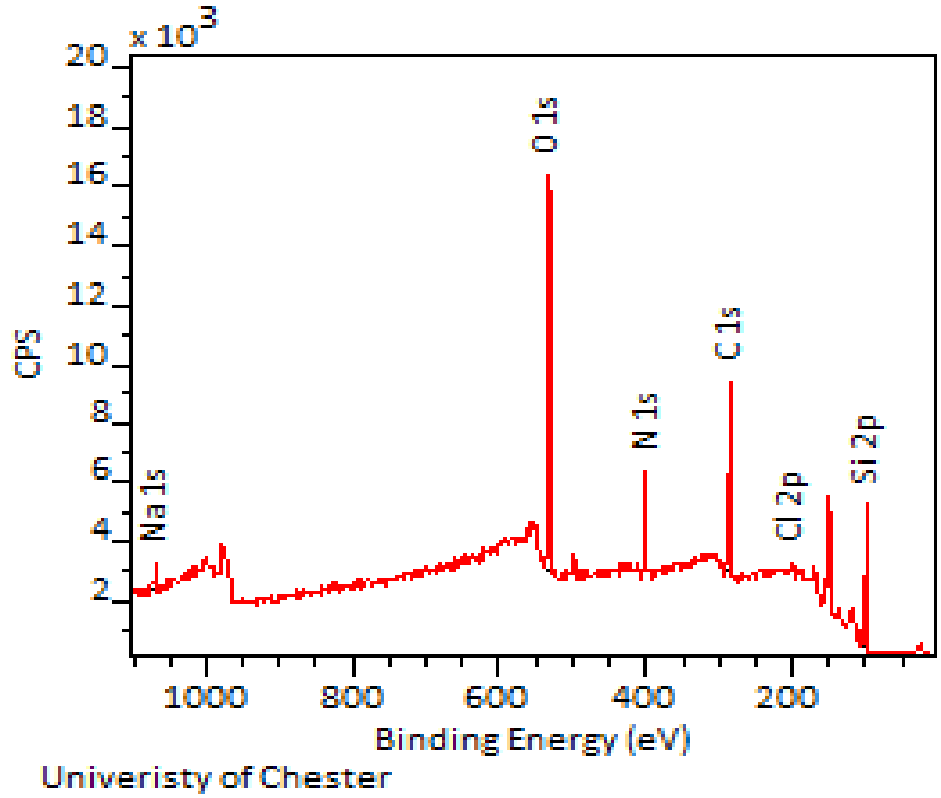

Figure A.25 Survey spectrum of silicon incubated with *NCTC13360* after 7 hours.

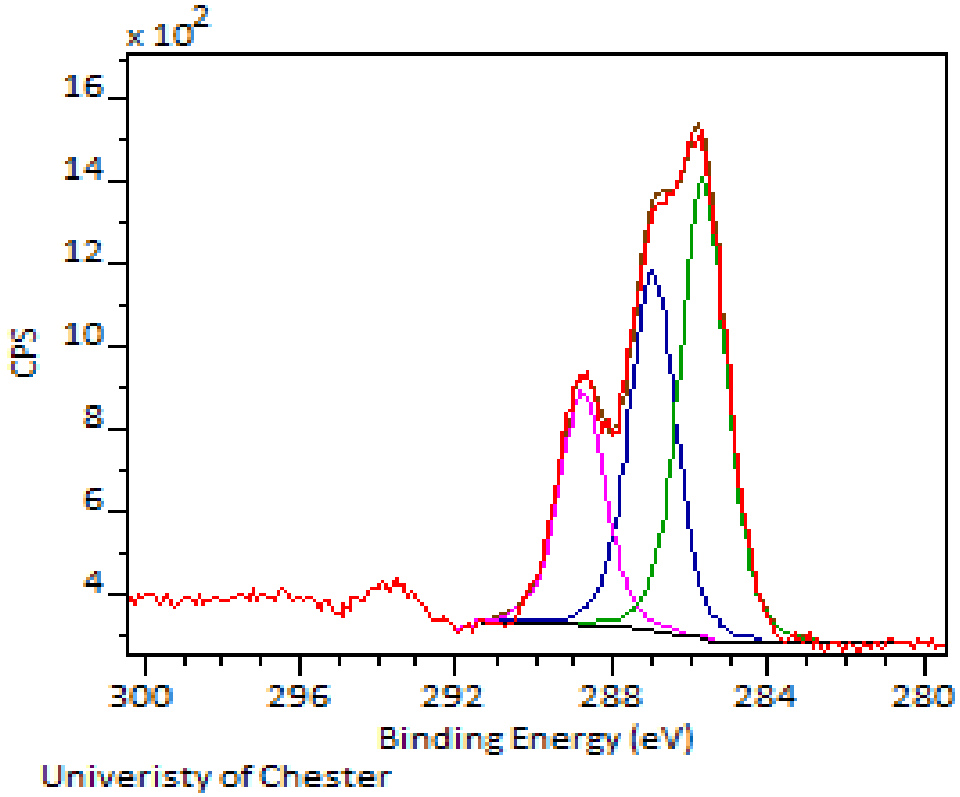

Figure A.26 C 1s peak fit of silicon incubated with *NCTC13360* after 7 hours.

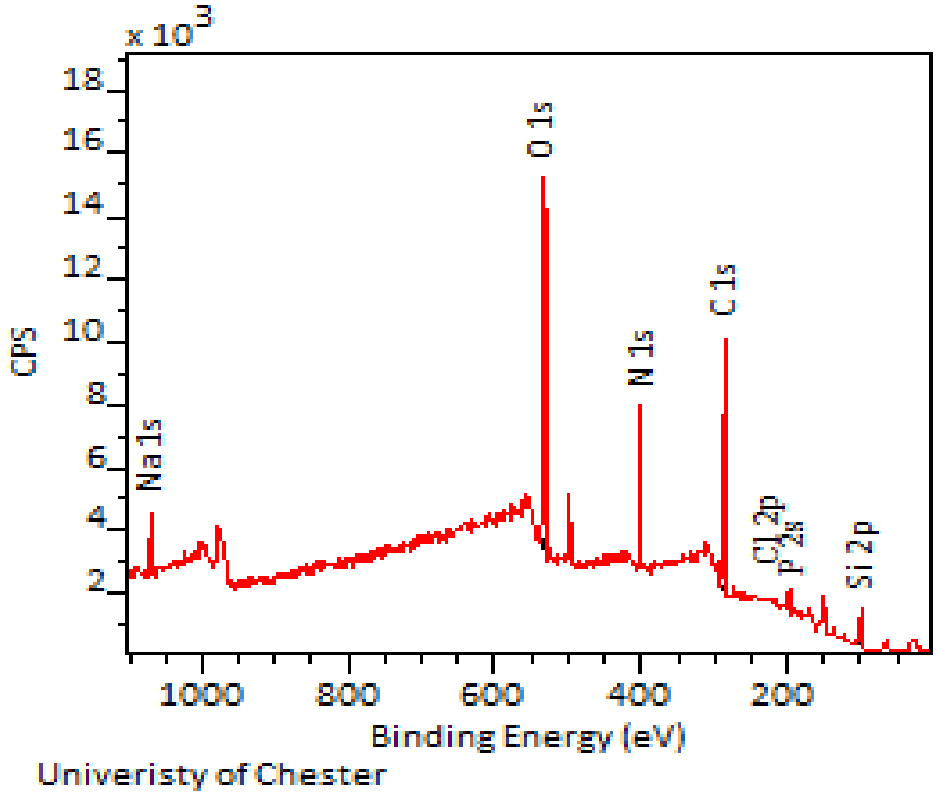

Figure A.27 Survey spectrum of silicon incubated with *NCTC13360* after 7 hours repeated sample.

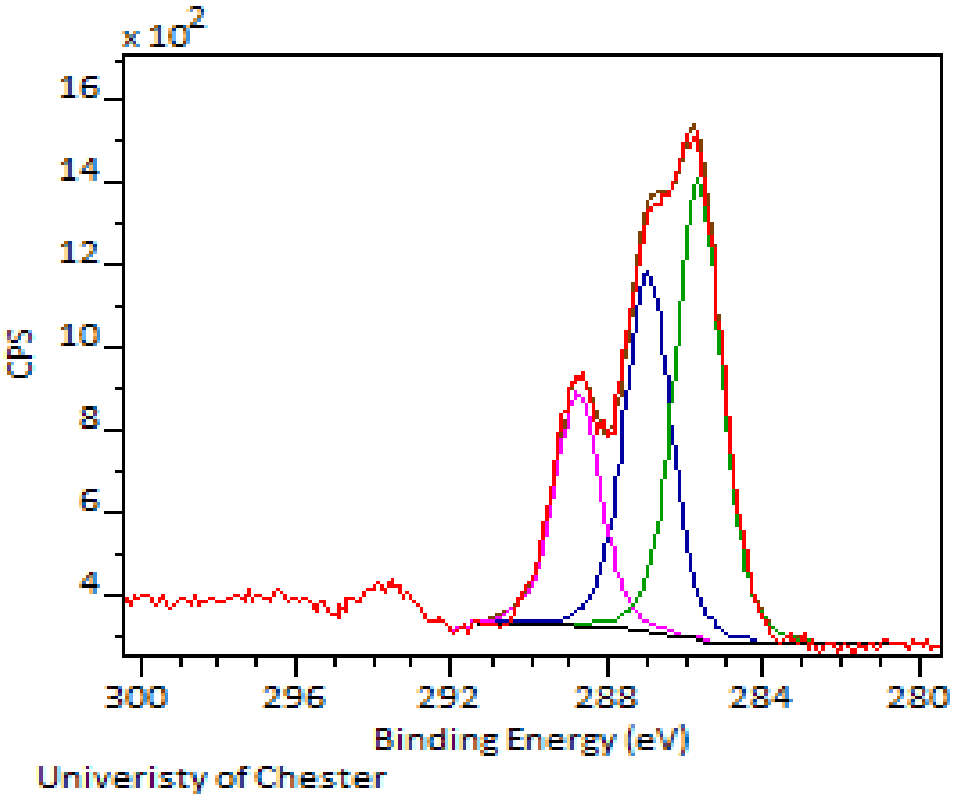

Figure A.28 C 1s peak fit of silicon incubated with *NCTC13360* after 7 hours repeated sample.

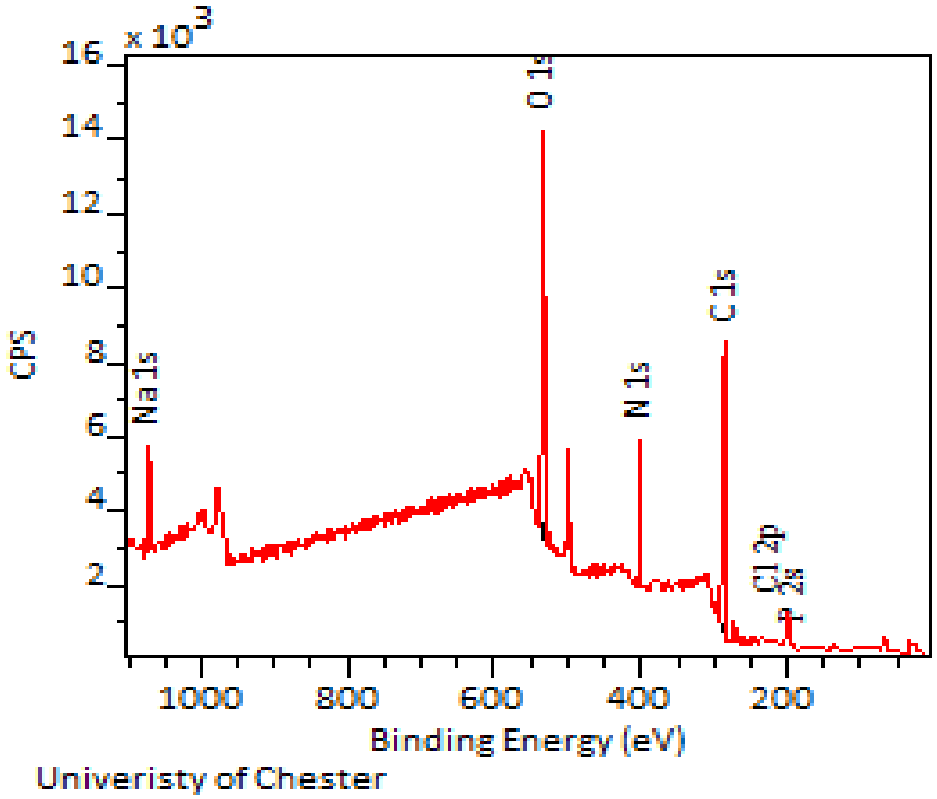

Figure A.29 Survey spectrum of silicon incubated with *NCTC13360* after 8 hours.

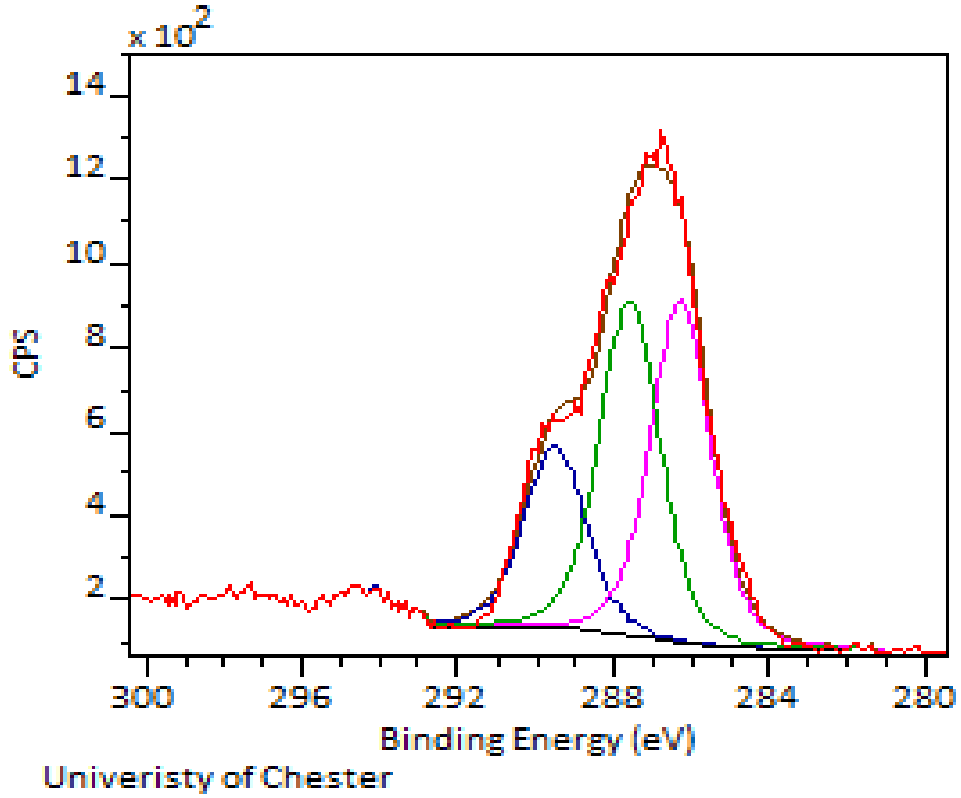

Figure A.30 C 1s peak fit of silicon incubated with *NCTC13360* after 8 hours.

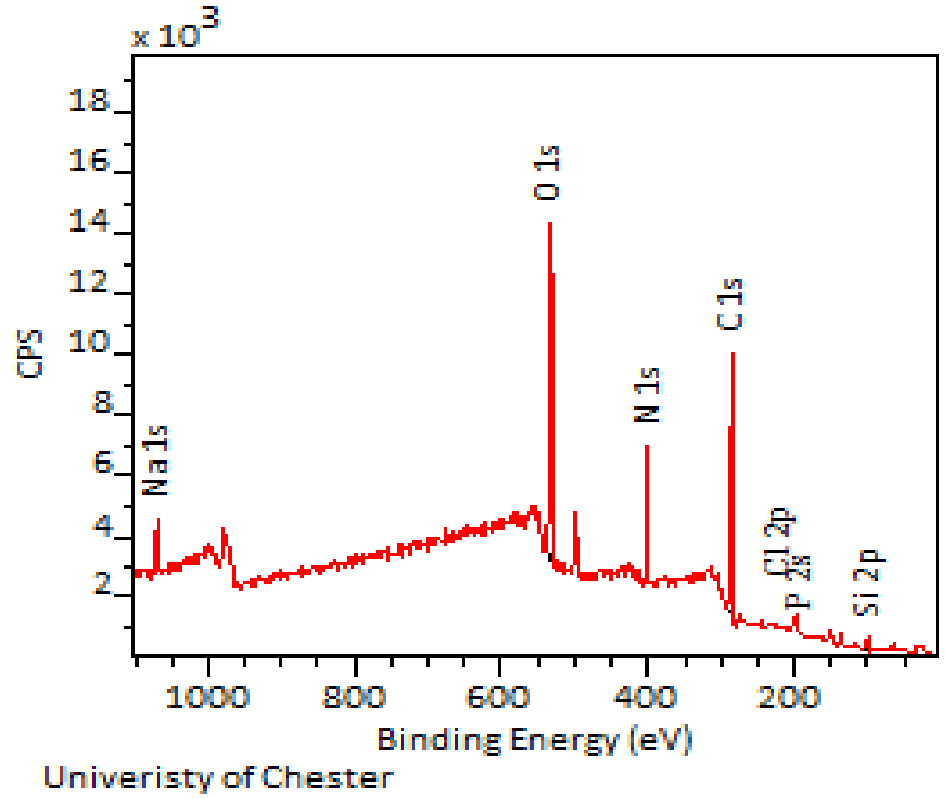

Figure A.31 Survey spectrum of silicon incubated with *NCTC13360* after 9 hours.

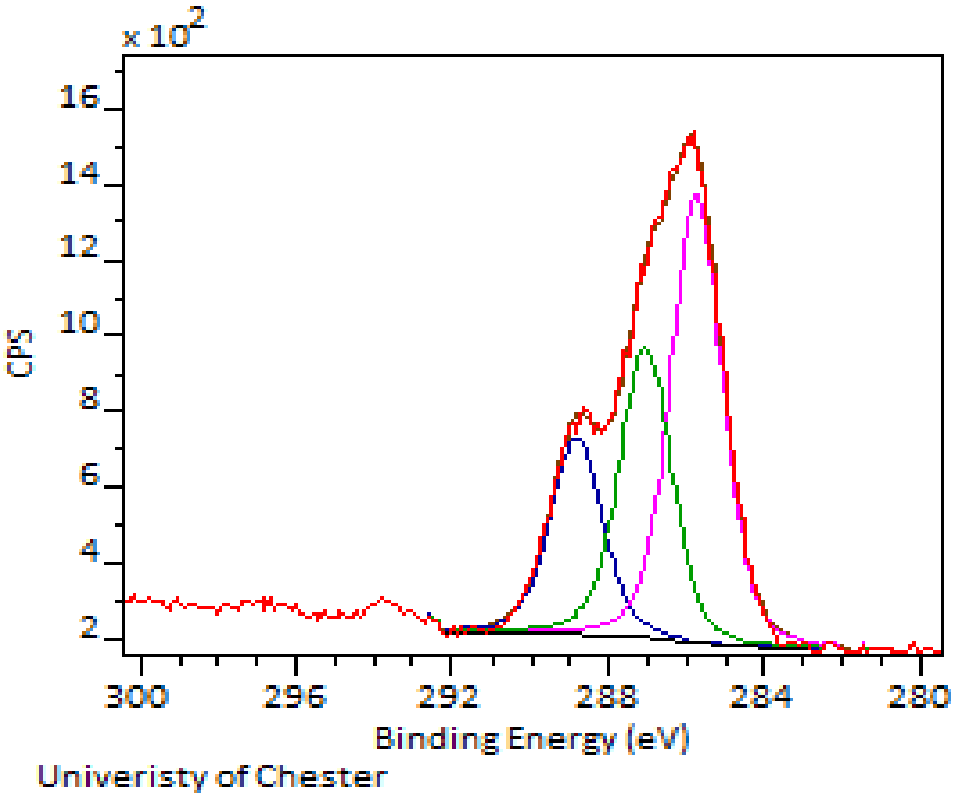

Figure A.32 C 1s peak fit of silicon incubated with *NCTC13360* after 9 hours.

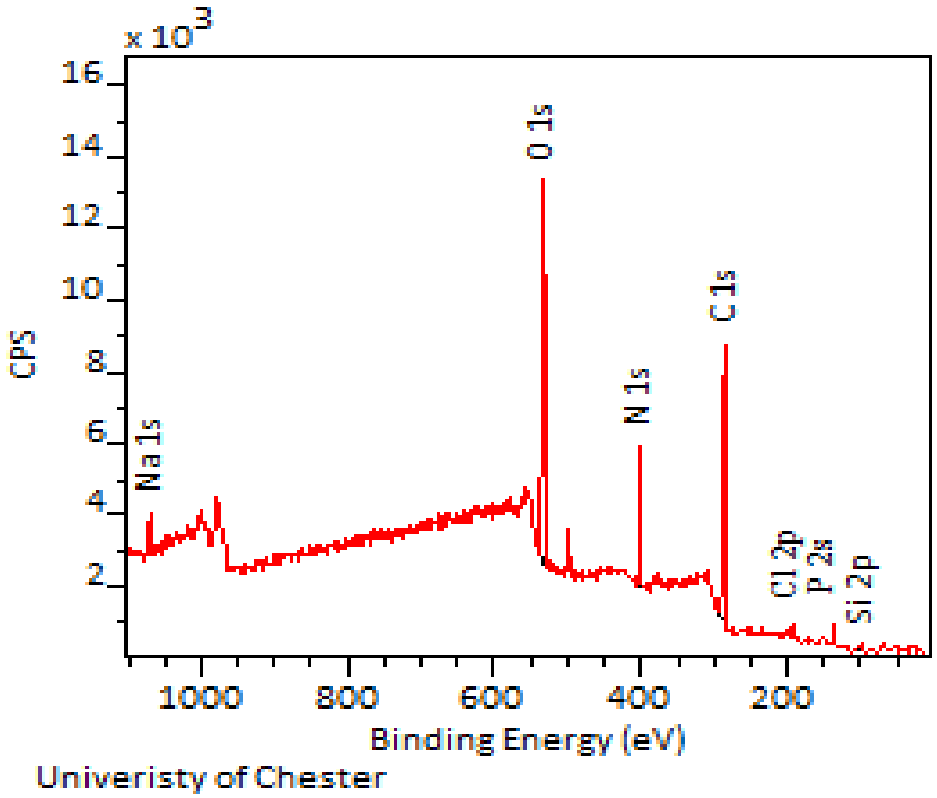

Figure A.33 Survey spectrum of silicon incubated with *NCTC13360* after 10 hours

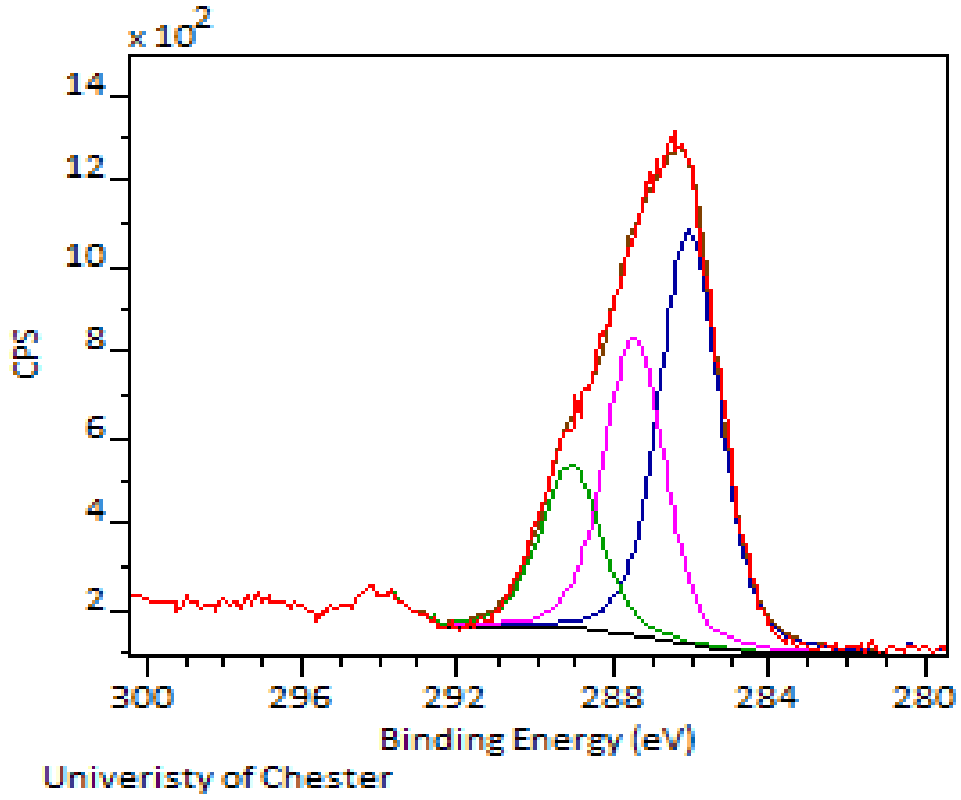

Figure A.34 C 1s peak fit of silicon incubated with *NCTC13360* after 10 hours.

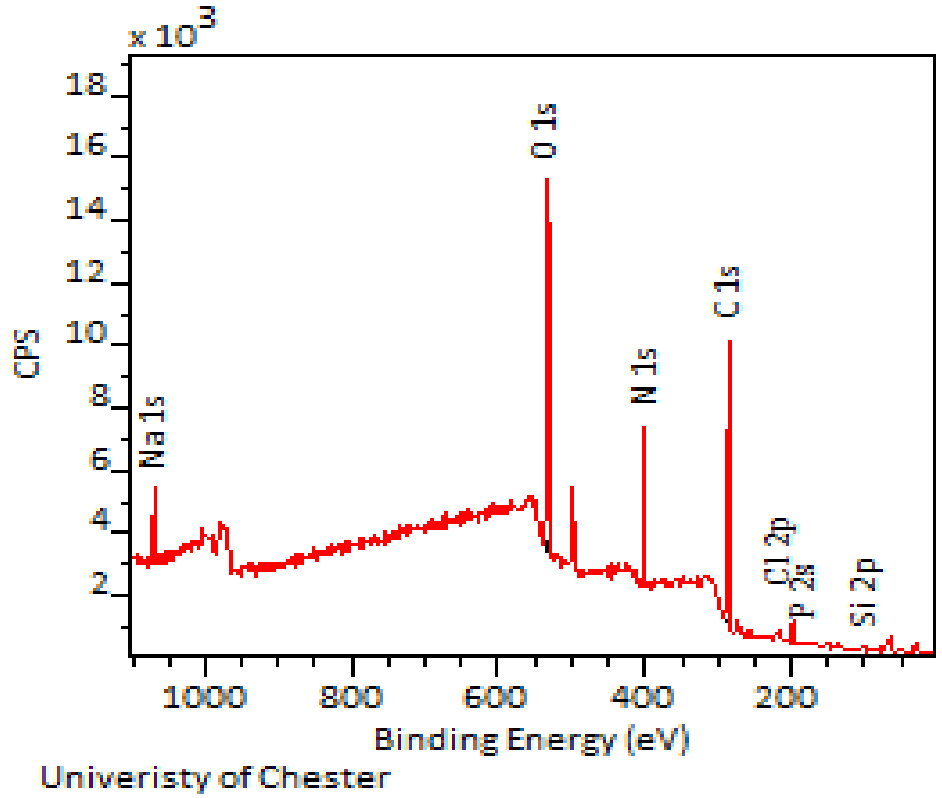

Figure A.35 Survey spectrum of silicon incubated with *NCTC13360* after 12 hours.

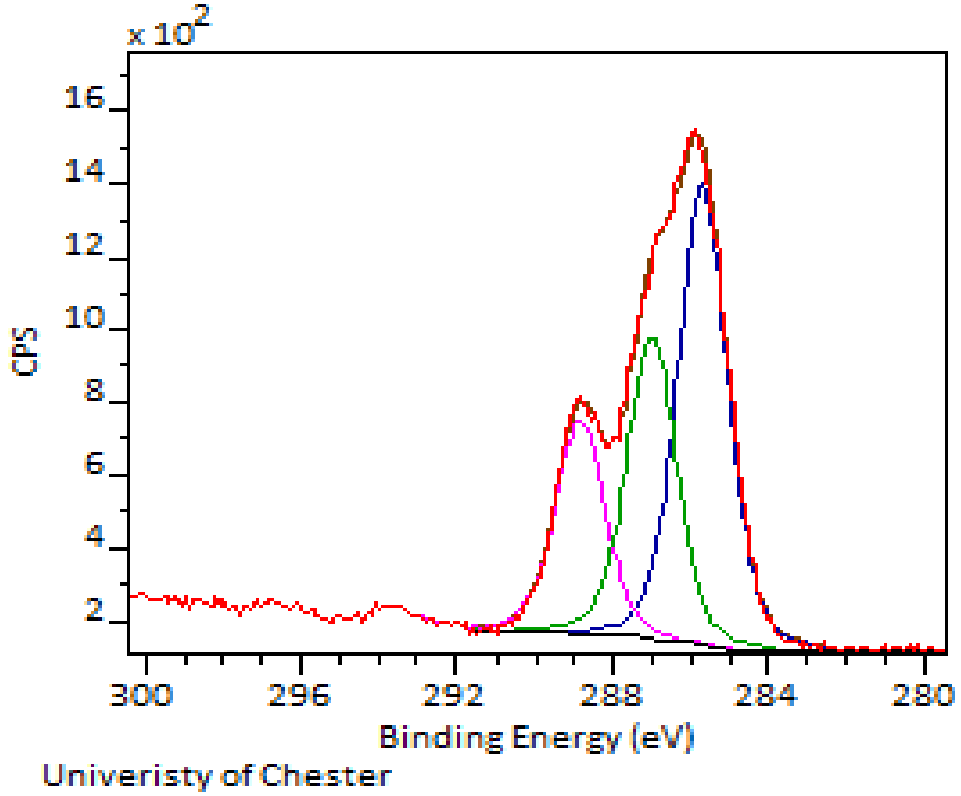

Figure A.36 C 1s peak fit of silicon incubated with *NCTC13360* after 12 hours.

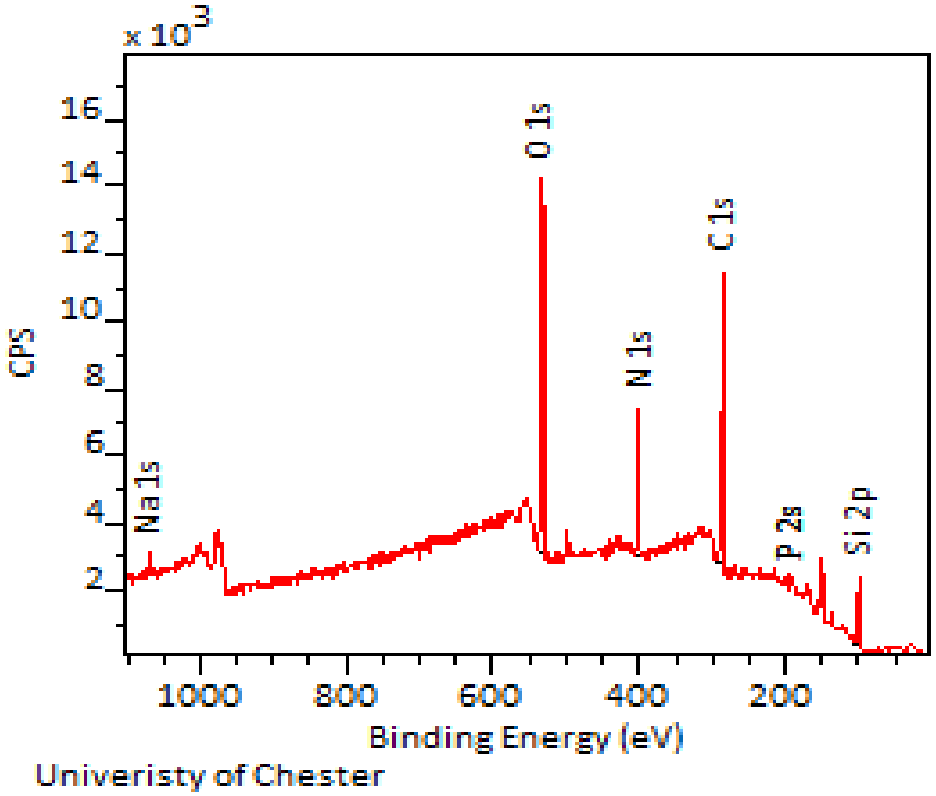

Figure A.37 Survey spectrum of silicon incubated with *NCTC13360* after 12 hours repeated sample.

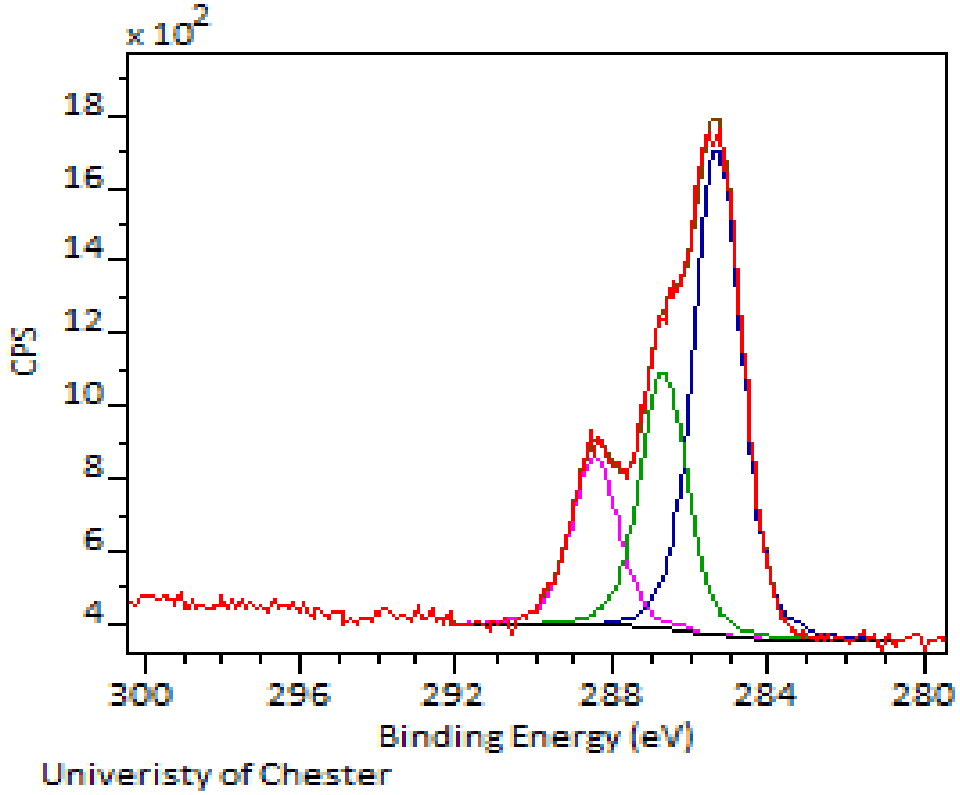

Figure A.38 C 1s peak fit of silicon incubated with *NCTC13360* after 12 hours redone.

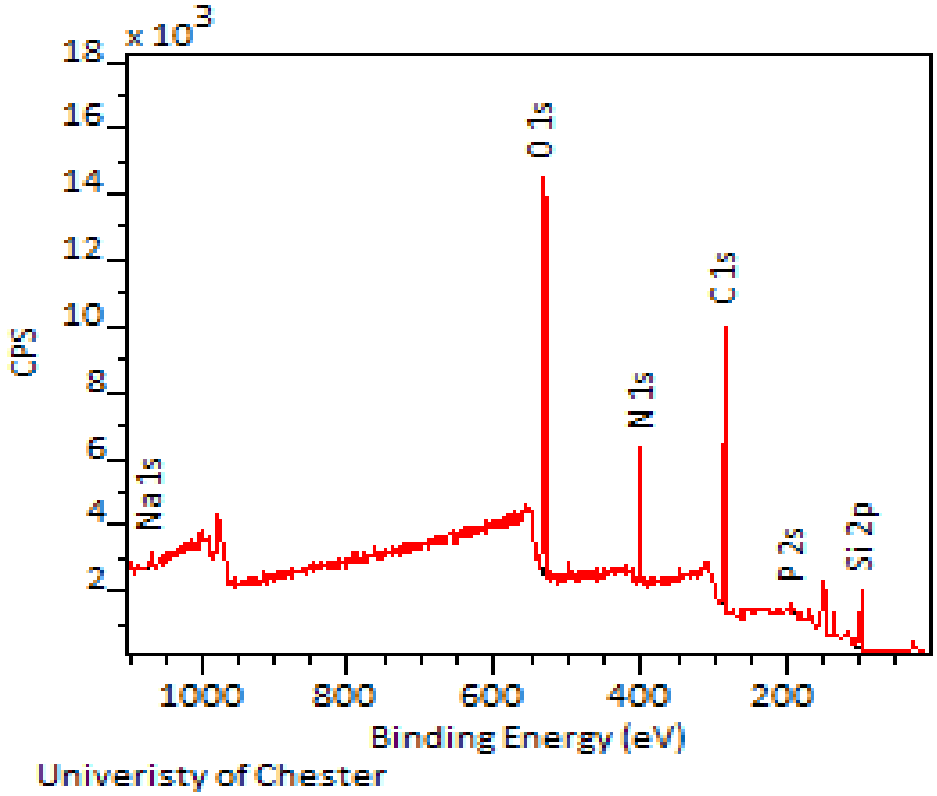

Figure A.39 Survey spectrum of silicon incubated with *NCTC13360* after 14 hours.

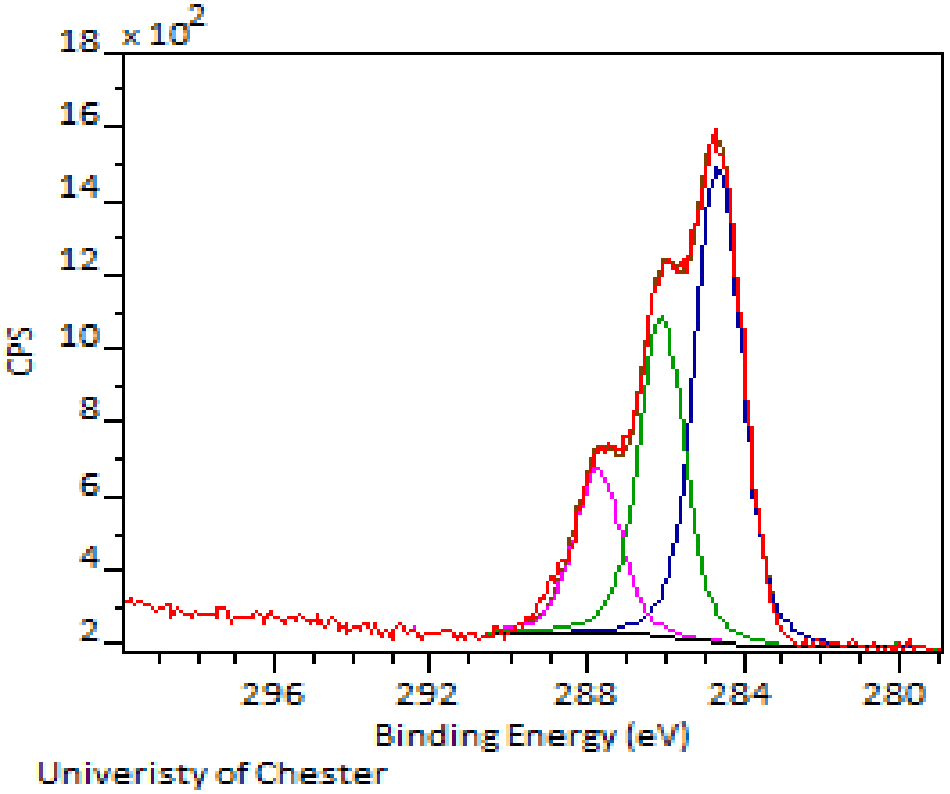

Figure A.40 C 1s peak fit of silicon incubated with *NCTC13360* after 14 hours.

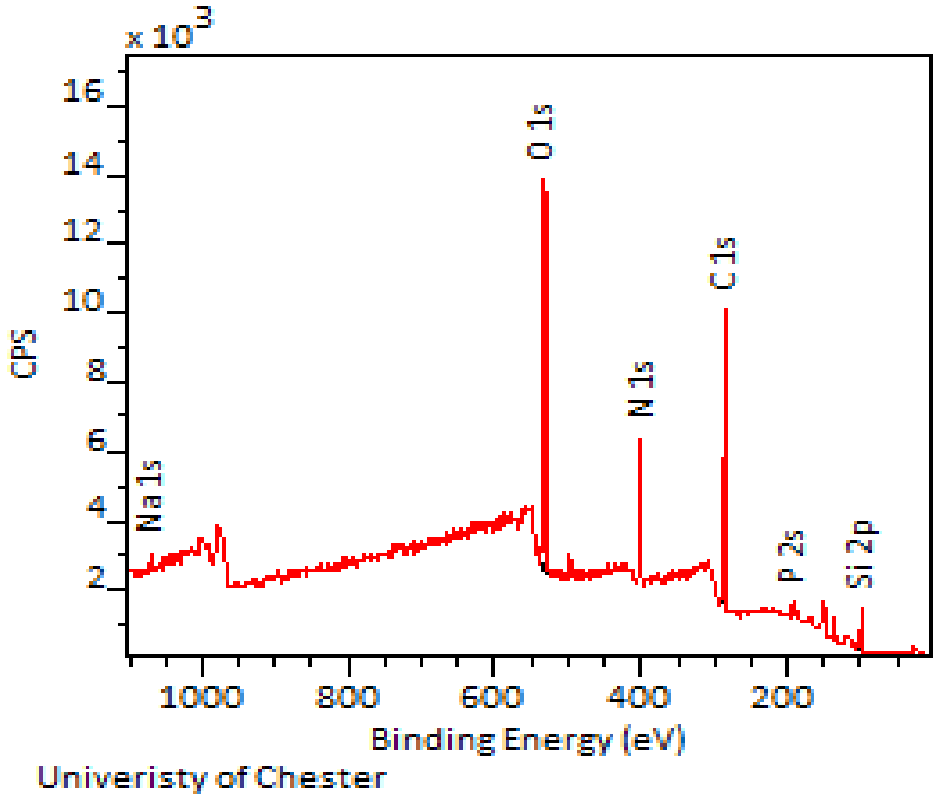

Figure A.41 Survey spectrum of silicon incubated with *NCTC13360* after 16 hours.

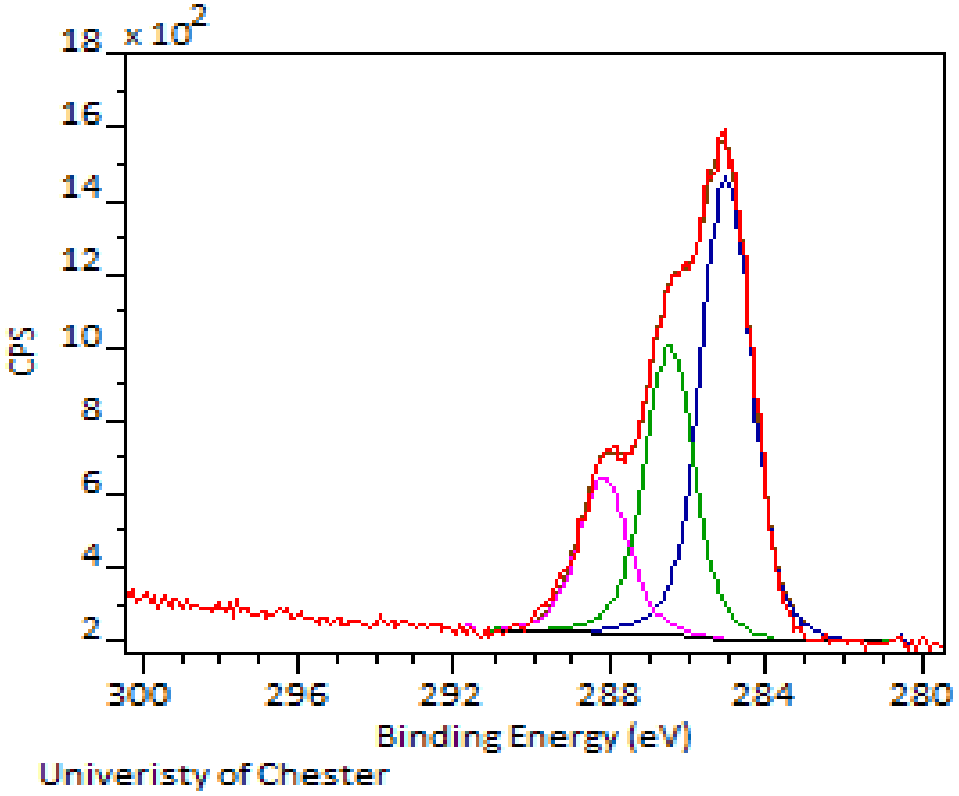

Figure A.42 C 1s peak fit of silicon incubated with *NCTC13360* after 16 hours.

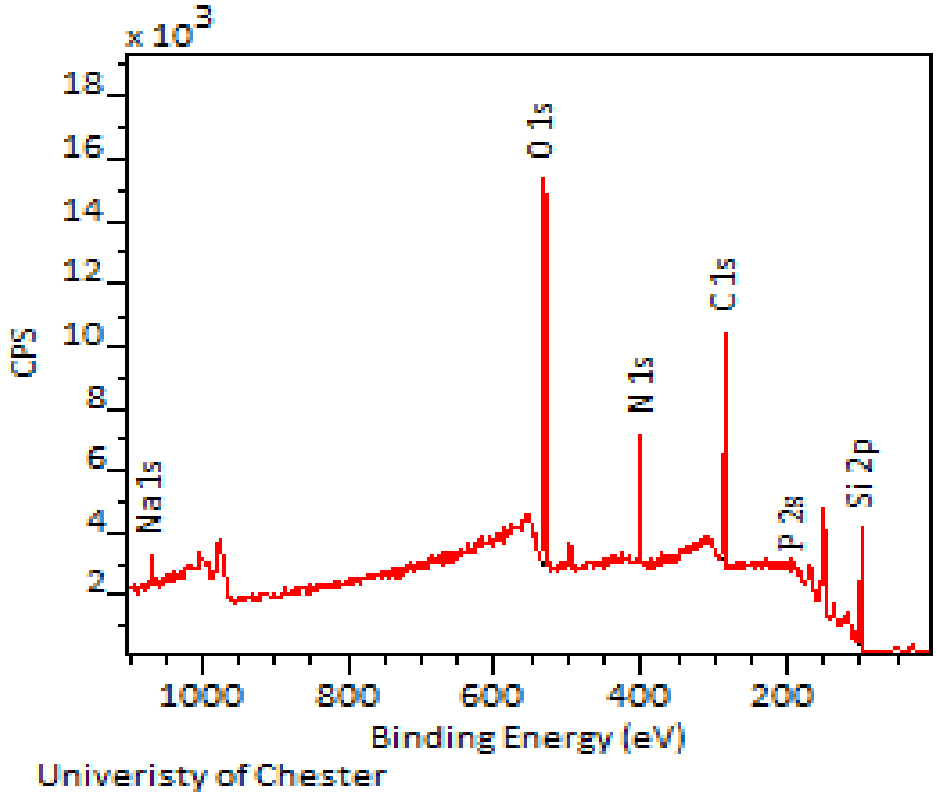

Figure A.43 Survey spectrum of silicon incubated with *NCTC13360* after 18 hours.

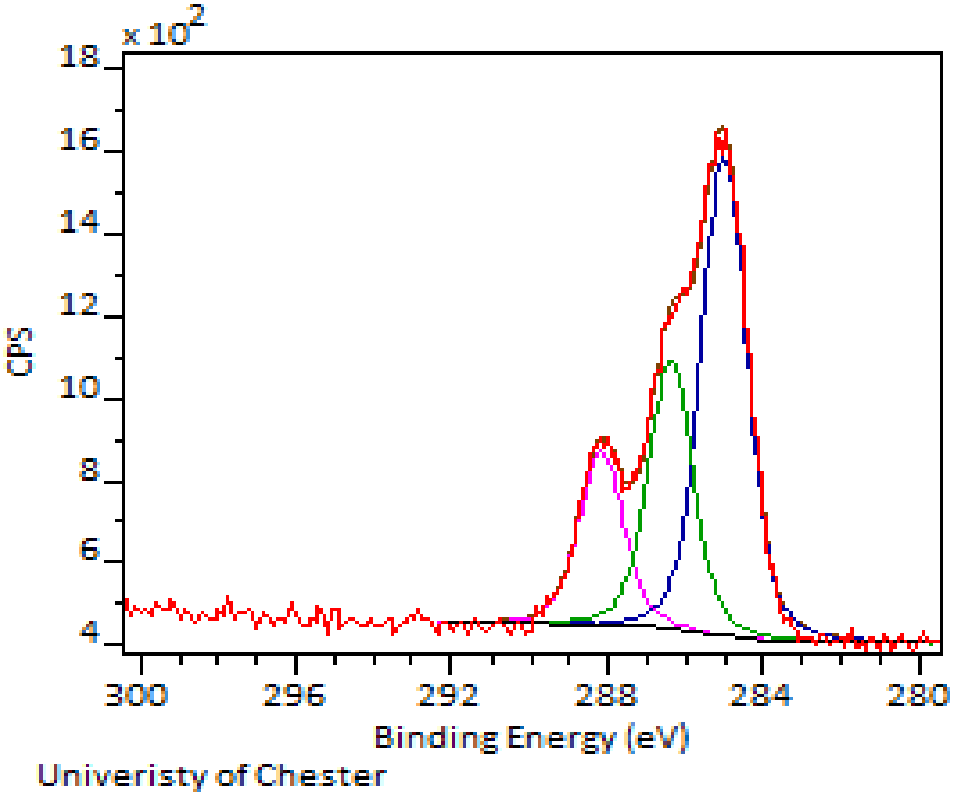

Figure A.44 C 1s peak fit of silicon incubated with *NCTC13360* after 18 hours.

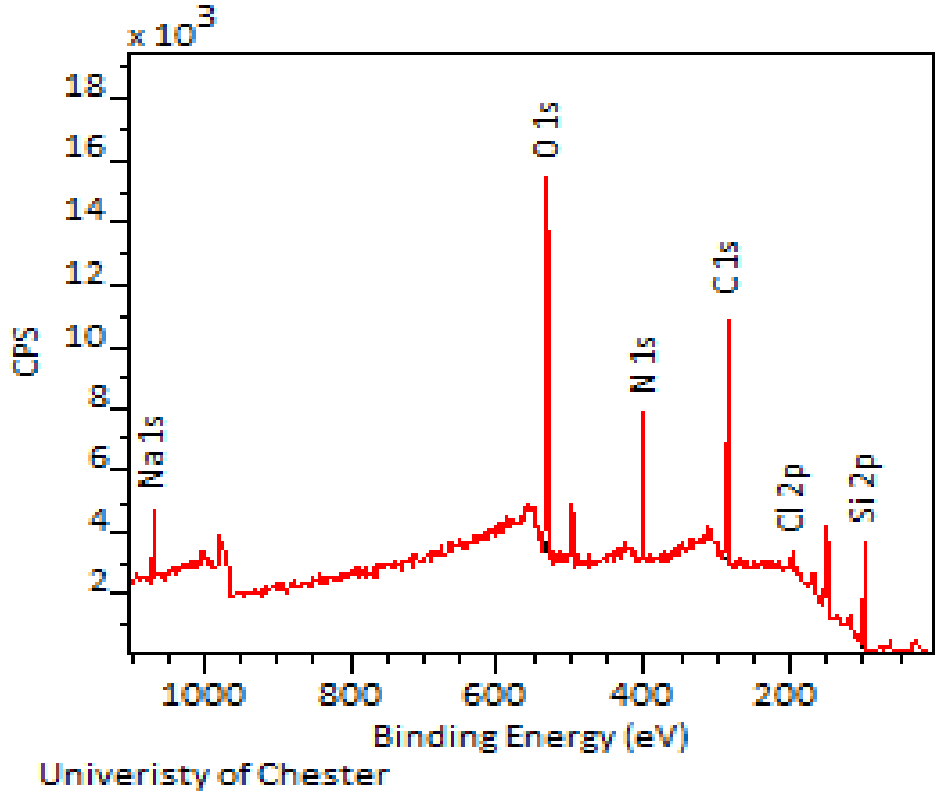

Figure A.45 Survey spectrum of silicon incubated with *NCTC13360* after 20 hours.

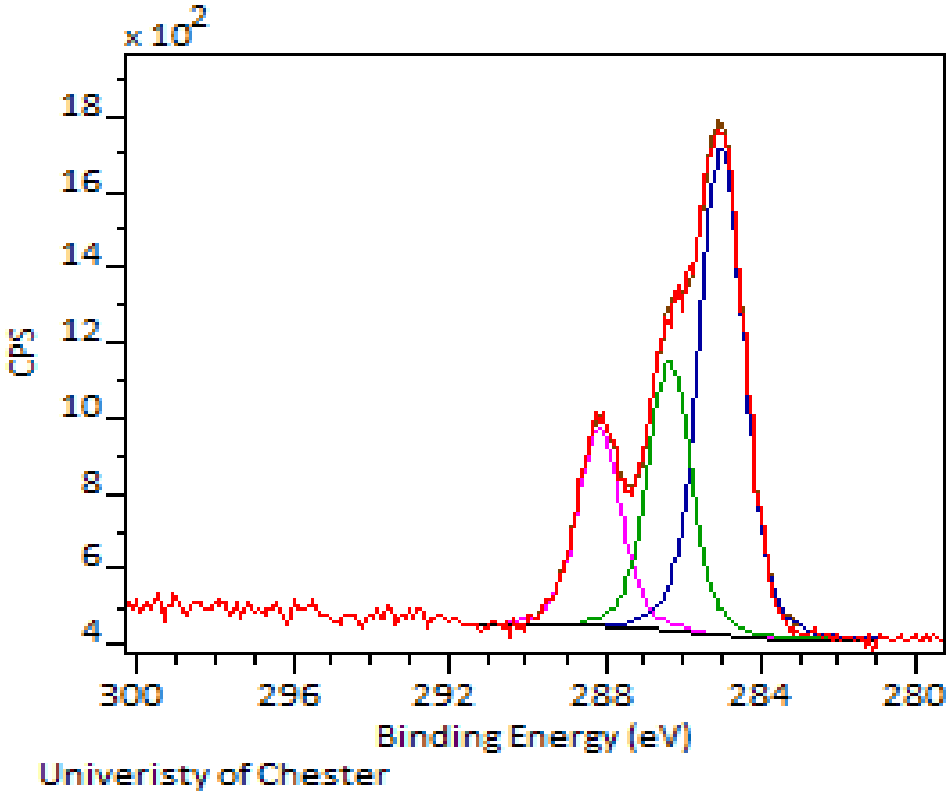

Figure A.46 C 1s peak fit of silicon incubated with *NCTC13360* after 20 hours.

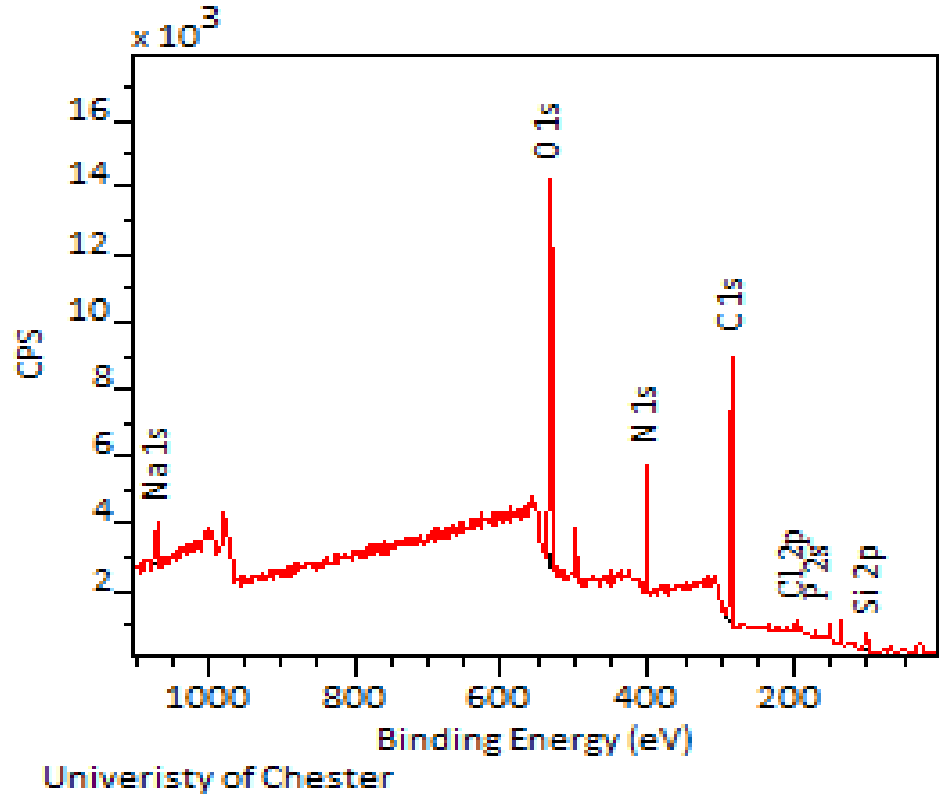

Figure A.47 Survey spectrum of silicon incubated with *NCTC13360* after 22 hours.

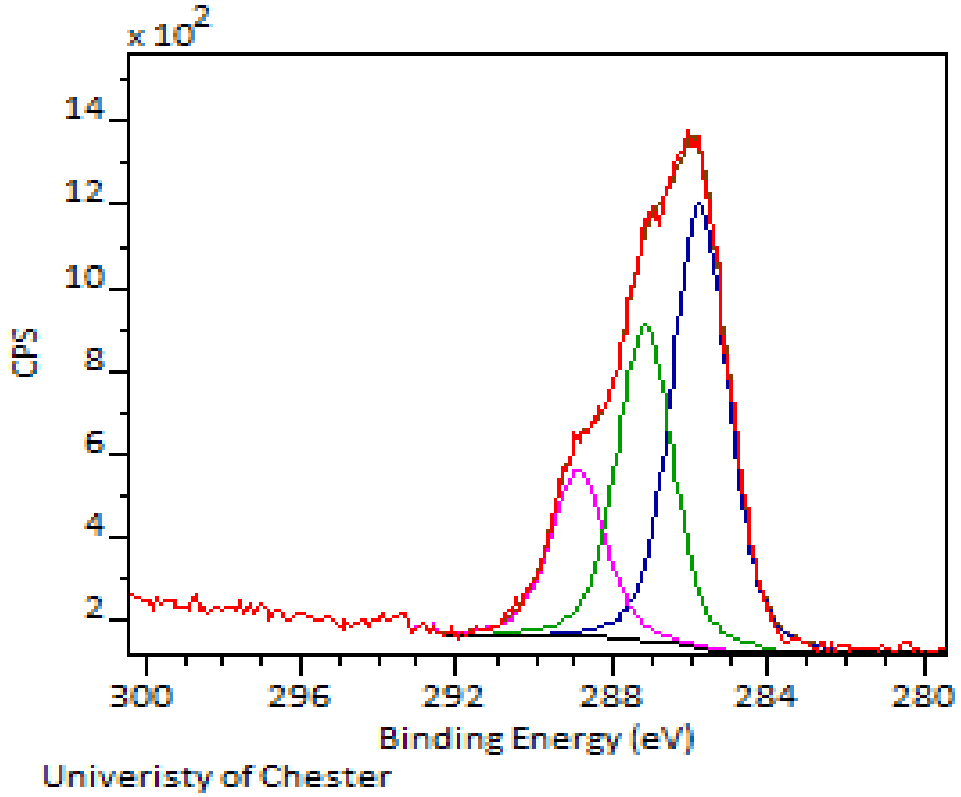

Figure A.48 C 1s peak fit of silicon incubated with *NCTC13360* after 22 hours.

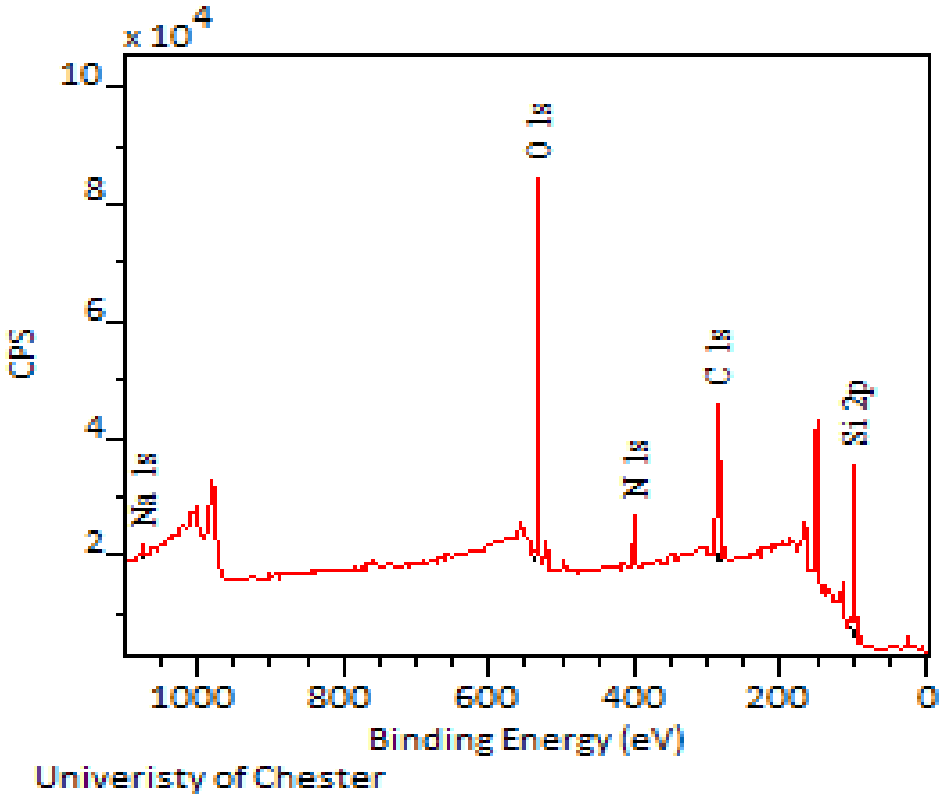

Figure A.49 Survey spectrum of silicon incubated with *ATCC35984* after 2 hours.

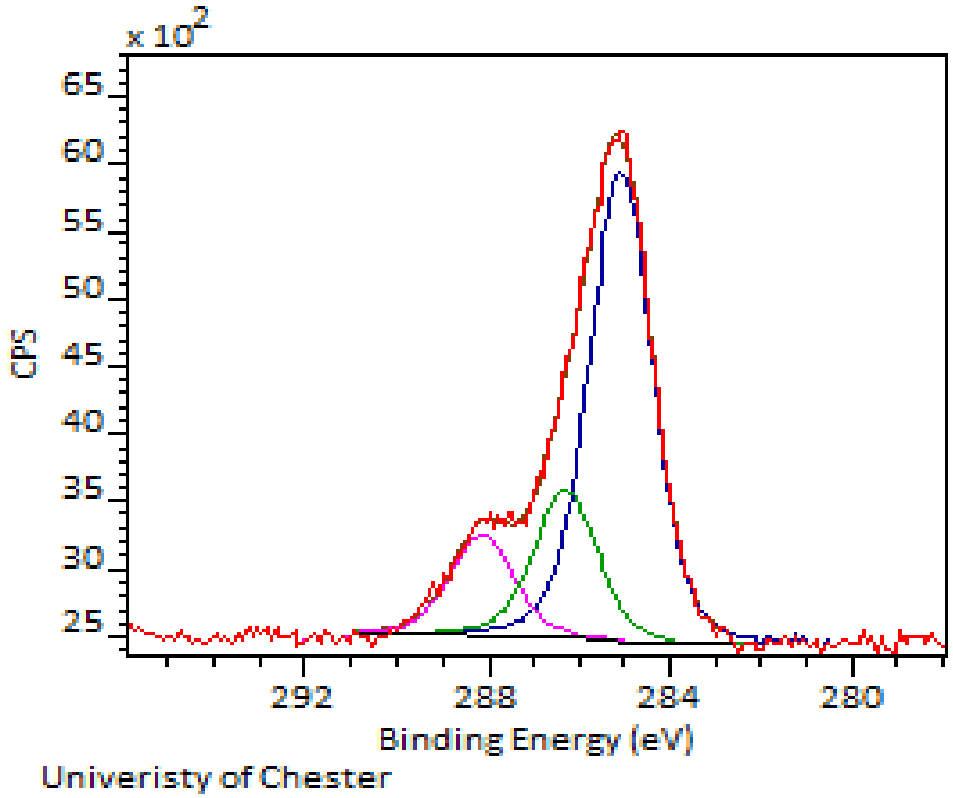

Figure A.50 C 1s peak fit of silicon incubated with *ATCC35984* after 2 hours.

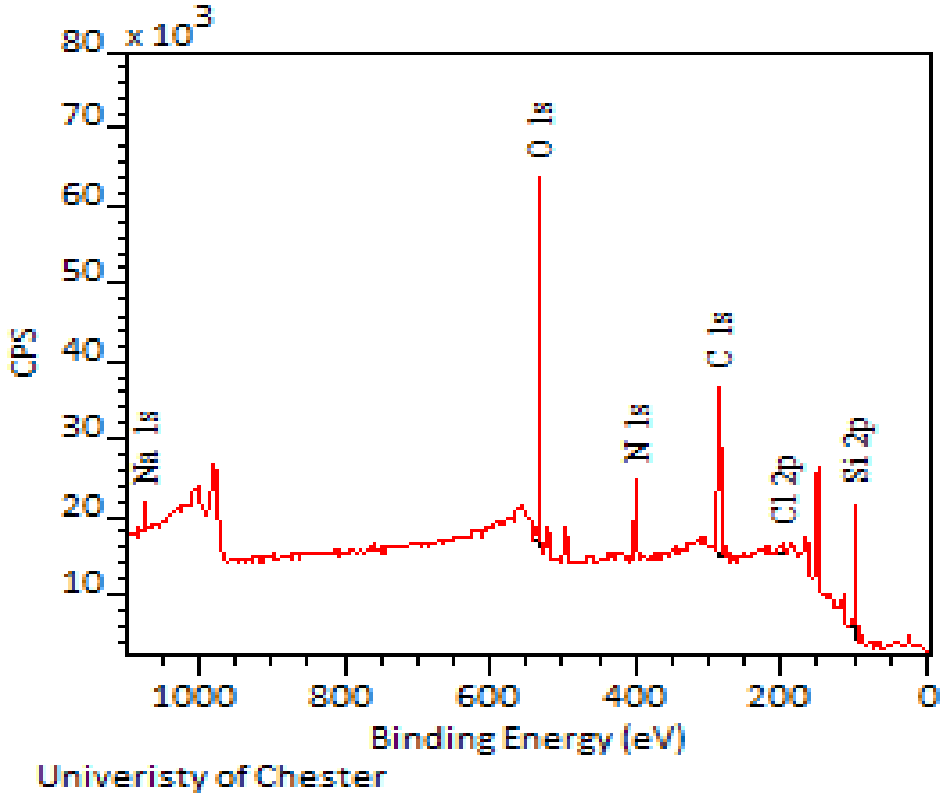

Figure A.51 Survey spectrum of silicon incubated with *ATCC35984* after 4 hours.

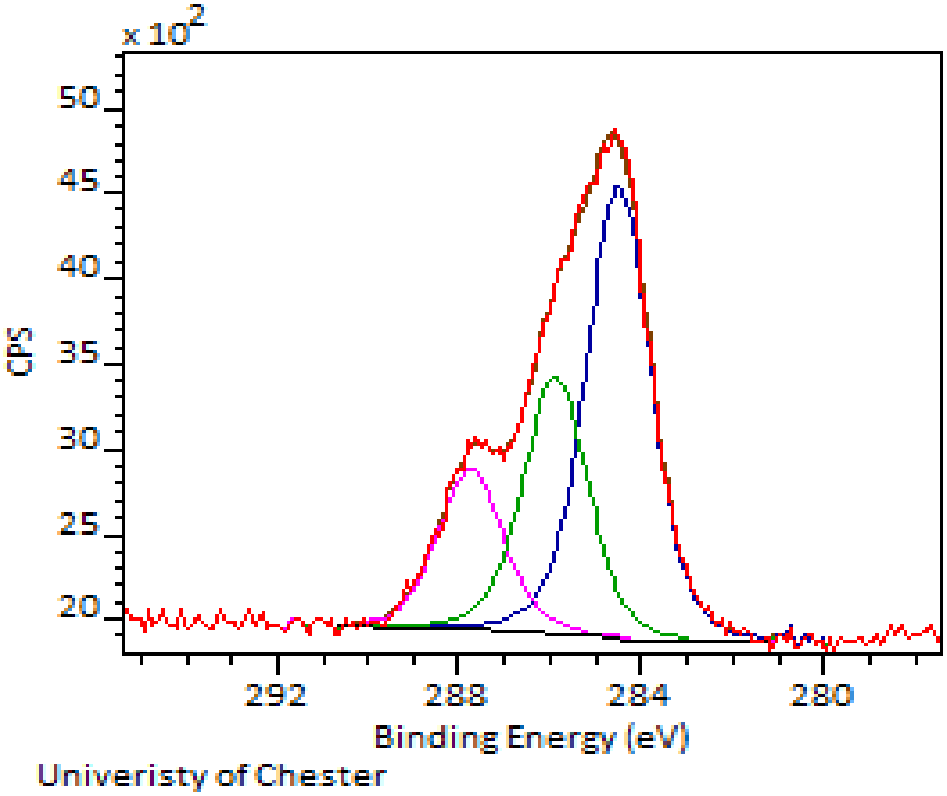

Figure A.52 C 1s peak fit of silicon incubated with *ATCC35984* after 4 hours.

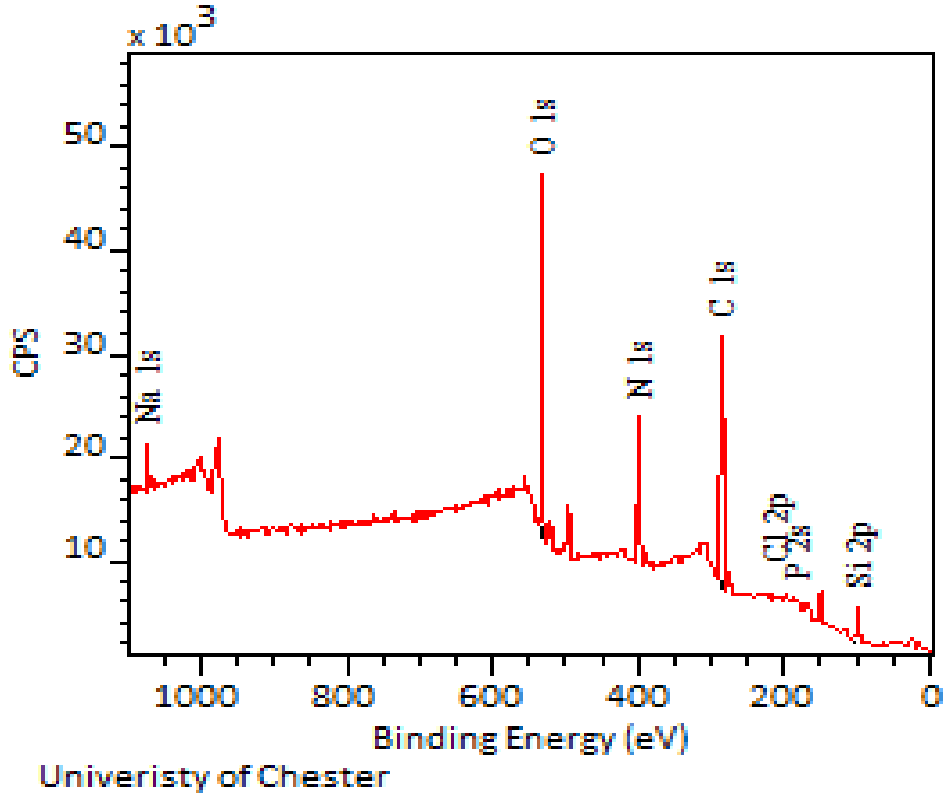

Figure A.53 Survey spectrum of silicon incubated with *ATCC35984* after 5 hours.

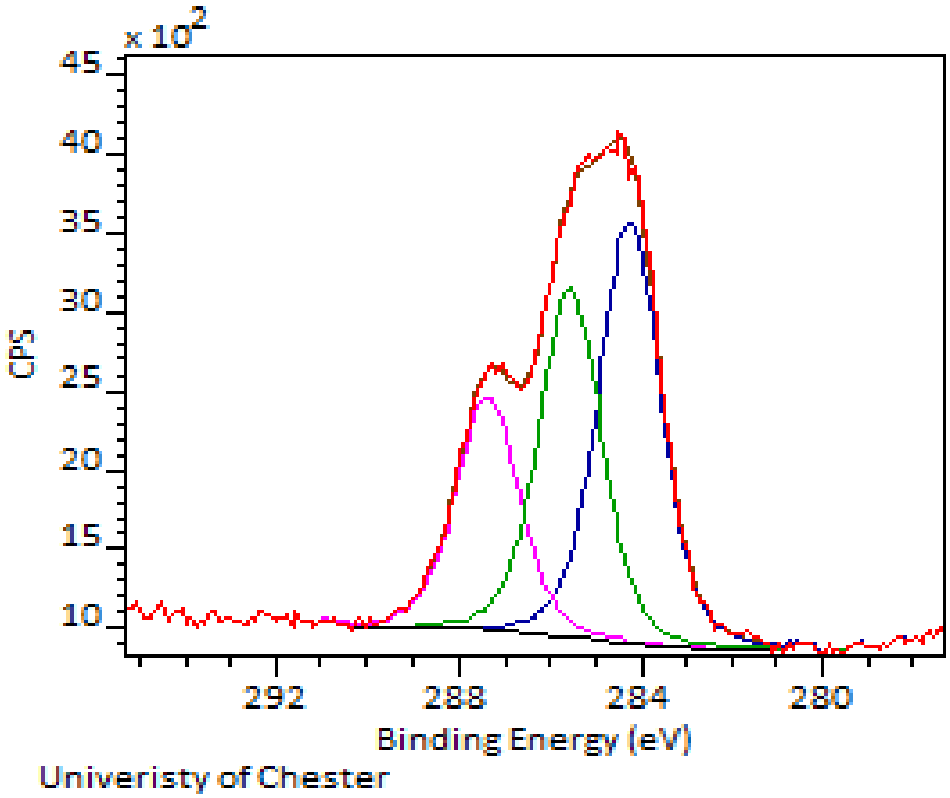

Figure A.54 C 1s peak fit of silicon incubated with *ATCC35984* after 5 hours.

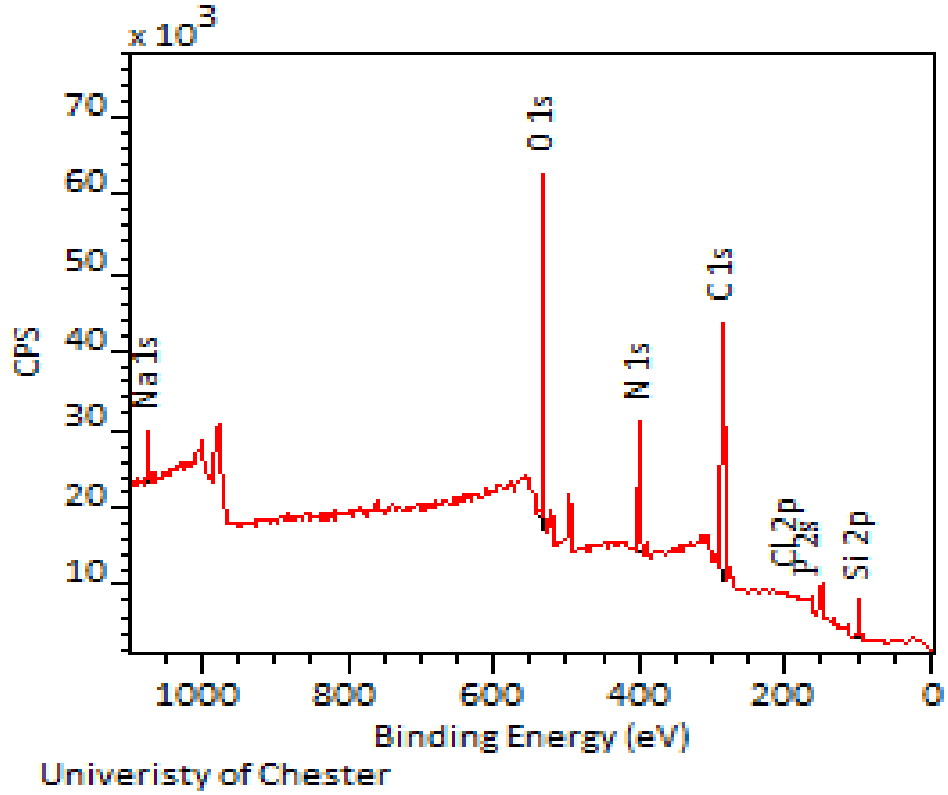

Figure A.55 Survey spectrum of silicon incubated with *ATCC35984* after 6 hours.

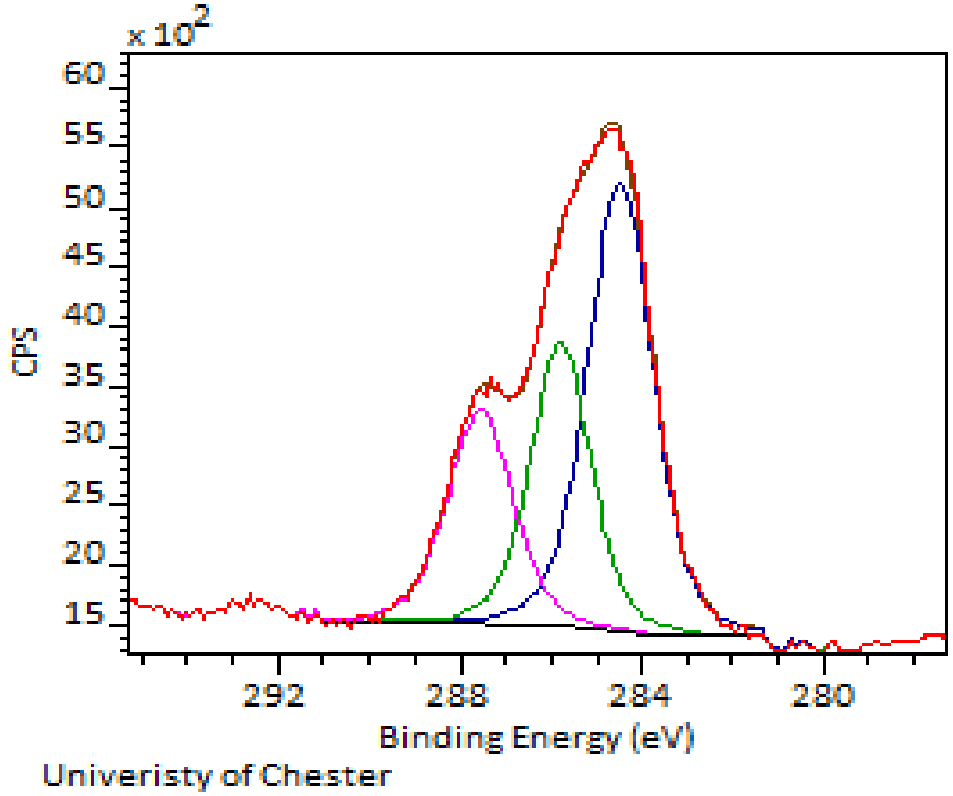

Figure A.56 C 1s peak fit of silicon incubated with *ATCC35984* after 6 hours.

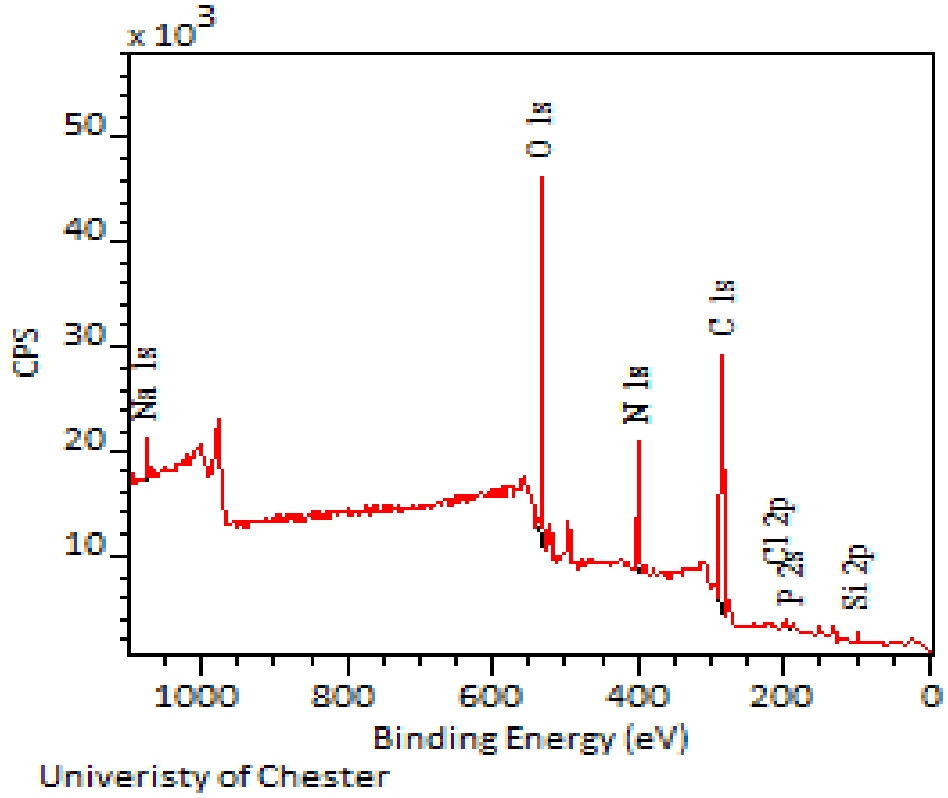

Figure A.57 Survey spectrum of silicon incubated with *ATCC35984* after 7 hours.

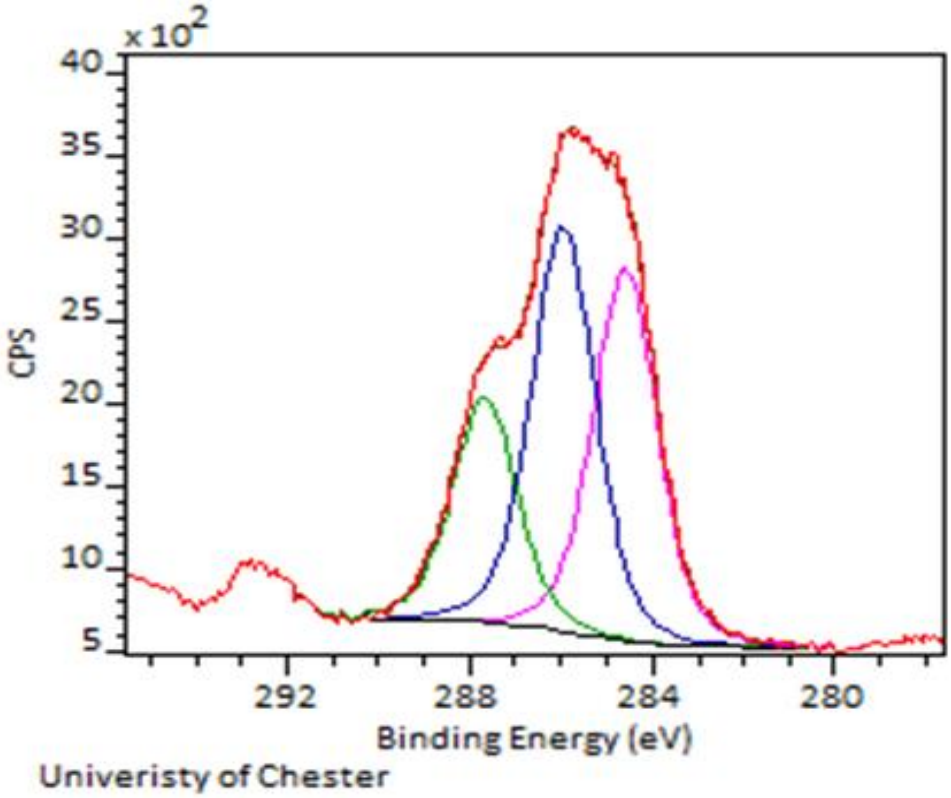

Figure A.58 C 1s peak fit of silicon incubated with *ATCC35984* after 7 hours.

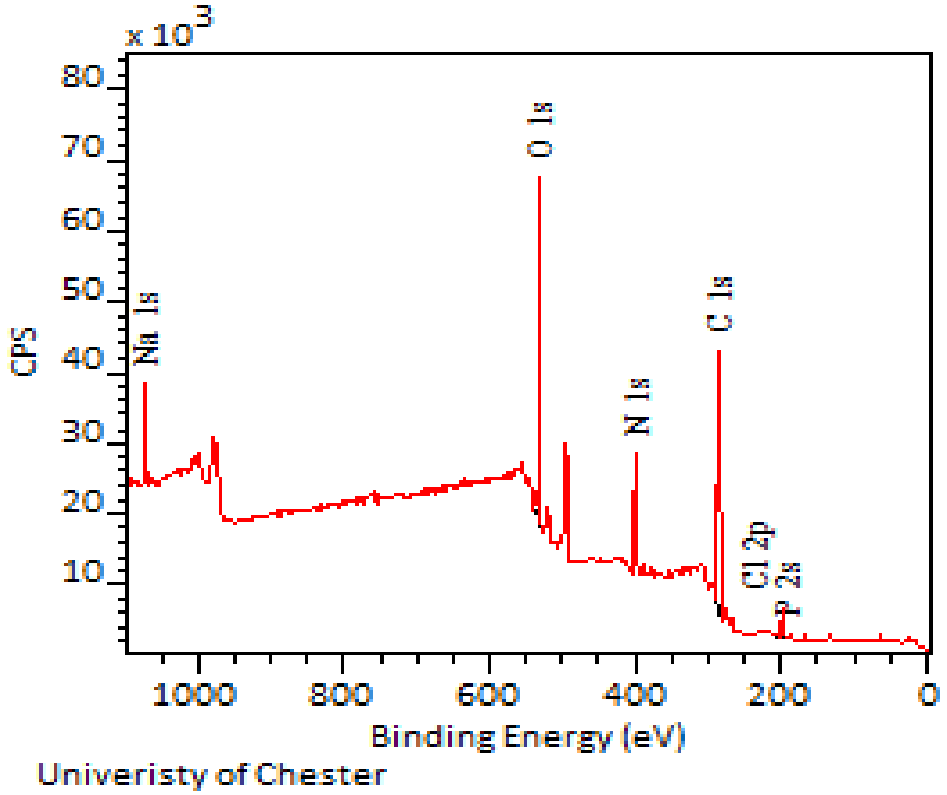

Figure A.59 Survey spectrum of silicon incubated with *ATCC35984* after 8 hours.

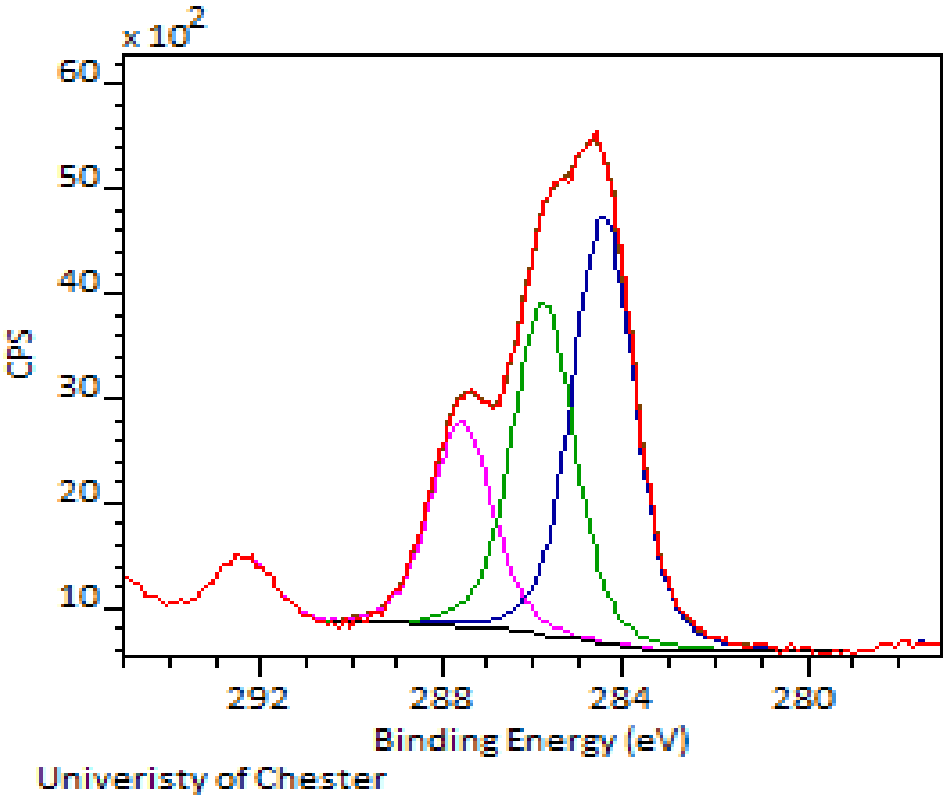

Figure A.60 C 1s peak fit of silicon incubated with *ATCC35984* after 8 hours.

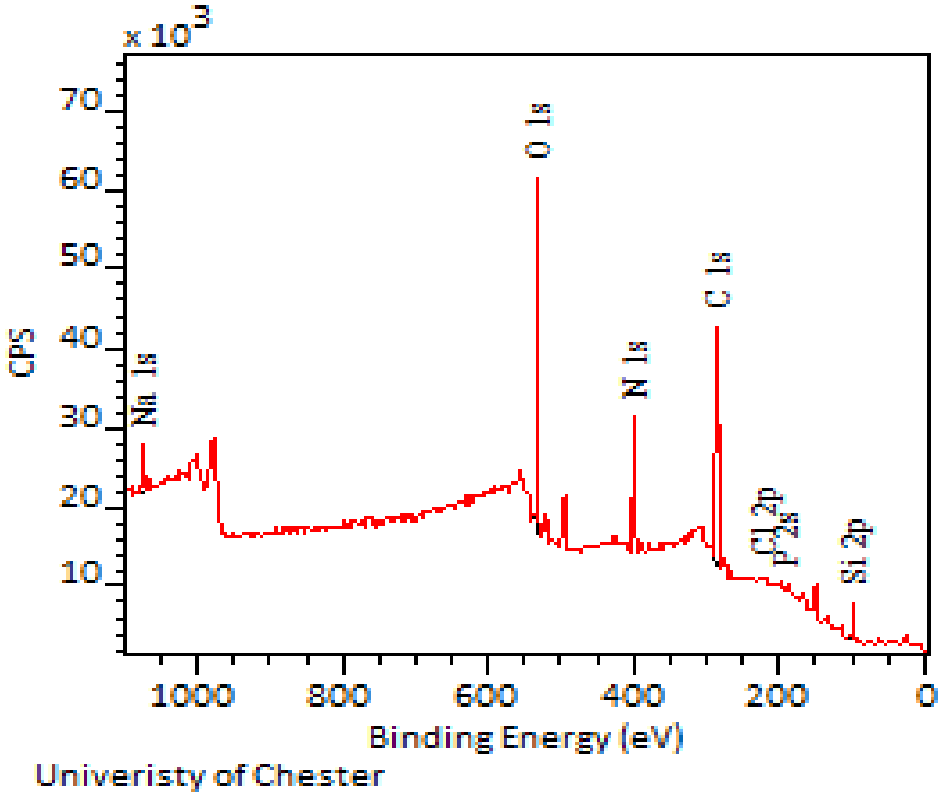

Figure A.61 Survey spectrum of silicon incubated with *ATCC35984* after 9 hours.

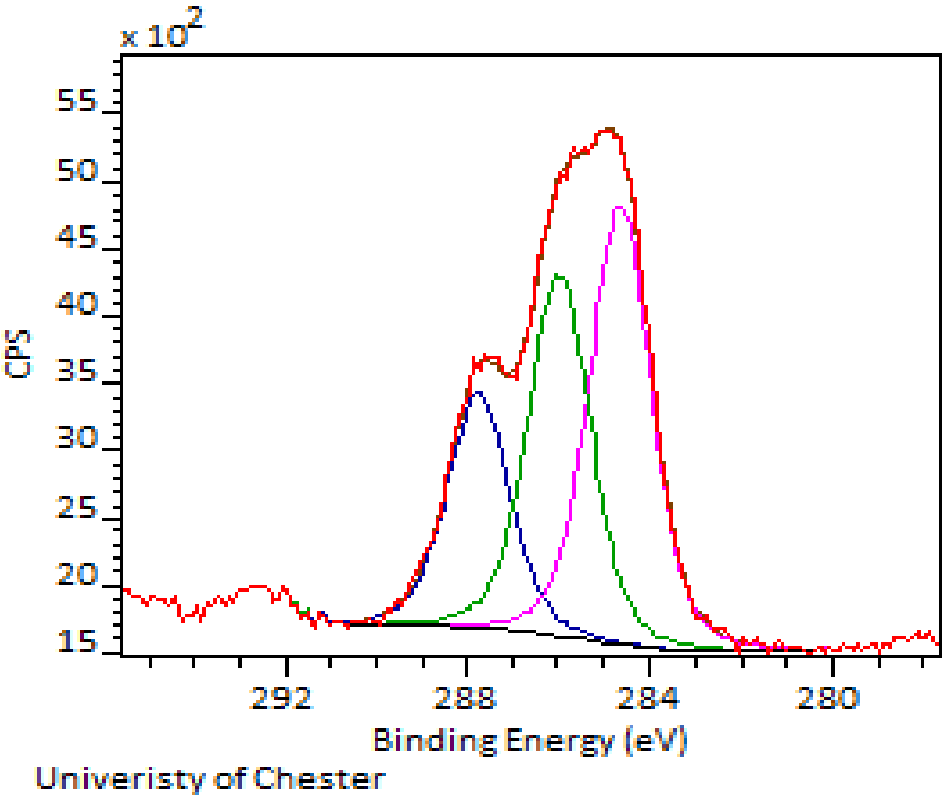

Figure A.62 C 1s peak fit of silicon incubated with *ATCC35984* after 9 hours.

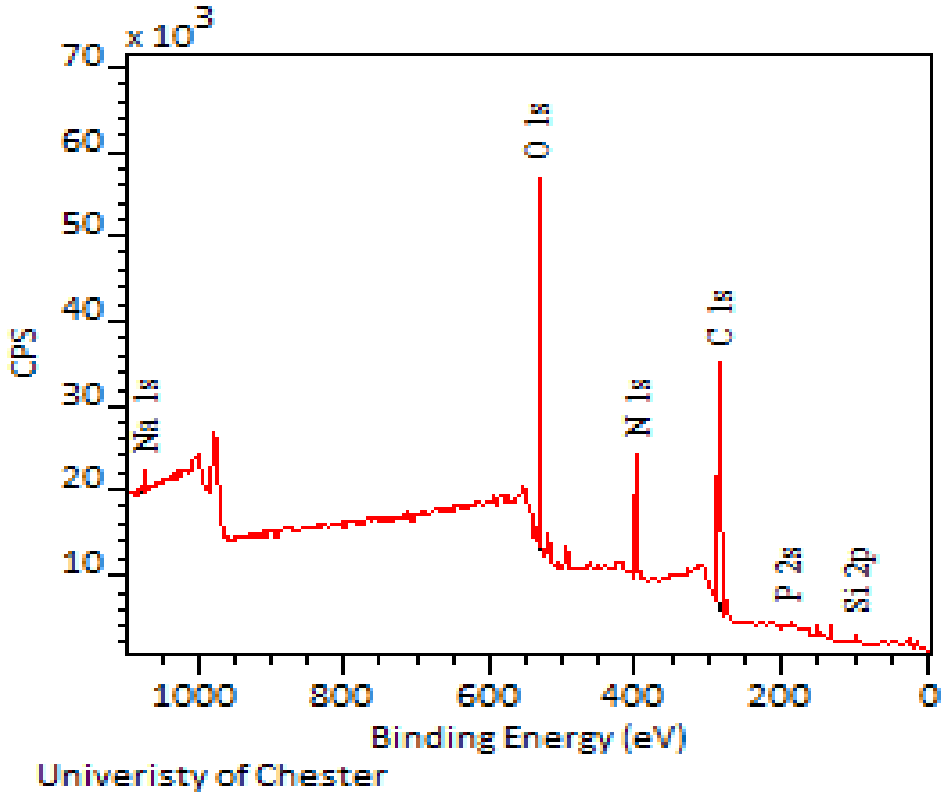

Figure A.63 Survey spectrum of silicon incubated with *ATCC35984* after 12 hours .

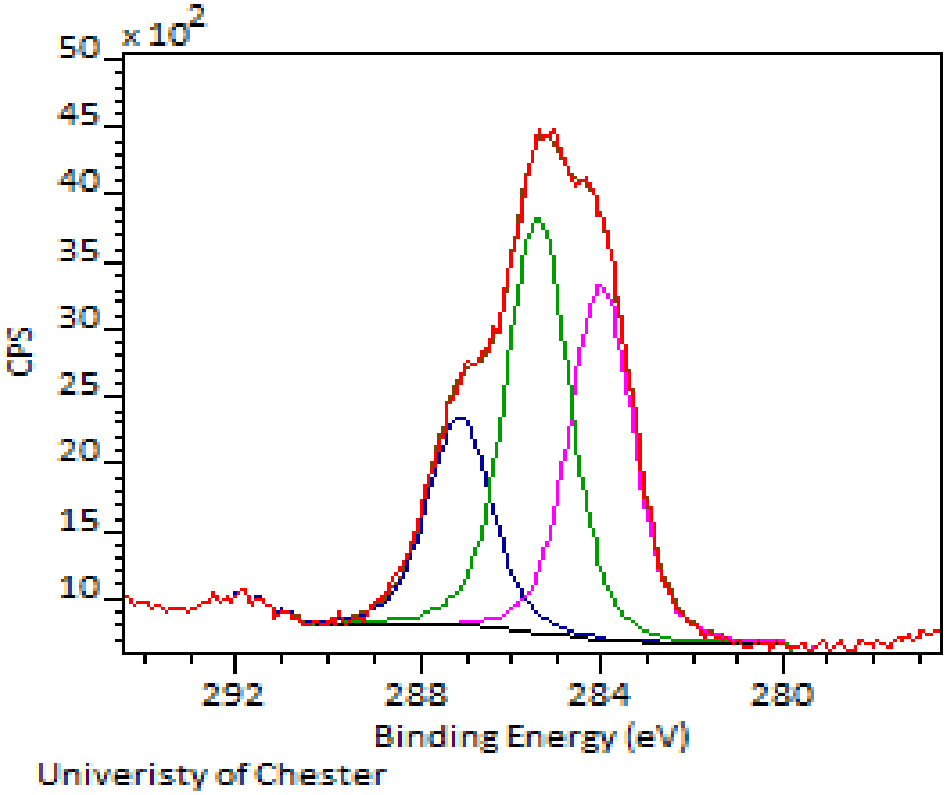

Figure A.64 C 1s peak fit of silicon incubated with *ATCC35984* after 12 hours.

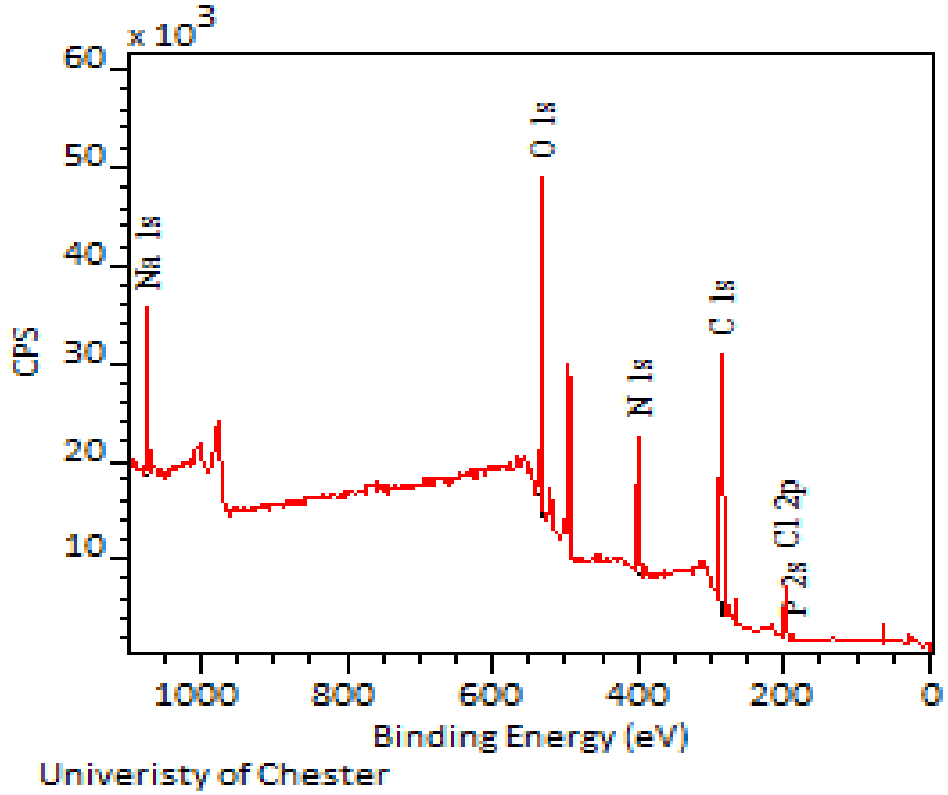

Figure A.65 Survey spectrum of silicon incubated with *ATCC35984* after 14 hours.

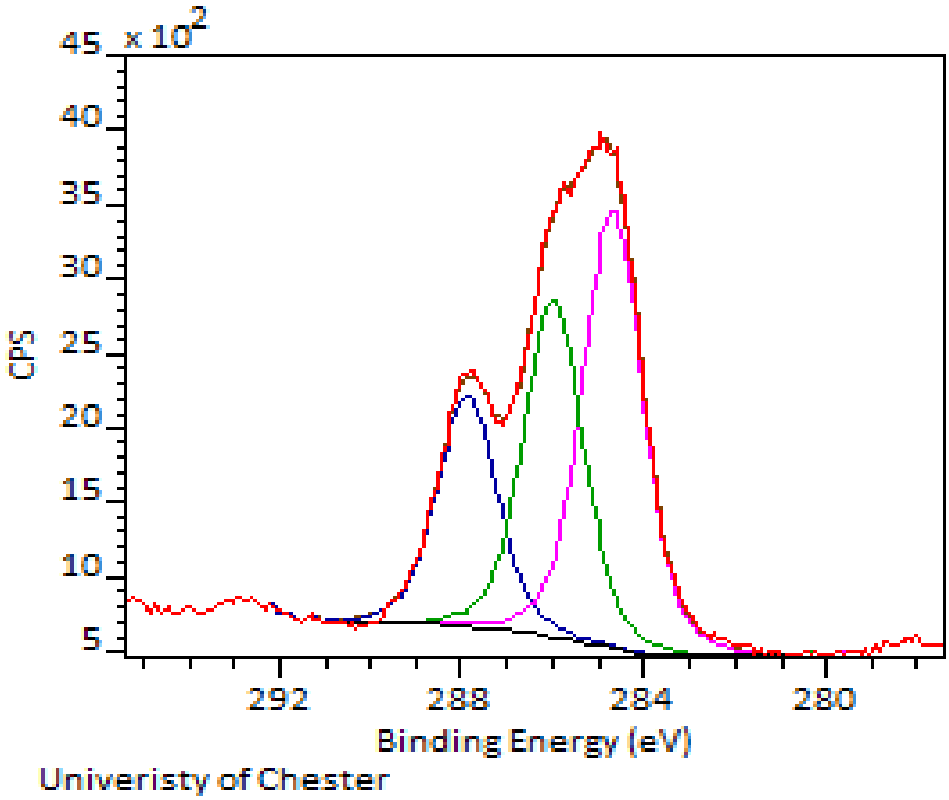

Figure A.66 C 1s peak fit of silicon incubated with *ATCC35984* after 14 hours.

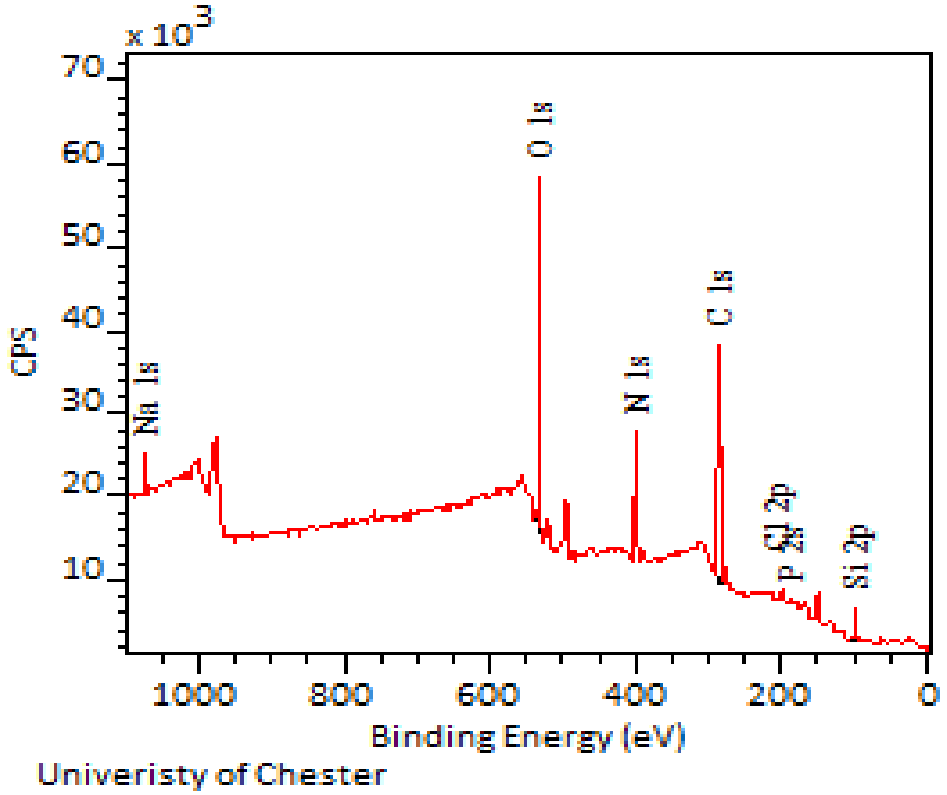

Figure A.67 Survey spectrum of silicon incubated with *ATCC35984* after 16 hours .

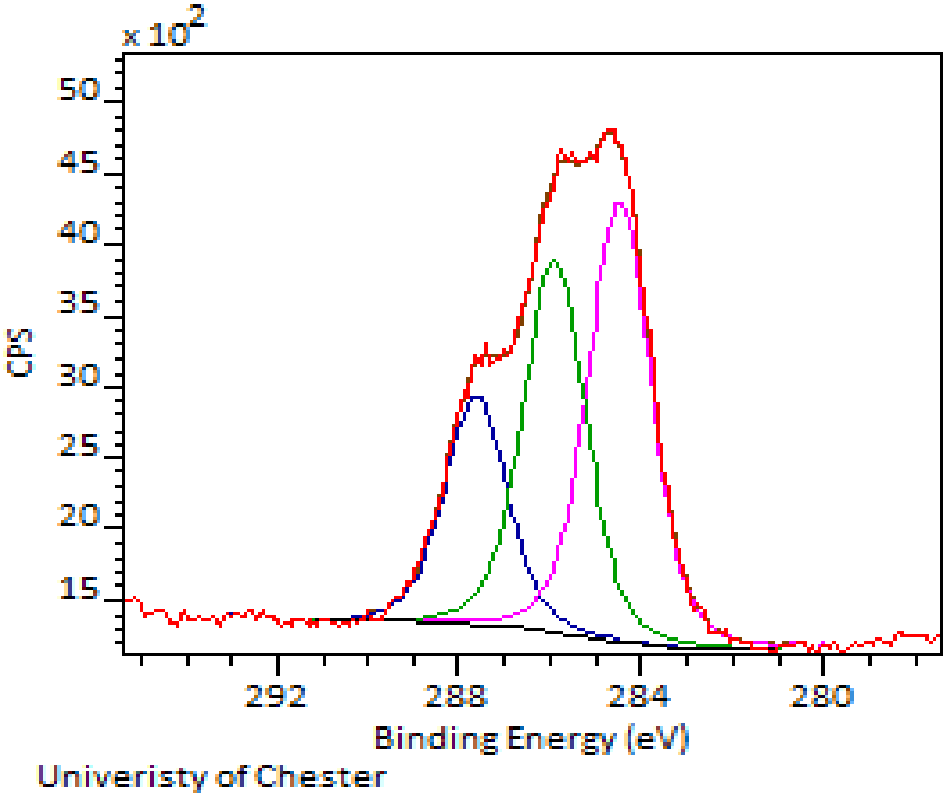

Figure A.68 C 1s peak fit of silicon incubated with *ATCC35984* after 16 hours.

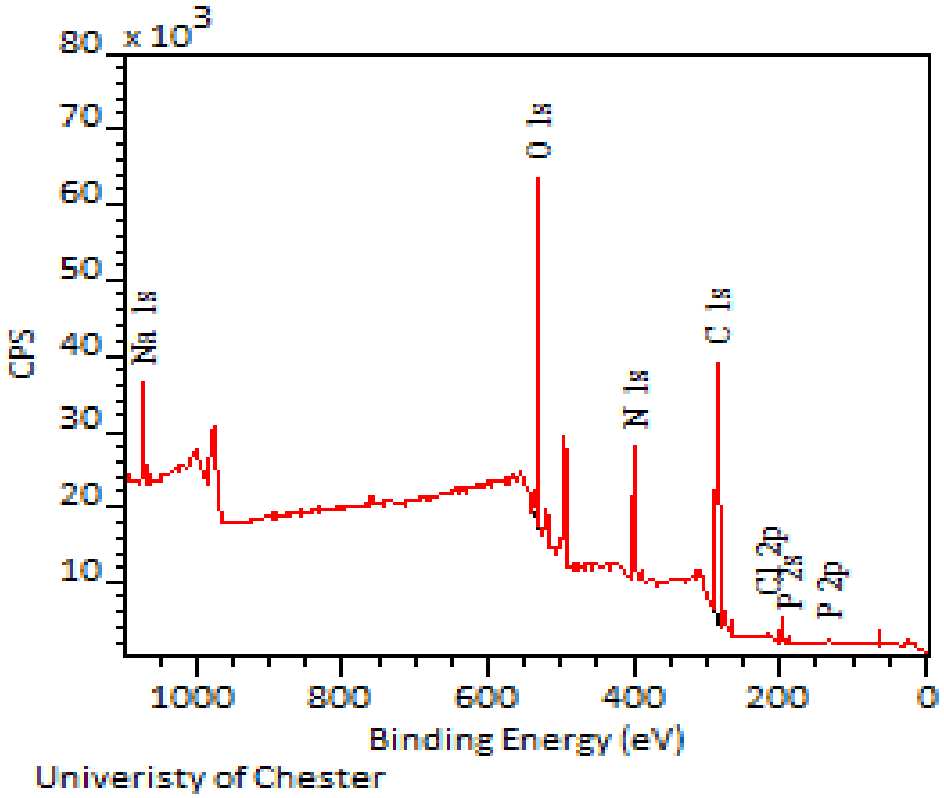

Figure A.69 Survey spectrum of silicon incubated with *ATCC35984* after 20 hours.

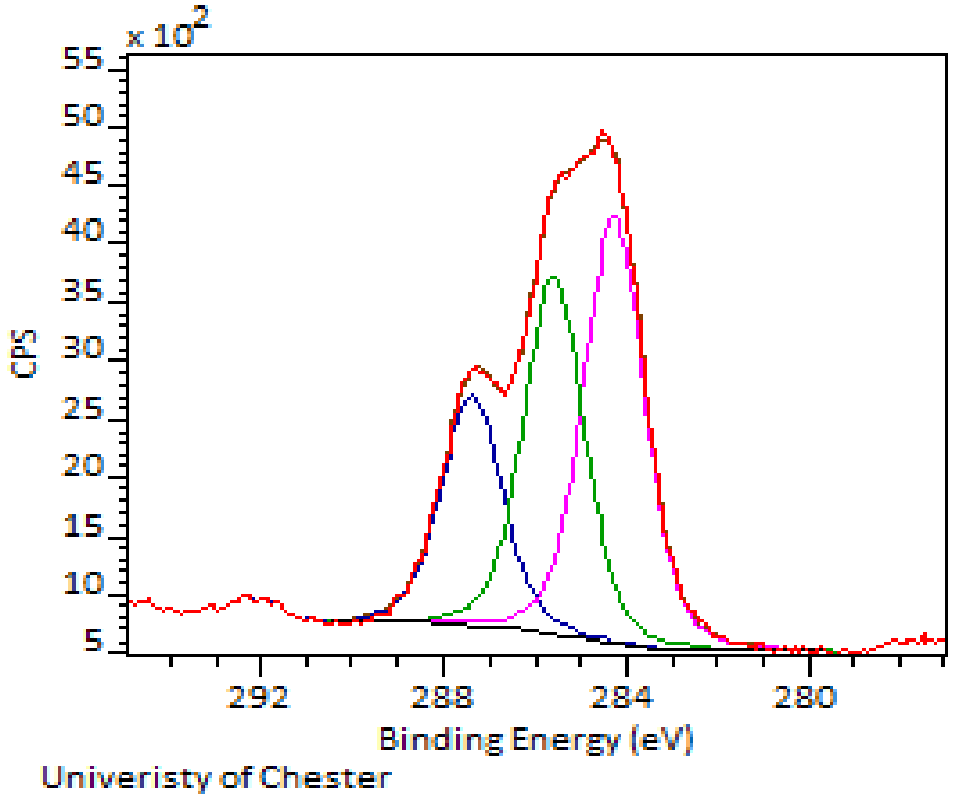

Figure A.70 C 1s peak fit of silicon incubated with *ATCC35984* after 20 hours.

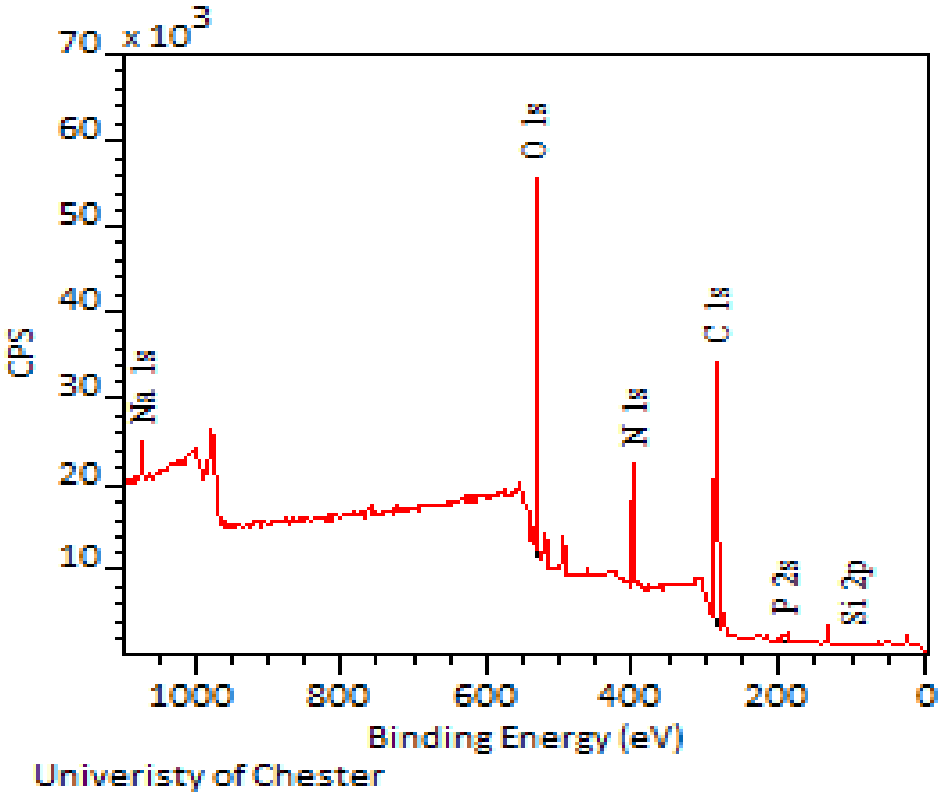

Figure A.71 Survey spectrum of silicon incubated with *ATCC35984* after 22 hours.

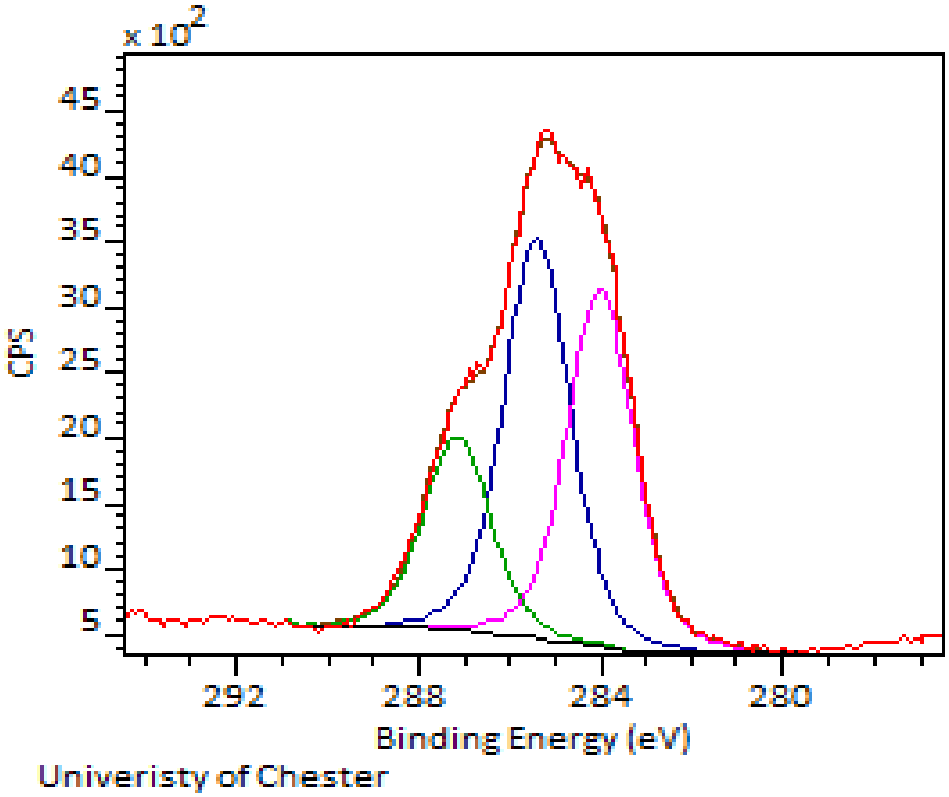

Figure A.72 C 1s peak fit of silicon incubated with *ATCC35984* after 22 hours.

Appendix B Frequency distribution plots

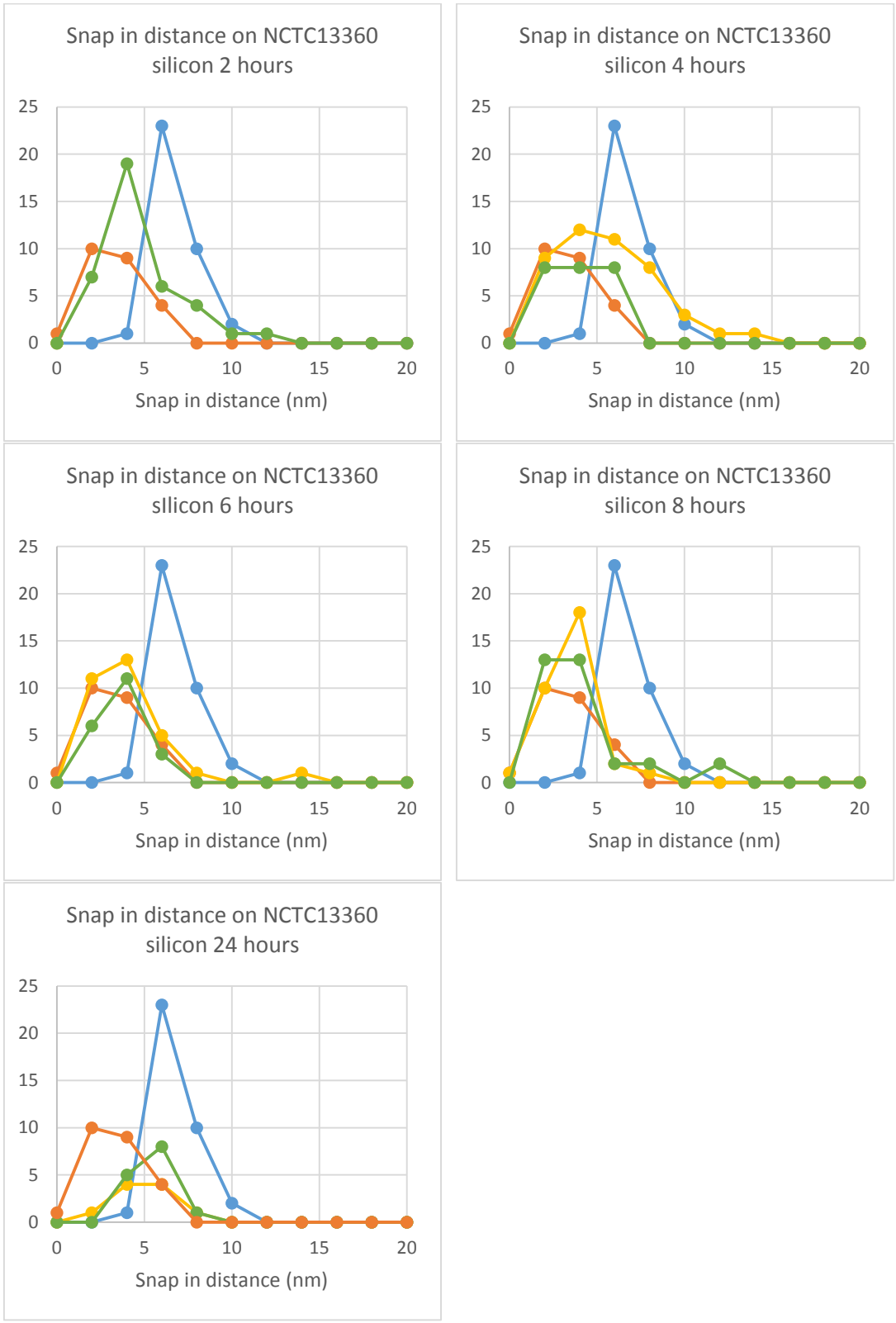

Figure B.1 Frequency distribution of snap in distance of incubated silicon at 2, 4, 6, 8 and 24 hours with *NCTC13360* where blue is TSB incubated silicon after 24 hours, orange is the *NCTC13360* pellet, yellow is the bacterial points of incubated samples and green is the non-bacterial points of incubated samples.

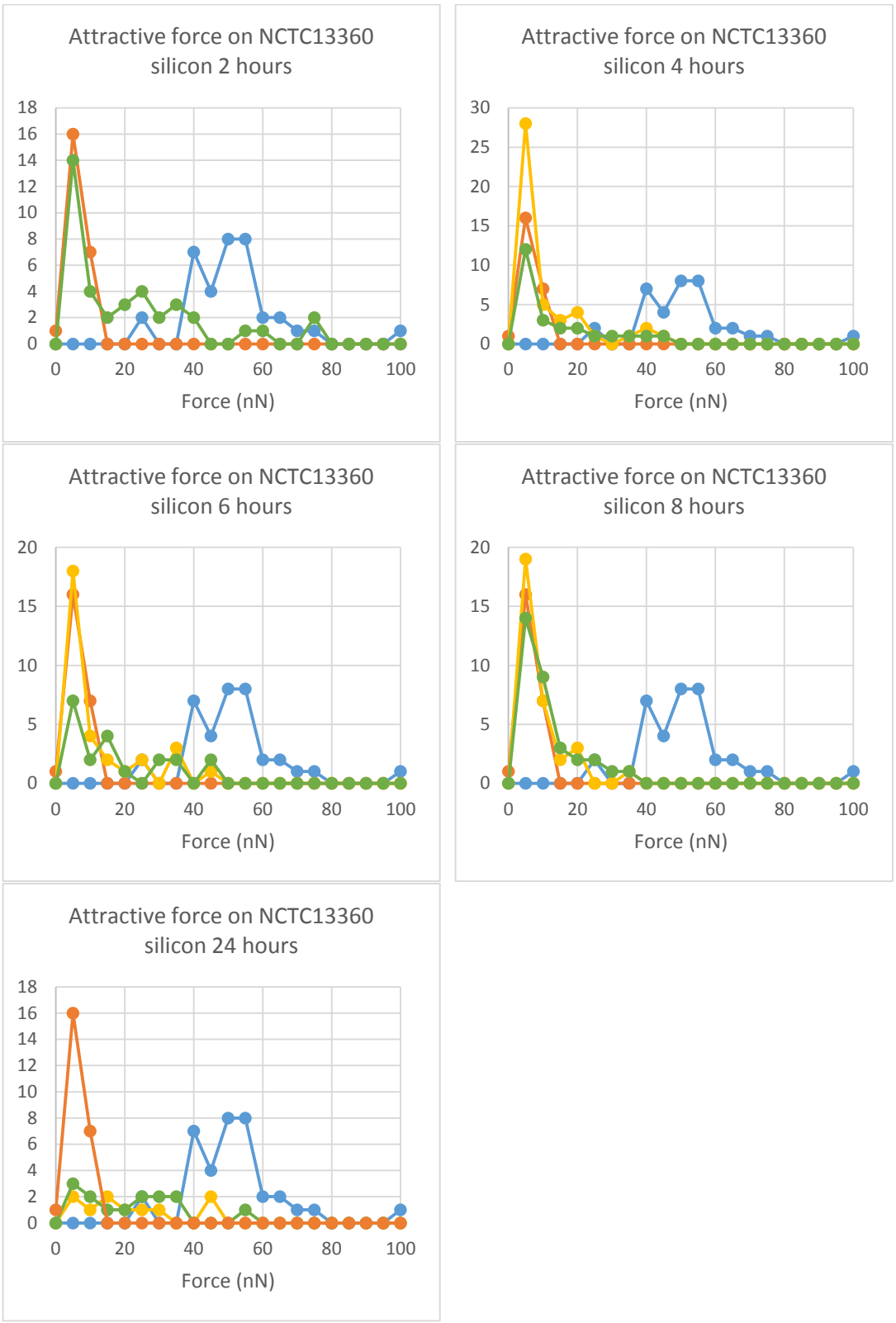

Figure B.2 Frequency distribution of attractive force of incubated silicon at 2, 4, 6, 8 and 24 hours with *NCTC13360* where blue is TSB incubated silicon after 24 hours, orange is the *NCTC13360* pellet, yellow is the bacterial points of incubated samples and green is the non-bacterial points of incubated samples.

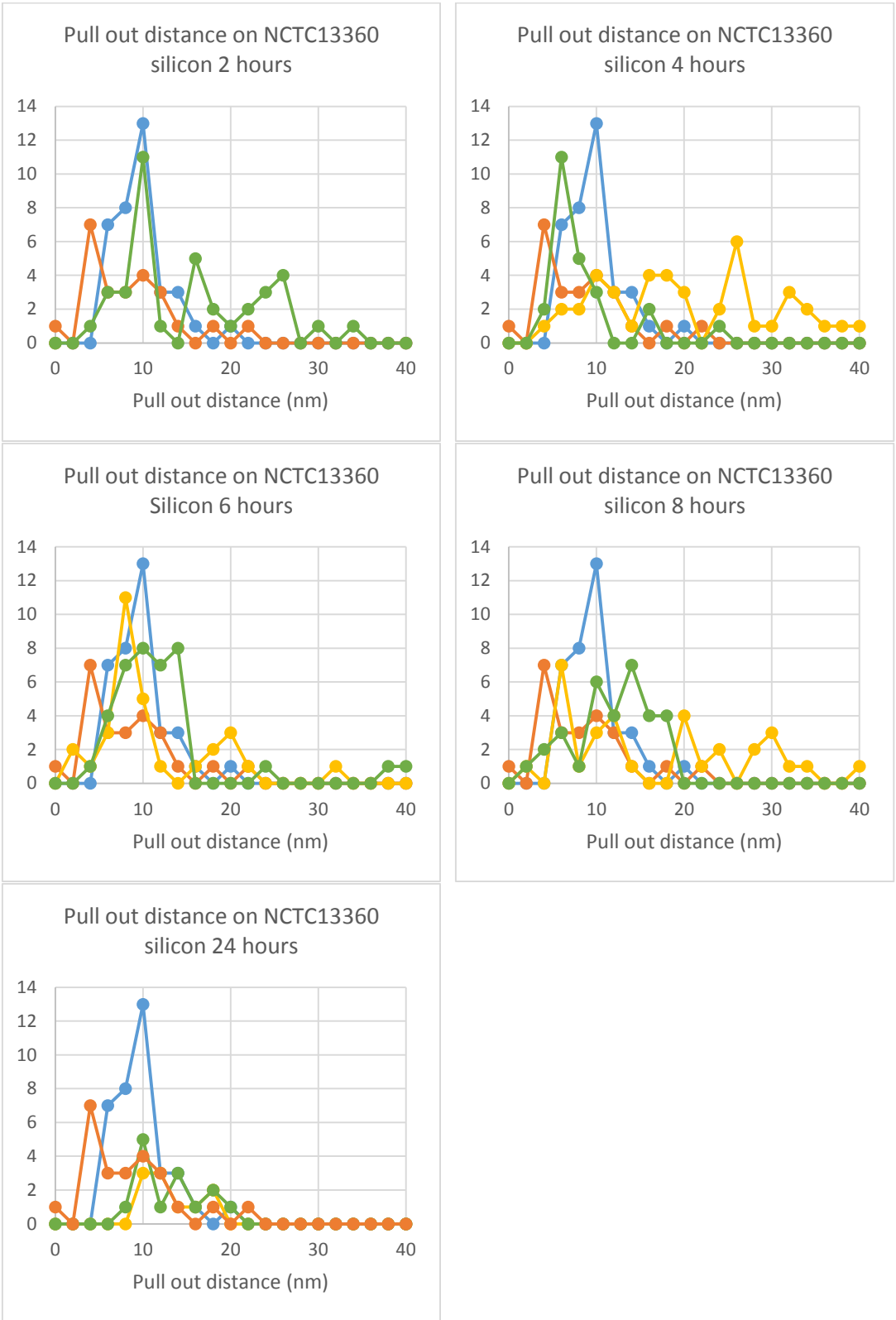

Figure B.3 Frequency distribution of pull out distance of incubated silicon at 2, 4, 6, 8 and 24 hours with *NCTC13360* where blue is TSB incubated silicon after 24 hours, orange is the *NCTC13360* pellet, yellow is the bacterial points of incubated samples and green is the non-bacterial points of incubated samples.

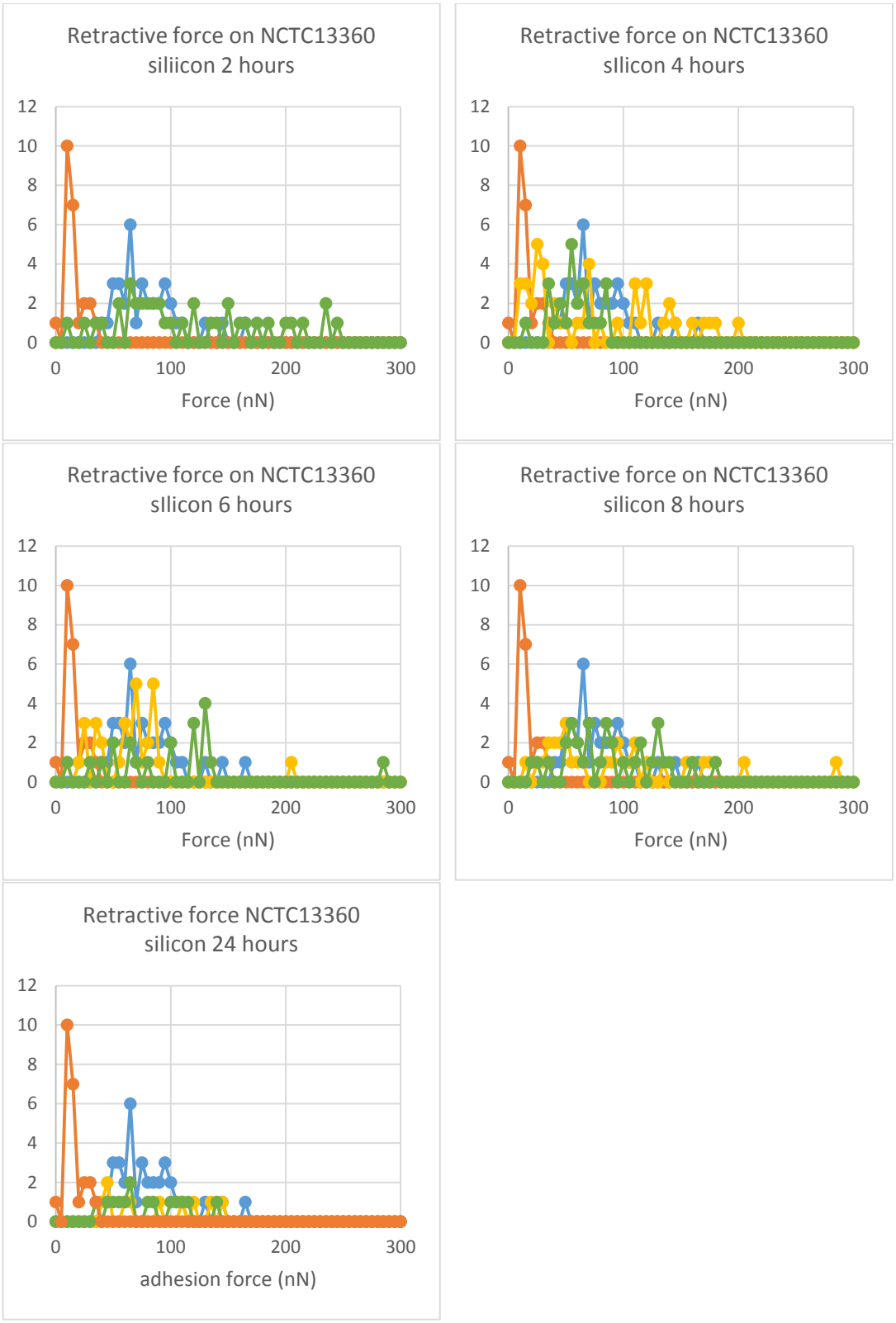

Figure B.4 Frequency distribution of retractive force of incubated silicon at 2, 4, 6, 8 and 24 hours with *NCTC13360* where blue is TSB incubated silicon after 24 hours, orange is the *NCTC13360* pellet, yellow is the bacterial points of incubated samples and green is the non-bacterial points of incubated samples.

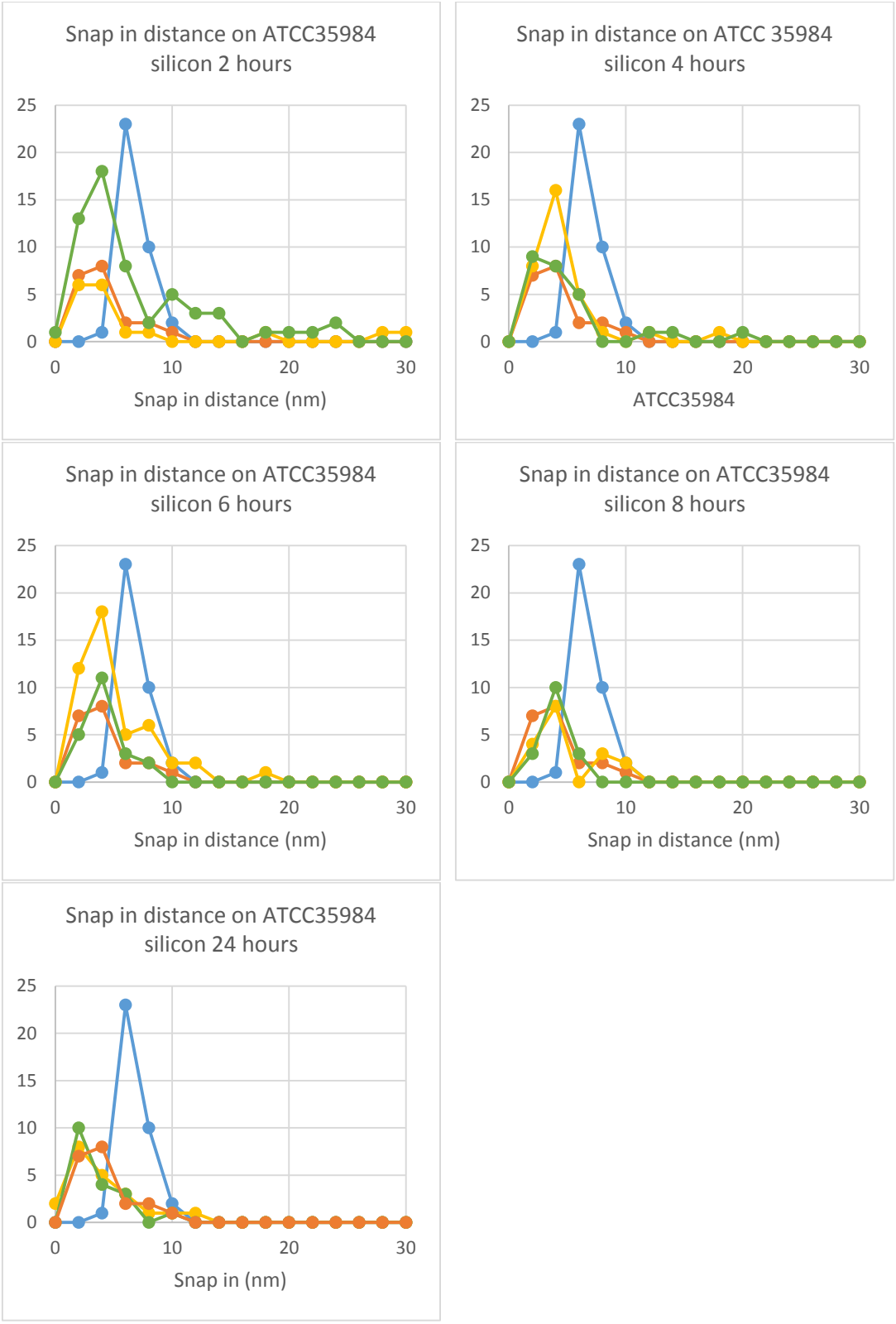

Figure B.5 Frequency distribution of snap in distance of incubated silicon at 2, 4, 6, 8 and 24 hours with *ATCC35984* where blue is TSB incubated silicon after 24 hours, orange is the *ATCC35984* pellet, yellow is the bacterial points of incubated samples and green is the non-bacterial points of incubated samples,

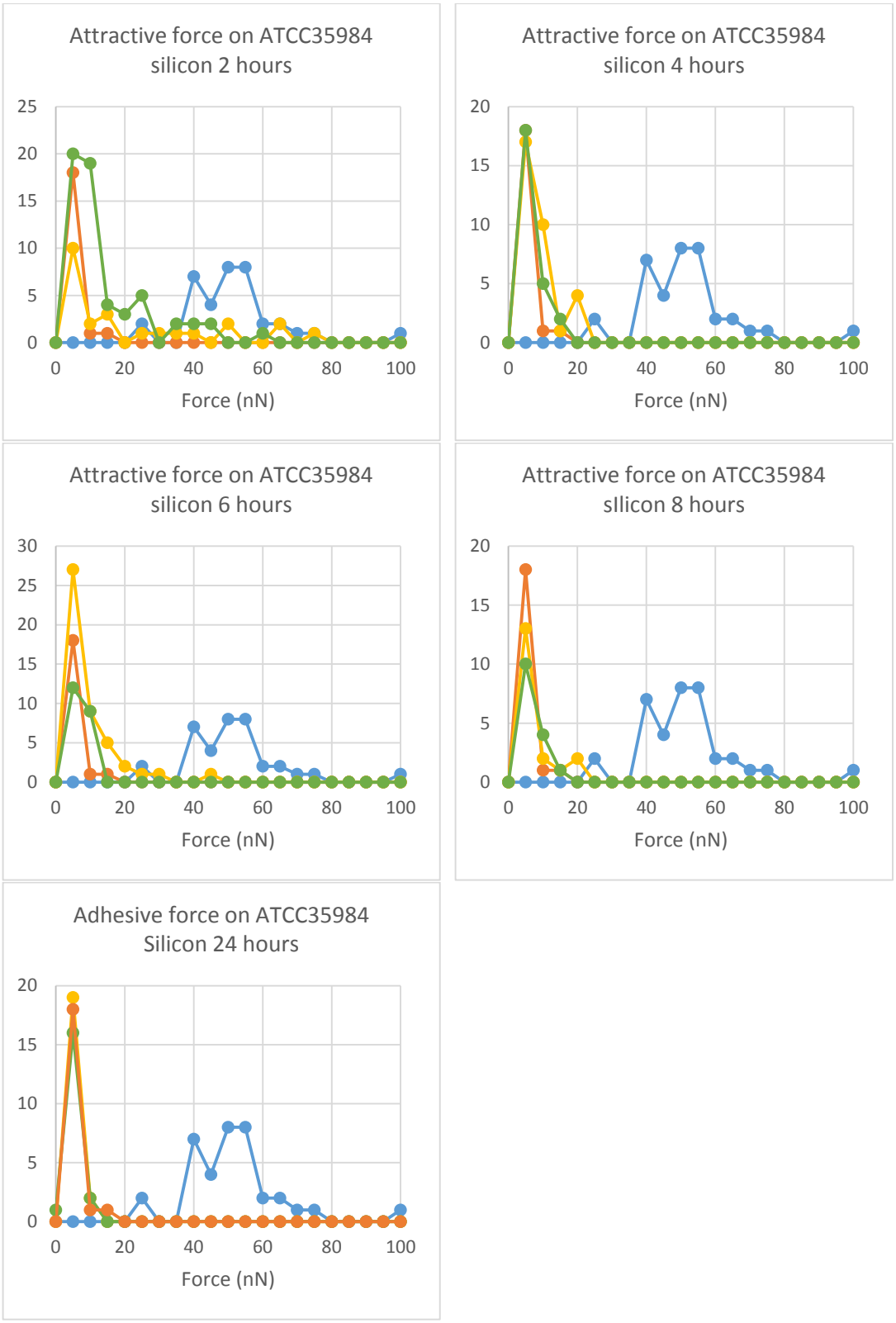

Figure B.6 Frequency distribution of adhesive force of incubated silicon at 2, 4, 6, 8 and 24 hours with *ATCC35984* where blue is TSB incubated silicon after 24 hours, orange is the *ATCC35984* pellet, yellow is the bacterial points of incubated samples and green is the non-bacterial points of incubated samples.

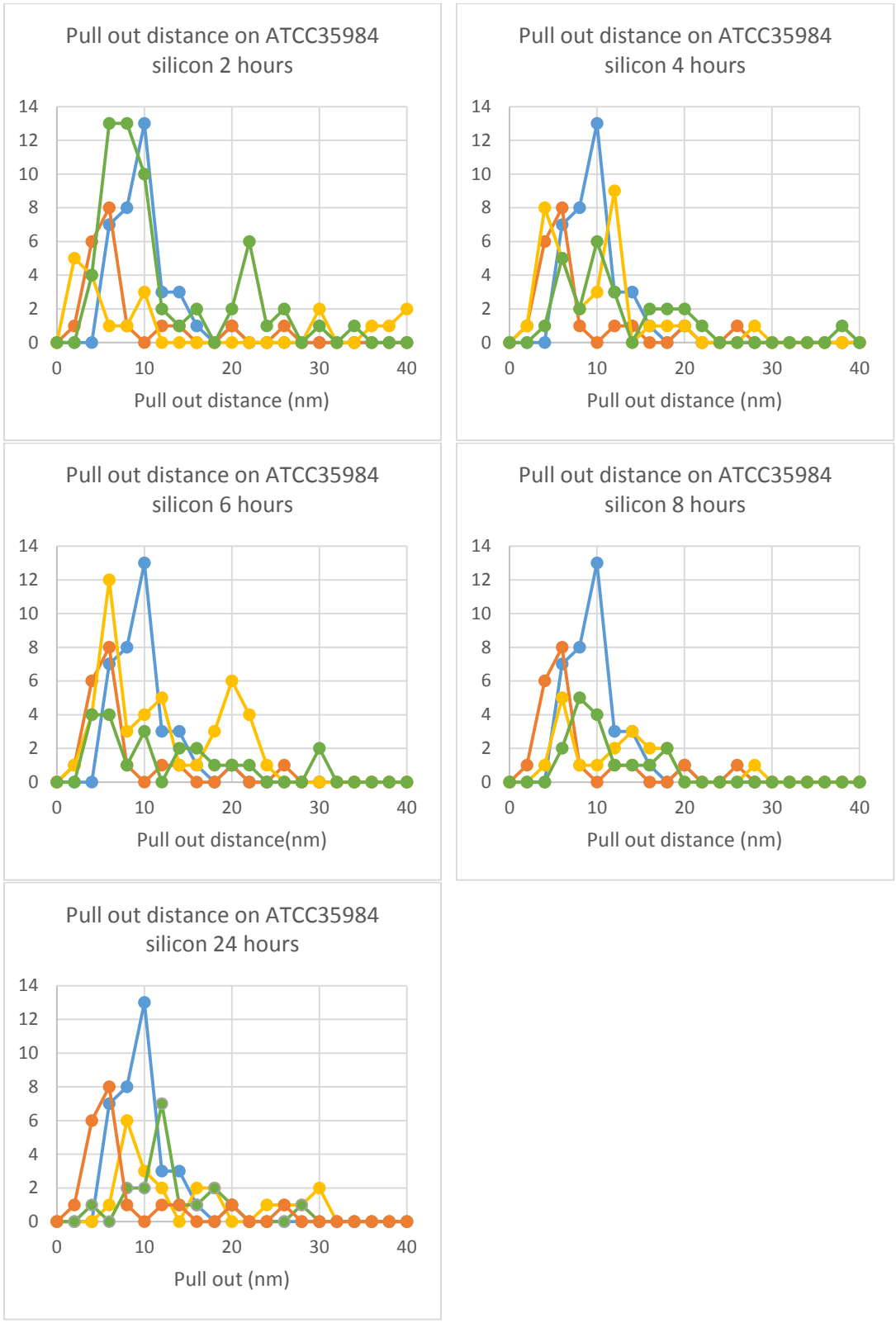

Figure B.7 Frequency distribution of pull out distance of incubated silicon at 2, 4, 6, 8 and 24 hours with *ATCC35984* where blue is TSB incubated silicon after 24 hours, orange is the *ATCC35984* pellet, yellow is the bacterial points of incubated samples and green is the non-bacterial points of incubated samples.

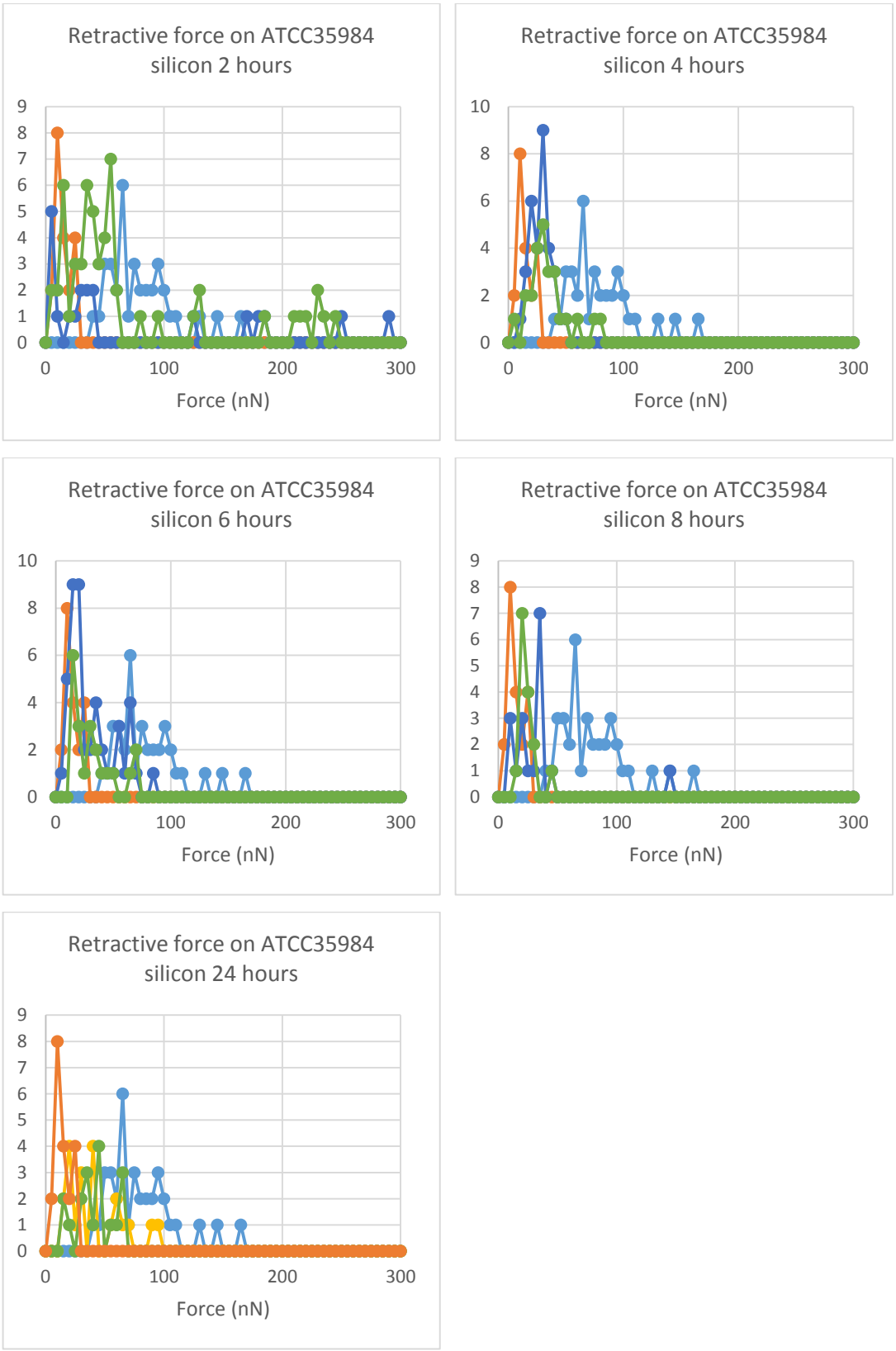

Figure B.8 Frequency distribution of retractive force of incubated silicon at 2, 4, 6, 8 and 24 hours with *ATCC35984* where blue is TSB incubated silicon after 24 hours, orange is the *ATCC35984* pellet, yellow is the bacterial points of incubated samples and green is the non-bacterial points of incubated samples.